

Reaction Injection Molding

ACS SYMPOSIUM SERIES 270

Reaction Injection Molding

Polymer Chemistry and Engineering

Jiri E. Kresta, EDITOR

University of Detroit

Based on a symposium sponsored by
the Division of Polymeric Materials Science and Engineering
at the 186th Meeting
of the American Chemical Society,
Washington, D.C.,
August 28–September 2, 1983



American Chemical Society, Washington, D.C. 1985



Library of Congress Cataloging in Publication Data

Reaction injection molding.
(ACS symposium series, ISSN 0097-6156; 270)

Includes bibliographies and indexes.

I. Injection molding of plastics—Congresses.

I. Kresta, Jiri E., 1934— . II. American Chemical Society. Division of Polymeric Materials: Science and Engineering. III. American Chemical Society. Meeting (186th: 1983: Washington, D.C.) IV. Series.

TP1150.R44 1984 668.4'12 84-24560
ISBN 0-8412-0888-3

Copyright © 1985

American Chemical Society

All Rights Reserved. The appearance of the code at the bottom of the first page of each chapter in this volume indicates the copyright owner's consent that reprographic copies of the chapter may be made for personal or internal use or for the personal or internal use of specific clients. This consent is given on the condition, however, that the copier pay the stated per copy fee through the Copyright Clearance Center, Inc., 21 Congress Street, Salem, MA 01970, for copying beyond that permitted by Sections 107 or 108 of the U.S. Copyright Law. This consent does not extend to copying or transmission by any means—graphic or electronic—for any other purpose, such as for general distribution, for advertising or promotional purposes, for creating a new collective work, for resale, or for information storage and retrieval systems. The copying fee for each chapter is indicated in the code at the bottom of the first page of the chapter.

The citation of trade names and/or names of manufacturers in this publication is not to be construed as an endorsement or as approval by ACS of the commercial products or services referenced herein; nor should the mere reference herein to any drawing, specification, chemical process, or other data be regarded as a license or as a conveyance of any right or permission, to the holder, reader, or any other person or corporation, to manufacture, reproduce, use, or sell any patented invention or copyrighted work that may in any way be related thereto. Registered names, trademarks, etc., used in this publication, even without specific indication thereof, are not to be considered unprotected by law.

PRINTED IN THE UNITED STATES OF AMERICA

**American Chemical
Society Library
1155 16th St. N. W.**

In Reaction Injection Molding; Kresta, Jiri E., ed. ACS Symposium Series; American Chemical Society: Washington, DC, 1985.

ACS Symposium Series

M. Joan Comstock, *Series Editor*

Advisory Board

Robert Baker
U.S. Geological Survey

Martin L. Gorbaty
Exxon Research and Engineering Co.

Roland F. Hirsch
U.S. Department of Energy

Herbert D. Kaesz
University of California—Los Angeles

Rudolph J. Marcus
Office of Naval Research

Vincent D. McGinniss
Battelle Columbus Laboratories

Donald E. Moreland
USDA, Agricultural Research Service

W. H. Norton
J. T. Baker Chemical Company

Robert Ory
USDA, Southern Regional
Research Center

Geoffrey D. Parfitt
Carnegie-Mellon University

James C. Randall
Phillips Petroleum Company

Charles N. Satterfield
Massachusetts Institute of Technology

W. D. Schultz
Oak Ridge National Laboratory

Charles S. Tuesday
General Motors Research Laboratory

Douglas B. Walters
National Institute of
Environmental Health

C. Grant Willson
IBM Research Department

FOREWORD

The ACS SYMPOSIUM SERIES was founded in 1974 to provide a medium for publishing symposia quickly in book form. The format of the Series parallels that of the continuing ADVANCES IN CHEMISTRY SERIES except that in order to save time the papers are not typeset but are reproduced as they are submitted by the authors in camera-ready form. Papers are reviewed under the supervision of the Editors with the assistance of the Series Advisory Board and are selected to maintain the integrity of the symposia; however, verbatim reproductions of previously published papers are not accepted. Both reviews and reports of research are acceptable since symposia may embrace both types of presentation.

PREFACE

THE NEWEST POLYMER PROCESSING METHOD, reaction injection molding (RIM), is based on the injection of monomers or reactive oligomers into a mold, followed by a fast polymerization reaction. The attractiveness of the RIM process is its economics—savings in energy and capital investments—compared to other polymer processing methods. Originally, the RIM technology used principles of urethane chemistry, but recently new nonurethane polymer RIM systems emerged, such as nylons, polyureas, polydicyclopentadienes, polyesters, and epoxies.

The automotive industry's strong interest in the RIM process has been the main thrust behind the development of new RIM systems. The replacement of steel body parts with glass-reinforced RIM panels could significantly decrease the weight of cars and thus improve their fuel economy. Efforts are now concentrated on improving the thermal and mechanical properties plus the dimensional stability of the polymer RIM systems, including improvements in processing aspects such as unmolding, curing, and paint-adhesiveness.

The first part of this book describes future trends of RIM in the United States and compares the economics of RIM and other polymer processing methods.

The second part of the book is devoted to the polymer chemistry and physics of urethane RIM systems. In this section, variables affecting the morphology, structure, properties, and catalysis of urethane RIM systems are discussed.

The new nonurethane RIM systems are covered in the third section, which includes studies on ketene-aminals, nylon polymerization, morphology, and new research trends.

The last part of the book covers the various aspects of RIM technology, such as mold release, glass-fiber reinforcement, mold filling, and new developments in RIM equipment.

Finally, I would like to thank all contributors for their efforts and all ACS editors for their patience and helpfulness in processing the manuscripts.

JIRI E. KRESTA
University of Detroit

September 4, 1984

The Future of RIM in the United States

L. M. ALBERINO¹ and T. R. MCCLELLAN²

¹D. S. Gilmore Research Laboratories, The Upjohn Company, North Haven, CT 06473

²Polymer Chemicals Division, The Upjohn Company, LaPorte, TX 77571

In organizing this presentation the process and material developments that have taken place in the RIM area were considered and the relationship that the market place has had as a driving force to these developments was investigated.

Therefore, in considering the current and future market figures in the RIM area, an attempt has been made to relate these to further process and material developments.

This paper is organized into three parts:
FIRST: Predicted RIM usage figures and other market information.
SECOND: Recent and future material developments for RIM processable systems.
THIRD: Process developments - including equipment developments and RIM process R & D which is leading to a better understanding of the RIM process.

With various modifications to handle RRIM, and with further modifications to be discussed later to handle solid components, the RIM process consists of (1) high pressure metering, (2) impingement mixing, and (3) a self-cleaning mix head.

It should be remembered throughout the discussions in this paper that RIM is a process and not a material.

In looking at market figures and projections for future volumes, three (3) facts emerge.

(1) The automotive market is currently the largest area of use

0097-6156/85/0270-0003\$06.00/0
© 1985 American Chemical Society

for RIM products and will continue to dominate in total volume for the next 5 years.

(2) Industrial consumer applications (sometimes called non-automotive) are predicted to grow at a faster annual rate than automotive areas - but they are starting from a much smaller base. (3) Market figures from different sources generally do not agree with each other. Agreement usually is fairly close in the automotive area and much further apart in the industrial consumer areas probably because the industrial consumer segment is dealing from a smaller base with many more varied and newer applications whose future is more difficult to project.

Some recent market figures (1) for the automotive area are shown in Table I.

TABLE I. AUTOMOTIVE RIM AND RRIM (1)

	Million Pounds	
	1982 Model Year	1984 Model Year
RIM ELASTOMERS	32	53
RRIM	0.1	8.6
INTERIOR TRIM FOAM	13 to 15	17 to 19

These figures are for domestic passenger car production. The figures for Elastomer in automotive are primarily fascia. RRIM is high modulus glass filled material and in the future includes reinforced fascia. Interior trim foam figures are for those made via RIM.

Other sources have listed the automotive RIM market at approximately 41 MM lbs. in 1982 (BCC) growing to nearly 95 MM lbs. in 1987, while still another study reports ~ 59 MM for automotive elastomers in 1982 -(Plastics Technology). This last figure of 59 MM lbs. includes application in buses, trucks, and recreational vehicles. Table II gives data for industrial consumer products. The types of applications in these areas have been discussed previously (2) but include such markets as electronic cabinetry, recreational, shoes, agricultural and various appliances.

TABLE II. INDUSTRIAL CONSUMER RIM MARKETS (1)

	<u>Million Pounds</u>	
	1982	1985
ELASTOMERS	1	5
URETHANE STRUCTURAL FOAM	6 to 9	12 to 15

Other sources have put the INDUSTRIAL CONSUMER elastomer figures for 1982 at 7 MM lbs. and figures for 1987 as high as 200 MM lbs. have been mentioned.

All the market figures, however, predict further strong growth in the RIM area well above the growth figures for other processes.

An indication of further growth are figures for RIM equipment, as shown in Table III. These figures are for actual high pressure units (not-self contained molds). Taken in conjunction with the volumes all the above figures indicate strong market forces to fuel further developments in the area of materials and process research.

TABLE III. RIM EQUIPMENT

<u>NUMBER OF RIM MACHINES IN PLACE</u>		
<u>1982</u>	<u>1984</u>	<u>1987</u>
400	475	700

In reviewing the material developments, we chose to look at the types of materials from a polymer physics or engineering point of view. Historically, the major growth in RIM has been with urethane segmented block copolymers. Specifically, because of the automotive applications these have been elastomers with approximately 50% hard segment levels. Hard segments (3) are the reaction product of the isocyanates and the extender (such as ethylene glycol or 1,4 BDO). Continued growth is seen in this area - whether the extender is a glycol or amine - with most of the growth for this type of elastomer being in automotive applications. However, other ranges of hard segment levels for

urethanes as well as non-urethane are emerging in new applications for automotive as well as non-automotive.

Therefore, as a means of organizing materials by structure and morphology, rather than strictly by application, the discussion on materials development has been divided into three groups:

Group 1: Hard segment levels < 50%. This group includes engineering rubbers (high performance elastomers) and would include some automotive fascia.

Group 2: Elastomers/elastoplastics: 50 - 60% hard segment.

Group 3: Plastics: > 65% hard segment.

Part of the reason for doing this is because these types of materials generally are processed somewhat differently, in formulating the polymers emphasis is given to different parameters, and in general, the overall markets are in different application areas.

Table IV shows a breakdown by hard segment level for these different materials - mainly for isocyanate based polyurethanes and polyurea urethanes .

Table V shows general features of Engineering Rubbers (high performance elastomers) produced via RIM.

These are materials which would have outstanding dynamic mechanical properties allowing them to be used in applications which demand excellent fatigue resistance and minimum heat build-up with cycling.

The market figures also include some elastomers which would not qualify for the above definition -however, they are included in this group because of the hard segment level.

Historically, the lower modulus (~ 90A, 30-40% hard segment) end of the market has been served by cast urethanes - especially the amine cured prepolymer types.

This area is expected to see further growth for RIM, part of which will come at the expense of cast systems (4). Many new formulations with improved properties will become possible through the use of "HOT RIM" equipment which will allow low melting solid isocyanate MDI prepolymers to be used along with low melting solid polyols in the "B" side.

Going up somewhat in hard segment content to the 50-60% range affords (at least in polyurethane or urea-urethane RIM) the elastomers and 'elastoplastics', or perhaps a better word than elastoplastics would be toughened plastics.

Table VI contains the general properties for 50-60% HARD SEGMENT polymers. This table contains polymers which have been developed in the past such as the Polyurethanes in the 55 to 65 Shore D hardness (Fascia materials), as well as Poly(urea-urethanes) which are more recent developments. This hard segment range also covers 65 to 75D intermediate modulus materials which are in reality toughened plastics. The raw materials prices are for comparison purposes.

Tables VII and VIII summarize present and future RIM engineering plastic developments. This is an emerging area for RIM processable materials part of which will be made possible by recent equipment developments such as hot RIM .Polyurethane materials which now exist in this hard segment range are plastics

TABLE IV. RIM (SEGMENTED) POLYURETHANE VOLUMES

% HARD SEGMENT	Million Pounds	
	1982	1987
LESS THAN 50	44.5	66.8
50 to 60	33.9	89.8
GREATER THAN 65	0.30	3.2

TABLE V. ENGINEERING RUBBERS (HIGH PERFORMANCE ELASTOMERS) PRODUCED VIA RIM

	Polyurethane	Poly(urea- urethane)
SHORE A RANGE	40 to 95	40 to 95
T _G , °C	- 70 to -20	-70 to -20
RESILIENCE (Rebound,%)	20 to 70	40 to 70
100% TENSILE MODULUS,psi	200 to 1200	200 to 1200
DIE "C" TEAR,pLi	100 to 450	100 to 450
USE TEMPERATURE LIMIT,°C	120	140*
R.M. COST, \$/lb.	0.80 to 1.60	1.00 to 1.80

*Flutter Modulus - Temperature Profile

TABLE VI. ELASTOMERS/ELASTOPLASTICS (50 to 60% HARD SEGMENTS)

	Polyurethane	Polyurethane	Poly(urea- urethane)
SHORE D RANGE	55 to 65	65 to 75	55 to 65
FLEXURAL MODULUS,psi	25 to 50,000	50 to 100,000	25 to 50,000
FLEXURAL MODULUS RATIO(-30°C/70°C)	4.5 to 5.5	4 to 5	3.5
AUTOMOTIVE HEAT SAG 4", 1 hr.,120°C	0.3 to 0.4	0.2	0.2 to 0.4
NOTCHED IZOD,ft-lb/In	---	10 to 20	---
APPROXIMATE R.M. COST \$/lb.	0.8 to 1.00	0.80 to 1.00	1.00 to 1.10

TABLE VII. ENGINEERING PLASTICS (> 65% HARD SEGMENT)

	Polyurethane	Poly(urethane- Isocyanurate)	Epoxy
SHORE D HARDNESS	75	75 to 80	—
FLEXURAL MODULUS, psi	200,000	250,000 to 330,000	374,000 to 415,000
HDT, °C at 264 psi	90 to 100	150	64 to 102
NOTCHED IZOD, ft-lb./In	0.5 to 1.0	0.5 to 1.0	< 0.5
APPROXIMATE COST, \$/lb.	0.80 to 1.00	0.80 to 1.00	1.20 to 2.65
COMMENTS	Needs Post Cure (Annealing)	Needs Rein- forcement For High Impact	Needs Rein- forcement For High Impact

TABLE VIII. ENGINEERING PLASTICS (> 65% HARD SEGMENT)

	Polyester	Nylon 6 Type	Polyamide Type (Enamine)
SHORE D HARDNESS	High	70	72
FLEXURAL MODULUS, psi	High	196,000	182,000
HDT, °C at 264 psi	—	73	Heat Sag 325 F., 1/2 Hr. 0.23 in.
NOTCHED IZOD, ft-lb./In.	—	9.8	LT 1.0
APPROXIMATE COST \$/lb.	0.85	1.60	—
COMMENTS	Contains Styrene	Moisture Sensitive Catalyst and Special Equipment	—

with similar mechanical properties to toughened styrene and high impact ABS (5).

The urethane modified Isocyanurate material can be processed on present equipment. This material has very high modulus and very high HDT (6) with has fast demold characteristics. Unfortunately it also has low impact and needs long fiber reinforcement for good impact. Epoxy RIM materials (7,8) also would have high modulus and low impact and therefore would need long fiber reinforcement. Currently undergoing development are Polyester materials (Table VIII). Cost may be its best property (7). The nylon 6 type of material has received greatest attention in terms of commercial interest (10). However this type of material needs special equipment, has a catalyst system which is sensitive to moisture, as well as the polymer itself being moisture sensitive. It does offer outstanding impact/thermal properties.

The enamine type of material was presented several years ago (11). As it exists now there are problems with impact. It is however an indication of the continuing research effort being made in the RIM area by evaluating new materials.

A further example of the new materials research being done on RIM processable polymers are the high modulus urethane-epoxy IPN's, shown in Table IX (12). These materials are shown compared to a toughened plastic polyurethane: 146,000 psi flexural modulus urethane material. The urethane-epoxy IPN's are based on two epoxies (Bisphenol A type and Novalak type). Process developments in the RIM area have involved equipment developments, RIM Process R & D and some aspects of reinforced vs filled RIM.

Since some of the emerging non-urethane based RIM materials development technology involves specialized equipment, it would be instructive to briefly compare some of the differences in processing especially since RIM is a process and not a material. Table X shows some of these basic differences between current RIM technology and recent Hot RIM candidates. Besides the obvious differences,

- . urethane processing demands exact stoichiometry
- . current new candidates such as Nylon 6 or polyesters have no exact stoichiometry.

Only the urethane modified isocyanurates which can be processed on current RIM equipment have no exact stoichiometry.

Many current urethane components when mixed together are incompatible and therefore need very intensive mixing in the mixhead. In addition, aftermixers and other aspects of tool design can be very critical in order to insure proper mixing. Some of the new candidates appear to be more compatible in their reaction profile. Thus one should use caution when judging processing of 'urethane' type systems on equipment designed specifically for other polymers -RIM still is intensive mixing.

Historically, many new polymer technologies have developed through experimental means such as applications and product development. Such is the case also with RIM. Only fairly recently has process research been performed on the RIM process which has led to a more fundamental understanding of the process as a whole. RIM process research has been divided into three

TABLE IX. HIGH MODULUS URETHANE-EPOXY IPN'S

	Urethane	Urethane BPA Epoxy	Urethane Novalak Epoxy
30:70 Diol:Polyol	50.4	40.3	40.3
Isonate ^R 191 (1)	49.5	39.6	39.6
Epoxy	—	20.0	20.0
Hardness Shore D	78	65	83
Flexural Modulus, psi	145,000	231,000	244,000
Izod Notched Impact ft-lb/In	6.0	5.0	—
Elongation at Break	30	20	10

TABLE X. BASIC DIFFERENCES BETWEEN CURRENT RIM TECHNOLOGY AND RECENT "HOT RIM" CANDIDATES

OBVIOUS DIFFERENCES SUCH AS:

- Solid Components
- High Mold Temperatures
- Heat Traced Lines and Pumps
- Slower Cycle Times

OTHER DIFFERENCES

- Urethane Processing Demands Exact Stoichiometry
- Current New Candidates have no exact Stoichiometry or are much less sensitive to stoichiometry
- Many urethane components are incompatible and need very intensive mixing
- Current new candidates are more "compatible" and mix easier —may not need an aftermixer

"unit" operations; (1) the mixing process, (2) Reaction kinetics and heat transfer modeled for the RIM process, and (3) mold filling studies.

Figure 1 summarizes impingement mixing in the RIM process as described by Macosko and coworkers (13). The "quality" of mixing is improved by making the striation thickness small enough so that diffusion occurs rapidly. The mixing quality was found to correlate with the Reynolds Number (N_{RE}). Good mixing occurred for N_{RE} of 200. As more information of this nature is gained on the mixing process, a better understanding of the relationship between material mixed in the mix head to material exiting the after mixer will result.

Understanding the reaction and heat transfer processes in the RIM Process has led to models which can predict temperatures in a RIM molded part and through kinetics the monomer conversions can be measured as a function of in mold dwell times. Temperature profiles at various depths in the molded part can be predicted and correlated with processing and properties (14). Information such as this should aid the designers of parts molded in the RIM process by allowing them to account for the effect of different temperatures in the molded item due to thickness differences - affects such as too high exotherm temperature causing blistering and polymer degradation, stresses due to thermal effects, too rapid crystallization - or no crystallization due to temperature extremes.

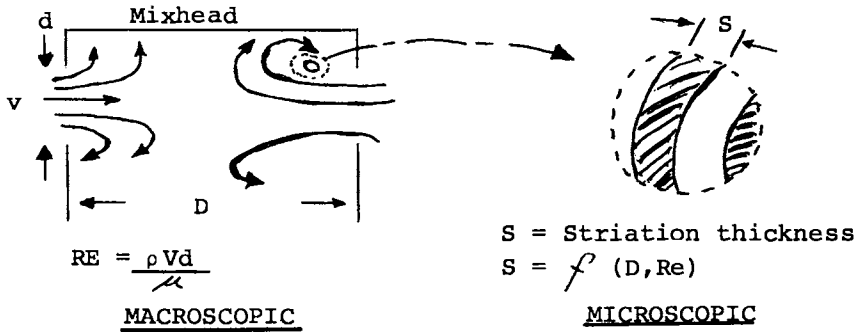
The third "unit operation" process currently under study in RIM is the mold filling process (15). Measuring the pressure drop in the mold filling step allows the calculation of the viscosity. Two cases exist; that where viscosity is constant (little or no reaction) and the case where viscosity is a function of temperature and conversion. The latter case requires a numerical solution to determine the viscosity. The type of information that can be gained from these studies is directly relatable to how well a material will RIM process in a tool -again this type of information should aid in tool design.

An area of RIM which very rapidly advanced through machinery and equipment developments is the so called REINFORCED RIM or (RRIM) technology now an accepted and proven commercial process after only several years of intense machine development (16). The kinds of solid additives which in reality can be processed on RRIM equipment are fillers not reinforcing agents, due to their low aspect ratio.

The RIM process as it now stands, either as RIM or RRIM puts limitations on the type of material that could advantageously be used in the process. One must use a material with a certain level of toughness in order to obtain useful structural parts.

Table XI demonstrates the effect of fiber length on properties for a type of RIM processable material - the urethane modified isocyanurate which has low impact. Table XI compares milled glass fibers with 1/8" chopped strand. The longer aspect length chopped strand provides for true reinforcement. However, it cannot be used in current RRIM equipment.

The use of long fibers - such as in continuous strand mat (RIM Mat Molded) affords composite material with potentially



○ TYPICAL URETHANE SYSTEM WITH ~ 6 SEC GEL,

RE ≈ 200
critical

RE < 200 ⇒ Diffusion control of reaction rate.

RE > 200 ⇒ Kinetic control of reaction rate.

○ IN A DIFFUSION CONTROLLED SYSTEM, THE FASTER THE GEL TIME, THE BETTER THE MIXING MUST BE.

BETTER MIXING → SMALL STRIATION THICKNESS → FASTER DIFFUSION

Figure 1. Impingement mixing in the RIM process (13).

TABLE XI. EFFECT OF GLASS FIBER LENGTH ON IMPACT STRENGTH

	Unfilled	15% Glass
A. Milled Glass Fiber (RIM; Admiral)		
Izod	1.2	0.5
Gardner	0.8	0.3
B. 18" Chopped Strand (Compression Molded)		
Izod	0.5	1.8
Gardner	0.3	0.2
C. Continuous Strand Mad (RIM; DSG-395-12)		
Izod	0.4	9.4
Gardner	0.3	1.0

very useful properties. Unsaturated polyester and many epoxies would be in this same situation. Mat molding points up an area of future R & D using the RIM process. RIM mat molding - a kind of RIM process - while still in the early stages of development may hold the promise of providing SMC like materials through the RIM process. Table XII further illustrates some of the properties achievable with this technique.

Other developments for RIM in the future include Internal Mold Release - the successful application of this technology should bring the overall cycle-time for a RIM process down to that of thermoplastic injection molding.

In summary, the future of the Reaction Injection Molding process in the USA definitely appears to be extremely positive. Fueled by growing market awareness and interest, especially in the Industrial Consumer area, new material and process developments should bring forth a variety of new applications. The automotive market for RIM continues to be strong, and for the near term will be the major driving force for new material developments.

TABLE XII. RIM MAT MOLDING WITH
DSG 395-12 SYSTEM

% GLASS	0	25	33
LAYERS OF MAT	—	2	3
LAYERS OF VEIL	—	2	2
<u>PROPERTIES</u>			
SPECIFIC GRAVITY	1.16	1.33	1.24
SHORE D	83	85	84
FLEXURAL STRENGTH,psi	9,300	16,500	23,300
FLEXURAL MODULUS,psi	248,000	610,000	715,000
NOTCHED IZOD,Ft-lb/In.	0.5	7.9	11.0

Literature Cited

1. The Upjohn Co., Polymer Chemicals Div., LaPorte, TX.
2. L. M. Alberino, "Future of RIM Development in the U.S.A. in the 1980's", *Polymer Sci & Tech.* 18, Reaction Injection Molding and Fast Polymerization Reactions, Ed. J. E. Kresta, Plenum Press (NY).
3. R. J. Lockwood and L. M. Alberino, p. 363 "Urethane Chemistry and Applications", K. N. Edwards, ACS SYMPOSIUM SERIES No. 172, American Chemical Society, Washington, D.C., 1981.
4. T. R. McClellan, "The MDI Bridge", Polyurethane Manufacturers Association, San Diego, Nov. 4, 1979.
5. Upjohn Data, D. S. Gilmore Research Labs., North Haven, CT, 06473.
6. P. S. Carleton, D. J. Breidenbach, and L. M. Alberino, 1979 NATEC, SPE(1979), Detroit, MI.
7. Shell Chemical Co., Technical Bulletin 56: 513-81R, W. Saidle and R. L. Mitchell.
8. R. S. Kubiak and R. C. Harper, 1979 NATEC, SPE(1979), Detroit, MI.
9. G. M. Peters, 38th Annual Conference SPI RP/C Proceedings, Feb. 7-11, 1983, Houston, TX.
10. Plastic Technology, p. 22, 28 (9) August 1982.
11. D. F. Regelman and L. M. Alberino, "Organic Coatings and Plastics Chemistry", American Chemical Society, Atlanta, GA (1981).
12. Pearce et al, Organic Coatings and Plastics Chemistry, 45, 279 Aug. 23-28, 1981 (NY).
13. P. Kolodziej, C. W. Macosko, and W. E. Ranz, "The Influence of Impingment Mixing and Stiration Thickness Distribution and Properties in Fast Polyurethane Polymerization". *J. Polymer Eng's and Sci.*, 22 (6) April 1982.
14. N. P. Vespoli and L. M. Alberino, "Computer Modeling of the Heat Transfer Processes and Reaction Kinetics of Urethane Modified Isocyanurate RIM Systems", AIChE Diamond Jubilee Meeting, Washington, D.C. Nov. 1 & 2, 1983.
15. J. M. Castro and C. W. Macosko, "Studies of Mold Filling and Curing in the Reaction Injeotion Molding Process," *AIChEJ.*, 28 No. 2 250 (1982).
16. P. Z. Han, 37th Annual Conference RP/C Institute SPI, Jan. 11-15, 1982, Washington, D.C.

RECEIVED April 30, 1984

Polyurethane RIM: A Competitive Plastic Molding Process

E. T. LLOYD and M. C. CORNELL

The Dow Chemical Company, Freeport, TX 77541

Extensive use of flexible polyurethane fascia on automobiles has established RIM (Reaction Injection Molding) as a viable plastic molding process. Improvements in this process are continuously occurring which increase productivity, versatility, and the competitive economics of RIM versus other plastic molding techniques such as compression molding or thermoplastic injection molding. This paper examines the relative economics of state-of-the-art RIM versus these other molding techniques to make large, complex parts. Factors considered include productivity, raw material consumption and cost, process energy, tooling, fixturing, hourly labor and capital. Developments in RIM technology such as internal mold release promises to further increase the attractiveness of the RIM process.

The growth of reaction injection molding (RIM) has been quite dramatic since the commercialization of this process in the mid-1970's. Forecasts by Dow and others indicate that this growth rate will continue over the next several years due to emerging new applications, both within and outside the transportation industry. Certainly, a primary reason for this growth stems from the bottom line economic advantage in producing large parts via the RIM process versus other plastic fabrication techniques.

This economic advantage results from the attributes of the RIM process, which include simple, fast mixing of highly reactive liquid components and the elimination of a messy and time consuming solvent flush between shots which is common with mechanical mixing dispensing equipment. Because the tool is filled with liquid monomers, RIM allows the production of both large and complex shapes using lightweight and/or lower cost clamping presses and molds; thus saving on capital.

Although polyurethane has been the principle polymer commercialized in the RIM process, modified polyurethane and

0097-6156/85/0270-0015\$06.00/0
© 1985 American Chemical Society

non-polyurethane RIM systems are rapidly moving toward commercialization.

Polyurethane RIM (PU-RIM) was selected for the initial RIM application of automotive fascia not only because it provides the required damage resistance and other performance requirements, but also because the reactivity of the urethane raw materials, isocyanate and polyol, provide acceptable productivity. Because the urethane monomers can be nucleated, high quality sink free surfaces that are suitable for automotive exteriors are produced at the time of demold. Little, if any, post mold surface repair is needed in preparation for painting the RIM part.

PU-RIM is most advantageous in molding large, complex parts where surface quality and damage resistance are important, i.e. automotive fascia and nonstructural body panels. It is also a more efficient process than casting for molding smaller sized but large volume elastomeric items such as shoe soles, beer barrel skirts and window gaskets.

This paper will explore the effect of these attributes toward making the RIM process competitive with other plastic molding techniques. It will also illustrate the impact that pending developments in RIM technology, such as internal mold releasing systems, will have in making PU-RIM even more economically viable.

For this case study, a vertical body panel such as that being molded of glass reinforced polyurethane-RIM (PU-RRIM) for the Pontiac Fiero fenders and door panels was chosen. The average projected surface area for a typical fender and door panel is about 750 sq. in. and 1,000 sq. in. respectively. The fender was selected for this study.

A body panel was chosen as our target application because major plastic molding techniques: RIM, compression molding and injection molding can be used to fabricate these parts. With the appropriate polymer system all three processes can be used to mold parts which essentially meet performance requirements. For RIM the chosen standard is the typical glass filled polyurethane system now being used. Injection molding is represented by a polycarbonate-polybutyleneterephthalate blend (PC alloy). For compression molding, a low profile SMC composition is our standard. Typical compositions of these plastics are shown in "Table I".

Table I. Typical Material Compositions, (%)

PU-RRIM	- Polyol	27.9	- Isocyanate/MDI Based	43.6
	- Ethylene Glycol	8.4	- Fiberglass	20.0
	- Catalyst	0.1		
PC ALLOY	- Bis A/Phosgene Polycarbonate			42
	- Polybutyleneterephthalate Polyester			53
	- Polybutadiene			4
SMC	- Polyester Resin	19	- Magnesium Oxide	2
	- Calcium Carbonate	35	- Styrene	1.7
	- Glass Fiber	30	- Zinc Stearate	1
	- Low Profile Agent	7	- Catalyst	.3
	- Polyethylene	4		

Performance requirements for other large plastic parts like fascia, hoods, and deck lids would most likely eliminate one or another of these polymers and/or molding processes from consideration. For example, SMC is not considered to have sufficient impact resistance for fascia; and RIM and engineering thermoplastic materials have yet to be developed for structural applications which also require a high surface quality, i.e. hoods and deck lids. These other parts were thus not chosen for this study.

As in any economic study certain assumptions must be made. It is not the intent of this paper to analyze cost factors in fine detail, but rather to examine and compare the major direct cost contributors in molding large plastic parts by these major process techniques. These direct cost factors are productivity, raw materials, process energy, tooling, fixturing, hourly labor and capital. Indirect costs that are based on these direct cost items are not considered in this study. Such indirect items include supervision, maintenance, general plant overhead, insurance, taxes and building depreciation.

In addition to Dow's own technology base in RIM, injection molding and compression molding, the data in this study was developed from literature references and from consultation with authorities in the automotive industry, material suppliers and equipment manufacturers.

Assumptions

It is assumed that the body panel will be made in an existing facility of a medium sized molder having state-of-the-art equipment. For RIM, a typical plant was deemed to have twelve clamps with one metering unit and glass dispersion unit servicing four clamps. Such RIM plants are indeed typical of the industry. The comparable output for a SMC operation would employ 13 clamp units. A comparable output in an injection molding operation would require seven large extruders of at least 2,500 ton clamping capacity. While very few injection molders in North America have this capability, a seven unit injection molding line was assumed for this study. These "typical" operations were determined as a basis for spreading direct capital items, such as bulk handling and storage systems, which were common to the entire plant.

The plants are assumed to be operating at capacity, making the fullest utilization of capital over a 48 week/year production schedule operating three shifts/day and five days/week (annual operating hours @ 5,760). A minimal amount of production overtime to meet demand was assumed if this was cost effective versus purchasing additional tooling. Labor was calculated at \$20.00/hour over 52 weeks.

A demand of 200,000 of these 750 square inch body panels was assumed for a model year. Costs for painting are assumed to be constant and are not considered in this study. Rather costs are calculated to produce the body panel ready for the painting operation, including any surface preparation and repair that might be required.

Direct Cost Factors

Productivity

Productivity factors are shown in "Table II". With today's technology, it is possible to operate both SMC and injection molding clamps during an entire shift. However, because RIM requires frequent application of an external mold release, approximately one hour per shift is required to perform both major and minor cleaning of the tool. Thus for RIM, only an 87.5% process efficiency was assumed.

Table II. Productivity (200,000 Parts/Year)

	SMC	PC ALLOY	PU-RRIM
Scrap Rate, %	3	3	2
Production Demand, M	206	206	204
Cavities/Mold	1	1	1
Cycle Time, Sec.	150	90	120
Annual Capacity, M	138.2	230.4	172.8
Efficiency, %			
: Process	100	100	87.5
: Operating	80	80	80
Clamp Output, M	110.6	184.3	121.0
Clamps/Production Demand	1.86	1.12	1.69
Molds	2	1	2

Operating inefficiencies of 20% are assumed by the automotive industry due to maintenance, tool changes, absenteeism, and other unscheduled interruptions.

Clamp output is defined as the annual clamp capacity less both process and operating inefficiencies. The clamps required to meet production demand is the ratio of production demand/clamp output. This relationship is used in determining fixed cost such as tooling, fixturing, hourly labor, and plant capital.

Raw Material Costs

Data summarizing raw material usage and cost development is provided in "Table III". Raw material usage is based upon part weight, material waste, and production demand. Today, body panels of PU-RRIM and PC alloy are molded at thicknesses of .125 inch. Due to the higher flexural modulus of SMC, such parts are molded with the thickness reduced to .100 inch. Thickness reductions are projected for all materials, however such speculative material use reduction measures were not considered.

Waste material can be generated either as raw material loss, part trimmings or defective parts. In the case of PC alloy, the waste generated from trimming (approximately 10% of injection weight) and defective parts (approximately 3%) is recoverable via grinding and reprocessing. Recoverable waste was thus not considered as a factor when evaluating PC alloy material usage.

Table III. Raw Materials

	SMC	PC ALLOY	PU-RRIM
Thickness, in.	.100	.125	.125
Specific Gravity	1.80	1.22	1.14
Part Wt. (750 in ²), lbs	4.88	4.13	3.86
Waste			
: Raw Material, %	4	Recoverable	--
: Trim/Part, lbs	--		.57
: Defective Parts, %	3		2
Material/Part, lbs	5.23	4.13	4.52
Material/200,000 Units	1046	826	904
Cost/lb, \$	0.90	1.60	1.02
Material Cost/Year, M\$	941	1322	922
Mold Release, M\$	--	--	40
Total	941	1322	962

Trim waste (aftermixer, runner, gate, and flash) accounts for 10-15% of the injection weight for PU-RRIM, and along with defective parts (2%), produce non-recoverable material which must be reflected in total material usage.

Trim losses are negligible for SMC. Nonrecoverable raw material loss associated with prepreg fabrication and defective parts due mainly to poor material flow contributes about 4% and 3% respectively to the total material usage for this molding process.

Material cost is derived from published list price. In the case of SMC, it is assumed that a molder of this size will purchase prepreg at \$.90/lb rather than compound SMC from basic ingredients.

External mold release is a raw material consideration for only PU-RRIM and is estimated to contribute \$0.20 to the overall part cost.

Process Energy

A comparison of energy cost for SMC, PC alloy, and PU-RRIM is shown in "Table IV". RIM compares favorably with the other process technologies. Process energy for liquid molding systems are typically lower than for injection molding systems, due primarily to reduce process temperatures. The monomers for PU-RRIM are commonly held slightly above room temperature (37°C) while mold temperatures run 70°C. These same process parameters for injection molding are typically 300°C and 180°C respectively. Energy consumption in compression molding falls between these extremes.

Table IV. Process Energy

	SMC	PC ALLOY	PU-RRIM
Component Temperature, °C	23	300	37
Mold Temperature, °C	170	180	70
Process Energy/lb, M BTU	18.6	39.0	16.6
Material/Year, M lbs	1006	851	904
Energy Cost @ \$0.575/KWH, M\$	315	559	253

Process energy for SMC, PC alloy, and PU-RRIM is reported to be 18.6M, 39.0M, and 16.6M BTU/lb.(1) The utility (electrical) rate for primary (custom or captive molder) customers in the Detroit area is reported at \$.0575/kilowatt-hour.(2)

Tooling/Fixtures

The evaluation of tooling and fixturing costs is summarized in "Table V". These materials are depreciated over 1-2 years (1 year in this study) because of the frequent engineering and styling changes of the part. This cost is therefore differentiated from capital cost.

Table V. Tools and Fixtures

	SMC	PC ALLOY	PU-RRIM
Tools	2	1	2
Cost/Tool M\$	300	250	225
Tool Cost, M\$	600	250	450
Fixtures, M\$	---	---	75
Total, M\$	600	250	525

Lower productivity of SMC and PU-RRIM is evidenced by the need for two tools to meet specified production demands of this study. It was assumed that overtime would be used rather than purchasing a second tool for PC alloy.

Full part support during post cure, prime and topcoat bake required for PU-RRIM adds an additional fixed cost to this process. These support fixtures typically range from \$200 - \$500 each. The price used in this study is \$350/fixture. Assuming fixture turnaround time of four hours, including part washing; post cure; primer and topcoat, a plant would thus require a number of support fixtures equal to four times the hourly production volume. With a clamp output of 21 parts/hour, a plant operation would require 84 fixtures. In addition, extra fixtures for reworks are needed. It was assumed that 126 fixtures would be needed by this "typical" plant.

Hourly Labor Cost

"Table VI" summarizes the derivation of hourly labor cost for typical SMC, PC alloy, and RIM operations producing 200,000 units. Manpower requirements are needed for raw materials handling, press operation, part trim, inspection and repair.

SAC manpower is allocated to raw material handling for the fabrication of the preform. Raw material handling in RIM would require manpower to formulate, disperse glass in the polyol component and chemically analyze components and formulated B-sides. Manpower allocated to material handling in an injection molding plant would be negligible.

In compression and injection molding operations the press operator demolds and trims the part. This same operator in a RIM

plant demolds the part, picks any flash left in the mold and applies the external release agent. This operator is normally accompanied by a full time assistant whose responsibilities include flash removal, void treatment and inspection of the part in preparation for painting.

Table VI. Hourly Labor

	SMC	PC ALLOY	PU-RRIM
Men/Press			
: Raw Material Handling	1.0	--	0.2
: Press Operation	1.0	1.0	1.0
: Trim	--	--	1.0
: Inspect/Repair	2.0	--	0.3
Presses	1.86	1.12	1.69
Men/Shift	7.44	1.12	4.23
Labor @ \$20/Hr, M\$	930	140	530

SMC typically requires post mold rework to provide a Class A surface. Consequently, additional manpower is allocated for inspection and repair for SMC to fill and sand the parts in preparation for painting. Some manpower is allocated for minor repair of PU-RRIM parts. The inspect/reject function in an injection molding operation is normally handled by the clamp operator.

Capital

"Table VII" summarizes the cost of process equipment and associated raw material handling equipment required to process SMC, PC alloy and PU-RRIM. A range of prices as well as an average price is indicated. For the purpose of this study this average price was used.

Table VII. Summary of Estimated Capital, \$M

PROCESS	ITEM	RANGE	AVERAGE
RIM	Material Handling	225 - 435	330
	Glass Dispersion/4 Clamps	100 - 200	150
	Metering Unit/4 Clamps	100 - 200	150
	Clamps	100 - 200	150
Compression Molding	Prepreg Storage & Preform Preparation	---	260
	Clamp	250 - 1500	875
Injection Molding	Material Handling (7 Extruders)	250 - 310	280
	2,500 Ton Extruder/Clamp	800 - 1000	900
	Grinder/3 Extruders	25 - 35	30

"Table VIII" summarizes the capital needs of a production

facility to meet the 200,000 part production demand. The material handling and conditioning costs were amortized over the entire plant operation. Also included are estimated installation costs based on 20% of the capital cost. These fixed costs were depreciated over seven (7) years using a straight line (SL) depreciation schedule.

Table VIII. Capital, \$M

	SMC	PC ALLOY	PU-RRIM
Raw Material Handling	Pre-preg 40	Pellet 40	Liquid/Filter 110
Process Equipment	Clamps 1630	Extruder/Clamp 910	Metering Unit and Clamps 320
Installation @ 20%	330	190	90
Total Capital	2000	1140	520
Depreciation, 7 yrs S.L.	286	163	74

"Table IX" summarizes all of the direct costs considered in this economic model. Analysis of this data indicates that PU-RRIM and PC alloy injection molding are the most economical polymer/processes for our body panel example.

Table IX. Direct Cost, \$M

	SMC	PC ALLOY	PU-RRIM	IMR PU-RRIM	PU-RRIM
Raw Material	941	1322	962	922	801
Process Energy	315	559	253	250	247
Tools/Fixtures	600	250	525	335	335
Hourly Labor	930	140	530	360	360
Capital	286	163	74	44	44
Total	3072	2434	2344	1911	1787
\$/Part	15.36	12.17	11.72	9.55	8.93

New Rim Technology

Examination of the economic data indicates several specific areas where PU-RRIM is penalized, among them are: long cycle time, process inefficiency (down time for mold clean), scrap, and the need for external mold release. These factors result in higher labor, unit capital and tooling costs for PU-RRIM when compared to injection molding. This situation provides a challenge to make PU-RRIM more economically viable.

Because of these limitations, the RIM industry has put a high priority on the development of an effective mold release agent which can be incorporated in the raw material component streams. An ideal RIM internal mold release (IMR) would essentially eliminate both the need to treat the tool between shots and mold

cleaning down time. This IMR should show no deterioration of component stability or other processing parameters, and not alter the physical properties of the polyurethane polymer. In particular, a RIM IMR must not interfere with the painting process nor be detrimental to paint adhesion or paint weathering characteristics.

Such RIM IMR technology has been developed by Dow and is in the final stages of production qualification at major RIM molders. While the details of this technology are beyond the scope of this paper, the impact of an effective IMR on RIM economics can be addressed. This data is shown on "Table X", where one can see cycle times reduced from 120 seconds to 90 seconds; the elimination of nonproductive mold cleaning time; and the elimination of scrap resulting from external mold release buildup. The reduction in part cost is significant; the unit cost for the body panel is reduced from \$11.72 to \$9.55 for an 18.5% production cost reduction.

Table X. RRIM IMR

-- Increase Press Output	121 M	--->	176.9 M
- Cycle Time	120 Sec	--->	90 Sec
- Process Efficiency	87.5 %	--->	96 %
- Defective Parts	2 %	--->	1 %
-- Reduce Capital			
- Clamps	1.69	--->	1.14
-- Reduce Tooling	2	--->	1
-- Reduce Labor	4.23 Men	--->	2.85 Men
-- Elimination of EMR	< \$0.20/Part >		

In addition to IMR, another area offering economic improvement for PU-RRIM is the reduction in raw material cost via incorporation of less expensive fillers. Today, PU-RRIM body panels use 20% milled or flaked fiberglass at \$.93/lb. Alternative fillers are available at a much reduced price. For example, development work incorporating an industrial mineral fiber, wollastinite, has shown some promise. The list price for wollastinite is \$.25/lb. Raw material cost, on a per pound basis by substituting wollastinite for fiberglass is a reduction from \$1.02 to \$.84. The overall economic impact from both IMR and wollastinite is a per part manufacturing cost reduction to \$8.93, and additional 5.3% over systems containing IMR alone, and a 23.8% improvement from today's technology.

A summary of the economic impact of IMR and less expensive filler (wollastinite) on the direct cost of manufacturing PU-RRIM body panels considered in this study is found in "Table IX".

In conclusion, it has been demonstrated that existing PU-RRIM technology offers a good balance of economics, processing and performance. The pending utilization of internal mold release will further enhance the attractiveness of the PU-RIM process. RIM technology is favored when the application requires large parts with complex shapes, Class A surface, and damage resistance. The

model presented here can be utilized to evaluate the economic impact of both material modification and process improvements in molding large RIM articles such as body panels and fascia.

Literature Cited

1. Plastic Parts by Reactive Processing - "A Technology for the Future", William L. Kelley, SAE Technical Paper Series - 820419.
2. Phone conversation with Detroit Edison.

RECEIVED September 28, 1984

Phase Separation Studies in RIM Polyurethanes Catalyst and Hard Segment Crystallinity Effects

R. E. CAMARGO¹, C. W. MACOSKO, M. TIRRELL, and S. T. WELLINGHOFF

Department of Chemical Engineering and Materials Science, University of Minnesota,
Minneapolis, MN 55455

Production of polyurethane elastomers by reaction injection molding, RIM, is now a well established technique. Since RIM involves a fast exothermic polymerization, the development of structure and properties in the materials thus produced is constrained by processing and polymerization conditions. The particular properties of polyurethane elastomers derive to a large extent from phase separation into hard, crystalline or glassy regions that reinforce and the soft rubbery phase. Figure 1 gives a simplified representation of such a microstructure. The hard segments are composed of sequences of a diisocyanate reacted with a short chain diol or diamine, the extender. In the particular instance of Figure 1, the hard segments are shown as crystalline, but they can also be amorphous. The soft segments are composed primarily of a long chain diol or triol (equivalent weight of 1000 or greater), and also of diisocyanate-extender sequences scattered throughout the matrix.

Major factors affecting the final properties of the polymer are the composition and the degree of order within each phase, and the topology or connectivity of the microphase structure, i.e. sharpness of the domain boundaries and mixing of the phases.

Several studies have been published in recent years on the properties of RIM polyurethanes and polyurethane-ureas (1-7). Unlike most studies, however, we have restricted our attention to simplified linear systems in order to establish the effect of reaction rates and mold temperatures on the phase separation and molecular weight of segmented polyurethane elastomers produced by RIM(6).

In our earlier work, we prepared rapidly polymerized samples with high molecular weight and finely dispersed hard and soft phases of low hard segment crystallinity. A high temperature dependency of the storage modulus was characteristic of this structure. At low reaction rates the polymerization proceeded almost isothermally at large undercooling. Incompletely reacted, low molecular weight, oligomers of high hard segment content phase separated into large spherulitic structures, between which was isolated material of rather low fracture strength. Evidently, early formation of hard segment

¹Current address: Raychem Corporation, Corporate Technology, Menlo Park, CA 94025.

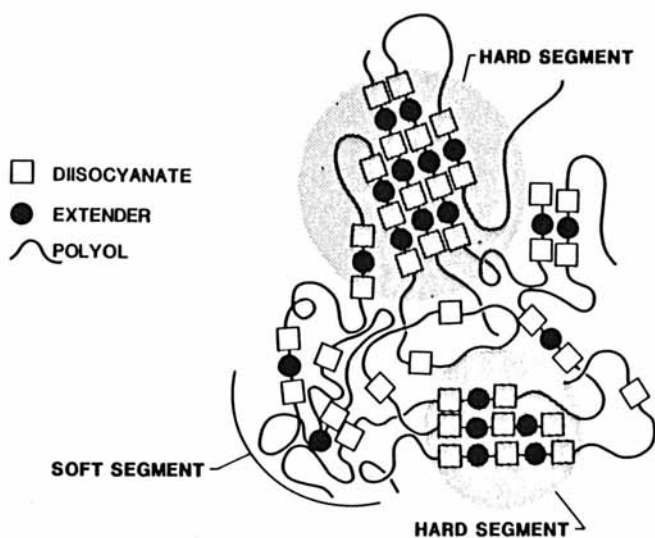


Figure 1. Schematic representation of the segmented micro structure in a semicrystalline polyurethane block copolymer.

crystallites, can remove unreacted isocyanate groups from solution preventing further reaction with the polyol (6-8).

Scope of the Present Works

We have extended the previous experiments(6) to a wider spectrum of catalyst concentrations, at hard segment levels typical of those used in the production of RIM fascia automobile parts (ea. 45-50% hard segment). As in our previous work,(6) only difunctional reactants at matched stoichiometries of the reactants have been used. This ensures linear, soluble polymers and allows molecular weight characterization.

To study the role of hard segment crystallizability, two series of polymers were prepared from special reactants as described in the experimental section. In addition some comparative results have been obtained by varying the molecular weight of the polyols used.

Experimental

Materials. The polyurethanes used are based on polypropylene oxide diol, capped with a certain amount of polyethylene oxide to provide high primary hydroxy content, and thus high reactivity. The main characteristics of the polyols are listed in Table I. Crystallizable hard segments were made from 4,4'-diphenylmethane diisocyanate, MDI (Rubinate 44, Rubicon Chemicals) and 1,4-butanediol, BDO (GAF Chemicals) or 1,2-ethanediol, EDO (ethylene glycol, Fisher Scientific). Amorphous hard segments were obtained using 2,4'-diphenylmethane diisocyanate, 24-MDI (this non-commercial material was kindly provided by Dr. D. Spence from Rubicon Chemicals) and BDO, or 44-MDI and n-methyl-diethanol amine, MDEA (Union Carbide Corp.). In either case hard segment crystallization is inhibited by molecular asymmetry (24-MDI/BDO) or by branching (MDI/MDEA). The catalyst used in all cases was dibutyltin dilaurate, DBTDL (T-12, M. & T. Chemicals).

Sample Identification. Given the number of samples and compositions, a general code was created as explained in Table II. In this table, the polyol type is identified by molecular weight and ethylene oxide content. Thus 40/15 refers to a polyol with $M_n = 4000$ and 15% (w/w) of ethylene oxide end capping agent. The last two labels in Table 2 indicate mold temperature and catalyst content.

Reaction Injection Molding. Molded polymer samples were produced in our laboratory-size RIM machine (9). Details of reactant preparation and molding procedures are found elsewhere (9-10). Briefly, the polyol and extender are blended as received at the desired stoichiometry. Catalyst is added when required and the mixture

*In this paper, the hard segment content is defined as the percent by weight of the isocyanate and extender in the polymer at a fixed stoichiometry or isocyanate index.

Table I. Characteristics of Polyols Used

Commercial Name	Supplier	$M_n^{(1,2)}$	$M_w/M_n^{(3)}$	% (w) EO ⁽²⁾	% Primary OH's ⁽²⁾	ID Code ⁽⁴⁾
Niax 1256 (special)	Union Carbide Corp.	1999	1.11	30.4	83	20/30
Niax E-351	Union Carbide Corp.	2772	1.15	15	75-80	28/15
Thanol E2103	Texaco Chemicals	2306	1.12	25	80	23/25
Poly G 55-28	Olin Corp.	4080	1.20	15	80-85	40/15

(1) Calculated assuming hydroxyl functionality of two
(2) Data from supplier
(3) From GPC measurements
(4) Corresponds to $(M_n/100)/(\%EO)$

Table II. A Sample Identification Code

A) CHEMICAL CODE AND RANGE OF VARIABLES:

ISOCYANATE TYPE	EXTENDER TYPE	POLYOL TYPE	HARD SEGMENT % (1)	MOLD TEMPERATURE °C	CATALYST CONTENT 1000 x % CAT
MDI = M	BDO = B	20/30	48	70	00
	EDO = E	23/25			
	MDEA = M	28/15	to	to	to
24-MDI = 24M		40/15	51	140	75

(1) Defined in text

B) AN EXAMPLE:

M - E - 23/25 - 48 - 70 - 30

M — MDI
 E — EDO
 23/25 — polyol: 23/25
 48 — hard segment: 48%
 70 — mold wall: 70 °C
 30 — catalyst content: 0.03%
 extender: EG
 isocyanate: MDI

subsequently degassed at room temperature for approximately eight hours. The pure MDI is melted and filtered at ca. 50°C immediately before each run. The chemicals are loaded in the machine tanks and blanketed with nitrogen. All lines and tanks are kept at 55 ± 5°C at all times. During the injection cycle, the materials are injected at the rate of ca. 0.1 kg.sec⁻¹ through a recirculating, self-cleansing, impingement mixing head, and into a rectangular, end-gated, teflon-coated mold (125 x 125 x 3 mm), opened and closed by a hydraulic press. Mold temperature is maintained by means of electrical resistances. The mold temperature in most runs was kept at 70°C. After demolding, the polymer plaques were postcured in an oven at 120°C for 1 hour, and aged at room temperature for at least one week prior to analysis.

Dynamic Mechanical Spectroscopy (DMS). Rectangular bars (3 x 12 x 45 mm) were cut from the molded plaques and dynamic mechanical spectra (DMS) obtained using a Rheometrics System-4. Values of G', G'' and tan δ at various temperatures were obtained by oscillatory torsion of the bars at 1 Hz and 0.2% shear strain; temperatures were varied between -100°C and 120°C at 5°C intervals in the transition regions and at 10°C intervals elsewhere. Thermal soak times were five minutes in all cases.

Wide Angle X-Ray Scattering. WAXS data was obtained on 25 x 25 x 3 mm samples; reflected intensity was recorded as a function of scattering angle (2θ) at 1° min⁻¹, with a Siemens D500 diffractometer, using monochromated Cu-λ radiation.

Differential Scanning Calorimetry. DSC scans were made at 20°C min⁻¹ on a Mettler TA3000 system equipped with a DSC-30 low temperature module. Temperature calibration was done with a multiple indium-lead-nickel standard. An indium standard was used for heat flow calibration. Thin shavings (ca. 0.5 mm thick) were cut with a razor blade from the cross-sectional edge of a plaque. These sections contained both surface and center portions.

Gel Permeation Chromatography. A Waters (model 150-C ALC/GPC) liquid chromatograph with a refractive index detector was used for molecular weight characterization. The unit was equipped with two sets of silanized Dupont bimodal columns (Zorbax PSM 60S/100S), with molecular weight range 2 x 10² to 10⁶ and total retention volume of 24 ml. Samples were cut across the plaque thickness as with DSC. Polymer solutions were prepared in N,N'-dimethyl-formamide, DMF, at 0.1% (w/v) and filtered through 0.45 micron nylon filters (Rainin Instruments). Injection volume was 0.2 ml and the solvent temperature in the columns was 80°C. Flow rate was adjusted between 0.5 and 1.0 ml min⁻¹ to keep the pressure at ca. 80% of the maximum pressure setting (16MPa). The data for each run was continuously fed to a PDP 11/60 computer for storage and further analysis. Calculations were done using a polystyrene standard calibration, since polyurethane calibrations are currently unavailable.

Mechanical Properties. Stress-strain curves for two of the series studied M-B-40/15-49 and M-E-23/25-48 were done at Rubicon Chemicals (Woodbury, NJ), using the ASTYM D-412 method (tensile properties of rubbers) at a strain rate of 500 mm min⁻¹. Young's modulus was determined from the initial slope of the stress-strain curve of at least two to four samples.

Results

Dynamic Mechanical Spectra. Dynamic shear moduli, G' and G'' for BDO and EDO based materials are shown in Figures 2 to 4. For the 23/25 polyol, increased reaction rate (catalyst) leads to greater dependence of the storage modulus in the rubbery region. As in our previous findings,⁽⁶⁾ overall phase separation seems to be improved by lower reaction rates. Increasing polyol molecular weight to 4000 reduces differences in the modulus temperature behavior as a function of catalyst composition (cf. Figure 3).

Unlike in our earlier work ⁽⁶⁾ very few differences were observed in the glass transition temperature of the soft segments, T_{gs} as a function of catalyst content. Similar results were obtained by DSC (as discussed later). An increase in the polyol molecular weight, on the other hand, decreased the T_{gs} significantly (Figure 5). The T_g values obtained by DSC however, were about 10° lower than DMS data.⁹ Similar differences were found by Zdrahala et al. ⁽¹¹⁻¹²⁾ and Russo and Thomas ⁽¹³⁾.

We studied two factors which affect dynamic moduli vs. temperature behavior: catalyst concentration, or equivalently, reaction speed, and polyol molecular weight. One way of comparing the data is to look at the $G'(-30^{\circ}\text{C})/G'(70^{\circ}\text{C})$ ratio. This is a measurement of the flatness of the rubbery plateau. The two temperatures are rather arbitrary but they can be taken as practical limits of use for these elastomers, at least in automotive applications. Figure 6 shows the effect of catalyst concentration on the ratio $G'(-30^{\circ}\text{C})/G'(70^{\circ}\text{C})$ of different series. Higher catalyst content produces a polymer with more modulus temperature sensitivity. For the sake of completeness the series M-B-20/30-6 studied earlier ⁽⁶⁾ has been added. Figure 7 shows that polyol molecular weight decreases $G'(-30^{\circ}\text{C})/G'(70^{\circ}\text{C})$. We interpret this as an increase in the degree of phase separation. We would expect this trend to level off at higher molecular weight polyols.

Amorphous Systems. The linear viscoelastic properties of the amorphous series (M-M-23/25-51 and 24M-B-23/25-48) are very different from the ones discussed so far in that the T_{gs} 's are ca. 30°C higher than those found in semicrystalline MDI-BDO or MDI-EDO based systems.

In Figure 8 we compare G' and G'' for samples produced under similar conditions from symmetric and asymmetric MDI isomers. The storage modulus of the 24-MDI based material drops by about three orders of magnitude after T_{gs} . Above 50°C, dynamic mechanical measurements were discontinued due to extreme softening of the

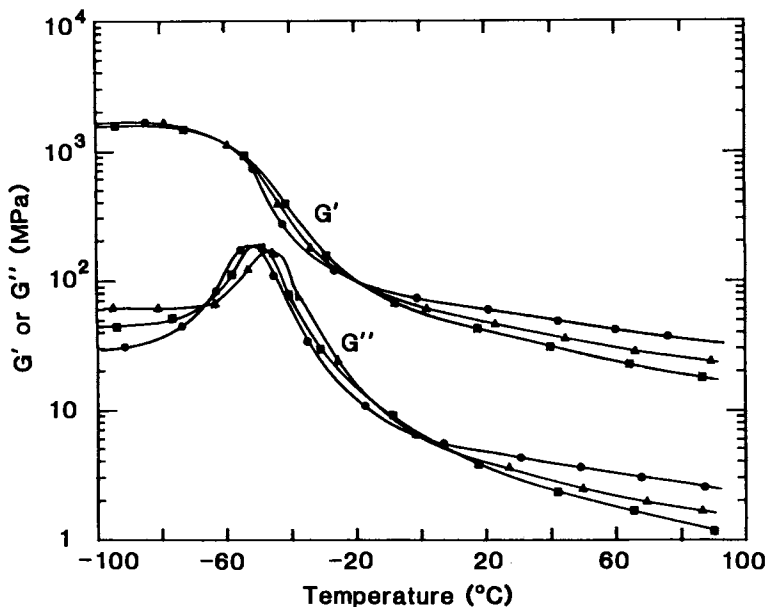


Figure 2. Dynamic mechanical properties for the M-B-23/25-48 series as a function of catalyst concentration. %DBTDL x 1000: ●, 05; ▲, 30; ■, 75.

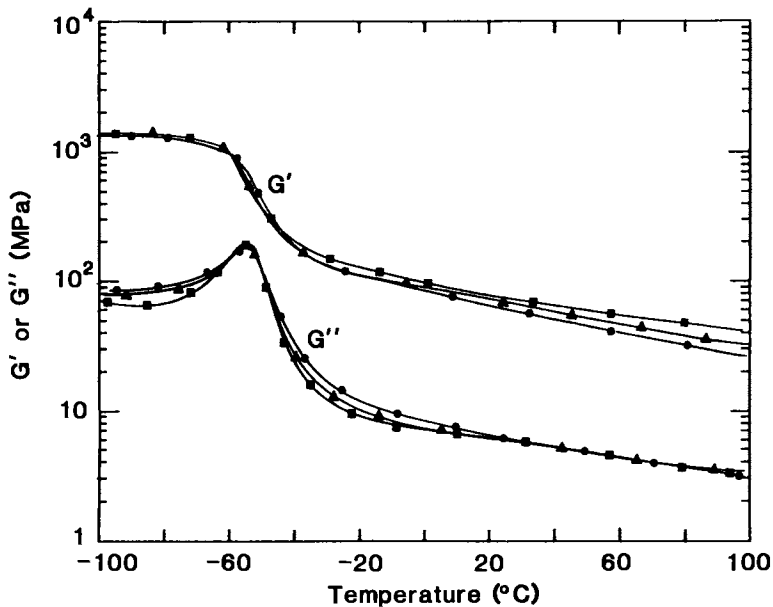


Figure 3. Dynamic mechanical properties for the M-B-40/15-49 series as a function of catalyst concentration. %DBTDL x 1000: ●, 05; ▲, 30; ■, 75.

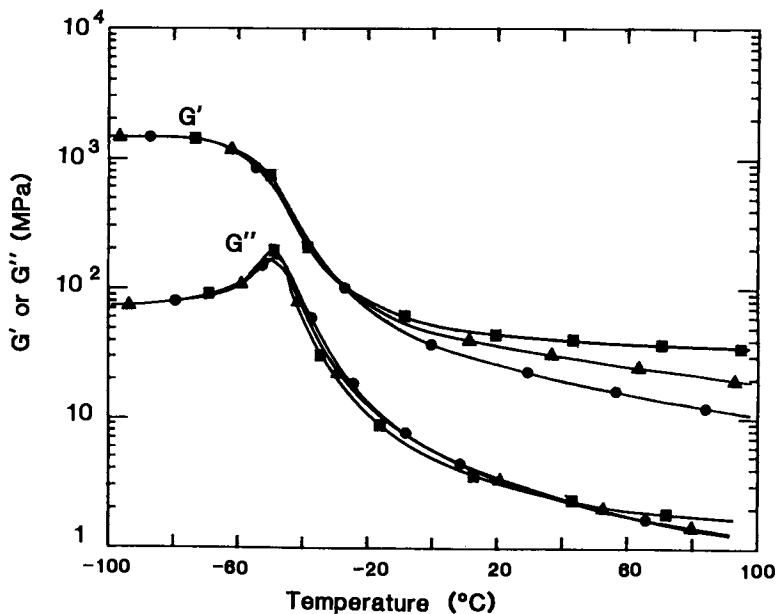


Figure 4. Dynamic mechanical properties for the M-E-23/25-48 series as a function of catalyst concentration. %DBTDL x 1000: ■, 00; ▲, 10; ●, 75.

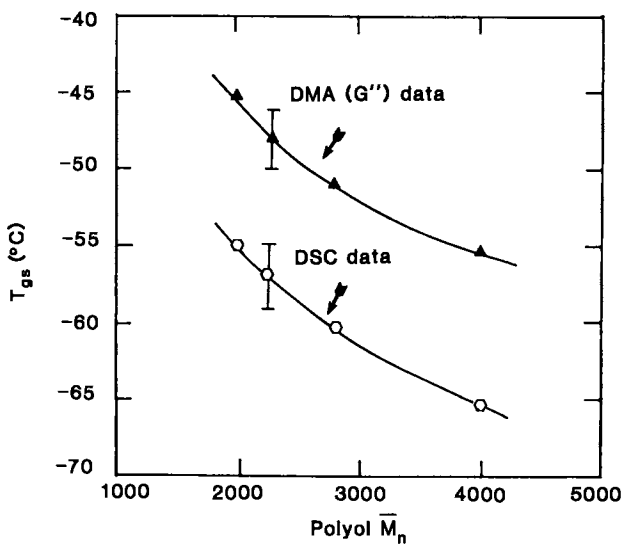


Figure 5. Soft segment glass transition temperature, T_{gs} as a function of polyol molecular weight.

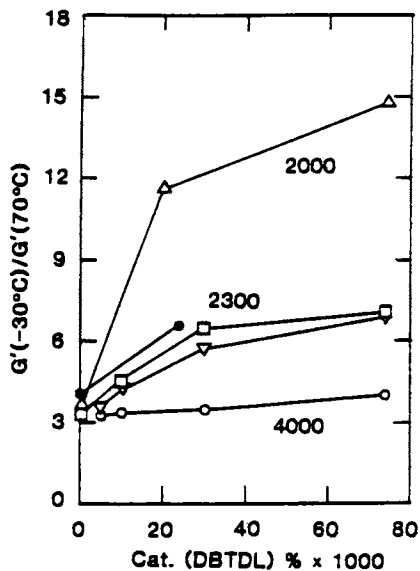


Figure 6. Modulus ratio, $G'(-30^\circ\text{C})/G'(70^\circ\text{C})$ versus concentration of DBTDL catalyst. (Δ) M-B-20/30-60; (∇) M-B-23/25-28; (\circ) M-B-40/15-49; (\square) M-E-23/25-48.

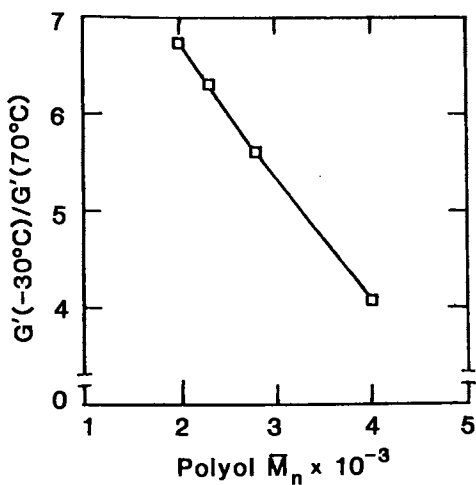


Figure 7. Effect of polyol \bar{M}_n on the modulus ratio, $G'(-30^\circ\text{C})/G'(70^\circ\text{C})$, M-B series.

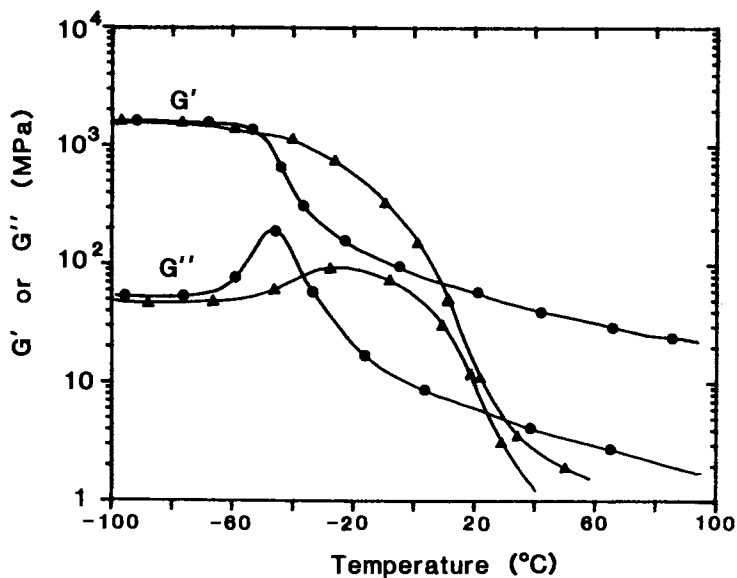


Figure 8. Comparison of dynamic mechanical properties for polyurethanes made from symmetric and asymmetric MDI isomers. Key: ●, based on 4,4'-MDI; ▲, based on 2,4'-MDI.

samples. G' and G'' vs. T curves for the MDEA based materials are similar to those of the 24-MDI shown in Figure 8.

Wide Angle X-Ray Diffraction. Scattered intensity vs. angle WAXS curves for MDI-BDO based materials were similar to those previously reported by us (6) and other investigators (14-15) (cf. Figure 9a). Again, at low catalyst concentrations, prominent reflections are observed; as catalyst concentration increases, the intensity of the sharp reflections decreases until almost an amorphous looking pattern is observed in very fast systems (e.g. 0.075% DBTDL). The MDI-EDO materials display similar behavior. With no catalyst, there are strong crystalline reflections at 3.41, 3.88, 4.23, 4.75, 7.82 and 15.5 Å (cf. Figure 9b). These d-spacings are in good agreement with those recently reported by Turner et al.(7) on similar systems. As catalyst concentration increases, most reflections are gradually weakened. However, some reflections still appear at very high catalyst concentrations (Figure 9b).

The MDEA and 24-MDI based samples display WAXS intensity curves characteristic of amorphous systems, thus confirming the absence of three dimensional order in the domains.

Differential Scanning Calorimetry. DSC scans for the M-B-23/25-48 series are shown in Figure 10. At low catalyst concentrations, there are two prominent endotherms at ca. 215°C and 225°C. As catalyst content increases, a new broad endotherm appears at ca. 190°C. These endotherms are characteristic of all polyol systems polymerized at high catalyst concentrations and/or high mold temperatures (Figure 11). Multiple endotherms in MDI/BDO polymers have been previously reported by other investigators (e.g. ref. 4, 14, 16, 17). Overall heats of fusion are a measure of crystallinity and crystal perfection and size and were higher (24 J/g) for samples with low catalyst content.

Figure 12 shows the DSC scans for the M-E-23/25-48 series are a function of DBTDL concentration. In general the multiple melting points for the MDI-EDO based hard segments are higher than the MDI-BDO based materials. Dominguez (4) also reports higher melting points in RIM materials produced from EDO and uretonimine modified MDI. However, his temperatures are below ours made with pure MDI. Heats of reaction in the MDI-EDO samples were somewhat higher than those of the MDI-BDO counterparts. The heat of fusion of the uncatalyzed composition was significantly higher than that of the catalyzed samples (40 J/g versus 25 J/g).

Molecular Weight Determination. As mentioned earlier, the GPC results for our samples are based on a polystyrene calibration curve. As such, all numbers must be regarded on a relative basis. PS based weight average molecular weights, M_w , were about 10^5 for highly reacted samples. Actual M_w values may be lower even by a factor of 2, based on calculations for an stepwise polycondensation with 99% conversion (18). M_w versus DBTDL concentrations for a typical series are shown in Figure 13. As observed the effect of a hotter mold wall

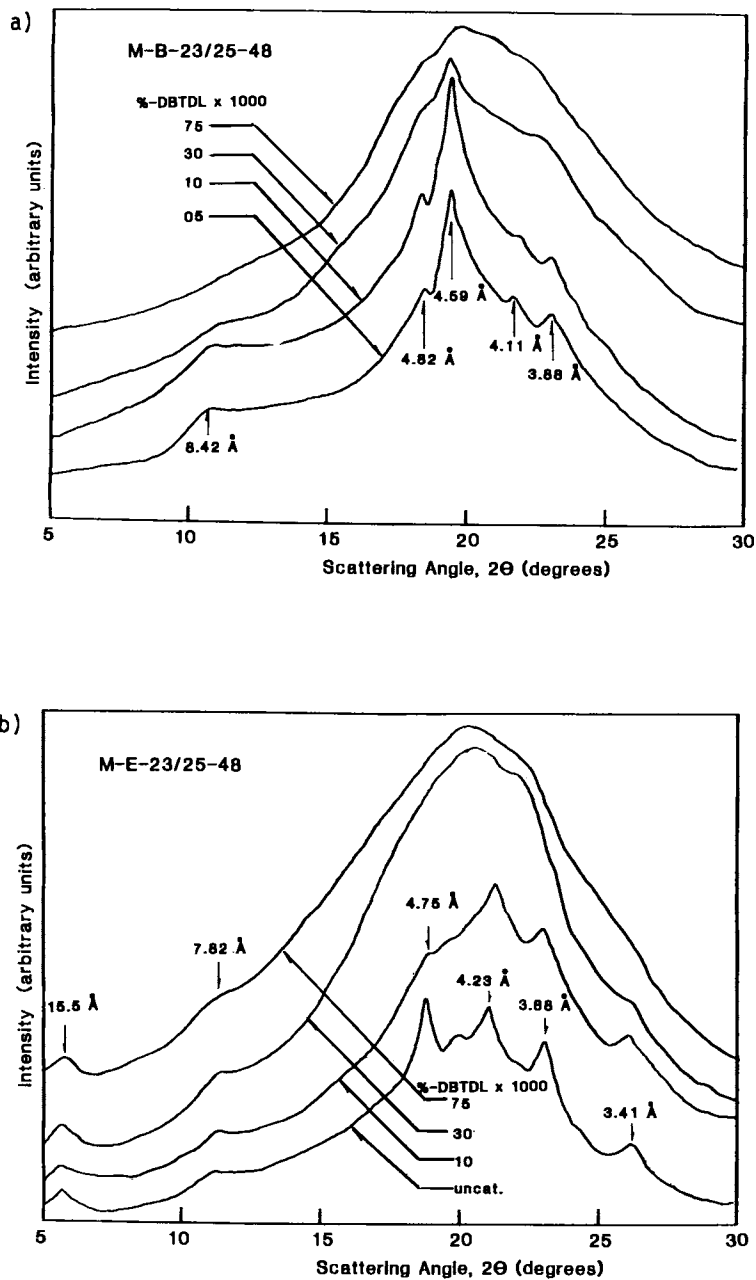


Figure 9. WAXS diffraction curves for the a) M-B-23/25-48 series and b) M-E-23/25-48 series at different levels of catalyst (DHTDL).

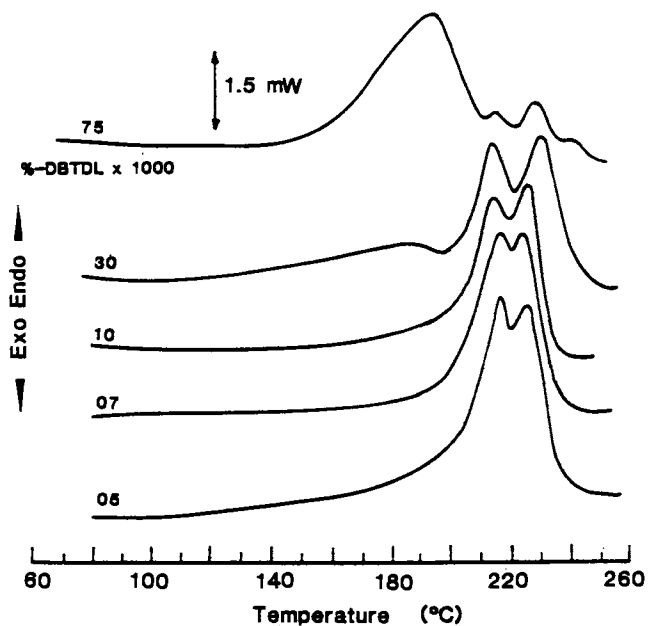


Figure 10. DSC curves for the M-B-23/25-48 series at different concentrations of DBTDL catalyst.

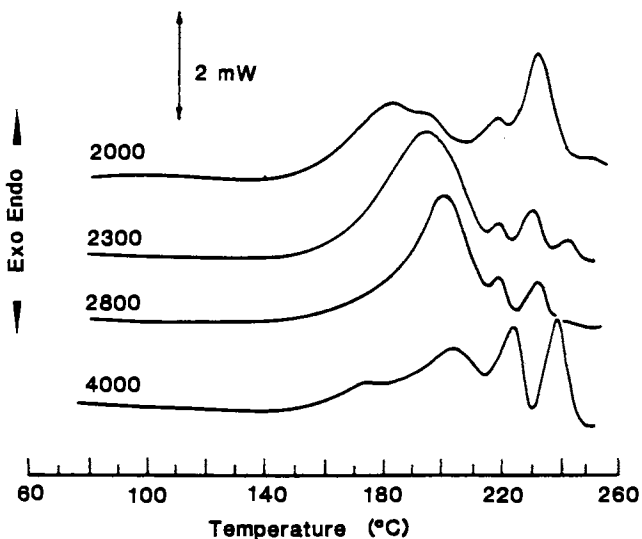


Figure 11. DSC curves for different polyurethanes at 0.075% DBTDL (fast systems). Effect of the polyol M_n in M-B series.

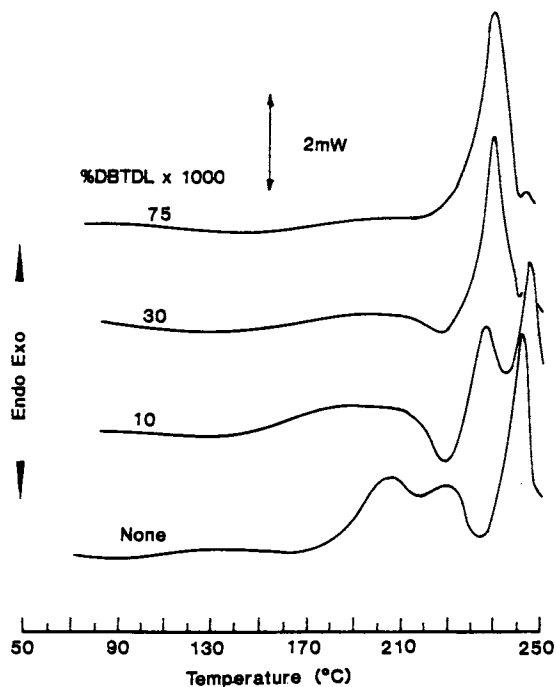


Figure 12. DSC curves for the M-E-23/25-48 series at different concentrations of DBTDL catalyst.

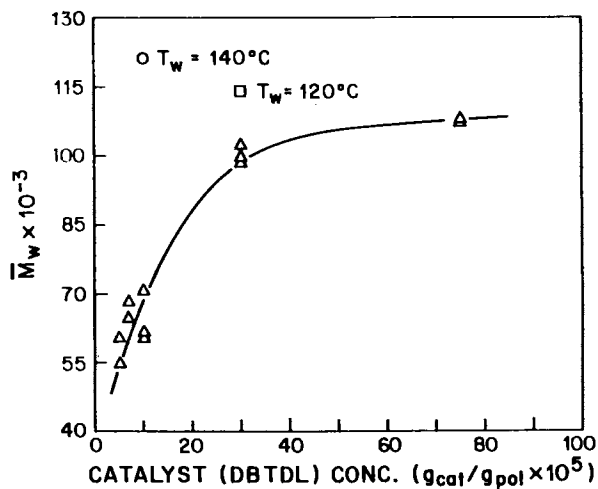


Figure 13. Molecular weight, \bar{M}_w , versus catalyst content for the M-B-23/25-48 series. Unless otherwise noted, mold temperature was 70 °C.

at constant catalyst composites is to increase the molecular weight of the sample. Figure 14 compares the different series, with M_w 's normalized by the highest value in the series. Except for the M-B-20/30-60 series in which the mold temperature was 100°C all other samples were molded at 70°C.

All samples show a sharp decrease in M_w at 0.02-0.03% DBTDL. Judging from the results of the M-B-20/30-60 series, an increase in mold temperature allows for larger decreases in catalyst composition without major effect on the molecular weight. Information like this is valuable in establishing optimum levels of catalyst or molding conditions.

The M_w of the amorphous samples were generally high (i.e. around 10^5). It is important to note that these results hold even for the uncatalyzed sample of the M-M-23/25-51 series. In terms of reaction speed this sample is comparable to EDO or BDO based materials with ca. 0.01-0.02% DBTDL, probably due to the presence of the catalytically active tertiaryamine group in the MDEA molecule (10). Nonetheless, the molecular weight is comparable to that of much faster samples. This, as we will discuss later is due to general absence of phase segregation during the reaction in the MDEA based materials.

A final and important observation must be made concerning molecular weight results. Ideally the polydispersity (M_w/M_n) of these samples should be close to 2.0. Indeed this was found in most samples with two remarkable exceptions. A decrease of catalyst content in the M-B-40/15-49 and M-E-23/25-48 series lead to higher polydispersity values. The uncatalyzed sample of the M-E-23/25-48 series for instance had a polydispersity of 8.0. Moreover, the GPC traces in these materials indicated the presence of shoulders. Upon close examination, at least one of the shoulders could be assigned to the polyol originally used in the composition, as seen in Figure 15 for the M-E-23/25-48-70-00 sample. Similar results were observed for the M-B-40/15-49-70-05 sample.

Examples of high polydispersity ratios and bimodal distributions have been previously rationalized by heterogeneous reaction conditions. Tirrell et al.(19) found M_w/M_n values well over 2.0 and low molecular weight shoulders in slow, low temperature RIM polymerized urethanes based on polycaprolactone diols. Xu et al. (20) have recently performed selective extraction experiments on urethanes based on toluene diisocyanate, TDI, and hydroxyl terminated polybutadiene. They have shown that two different chain length distributions are a consequence of insoluble initial components.

Tensile Properties. Stress-strain data for the M-E-23/25-48 series is shown in Figure 16. Elongations at break drop rapidly with lower DBTDL concentrations. Young's modulus was measured at about 42 MPa (6,000 psi). Similar results were obtained in samples of the M-B-40/15-49 series where Young's modulus in this case was ca. 60MPa (8,700 psi).

It is important to compare these results to molecular weight data presented in the previous section. A drop in molecular weight

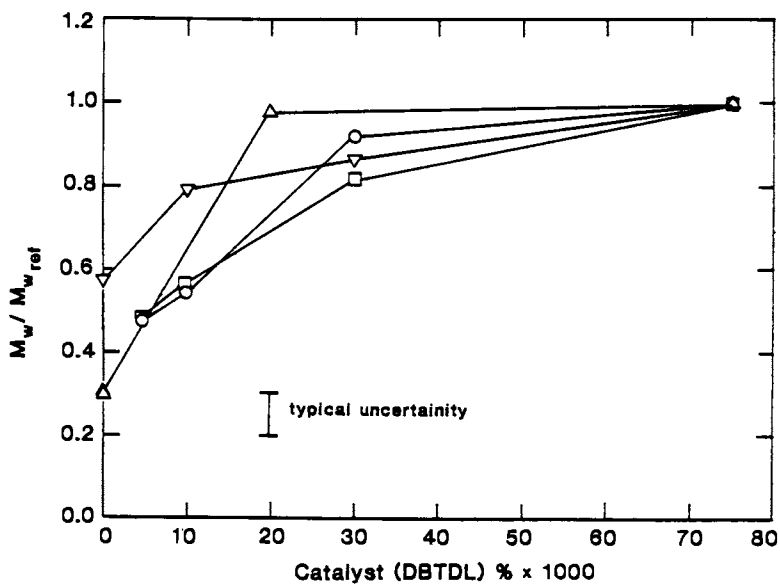


Figure 14. Normalized molecular weights versus catalyst concentration for different series. $M_w \text{ ref.}$ = value at highest catalyst. Key: Δ , M-B-20/30-60-100; \circ , M-B-23/25-48; \square , M-B-40/15-49; ∇ , M-E-23/25-48.

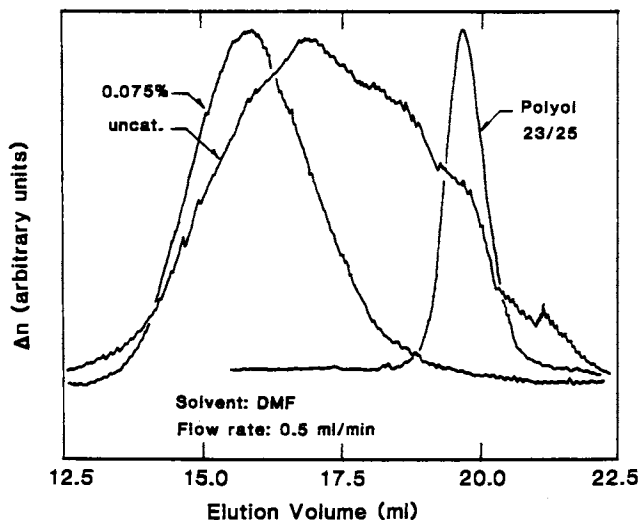


Figure 15. GPC traces for catalyzed (M-E-23/25-48-70-75) and uncatalyzed (M-E-23/25-48-70-00) RIM samples and the starting polyol, 23/25. Note the correspondence between the shoulder in the uncatalyzed sample and the polyol.

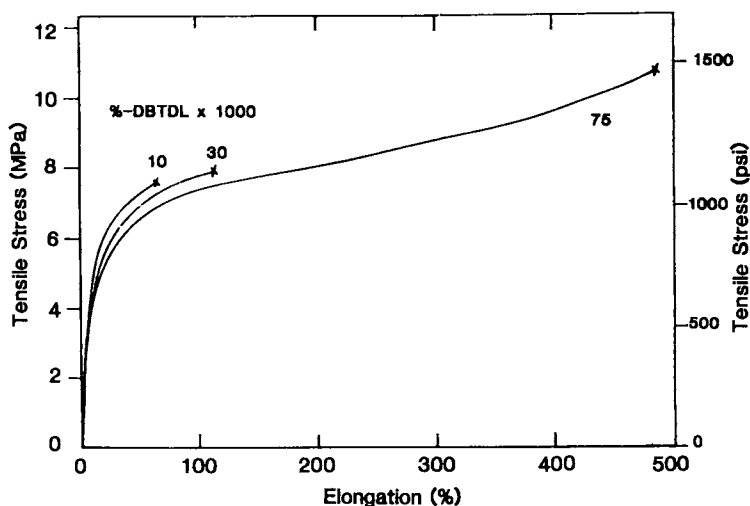


Figure 16. Stress-strain curves for the M-E-23/25-48 series as a function of catalyst concentration.

of ca. 20% represent changes in elongation from 500% to 100%. Only those samples with 0.075% DBTDL display stress-strain data typical of elastomeric materials. Evidently in linear polyurethanes produced by RIM, only with high catalyst levels are molecular weights in the region where mechanical properties became insensitive to molecular weight (21). This characteristic certainly justifies the use of triols or multifunctional isocyanates in commercial RIM systems, provided that morphology and domain formation are not significantly affected.

Discussions

Crystalline Systems. Lower T_{gs} , flatter rubbery plateau modulus, higher hard segment crystallinity, all support the view that phase separation is more complete MDI-BDO and MDI-EDO based polyurethanes as catalyst concentration decreases.

Highly catalyzed materials display a temperature sensitive plateau modulus and lower hard segment organization as evidenced by WAXS and DSC data. These samples are flexible and tough with good tensile properties. Recent FTIR data indicates that there is a high degree of hard segment association through hydrogen bonding (10,22). The evidence suggests that rapidly polymerized specimens can be viewed as a disperse, highly interconnected network of loosely organized hard segments reinforcing a polyether rich soft segment matrix. Additional arguments to support this hypothesis follow.

Hashimoto and coworkers (23) analyzed the effects of interdomain mixing and phase boundary mixing (i.e. broader interphases) on the linear viscoelastic properties of block copolymers. Briefly, both mixing and interphase broadening increase the temperature dependence of the storage modulus. Changes on the loss modulus, however, are different in the two cases. Interdomain mixing results in shifts of the transition peaks toward each other with little or no broadening. Interphase boundary mixing, on the other hand, produces a broadening of the transition peaks but negligible shifts of the transition temperatures.

Based on the above interpretation, the main effect of increased catalyst concentration is to produce more diffuse boundaries between the hard and the soft domains, since differences in T_{gs} among the samples are small, while differences in temperature dependency of the modulus are large as indicated by Figure 6. It is interesting to observe in this figure also that all curves converge to a limiting modulus ratio value of about 3.0, $G'(-30^{\circ}\text{C})/G'(70^{\circ}\text{C})$. A survey of literature data (5,12,24) indicates that for polyether urethane elastomers of similar hard segment concentration, the modulus ratio values are greater or equal to this limiting value. It is therefore reasonable to assume that 3.0 corresponds to a system that is completely phase separated with very sharp boundaries. In very slow systems this situation is accomplished by an early precipitation of mobile hard segment oligomers which form reasonably stable crystalline structures. However, there is a low degree of connectivity between hard and soft segments because the tight packing

of the crystalline structures prevents further reaction of groups attached to crystalline chains.

As the reaction speed increases, high conversions can be achieved in a time interval shorter than the characteristic time for phase separation. Moreover, nonisothermal effects become important. Due to the exothermic nature of the reaction, the temperature of the reactive medium is greatly increased possibly to the region of phase compatibilization. At this point the system can cool down, but domain formation is difficult due to high molecular weight and high viscosity. Thus only a finely interconnected structure results. Reduced segment mobility prevents the hard segments from reaching a high degree of crystalline organization.

Increasing the molecular weight of the polyol decreases the critical value of the interaction parameter χ_{AB} for phase separation and thus increases the driving force for phase separation. Hence the flatter modulus plateau in the samples of the M-B-40/15-48 series. Another variable that may also contribute to the higher degree of phase separation in the M-B-40/15-48 series is the lower ethylene oxide content of the polyol (Table 1). Since the polyethylene oxide segment is more polar than the polypropylene oxide ones, we expect ethylene oxide to promote phase mixing. Recently, Kojima and coworkers (24) have shown that the temperature dependence of modulus in RIM urethanes increases as the content of ethylene oxide in a triol of constant equivalent weight increases.

The picture presented thus far is also supported by other experimental data. WAXS and DSC data show that rapidly polymerized samples do not display a high degree of crystallinity in the hard segments. Annealing studies of some of our samples indicate that the broad peak at ca. 190°C can be slowly converted to a peak at ca. 220°C. If annealing is done at high enough temperature (210°C or higher), a new DSC endotherm appears ca. 235°C(10). This is in agreement with recent work of Thomas and Briber (25) and Blackwell and Lee (26) who have independently proposed the existence of at least two different crystal structures in MDI/BDO based hard segments.

Perhaps one of the most important effects of a low reaction rate and premature phase separation is the decrease in molecular weight of the material. This clearly must be avoided as it seriously decreases the tensile properties of the polymer. There exists therefore a balance between the degree of phase separation and organization that can be achieved and the maximum molecular weight. As the latter has more importance regarding the performance of the material, it is necessary in real systems to turn to other alternatives such as the use of triols or graft polyols to increase molecular weight without seriously affecting the ability of the system to reach a certain degree of phase separation.

Finally, a word must be said regarding spacial variations. In real samples, large temperature gradients develop during the polymerization. Generally monomers near the mold wall, react slower, and thus can undergo phase separation at an early stage, decreasing the local molecular weight of the material. Center to surface

variation tend to be magnified at intermediate catalyst concentrations (e.g. 0.01 to 0.05% DBTDL). At concentrations lower than these, the overall system is slow and early phase separation occurs throughout the part. At very high catalyst concentrations, the reaction is fast even near the mold wall. High conversions can be reached before appreciable phase separation can affect molecular weight. For this reason, surface to center differences are also minimized (cf. ref. 6, Figure 5).

Non-crystalline Systems. As inferred from the experimental data, those systems based on 24-MDI or MDEA are highly compatible and have a low modulus at room temperature. They only display a single T_g much higher than the one of the crystalline systems described in the previous section.

It is useful to compare the T_g values obtained for the amorphous M-M-23/25-51 and 24-M-B-23/25-48 series to predictions for random homo-geneous systems. Using for instance Fox's equation (27):

$$\frac{1}{T_g} = \frac{w_s}{T_{gs}} + \frac{w_h}{T_{gh}}$$

where w_s and w_h are the weight fractions of the soft (s) and hard (h) phases and T_{gs} and T_{gh} are the corresponding glass transition temperatures. T_{gs} for the polyethers used in this work is -65°C (10). Hwang et al. (28) reported $T_{gh} = 54^\circ\text{C}$ for the MDI/MDEA hard segment. T_{gh} for the 24-MDI/BDO hard segments has been measured at 74°C using a copolymer polymerized in solution (10). As observed from Table III, the predictions of Fox's equation are in good agreement with the values measured in this work, indicating once again that these systems are highly compatible.

Summarizing then, the amorphous glycol extended systems have a large degree of phase compatibility and poorly defined elastomeric behavior. The absence of crystallinity reduces the driving force available for phase separation. This is necessary to overcome specific hard-soft segment interactions such as hydrogen bonding that tends to reduce the interaction parameter between the blocks. Crystallinity is not the only mechanism available to increase χ_{AB} . Other specific intradomain interactions such as π -electron attractive forces can also help phase development without crystallinity as shown by Camberlin et al. (29). In polyurethane-urea systems, a strong hydrogen bonding (most likely a 3-D arrangement) can explain the phase separation and excellent properties of these polymers without crystallinity.

The absence of intersegmented interactions can make an otherwise compatible system become more phase separated. These have been well illustrated by the work of Cooper et al. (30) who have prepared MDI/MDEA based systems using polytetramethylene oxide and polybutadiene based soft segments. Since with PBD soft segments there is no possibility of hard-soft segment hydrogen bonding, these materials show a more complete phase separation than in the PTMO materials.

**American Chemical
Society Library
1155 16th St. N. W.
Washington, D. C. 20036**

In Reaction Injection Molding, ACS Symposium Series, Washington, DC, 1985.

Table III. DMA and DSC Data for Glycol Extended Amorphous Samples

SAMPLE	T _g ⁽¹⁾	T _g ⁽²⁾	T _g ⁽³⁾	G'(-30°) MPa	$\frac{G'(-30\text{ }^{\circ}\text{C})}{G'(70\text{ }^{\circ}\text{C})}$
M-M-23/25-51-70-19	-12	-18.6	-18.7	794	>100
24M-B-23/25-48-70-150	-22	-23.5	-15.6	832	>100

(1) From dynamic mechanical spectra
(2) From differential scanning calorimetry
(3) Predicted from Fox equation (see text)

Summary and Conclusions

Through this work we have demonstrated the following points concerning phase separation and properties in bulk RIM polymerized polyurethane elastomers:

- The final degree of phase separation, and the molecular weight, in semi-crystalline systems are highly dependent on the rate of polymerization, controlled mainly by the catalyst concentration.
 - Low reaction rates favor the crystallization of oligomeric materials during the polymerization. Although the samples show a high degree of phase separation and hard segment crystallinity, the hetero-geneous conditions of the reaction decrease the molecular weight, resulting in a brittle material with poor tensile properties.
 - At high reaction rates most of the polymerization takes place before phase separation. The final degree of phase separation and hard segment organization depend mostly on the molding conditions and thermal history of the material. Under normal RIM conditions the system can be regarded as a finely interconnected network of hard segments dispersed throughout a polyether rich hard segment matrix. This high dispersion of poorly organized hard segments yields a high temperature dependence of the storage modulus.
 - Increasing the polyol molecular weight increases the length of the segments and increases phase incompatibility. At high enough polyether molecular weight, the effect of catalyst concentration on the temperature dependence of the modulus becomes less apparent.
 - Comparison between ethanediol and butanediol extenders indicates that the former produces hard segment crystals with a higher melting temperature. Because of higher urethane group concentration in the ethanediol based hard segments, these tend to have higher cohesion thus giving higher T_m .
- The use of monomers that produce amorphous hard segments produces highly compatible systems with poorly defined rubbery plateau and elastomeric behavior. Because no heterogenous conditions develop during the reaction, molecular weight in amorphous polyurethane systems tends to be less affected by reaction rates or polymerization conditions.
- Hard segment crystallizability, and/or other specific interactions such as π -electron forces between aromatic groups or 3-D hydrogen bonding provide higher cohesive intersegmental forces.

Acknowledgments

This work was supported by cooperative funding from the National Science Foundation, Grant NSF-CPE-8118-232, the General Motors Corporation and the Union Carbide Corporation. The authors are also indebted to Drs. D. Spence and J. Ferrarini from Rubicon Chemicals, R. Lloyd from Texaco Chemicals, J. O'Connors from Olin Park and R. Gerkin and L. Lawler from Union Carbide for providing us with the raw

chemicals used in this work. Invaluable assistance by K. Dulin, J. Horns and J. Andrews in sample preparation and characterization is acknowledged. One of the authors (R.E.C.) would also like to thank the 3M Company for fellowship support through this project.

Literature Cited

1. R.M. Gerkin and F. E. Critchfield, Paper 741022, Soc. Automotive Engineers Mtg. Toronto, Canada, Oct., 1974.
2. I.D. Fridman, E.L. Thomas, L.J. Lee and C.W. Macosko, Polymer **21**, 393 (1980).
3. D.M. Rice and R.J.G. Dominguez, Polym. Eng. Sci., **20**, 1192 (1980).
4. R.J.G. Dominguez, Polym. Eng. Sci., **21**, 1210 (1981).
5. R.B. Turner, H.L. Spell and J.A. Vanderhider, in "Reaction Injection Molding and Fast Polymerization Reactions," J.E. Kresta, Ed., p. 63, Plenum Press, N.Y., 1982.
6. R.E. Camargo, C.W. Macosko, M. Tirrell, and S.T. Wellinghoff, *ibid.*, p. 95; Polym. Eng. Sci., **22**, 719 (1982).
7. J. Blackwell, J. Quay, and R.B. Turner, Polym. Eng. Sci., **23**, 816 (1983).
8. P. Kolodziej, C.W. Macosko, and W.E. Ranz, Polym. Eng. Sci., **22**, 388 (1982).
9. L.J. Lee, and C.W. Macosko, S.P.E. ANTEC Tech. Papers, **24**, 151 (1978); U.S. Patent 4,189,070 (1979).
10. R.E. Camargo, Ph.D. Thesis, Dept. of Chemical Engineering and Mat. Sci., U. of Minnesota, 1983.
11. R.J. Zdrahala, R.M. Gerkin, S.L. Hager and F.E. Critchfield, J. Appl. Polym. Sci., **24**, 2041 (1979).
12. R.J. Zdrahala, S.L. Hager, R.M. Gerkin and F.E. Critchfield, J. Elastom. Plast., **12**, 225 (1980).
13. R. Russo and E.L. Thomas, J. Macromol. Sci., Phys., **B22**, 553 (1983).
14. A.L. Chang, R.M. Briber, E.L. Thomas, R.J. Zdrahala, and F.E. Critchfield, Polymer, **23**, 1060 (1982).
15. N.S. Schneider, C.R. Desper, J.R. Illinger, and A.O. King, J. Macromol. Sci., Phys., **B11**, 527 (1975).
16. R.W. Seymour, and S.L. Cooper, Macromolecules, **6**, 48 (1973).
17. T.R. Hesketh, J.W.C. Van Bogart, and S.L. Cooper, Polym. Eng. Sci., **20**, 190 (1980).
18. F. Lopez-Serrano, J.M. Castro, C.W. Macosko and M. Tirrell, Polymer, **21**, 263 (1980).
19. M. Tirrell, L.J. Lee, and C.W. Macosko, A.C.S. Symp. Series, **104**, 149 (1979).
20. M. Xu, W.J. MacKnight, C.H.Y. Chen and E.L. Thomas, Polymer, **24**, 1327 (1983).
21. J.H. Saunders, Rubber Chem. Technol., **33**, 1259 (1960).
22. F.M. Mirabella, Northern Petrochemical Co., Personal Comm., 1983.
23. T. Hashimoto, Y. Tsukahara, K. Tachi, and H. Kawai, Macromolecules, **16**, 648 (1983).

24. H. Kojima, H. Nishimura and M. Funaki, Reports of the Research Lab. Asahi Glass Co., 31, 109 (1981).
25. R.M. Briber and E.L. Thomas, J. Macromol. Sci., Phys., B22, 509 (1983).
26. J. Blackwell and C.D. Lee, submitted for publication, 1983.
27. F.W. Billmeyer, "Principles of Polymer Science," 2d. ed., Wiley, 1984.
28. K.K.S. Hwang, C.Z. Yang and S.L. Cooper, Polym. Eng. Sci., 21, 1027 (1981).
29. Y. Camberlin, P. Pascault, M. Letoffe, and P. Claudy, J. Polym. Sci., Polym. Chem. Ed., 20, 1445 (1982).
30. C.Z. Yang, K.K.S. Hwang and S.L. Cooper, Macromol., to appear.

RECEIVED October 5, 1984

Investigations of the Structure-Property Relationships for RIM Polyurethane Elastomers

Effect of an Amine Additive

ROBERT B. TURNER¹, CHRISTINE E. MACDONALD¹, JOHN BLACKWELL²,
JEFFREY R. QUAY², and CHUN DONG LEE²

¹The Dow Chemical Company, Freeport, TX 77541

²Department of Macromolecular Science, Case Western Reserve University, Cleveland, OH 44106

Structural and mechanical data have been compared for RIM polyurethanes prepared from uretonimine modified diphenylmethane 4,4'-diisocyanate (MDI), ethylene glycol (EG), and a polypropylene oxide soft segment polyol (Mn 5000), with and without the addition of a polyether diamine (PEDA). A series of specimens containing 18 parts and 30 parts EG (per 100 parts by weight of polyol) were prepared with and without the addition of a PEDA, and were examined before and after thermal annealing (120°C for 1 hour). X-ray analyses show that the hard domain crystallite size and degree of crystallinity is increased by thermal annealing in the specimens prepared without PEDA. Significantly, the same structural improvement is achieved by use of the PEDA additive without the annealing step. These results are seen to correlate with the thermal and mechanical data, and show that the improvement in heat sag behavior can be effected by use of the PEDA additive without annealing. It is suggested that the mechanism for this improvement may involve MDI-capped PEDA as a nucleation site for the hard domains.

At present there is considerable interest in the structure and properties of reaction injected molded (RIM) polyurethanes elastomers for many applications, including automobile bodies. Polyurethane elastomers are multiblock copolymers comprised of alternating polyurethane and polyether or polyester segments. At use temperatures the polyurethane and polyol segments are respectively below and above their glass transition temperatures, and are designated hard and soft segments. The elastomeric properties are derived from phase separation, such that the polyurethane segments form hard domains within the soft segment matrix. These hard domains serve as physical cross-links and reinforcing filler particles [1-4]. A wide range of properties is possible, depending on the hard/soft ratio and the selected chemical structure.

0097-6156/85/0270-0053\$06.00/0
© 1985 American Chemical Society

In this paper we describe investigation of the structure and properties of RIM polyurethane elastomers prepared from diphenyl-4,4'-diisocyanate (MDI) with ethylene glycol (EG) as the hard segment chain extender and copoly(ethylene oxide/propylene oxide) as the soft segment. The softening point of these polyurethanes is frequently in the range 80 - 100°C, but is found to increase as a result of thermal annealing [5-6]. Greater improvement in the thermal properties, and also in the mechanical properties such as impact strength, flexural modulus, and heat sag, can be achieved by addition of organic diamines to the polyol/chain extender [5-7]. We are investigating the physical structure of these RIM polyurethanes in order to understand the effect of the diamine additives on the properties. A preliminary account of this work has been published previously [8].

Poly (MDI/EG) hard segments can crystallize, and the development of crystallinity is thought to be part of the driving force for phase separation. The X-ray diffraction characteristics of MDI/EG polyurethanes are now well understood.

Figure 1 shows the X-ray pattern of an oriented film of a polyurethane elastomer prepared using MDI and EG. The hard/soft ratio is approximately 50/50, and the specimen had been stretched 720% and annealed for 14 days at 130 degrees C. The soft segments are amorphous and all the Bragg reflections arise from the crystalline hard domains. Of particular interest are the sharp meridional reflections at $d = 15.0$ and 7.5\AA , which are indexed 001 and 002, respectively, and arise from planes perpendicular to the chain axis (i.e. the direction of draw) [9-10]. These reflections have been used [11] to estimate the crystallite thickness along the chain axis and also the extent of paracrystalline distortion as functions of elongation and annealing. It was found that non-crosslinked polyurethanes prepared using EG as the hard segment showed a small but significant increase in axial crystallite width (from 75 to 85Å in the present example) as a result of elongation and annealing, and these results point to a hard domain structure formed by lateral aggregation of parallel hard segments. These meridional reflections are easily identified in less crystalline unoriented specimens, because they are well away from the amorphous halo ($6-4\text{\AA}$), and hence their intensities can be used to compare the relative crystallinity of specimens produced by different processing techniques.

We have used X-ray methods to compare the crystallite size of RIM specimens prepared with and without use of a polyether diamine (PEDA) additive. These results are compared with differential scanning calorimetry data on the hard domain melting behavior and dynamic-mechanical studies of the extent of phase separation. Mechanical data on flexural modulus, elongation, impact strength, and heat sag behavior have been obtained for the same specimens and have been correlated with the structural analyses.

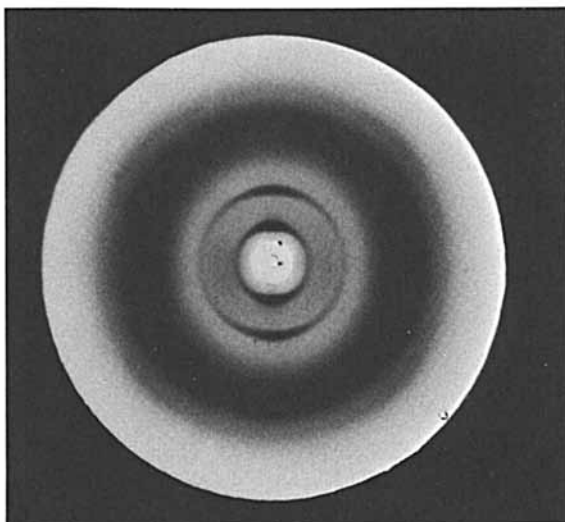


Figure 1. X-ray pattern of an oriented film of a polyurethane elastomer.

Experimental

Specimen Preparation. These polymers were polymerized using a Krauss-Maffel PU 80/40 RIM (reaction injection molding) machine using a suitable catalyst (Witco Fomrez UL-28). 6" x 6" x 1/8" plaques were produced in a P20 steel mold heated to 160°F (71°C). The MDI was Upjohn's Isonate 143L, which is diphenylmethane 4,4'-isocyanate modified with 15% uretonimine. Ethylene glycol (EG) was used as the chain extender and the soft segment was a polyether triol with a molecular weight (M_n) of 5000 prepared from propylene oxide and capped with ethylene oxide. The polyether diamine (PEDA) is an amine-terminated poly(propylene oxide). Two sets of specimens were prepared containing 18 and 30 parts EG per 100 parts by weight of polyether triol at a 105 isocyanate index. These will be referred to as the 18 EG and 30 EG series, and contain approximately 43% and 64% hard segments. Diamine modified specimens were prepared by the addition of PEDA to the 18 or 30 parts EG systems. In view of the difference in molecular weights of EG and the PEDA, this results in only a small increase in the proportion of MDI and hence in the hard segment content. The specimens were examined in the as prepared state and after annealing for 1 hour at 120 degrees C.

X-Ray Diffraction. Data were obtained as 2 θ scans of the stationary specimens in the transmission mode using Ni-filtered CuK radiation and a Schintag Pad II computer controlled diffractometer. Intensity measurements were made from 2 θ = 4.0 degrees to 32.0 degrees using 0.2 degree steps and 60 second counting times. Axial crystallite sizes were derived from the 001 integral breadths, following correction for instrumental broadening.

Heat Sag. One inch wide and 1/8" thick strips were supported horizontally with a 4" overhang and were placed in an oven at 120 C, and the vertical drop of the end after 1 hour was recorded according to ASTM D3769-79.

Mechanical Testing. Impact strength was measured using ASTM method D-250-56 and is reported in foot-pound per inch of notch. Elongation and flexural modulus were measured on an Instron tester model number 1125 according to ASTM D-638 and ASTM D-790 tests respectively.

Differential Scanning Calorimetry. Specimens were heated at a rate of 20 degrees/minute using a Perkin-Elmer DSC-2C. All samples were normalized for sample weight and tested under a nitrogen atmosphere.

Dynamic Mechanical Spectroscopy. Samples were run in the tensile mode using a Rheometrics Model 605 Mechanical Spectrometer. Temperature scans were run from -160 to 240 C using a strain of 0.15% and a frequency of 1 Hertz. Samples were maintained in a nitrogen atmosphere during testing.

Results and Discussion. X-ray diffraction densitometer scans are presented in Figures 2 for the 18 EG and Figure 3 for the 30 EG series for RIM polyurethanes. DSC and Storage Modulus traces (EI) for the same specimens are shown in Figures 4, 5 and 6, and flexural modulus, elongation, impact strength, and heat sag data are given in Table I.

The densitometer scans of all the specimens show peaks at 15.0 and 7.5Å that demonstrate the presence of crystalline hard segments. These peaks are poorly resolved for the unannealed/without PEDA specimens but increase in intensity on annealing. Significantly, the unannealed/with PEDA specimens give diffraction patterns that are similar to those for the annealed/without PEDA specimens, and estimates of the peak areas indicate an approximate doubling of the crystallinity. Very little further improvement is obtained when the samples added with PEDA are annealed. Not surprisingly, the 30 EG series of specimens are more crystalline than the 18 EG series, which have a lower hard segment content. We have no estimates of the absolute degree of crystallinities, but these are clearly lower than in the oriented annealed specimen of the noncrosslinked polyurethane (Figure 1), for which the 15.0 and 7.5Å reflections have much higher relative intensity. The lower crystallinity of the RIM specimens is to be expected because of the crosslinking that occurs as a result of the use of trifunctional soft segments. We are currently developing methods to determine the absolute hard segment crystallinities from data of this type. Crystallite sizes determined for both series of specimens using the Scherrer equation and the integral breadth of the 15.0Å peak are given in Table II. The figure for the unannealed/without PEDA specimens must be viewed as very approximate given the quality of the data. Nevertheless, there is an increase in the crystallite size on annealing without PEDA specimens, from 54 to 76Å for 18 EG and from 61 to 75Å for 30 EG. The same increase is seen as a result of the use of the PEDA additive, and there is little further change on annealing. These widths are less than those seen in equivalent linear polyurethanes [10], and this is probably due to the effects of the crosslinking which inhibits organization of the hard domains.

Figure 4 and 5 and Table III show the DSC data for these RIM specimens. It is seen that ΔH for the hard segment melting in the unannealed/without PEDA specimens increases on annealing (for both the 18 EG and 30 EG series) and essentially the same increase occurs in the unannealed/with PEDA specimens. These effects correlate with the X-ray data showing a similar increase in the crystalline perfection of the hard domains with annealing or with the use of PEDA. The decrease in the melting temperature for the hard domain prepared with PEDA suggests that the PEDA is naturally associated with the hard segments, probably at the boundaries of the hard domains. It should also be noted that the use of PEDA reduces the average hard segment length, and this may also be a factor leading to the lower melting points of the PEDA specimens.

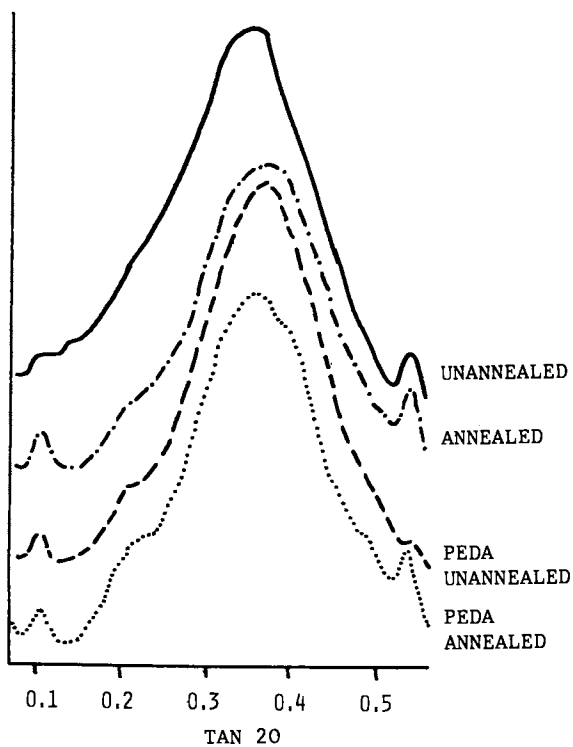


Figure 2. X-ray diffraction densitometer scans, 18 EG series.

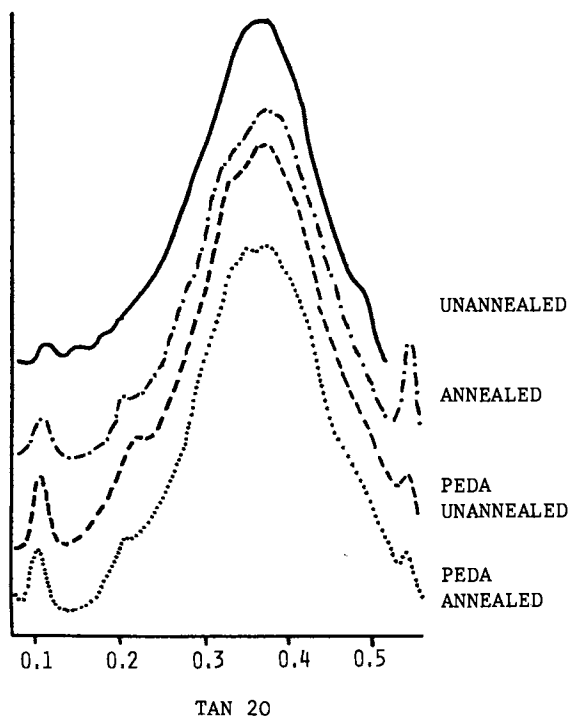


Figure 3. X-ray diffraction densitometer scans, 30 EG series.

Table I: Property Data For RIM Polyurethanes

30 EG Series	No Diamine Unannealed	No Diamine Annealed	PEDA Unannealed	PEDA Annealed
Flexural Modulus MP _a (psi)	413 (60,000)	400 (58,000)	617 (89,500)	599 (87,000)
Elongation (%)	122	172	100	214
Impact Strength, IZOD Nm/m (ft-lbs/in of notch)	287 (5.3)	314 (5.8)	650 (12.0)	705 (13.0)
Heat-sag after 60 min. at 120°C (in)	0.3	0.2	0.2	0.1
<u>18 EG Series</u>				
Flexural modulus MP _a (psi)	134 (19,500)	124 (18,000)	214 (31,000)	207 (30,000)
Elongation (%)	188	255	150	260
Impact Strength, Izod	No break	No break	No break	No break
Heat-sag after 60 min at 120°C (in)	0.7	0.5	0.4	0.5

Table II. Axial Crystallite Widths

SAMPLE DESCRIPTION	CRYSTALLITE SIZE
18 EG, Unannealed	54
18 EG, Annealed	76
18 EG, 7.5 PEDA, Unannealed	72
30 EG, Unannealed	61
30 EG, Annealed	75
30 EG, 7.5 PEDA, Unannealed	76

Table III. Melt Temperatures and Heats of Fusion

SAMPLE DESCRIPTION	T MELT (°C)	ΔH_f (CAL/g)
18 EG, Unannealed	229.4	17.1
18 EG, Annealed	228.5	24.8
18 EG, 7.5 PEDA, Unannealed	218.1	24.9
30 EG, Unannealed	228.7	24.3
30 EG, Annealed	229.2	36.2
30 EG, 7.5 PEDA, Unannealed	224.8	38.7

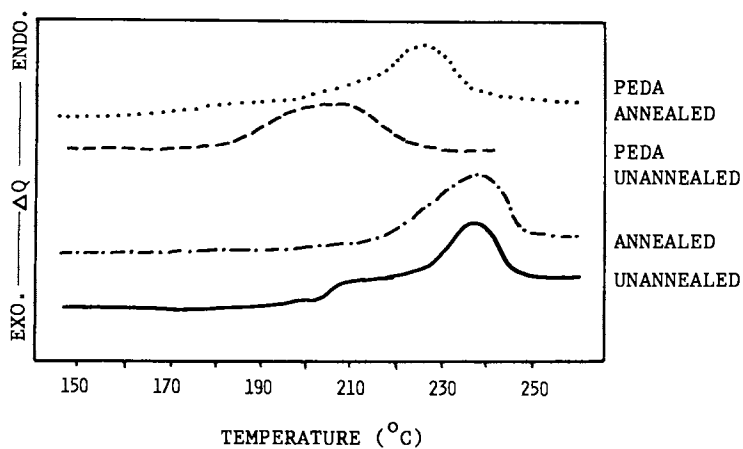


Figure 4. DSC scans, 18 EG series.

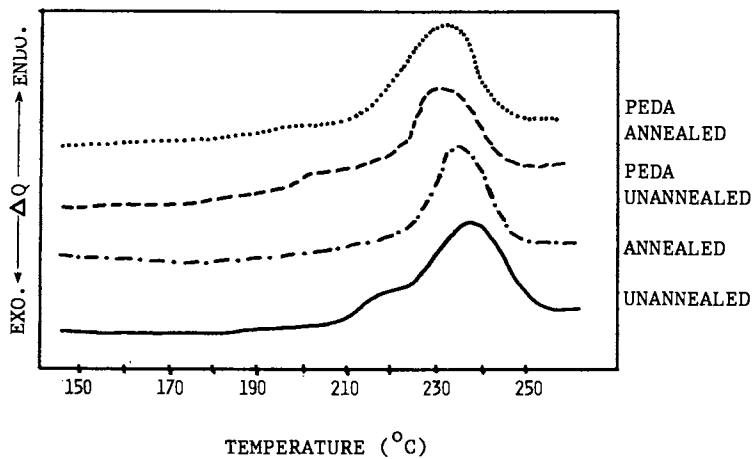


Figure 5. DSC scans, 30 EG series.

The dynamic mechanical data (Figure 6) point to enhanced phase separation as a result of annealing, as shown by the flatter storage modulus curves. The data show that a similar improvement is obtained by annealing without PEDA and by addition of PEDA without annealing. A similar conclusion is also derived from the heat sag data.

Thus the structural and mechanical data are mutually compatible and point to an increase in the order of the hard domains as a result of use of the PEDA additive, comparable to that which is achieved by annealing without use of the additive. At present we can only speculate on the mechanism whereby the PEDA leads to the higher order. The crystalline reflections are those of homopoly (MDI/EG) and hence the PEDA chains must be outside the crystalline regions, but the flexural modulus does increase indicating some hard domain association. Nevertheless, the PEDA could be intimately involved with the hard domains. The amine groups are much more reactive than the hydroxyls of the chain extender and polyol, and hence the first chemical reaction will involve PEDA and MDI. The MDI-PEDA-MDI units may serve as nucleation agents for the formation of the hard domains, perhaps because of their low solubility in the reaction mixture.

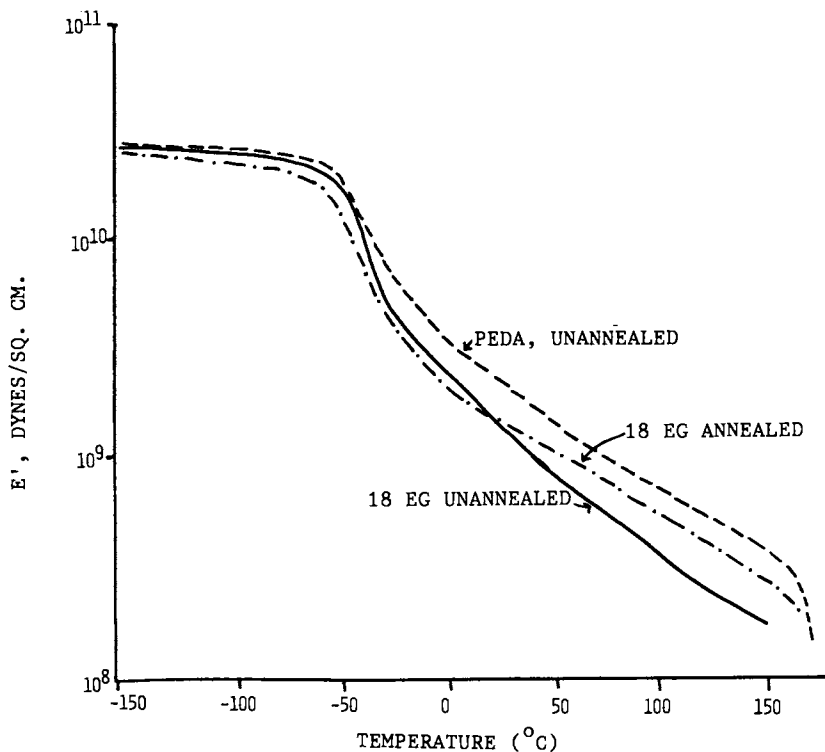


Figure 6. DMS scans.

Acknowledgments

The research at Case Western Reserve University was supported by a grant from the Dow Chemical Company.

Literature Cited

1. S. L. Cooper and V. Tobolsky, *J. of Appl. Polym. Sci.* 10 (1966).
2. D. C. Allport and A. A. Mohagu, in "Block Copolymers" (ed. D. C. Allport) Wiley-Interscience, New York, 1973.
3. A. Noshay and J. E. McGrath, "Block Copolymers--Overview and Critical Survey," Academic Press, 1977.
4. T. L. Smith, *Polym. Eng. Sci.* 17, 129 (1977).
5. M. C. Cornell, R. B. Turner, and R. E. Morgan, "Amine Modified Polyol for RIM Systems," 26th Ann. Tec. Conf., SPI, Polyurethane Div., 1981.
6. R. Dominquez, "The Effect of Annealing on the Thermal Properties of RIM Urethane Elastomers," in *Reaction Injection Molding and Fast Reaction Systems* (ed. J. Kresta) Plenum Press, New York, 1982.
7. J. A. Vanderhider and G. M. Lancaster, U.S. Patent 4,269,945 (1981).
8. J. Blackwell, J. R. Quay, and R. B. Turner, manuscript submitted to *Polymer Science and Engineering*.
9. J. Blackwell, M. R. Nagarajan, and T. B. Hoitink, *Polymer* 22, 1534 (1981).
10. J. Blackwell, M. R. Nagarajan, and T. B. Hoitink, *Polymer* 23, 950 (1982).
11. J. Blackwell and C. D. Lee, *J. Polymer Sci., Polymer Phys. Edns.*, in press.

RECEIVED October 5, 1984

Effect of Urethane RIM Morphology on Deviation from Second-Order, Straight-Line Dependence

A. DAMUSIS¹ and T. B. LIN

Polymer Institute, University of Detroit, Detroit, MI 48221

Conversion levels of polymerization at the deviation points from straight line dependence of the second order reaction graphs were correlated with the contents of rigid segments and of plasticizer in the urethane RIM formulations. Experimental data of exothermic temperature and of conversion levels versus reaction time were obtained in an adiabatic reactor and were programmed by a regression method using a computer. Formation of fringed micelle crystallites in the process of urethane RIM polymerization was a factor influencing deviation from the straight line dependence of regular kinetics. The crystalline aggregates were evaluated by the permanent set values and at three levels of temperature by the stress relaxation method.

In some cases RIM reaction kinetic data indicated the deviations from the straight line dependence of the second order reaction equation plots. Some agglomerations of polymer molecules were considered to be the cause of these deviations. Aggregates of molecules formed in the process of urethane RIM polymerization would restrict mobility of the reactive groups and would distort the regular kinetics.

Among these agglomerations the recent literature mentioned the formation of microheterogeneous systems (1), the coagulation of polymer molecules into gel particles (2), or the building of special network configurations (3).

In this study more attention was paid to the possible formation of fringed micelle crystallites by rigid segments of RIM formulations. These crystallites could be considered to be an important factor inhibiting the mobility of the reactive groups and consequently causing the deviations from the straight line dependence of the second order reaction kinetic plot.

The intermolecular fringed micelle nuclei could be formed under the influence of lateral intercohesion of the rigid segments (4,5,6).

¹Current address: 13255 Oak Ridge Lane, Rockport, IL 60441.

If the rigid segments of the polymers would arrange in orderly arrays, the intermolecular fringed micelles of crystallites would be formed.

The fringed micelle crystallites would be an organic part of the total network of the polymeric RIM system. The gel particles or microheterogeneous systems could be considered as separate phases suspended in the matrix of the polymer system.

The fringed micelle crystallites formed by aggregation of rigid segments would not only restrict the mobility of the reactive groups, but would also introduce physically bonded crosslinks into the amorphous polymer matrix (4,5,6).

Formed by the physical intercohesion forces among the rigid segments, the fringed micelle crystallites as the crosslinks would be weaker than the chemical covalent crosslinks. The physical crosslinks could be partially or completely decrystallized at the softening point. Under these conditions the chemical covalent bonds would not be broken.

If exposed to an external stress, cured RIM elastomers containing fringed micelle crystallites as crosslinks would show a faster decay of the physical crosslinks even at a moderately elevated temperature (7). The two factors, temperature and stress, according to literature data, could be very effective in decrystallization of the fringed micelle nuclei (7,8).

The determination of crosslink densities, covalent, and physical, at various temperatures by the stress relaxation method could help to elucidate to what degree and at what conversion level the fringed micelle crystallites would cause and affect the deviation from the straight line dependence.

At higher extensions of 300% and over, the fringed micelle aggregates would be oriented in the direction of the stress. Some bonds would rearrange, some new intermolecular physical bonds would be formed, and the system would result in a substantial permanent set. When dealing at a high extension with RIM elastomers of even moderate crystallinity, a permanent set proportional to the content of the crystalline portion could be expected (6).

Incorporating a plasticizer into the RIM formulations as a non-volatile residual solvent should at least partially inhibit the formation of the fringed micelle crystallites and thus depress the build-up of physical crosslinks by the aggregation of crystallites.

The goals of this study were determined by the above considerations. They were:

- what influence rigid-flexible segment ratios would have on the conversion level of the reaction at the deviation point;
- to what degree the plasticizer content would inhibit the development of physical crosslinks produced by the fringed micelle nuclei, and how it would relate to the conversion level at the deviation point;
- what influence the rising temperature would have on decrystallization of fringed micelle crystallites;
- what type of correlation existed between the physical crosslink decay, determined by stress relaxation method and by DSC exotherm-endotherm scans.

Experimental

Adiabatic Reaction. The experiments were conducted in an adiabatic reactor constructed at the laboratory of the Polymer Institute consisting of a 250 mls polyester container well insulated with a thick wall of a polyurethane foam poured in situ.

The adiabatic reactor, discussed and described in a series of papers (9,10,11,12), was suitable for fast exothermic urethane RIM reactions. It did not require sophisticated insulated equipment. Because of the high speed of the urethane RIM reaction and poor thermal conductivity of the reactants, the heat losses were minimal, particularly when the thermocouple was inserted into the center of the charge of the reactants.

The Arrhenius equation and the energy balance equation were used to obtain a modified version of the equation for the second order adiabatic reaction kinetics.

The Arrhenius equation for the second order reaction is:

$$k = A \cdot e^{-\Delta E/RT} \cdot C^2 \quad (1)$$

The energy balance equation is:

$$\begin{aligned} \rho \cdot C_p(T) \frac{dT}{dt} &= k(-\Delta H) \\ k &= \frac{\rho \cdot C_p(T)}{\Delta H} \frac{dT}{dt} \end{aligned} \quad (2)$$

The second order adiabatic reaction kinetic equation was obtained by combining Equations 1 and 2:

$$\frac{\rho \cdot C_p(T)}{-\Delta H} \frac{dT}{dt} = A \cdot e^{-\Delta E/RT} \cdot C^2 \quad (3)$$

The above equation in natural logarithm form is:

$$\ln \frac{\rho \cdot C_p(T)}{-\Delta H} \frac{dT}{dt} = \ln A \cdot C^2 - \frac{\Delta E}{RT} \quad (4)$$

The final form of the adiabatic reaction equation was obtained by moving the changeable value C from the right side of the equation to the left side and replacing it on the right side with the constant value of C_0 :

$$\ln \frac{\rho \cdot C_p(T)}{-\Delta H \cdot C_0 \left(\frac{C}{C_0}\right)^2} \frac{dT}{dt} = \ln A \cdot C_0 - \frac{\Delta E}{RT} \quad (5)$$

The left part of this equation was plotted on the ordinate, and the Kelvin temperature reciprocal $1/T$ on the abscissa. The necessary values were obtained experimentally, graphically, or were calculated by a regression method using a computer where:

$$\begin{aligned} \rho &= \text{density, g/cc} \\ C_p &= \text{heat capacity, cal.g}^{-1} \cdot \text{o.K}^{-1} \end{aligned}$$

- T = temperature, °K
 t = time, min.
 k = reaction rate, equivalent⁻¹·l⁻¹·min⁻¹
 H = heat of reaction, cal.mole⁻¹ of NCO
 A = activation energy, kcal.mole⁻¹ of NCO
 R = gas constant, 1.987 cal. mole⁻¹·°K⁻¹
 C₀ = initial concentration of isocyanate, equiv.·l⁻¹
 C = concentration of isocyanate at time t, equiv.·l⁻¹

RIM Formulations with Various Amounts of Rigid Segments.

1. Compositions of formulations. Five RIM elastomers A, E, F, G, and H, containing rigid segments in the range from 54.8 to 13.2%, were evaluated in the adiabatic reactor. Their compositions are presented in Table I. The components of the rigid segments were 1,4 butanediol and 4,4' methylene bis(phenylisocyanate), MDI. A high molecular triol, a polyoxypropylene derivative of glycerine modified with 10% acrylonitrile and 10% styrene, constituted the flexible amorphous part of the elastomer. A slow reacting triol was a good suspending medium for the fast reacting rigid segment. Such a composition of RIM formulation established favorable conditions to synthesize an orderly structure of the elastomer polymer with regularly repeating rigid and flexible segments. A regularly structured polymer (7) tended to crystallize rapidly in the polymerization process.

2. Kinetics of urethane RIM reaction in adiabatic reactor. The polyols of five RIM formulations (Table I) were thoroughly demoisurized at 60°C under vacuum. The reactants, polyols and quasi-prepolymer, based on MDI, were compounded in a dry container under a dry nitrogen blanket. After a thorough blending for 15 seconds by a mechanical stirrer, the reactants were poured into the adiabatic reactor. A thermocouple was inserted through an insulating cover into the center of the charge of the reactants.

The adiabatic temperature rise was continuously recorded. At ten-second intervals the samples were taken from the reactor for determination of isocyanate content. The withdrawn samples were poured into Erlenmeyer flasks containing exactly measured amounts of dibutylamine in toluene solution prepared in advance. The depletion of isocyanate was determined by the back titration with a standard HCl solution, ASTM 1638-70.

Time t, adiabatic rise of temperature T°K, and concentration of isocyanate C and C₀ were experimentally determined and recorded (Table II, columns 1, 2, and 6). Other values were programmed by a regression method using a computer (Table II, columns 3, 4, 5, 7, and 8). The initial concentration C₀ of isocyanate for each of the five elastomers, expressed in equivalents per liter, as well as density values, were calculated and compiled in Table I.

The kinetic adiabatic data of all these five elastomers were plotted with

$$-\ln x = -\ln \frac{\rho \cdot C_p(T)}{(\Delta H) \cdot C_0 \cdot (C/C_0)^2} \cdot \frac{dT}{dt}$$

on the ordinate axis, against the reciprocal of Kelvin temperature 1/T, on the abscissa.

The adiabatic reactor data for all five RIM elastomers with rigid segments from 54.8% to 13.2% were plotted in Figures 1, 2, 3, 4, and 5. The graphs presented a clear picture of the influence the

rigid-flexible segment ratio of the urethane RIM elastomer formulation had on the conversion level of the urethane RIM reaction at the deviation point. In Figure 6 the adiabatic temperature rise data versus the rigid segment contents were put together.

Table I. Urethane RIM Samples with Decreasing Contents of Rigid Segments

Designation of RIM Components	A	E	F	G	H
Polyoxypropylene derivative of TMP, equiv.	1	1	1	1	1
parts by wt.	2078	2078	2078	2078	2078
1,4-Butanediol, equiv.	12	9	6	3	1.5
parts by wt.	540	405	270	135	67.5
Quasi-prepolymer, equiv.	13	10	7	4	2.5
parts by wt.	2392	1840	1288	736	460
Initial concentration of isocyanate, equiv./liter	2.869	2.482	2.041	1.413	0.987
Theoretical crosslink density, $C_T \times 10^{-4}$ moles/cc	0.705	0.857	0.986	1.200	1.350
Rigid segment, (calculated) % by wt.	54.8	47.7	38.0	23.5	13.2
Flexible segment, (calculated) % by wt.	45.2	52.3	62.0	76.5	86.8
Tensile strength, psi	5138	3842	2921	2392	2092
100% Modulus, psi	3450	3260	1520	687	458
Elongation, %	403	460	500	600	650
Permanent set, %	110	80	60	55	12

Urethane RIM Elastomers Modified with Plasticizer. The standard RIM elastomer A (Table I) containing 54.8% of rigid segments was modified with plasticizer, tributyl phosphate, as follows: elastomer B with 5%, elastomer C with 10%, and elastomer D with 15%. The composition of all four of these elastomers is presented in Table III.

The kinetic tests of these elastomers were conducted in the same adiabatic reactor as described above. The main goal of evaluation of this group of elastomers was to determine the effect of the content of plasticizer on inhibition of the lateral intercohesion forces between the interspaces of the crystalline aggregates. The kinetic data were obtained experimentally, calculated by a regression method using a computer and graphically from the plots as above. The data obtained are presented in Figure 7.

Physical Properties of RIM Elastomers. The elastomers were compounded from demoiaturized and purified polyols and quasi-prepolymer. The well blended components were vacuumized and molded in steel molds measuring 6"x6"x0.070". The samples were cured for 1 hour at 120°C, conditioned for 1 week and submitted for determination of physical properties by Instron. The permanent sets were determined at an extension of 300%. The results are compiled in Tables I and III.

Table II. Values of the RIM Elastomer E from Adiabatic Reactor Programmed Using a Computer

From Adiabatic Reactor		Programmed by Regression Method Using a Computer					
Time t, sec.	Temp T, °K	$\frac{1}{T} \text{ K}^{-1}$	$\frac{dT}{dt}$	$C_p(T)$	$\frac{C}{C_o}$	$(\frac{C}{C_o})^2$	-ln X
0.0	306.3	.3265E-02	18.0	0.474	0.974	0.948	1.506
10.0	309.3	.3234E-02	13.5	0.475	0.939	0.881	1.718
20.0	311.5	.3210E-02	22.5	0.476	0.912	0.832	1.148
30.0	315.3	.3172E-02	30.0	0.477	0.868	0.754	0.754
40.0	320.3	.3123E-02	55.5	0.479	0.809	0.655	-0.001
50.0	329.0	.3035E-02	93.0	0.482	0.670	0.489	-0.816
60.0	345.0	.2899E-02	93.0	0.488	0.514	0.264	-1.444
70.0	360.0	.2774E-02	60.0	0.494	0.326	0.106	-1.927
80.0	370.0	.2700E-02	33.0	0.498	0.204	0.042	-2.277
90.0	376.0	.2660E-02	18.0	0.500	0.136	0.019	-2.482
120.0	382.0	.2617E-02	9.0	0.502	0.062	0.004	-3.366
150.0	384.9	.2598E-02	2.4	0.503	0.028	0.001	-3.732
180.0	386.10	.2590E-02	1.5	0.504	0.011	0.0001	-5.004
210.0	386.7	.2586E-02	0.75	0.504	0.003	0.0000	-6.682

Effects of Temperature on Physical Crosslinks Induced by Crystallites.

All five RIM elastomers, containing different amounts of rigid segments, and four RIM elastomers A, modified with a plasticizer, were evaluated for crosslink densities by stress relaxation method at a low extension of 50% and at three temperatures of 25°C, 50°C, and 100°C. Crosslink densities, c_r , were calculated using Equation 6:

$$\frac{3}{2} c_r \cdot RT = f\left(\alpha - \frac{1}{\alpha^2}\right) = \frac{d}{M_{c,r}} \cdot RT \quad (6)$$

The number average molecular weight between the crosslinks, $M_{c,r}$, could be calculated as well using the same equation. The values and dimensions of the equation are:

c_r = crosslink density or moles of effective crosslinks per unit volume x 10⁻⁴ moles/cc

R = gas constant, 8.313 x 10⁷ ergs/degree-mole

T = absolute temperature in Kelvin degrees

f = force per unit area of the original cross-section in dynes/square cm

L/L_o = extension ratio, L=stretched length, L_o=original length

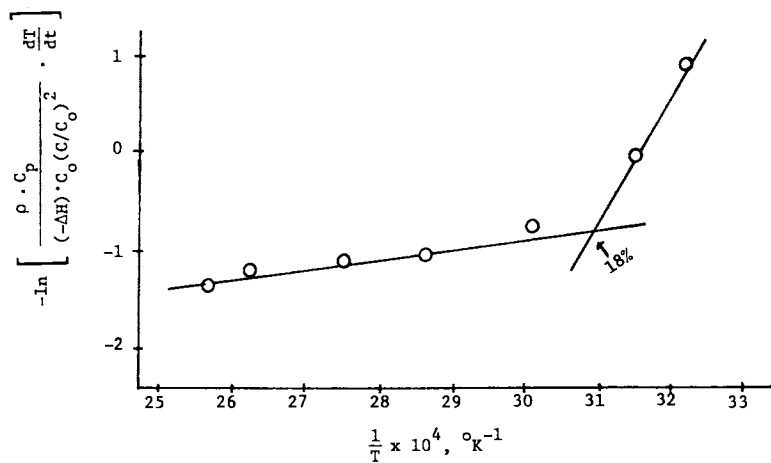


Figure 1. Kinetic plot of urethane RIM sample A with 54.8% rigid segment.

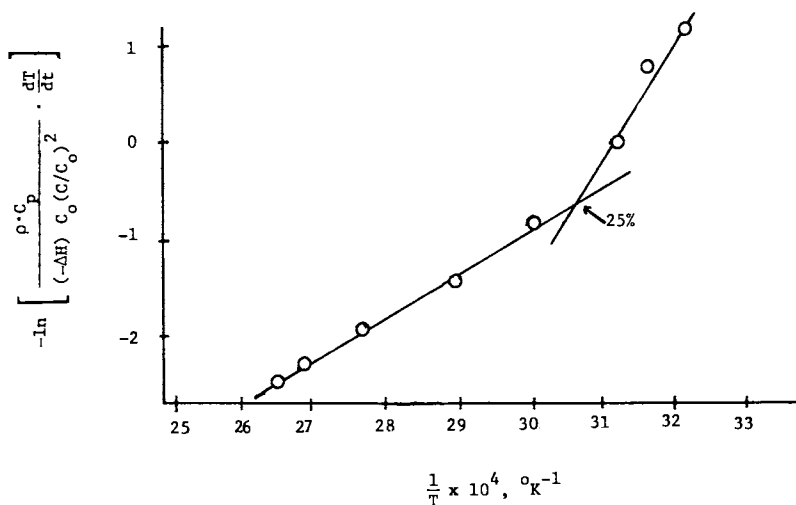


Figure 2. Kinetic plot of urethane RIM sample E with 47.7% rigid segment.

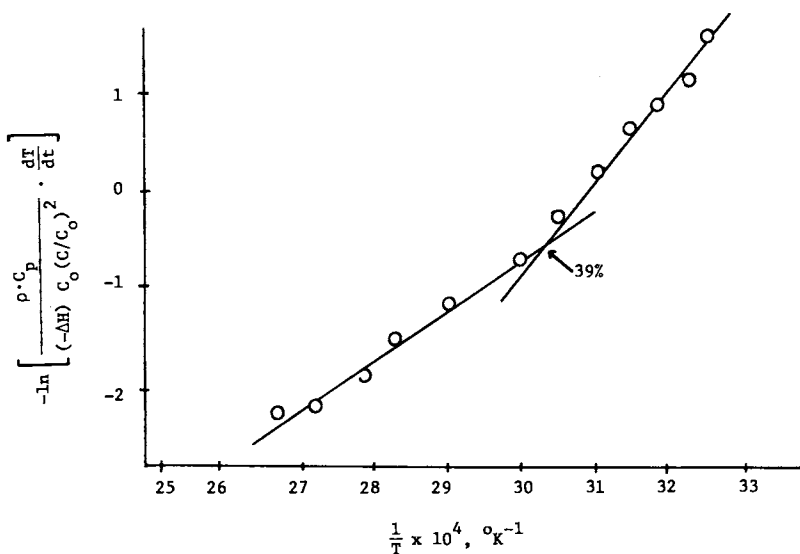


Figure 3. Kinetic plot of urethane RIM sample F with 38% rigid segment.

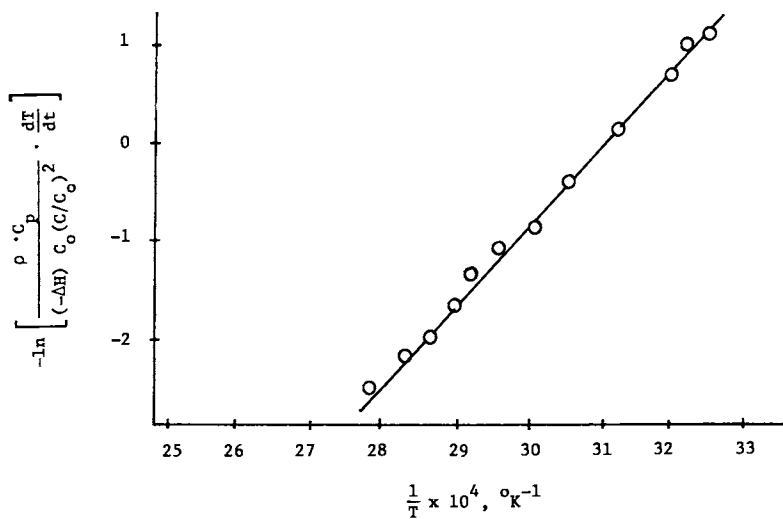


Figure 4. Kinetic plot of urethane RIM sample G with 23.5% rigid segment.

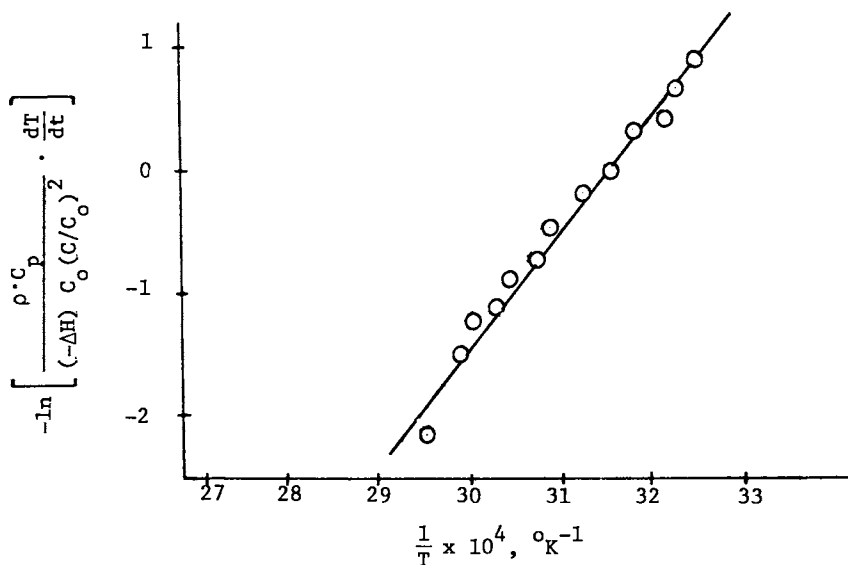


Figure 5. Kinetic plot of urethane RIM sample H with 13.1% rigid segment.

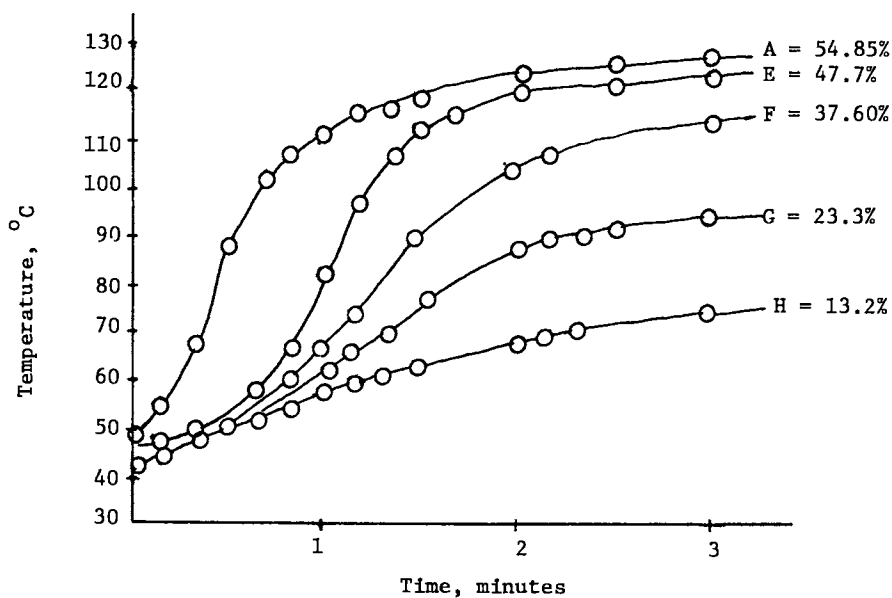


Figure 6. Effect of rigid segment on adiabatic reaction temperature.

d = density, g/cc
 $M_{c,r}$ = number average molecular weight of network chain
 between the crosslinks by stress relaxation.

The stress relaxation method was employed here for determination of total crosslink density, consisting of covalent crosslink density and of crosslink density caused by physical bonding of the rigid segment crystallites. The crystalline aggregates acted as physical crosslinks at ambient and at moderately elevated temperature (5,6).

Exposing the RIM elastomers to stress relaxation at low extension at three levels of temperature, the changes obtained in experimentally determined crosslink densities, minus the covalent calculated crosslink densities, indicated how fast the crystalline micelles were decaying at the elevated temperatures. The data obtained were recorded in Tables VI and VII.

Table III. Urethane RIM Samples with a Plasticizer Composition

Designation of RIM	A	B	C	D
	percents by weight			
Polyoxypropylene derivative of TMP, modified with acrylonitrile and styrene	41.46	39.40	37.30	35.23
1,4-Butanediol	10.78	10.24	9.70	9.26
Quasi-prepolymer, based on MDI, NCO equiv. 184	47.76	45.36	43.00	40.51
Plasticizer, tributyl phosphate	0.0	5.00	10.00	15.00
Moles of chemical crosslinks per 10^4 cc of polymer	0.705	0.669	0.636	0.606
Tensile strength, psi	5138	4544	2067	2786
Elongation, %	403	500	275	170
100% Modulus, psi	3450	2320	1820	1450
Permanent set, %	120	100	20	26

DSC Scans of RIM Elastomers. DSC measurements were run on five RIM elastomers, A,E,F,G, and H, in a Perkin-Elmer DSC-2 at $10^\circ\text{K}/\text{min.}$, 0.5 mcal/sec. , on $15 \pm 3 \text{ mg.}$ The elastomers were examined at the temperatures $300\text{--}520^\circ\text{K.}$ The data are presented in Figure 8.

Results and Discussions

Effect of RIM Composition on the Deviation Point from Straight Line Dependence. The data in Figures 1,2,3,4, and 5, and in Table IV indicated that the deviation point decisively depended on the amount of rigid segment in the elastomer formulation. The higher the content of rigid segment, the lower was the conversion level (RIM elastomers A,E and F in Figures 1,2 and 3). The urethane RIM elastomers G and H with relatively low amounts of rigid segment did not show any deviation from the straight line dependence (Figures 4 and 5).

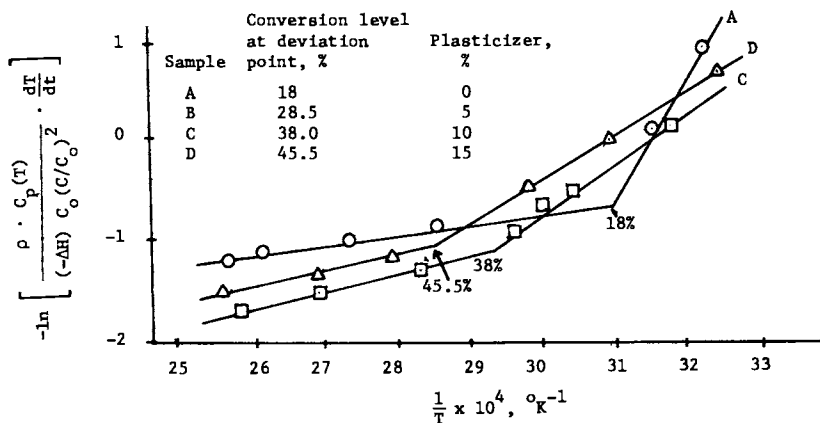


Figure 7. Effect of plasticizer on the conversion level at the deviation point.

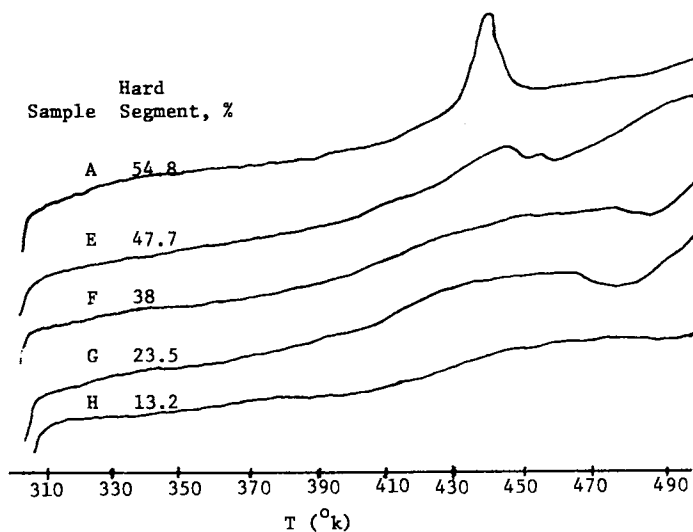


Figure 8. DSC scans of RIM elastomers with hard segment contents in the range of 54.8 - 13.2%.

A formulation similar to our elastomer A was reported by T.B. Lin in his doctoral thesis. The only difference was in the type of diisocyanate - our formulation was based on aromatic diisocyanate (MDI), and Lin's formulation was based on aliphatic diisocyanate, 1,4-isocyanatomethyl cyclohexane (p-BDI). 58% conversion level at deviation point was for the RIM elastomer based on aliphatic diisocyanate at triol-1,4 butanediol weight ratio of 70:30. 18% conversion level was for the elastomer A, based on aromatic diisocyanate at triol-1,4 butanediol weight ratio of 70:30. The effect of the aliphatic diisocyanate causing deviation from the straight line dependence was weaker than that of the aromatic diisocyanate.

Another example indicating the effect of RIM elastomer composition on the deviation from straight line dependence was taken from the paper of Stephen D. Lipshitz and Christopher W. Macosco (15).

The urethane formulation presented in the paper was based on 1,6 hexamethylene diisocyanate (HDI), an aliphatic diisocyanate, and on tripropylene glycol (TPG) prepolymer, cured with a medium molecular size triol with an equivalent weight per OH of 180 (mol. wt. 540). This formulation did not have rigid segments for formation of fringed micelle crystallites as physical crosslinks. Therefore, the kinetic plot of the adiabatic reaction data resulted in a straight line without any deviation point.

Table IV. Conversion Levels at Deviation Points from the Straight Line Dependence

Designation of RIM Elastomer	A	E	F	G	H
Content of rigid segment, %	54.34	47.70	37.60	23.30	13.20
Conversion level at deviation point, %	18.00	25.00	39.00	no deviation	

Effect of Plasticizer on Conversion Level at the Deviation Point.

The effect of plasticizer on the conversion level at the deviation point was very apparent (Table V, Figure 8). At 10% of plasticizer addition, the conversion level at deviation point increased twice (Table V, elastomers A and C).

The incorporation of plasticizer into the RIM elastomer A inhibited the formation of crystalline aggregates. The physical crosslink densities were significantly decreasing with the increasing amount of plasticizer (Figure 9).

Effect of Elevated Temperature on Decay of Physical Crosslinks.

1. RIM elastomers A,E,F,G and H with decreasing amount of rigid segments. The elastomers A,E,F,G and H (Table I) with decreasing amounts of rigid segments resulted in successively decreasing amounts of physical crosslinks densities (Table VI, Figure 10). The crosslinks caused by crystalline aggregates degraded with the rising

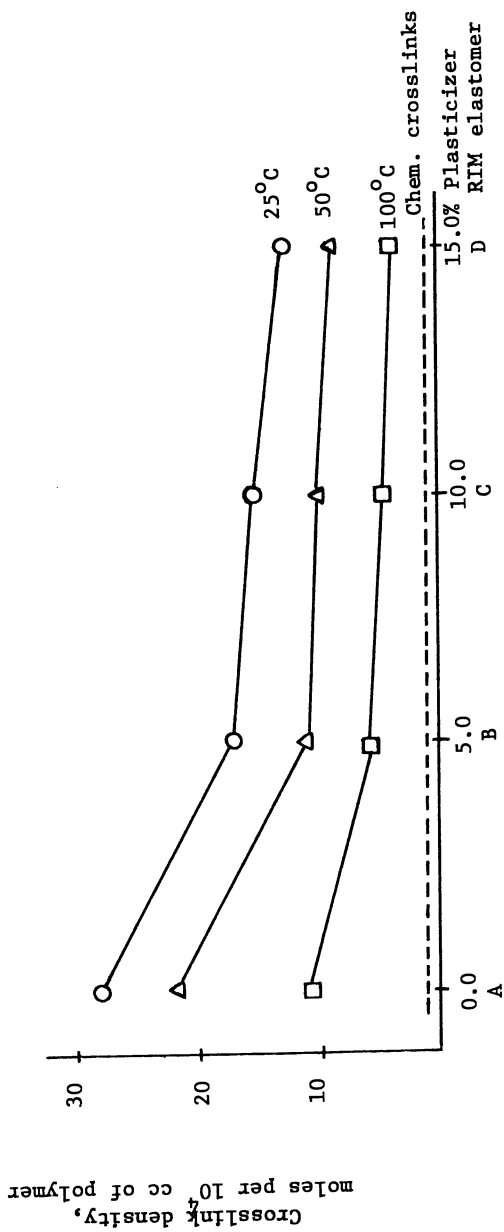


Figure 9. Decay of physical crosslink density with rising temperature in the presence of plasticizer.

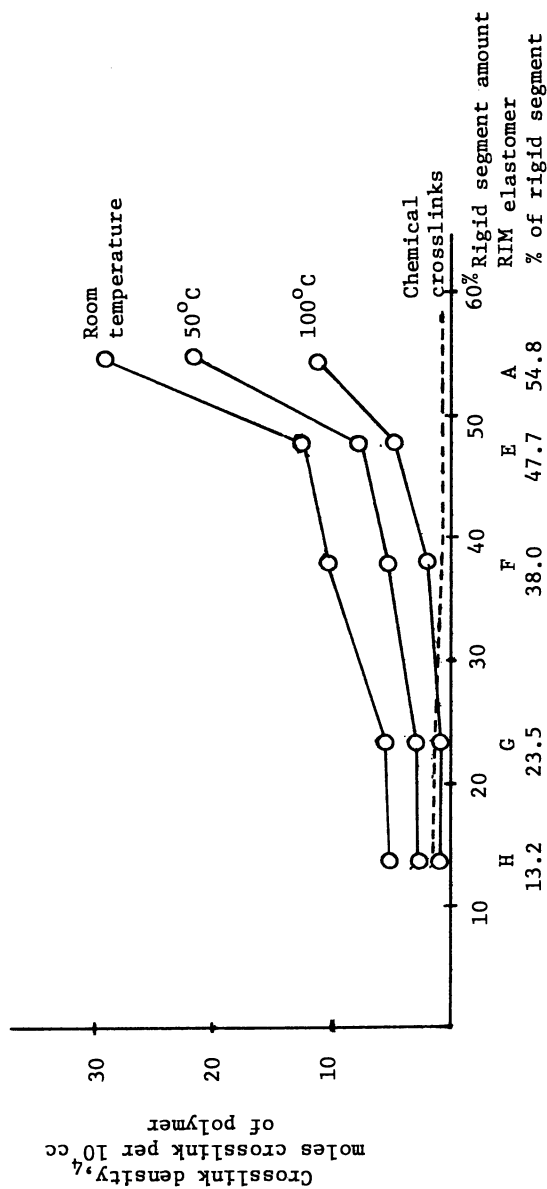


Figure 10. Decay of physical crosslink density with rising temperature at various rigid segment amounts.

temperature. Elastomer A, containing 54.8% of rigid segments, rapidly decreased in crosslink density with rising temperature, but even at 100°C still did not reach the level of the covalent crosslink density of 0.705 moles per 10⁴ cc of the polymer content. Approximately 37.2% of the physical crosslinks were still holding after one hour at 100°C. After one hour at 100°C, the elastomers E and F were closer to the covalent crosslink density. Approximately 20.8% of the physical crosslinks of the elastomer E and 3.5% of the elastomer F were still holding after one hour at 100°C. The elastomers G and H, which did not show any deviation from the straight line dependence, at 100°C have lost all physical crosslink density and even a small fraction of the covalent crosslink density. The data indicated that the content of rigid segments had a decisive effect on the retention of physical crosslinks, even at 100°C.

Table V. Effect of Plasticizer on the Conversion Level at the Deviation Points from Straight Line Dependence

Designation of RIM	A	B	C	D
Content of plasticizer, %	0.0	5.0	10.0	15.0
Conversion level, %	18.0	28.0	38.0	45.5

Table VI. Effect of Rigid Segment Content on Crosslink Density of RIM by Stress Relaxation

Designation of RIM % of Rigid Segment	A	E	F	G	H
Crosslinks in Moles per 10 ⁴ cc of Polymer	54.8	47.7	38.0	23.5	13.2
Of chemical network	0.705	0.816	0.972	1.20	1.36
Of actual physical and chemical network,					
Room temperature	28.10	12.36	10.63	5.13	5.20
50°C	21.82	7.34	5.58	3.02	3.10
100°C	11.00	3.22	1.31	1.04	1.12
Physical crosslinks not broken at 100°C in 1 hr.	37.21%	20.82%	3.50%	-	-

2. RIM elastomers A,B,C and D with increasing amount of plasticizer. The conversion level at deviation points increased with the increasing amount of plasticizer (Table V, Figure 9). Addition of plasticizer to the elastomer formulation inhibited the tendency to form fringed micelle crystallites, thus, with the increasing content of plasticizer, the physical crosslink density was significantly decreased. 5% plasticizer, added to the elastomer A, did not significantly decrease the tensile strength (Table III, B), increased elongation, and significantly decreased the physical crosslink density (Table VII, Figure 9). With increasing temperature, the elastomers

with low quantities of plasticizer lost the physical crosslink densities at the same rate as the non-plasticized elastomers (Table V).

Table VII. Effect of Plasticizer on the Actual Crosslink Density by Stress Relaxation

Designation of RIM % of Plasticizer	A	B	C	C
Crosslinks in Moles per 10 ⁴ cc of Polymer	0.0	5.0	10.0	15.0
Of chemical network	0.705	0.669	0.636	0.606
Of actual physical and chemical network,				
Room temperature	28.10	17.10	14.10	12.71
50°C	21.82	11.10	10.20	8.79
100°C	11.00	5.89	4.70	3.94
Physical crosslinks not broken at 100°C in 1 hr.	37.10%	31.77%	30.19%	27.54%

Permanent Set of Urethane RIM VS. Content of Rigid Segment. The permanent set, as reported in Tables I and II, was obtained at 300% elongation. The fringed micelle crystallites, exposed to such high extension, seemingly realigned in the direction of the stretch and formed new physical bonds which were permanently stable (17). The permanent set data in Table I indicated that the permanent set decreased with the decreasing content of the rigid segments of the RIM formulation. The permanent set data in Table III indicated that the permanent set decreased with increasing amounts of plasticizer (6). The correlation of the permanent set data with the content of the rigid linear segments, and the effect of the amount of plasticizer on the physical crosslink densities, indirectly indicated the presence of crystalline aggregates in the systems.

DSC Scans. The endothermic peaks of the DSC scans of the urethane RIM elastomers appeared in the area of 440°K (167°C). These peaks were more pronounced with the higher content of rigid segments than with the lower content of rigid segments.

The RIM elastomer A, exposed to the stress relaxation test after one hour at 100°C, was able to retain only 37.2% of its physical crosslinks. The dissipation of crystalline aggregates by the DSC measurements occurred at a temperature approximately 50° higher than determined by the stress relaxation method. Seemingly, the stress which was applied in the process of the stress relaxation method was an additional factor enhancing decrystallization of the physical crosslinks.

Conclusions

RIM elastomers based on aromatic diisocyanates and short linear diols are more inclined to form crystalline aggregates than the identical formulations based on cycloaliphatic and linear aliphatic diisocyanates and short linear diols.

The higher the rigid segment content, the lower the conversion level at the deviation point from the straight line dependence.

RIM elastomers without crystallizing components show no deviation from the straight line dependence of the kinetic plots.

Small amounts of plasticizer included in RIM formulations inhibit the formation of crystalline aggregates and the development of physical crosslinks.

The crystalline aggregates, probably the fringed micelle crystallites, act as physical crosslinks and decrystallize at elevated temperatures. RIM elastomers containing a higher content of rigid crystallizing segments show more resistance to thermal decay.

The decay of physical crosslinks determined by the DSC measurements occurs at a higher temperature than determined by the stress relaxation method.

Seemingly, stress is another factor besides temperature that enhances the decrystallization of the physical crosslinks.

Literature Cited

1. Dusek, K. J. Pol. Sci. 1967, 16, 1289-1299.
2. Bobalek, E.C.; Moore, E.R.; Levy, S.S.; Lee, C.C. J. Appl. Sci. 1964, 8, 625.
3. Lipatova, T.E. Pure and Appl. Chem. 1975, 47, 23.
4. Flory, P.J. J. Amer. Chem. Soc. 1962, 84, 2857.
5. Wunderlich, B. "Macromolecular Physics"; Academic: New York, 1976; Vol. II, pp. 16-17.
6. Meares, P. "Polymer Structure and Bulk Properties"; Van Nostrand: London, 1965; pp. 117-118, pp.154-156, pp. 230-233.
7. Rodriguez, F. "Principles of Polymer Systems"; McGraw-Hill: New York, 1970; pp. 3, 29 and 34.
8. Samuels, R.J. "Characterization of Deformation of Polycrystalline Polymer Films"; Sweeting, O.J., Ed.; Interscience: New York, 1968; Vol. 1, pp. 258-260.
9. Parts, A.G. Australian J. of Chem. 1959, 11, 251.
10. Douglas, J.M.; Eagleton, L.C. I. & E. C. Fundamentals 1962, 1, 116.
11. Allen, E.L. I. & E. C. Fundamentals 1969, 8, 828.
12. Camargo, R.E.; Macosko, C.W.; Tirrel, M.; Wellinghoff, S.T. Pol. Eng. Sci. 1982, 22, 719.
13. Damusis, A.; Asch, W.; Frisch, K.C. J. Appl. Pol. Sci. 1965, 9, 2965-2983.
14. Lin, T.B. Ph.D. Thesis, University of Detroit, Detroit, 1982.
15. Lipshitz, S.D.; Macosko, C.W. J. Appl. Pol. Sci. 1977, 21, 2029-2039.
16. Turner, R.B.; Spell, H.L.; Vanderhider, J.A. "Urethane RIM Elastomers"; Kresta, J.E., Ed.; Plenum Press: New York, 1982; p. 63.

17. Sweeting, O.J.; Lewis, R.N. "Molecular Constitution of Polymers"; Sweeting, O.J., Ed.; Interscience: New York, 1968; Vol. I, p. 35.
18. Cobler, J.G.; Long, M.W.; Owens, E.G. "Crystallinity and Melting Temperature"; Sweeting, O.J., Ed.; Interscience: New York, 1968; Vol. I, p. 728.

RECEIVED October 5, 1984

Structure-Property Relationships in RIM Polyurethanes

N. BARKSBY¹, D. DUNN¹, A. KAYE², J. L. STANFORD¹, and R. F. T. STEPTO¹

¹Department of Polymer Science and Technology, University of Manchester, Institute of Science and Technology, Manchester, M60 1QD, England

²Department of Mathematics, University of Manchester, Institute of Science and Technology, Manchester, M60 1QD, England

Polyurethane (PU) materials have been formed by RIM using a commercial isocyanate reacting with either various compatible or incompatible polyol blends, or with slurries containing polyol blends and glass fibres. The RIM equipment used, modified with a special dosing unit for processing glass fibre/ polyol slurries, is described. Polyol blend composition, varied by using different proportions of high and low molar mass triols and a chain extender, resulted in PUs with various hard block contents and crosslink densities. Tensile, flexural and dynamic mechanical properties at different temperatures have been investigated for the various PUs which ranged (at ambient temperature) from soft elastomers to stiff, yielding plastics. In this study, the use of incompatible polyol blends produced well phase-separated PUs for which the property-temperature dependence (-50 to 100°C) is much less than for PUs formed from compatible polyol blends. At elevated temperatures (>150°C), PUs formed from compatible polyol blends, containing higher proportions of low molar mass triols, retained their mechanical integrity compared with the rapid deterioration, (due to hard-phase melting), observed in the phase-separated PUs. Filled PUs showed the expected increases in stiffness and strength with concomitant decreases in elongation. Property changes in these composites are related to fibre loading and aspect ratio.

Formulations for producing polyurethanes (PUs) by reaction injection moulding (RIM) usually contain mixtures of polyols and diols in order to achieve the desired properties in the moulded part. The present work forms part (1) of a systematic investigation into the effects of polyol blends and glass fibres on the physical properties of unfilled and filled PUs formed by RIM. In the case of unfilled PUs, by using a multi-component polyol mixture, it is possible to investigate the effects on properties of (a) polyol structure, molar mass and functionality, (b) the relative proportions of diol-based hard blocks and triol-based soft blocks and (c) polyol blend compatibility. The

0097-6156/85/0270-0083\$06.00/0
© 1985 American Chemical Society

properties of filled PUs are determined primarily by the loading and aspect ratio (length-to-diameter) of glass fibres incorporated in the RIM composite materials. In either case, processing variables such as isocyanate/polyol reactant ratio, mould temperature and thickness used during RIM will also affect final materials properties.

RIM-PU Reaction Systems

The commercially available materials used in these studies included Suprasec VM10 isocyanate, PBA1478 polyol blend and Daltocel T32/75 triol (all ex. ICI Polyurethanes), LHT240 triol (ex. Union Carbide) and ethylene glycol. PBA1478 is an incompatible blend of polyols containing added catalysts, and T32/75 is a polyoxypropylene (POP) triol tipped with polyoxyethylene (POE) units, with POP:POE units in the weight ratio 85:15. The molar mass (M) of T32/75 is $5,260\text{g mol}^{-1}$, and in the present studies it was used in admixture with LHT240, a POP triol of lower $M(720\text{g mol}^{-1})$ and ethylene glycol (EG) as chain extender. The isocyanate used (VM10) has an isocyanate value of 26% (2) and is based on 4,4-diphenylmethane diisocyanate (MDI) and oligomers thereof. Two series of RIM materials based on VM10 isocyanate were prepared, designated Series I and Series II.

Series I: PUs using the incompatible PBA1478 unfilled and filled with hammer milled glass (HMG) and chopped strand glass (CSG). The hammer milled fibres (ex. Turner Bros.) had nominal mean length and diameter of $70\mu\text{m}$ and $12\mu\text{m}$: the chopped fibres (ex. Pilkington Fibreglass) were of uniform length and diameter, 1.5mm and $17\mu\text{m}$, respectively.

Series II: Unfilled PUs using various compatible polyol blends (PB) in which the code numbers in Table I represent in order the weight ratios of polyols T32/75, LHT240 and EG. A mixture of triethylene diamine and dibutyltin dilaurate was used as catalyst throughout. The various polyol-based reactants and derived RIM PUs are summarised in Table I, including isocyanate/hydroxyl ratios (multiplied by 100), expressed as the System Index. Thus, 100I represents stoichiometric equivalence, 104I a 4% excess by weighted equivalents of isocyanate and 97I a 3% excess of hydroxyl.

Description and Operation of RIM Equipment

A range of PU materials was produced in-house, using development filled-RIM equipment based on a Viking Engineering machine, model HP90, capable of operating up to a maximum material throughput of 90 kg min^{-1} (1.5kg s^{-1}). A schematic flow diagram of the HP90 machine is shown in Figure 1 which also shows (top right) the development dosing unit used to handle polyol slurries. For normal processing of unfilled PUs, the HP90 would not require the special dosing unit and the hydraulic tank (htp) would contain polyol, thus simplifying the polyol side to that shown in Figure 1 for the isocyanate side. Generally in filled-RIM, to avoid excessive and rapid wear of the axial piston metering pump (mpl) by the abrasive glass fibres contained in slurries, metering and dispensing of polyol slurries have to be achieved indirectly using a dosing unit which, in most commercially-available, filled-RIM machines is usually some form of positive displacement pump fitted with special wear-resistant parts. In the present machine, a novel dosing unit was used, shown

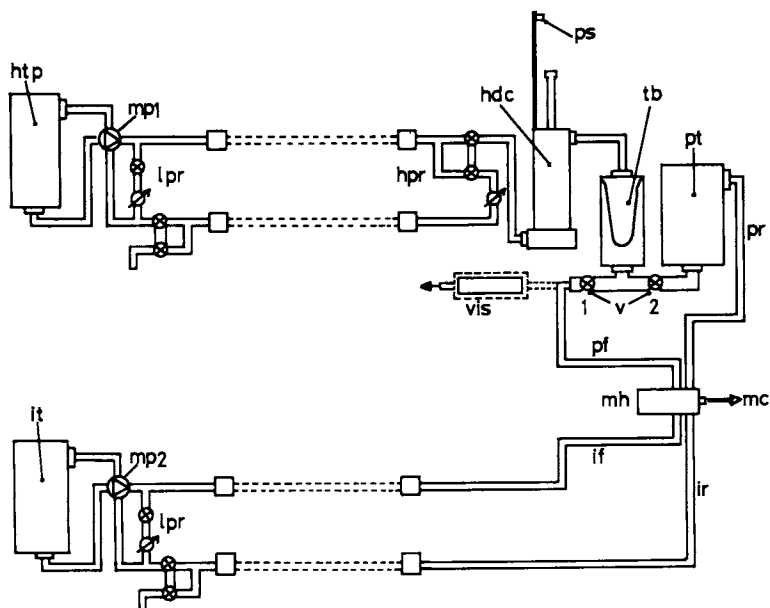


Figure 1. Schematic flow diagram of the HP90 RIM machine showing the polyol slurry dosing unit and on-line rheometer. Key: htp, hydraulic tank (for metering polyol); mp, metering pumps (1 and 2); lpr/hpr, low/high pressure recirculation loops; it/pt, isocyanate/polyol tanks; if/ir, isocyanate feed/return lines; pf/pr, polyol feed/return lines; mh, mixing head; mc, mould cavity; tb, transfer barrier; hdc, hydraulic displacement cylinder; ps, proximity switch; bv, ball valves (1 and 2); vis, viscometer.

Table I. Polyol Blends and Slurries Used with VM10 Isocyanate to Form RIM PUs

(i) = Incompatible Polyols; (c) = Compatible Polyols

*Slurry containing 18% HMG; †Slurry containing 5% CSG

	Polyol Blend/Slurry	Viscosity(25°C) Poise	Polyurethane from VM10	System Index
S				
E	PBA1478(i)	11.3	PU1478-97I	97I
R	PBA1478(i)	11.3	PU1478-104I	104I
I	PBA1478(i)	11.3	PU1478-114I	114I
E	PBA1478-H18*	15.6	PU1478-H18	104I
S	PBA1478-C5†	20.0	PU1478-C5	104I
I				
S	PB821(c)	7.7	PU821	103I
E	PB621(c)	7.8	PU621	103I
R	PB521(c)	7.7	PU521	103I
I	PB421(c)	7.5	PU421	103I
E	PB221(c)	4.3	PU221	103I
S	PB401(i)	11.1	PU401	103I
II				

in greater detail in Figure 2 in which the main feature is the transfer barrier (tb). Inside the transfer barrier, the polyol slurry is separated from hydraulic displacement fluid (hdf) by a flexible, nitrile rubber diaphragm. Polyol slurry at 25°C is contained in a separate, stirred holding tank (pt) which can be pressurized up to 10 bar and flow of material between holding tank and the bottom of the transfer barrier is controlled by ball valve 2 (with ball valve 1 closed). During dispensing of polyol slurry from the transfer barrier, ball valve (bv2) is shut and material is expelled through the 3-way ball valve (bv1) which allows flow either through the mixing head (mh) for processing PUs or through the viscometer (vis) during rheological measurements. (A fuller description of the viscometer and its operation are given in the succeeding paper (3).) The amount of polyol slurry expelled is determined using a precise volume of hydraulic fluid from metering pump (mp1) which operates the hydraulic dispensing cylinder (hdc) and displaces an equivalent amount (allowing for differential areas either side of the piston in this cylinder) of hydraulic fluid (hdf) into the top of the transfer barrier. The rubber diaphragm is expanded and expels the required amount of polyol slurry. The advantage of the transfer barrier system is that there are effectively no moving parts with the diaphragm itself being subjected to minimal stress, thus negating the abrasive nature of the slurry. Overfilling of the transfer barrier is prevented by ensuring that the total swept volume of the displacement cylinder is less than the maximum volume of the transfer barrier and by controlling the stroke of the cylinder piston with the proximity switch (ps).

During machine operation but prior to dispensing, materials are recirculated under low pressure (independently of the mixing head) to

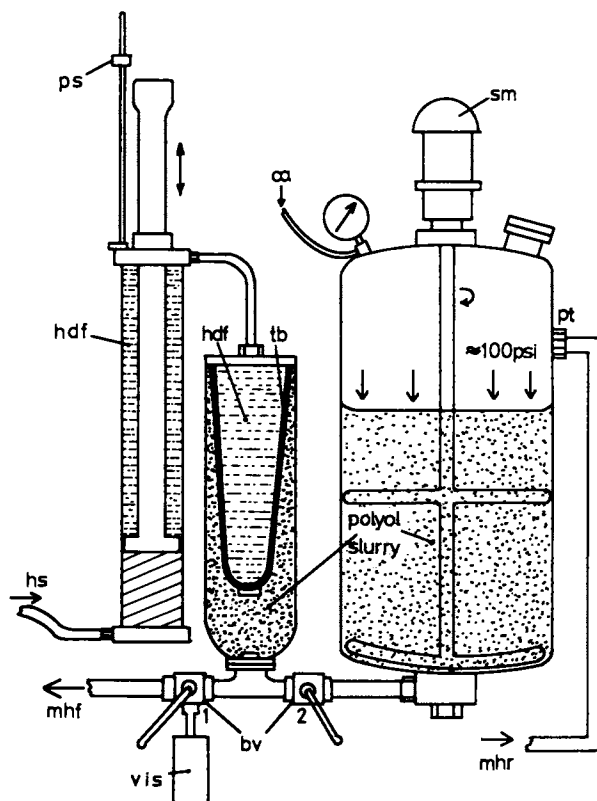


Figure 2. Schematic diagram of the RRIM dosing unit used for processing polyol slurries. Key: pt, polyol holding tank; ca, compressed air; sm, stirrer motor; hdf, hydraulic displacement fluid; tb, transfer barrier (nitrile rubber); ps, proximity switch; mhf/mhr, mixing head feed/return lines; hs, hydraulic supply from metering pump 1; bv, ball valves (1 and 2); vis, viscometer.

ensure homogeneous mixing and steady temperature/viscosity conditions. Considering Figure 1, polyol or polyol slurry is recirculated between transfer barrier (tb) and holding tank (pt) through valve (bv2) as described, whilst isocyanate is pumped to and from its holding tank (it) through a low pressure recirculation loop (&pr) using the metering pump (mp2). The machine can then be switched to a high pressure recirculation mode in which both polyol and isocyanate can be recirculated independently through the mixing head to ensure smooth flow through mixing jets/channels etc. at the potential dispensing pressure of approximately 200 bar (3,000 psi)

The mixing head used in conjunction with the modified HP90 machine is a Krauss-Maffei MK12-4K-F, fitted with a 12mm diameter, self-cleaning piston. During operation, the mixing head splits the reactant supplies into 4 streams thereby enabling 2 pairs of diametrically-opposed streams of polyol and isocyanate to impinge and mix in the circular mix chamber. The head is fitted with mixing nozzle assemblies whose orifice sizes can be continuously varied by externally adjustable pintles moving in fixed-diameter, circular jets. Thus, reactant streams pass through annular-shaped orifices whose sizes can be varied from effectively zero (pintle fully inserted, orifice completely shut) to a maximum (pintle withdrawn, orifice completely open) defined by the diameter of the circular jet. With reactant ratios, throughputs and viscosities established, efficient impingement mixing is achieved by setting the annular orifice sizes to give 200 bar (3,000 psi) pressure at the mixing head, giving corresponding reactant stream velocities of about 100 m s^{-1} .

Efficient mixing is achieved when flow conditions in the head are turbulent as defined in terms of the Reynolds number (Re) whose value should exceed a critical value (4) of about 50 for an impingement mixer. In its simplest form for flow in a circular orifice, the Reynolds number is given as

$$Re = \frac{4Q}{\pi d \mu} \quad (1)$$

where d is the orifice diameter and μ is the dynamic viscosity of the fluid. Q , the mass throughput of fluid, is given by the equation (5)

$$Q = \frac{\pi d^2 \rho k}{4} \sqrt{\frac{2g \cdot \Delta P}{\rho}} \quad (2)$$

where ρ is the fluid density, k is a nozzle factor and ΔP is the pressure drop on entering the mixing chamber. However, with the complex annular orifice arrangement in the Krauss-Maffei head, a simple definition of d in Equations 1 and 2 is impossible and only by eliminating d can an approximate expression for Re be obtained. Thus,

$$Re^2 = \frac{4Q\rho k}{\pi \mu^2} \sqrt{\frac{2g \cdot \Delta P}{\rho}} \quad (3)$$

Calculated values of Re using Equation 3, together with materials and machine variables are summarised in Table II for the various reactants described in Table I.

During RIM-PU processing, the mixing head was fixed to a

Table II. Materials and Machine Parameters Used during RIM Processing

Reactant	Viscosity, μ (P)	Throughput, Q (kg s ⁻¹)	Density, ρ (kg m ⁻³)	Reynolds Number, Re
Polyol Blends(25°C):	4.0-20.0	0.345-0.522	1036	270-615
Polyol Slurries(25°C):				
(i) PBA1478-H18	15.6	0.480	1170	206
(ii) PBA1478-C5	20.0	0.439	1068	150
Isocyanate(35°C):	1.0	0.178-0.238	1220	1980-2291

rectangular steel mould fitted with a "U"-shaped, static aftermixer connected to a runner and gate system running the entire length (700mm) of the cavity. The mould, clamped in a hydraulic press, was circulated continuously with water at 70°C with the reaction exotherm increasing the temperature of the polymerising material in the mould to about 150°C. Rectangular plaques, 700 x 400mm, of predetermined thickness in the range 1 to 6mm were produced using reproducible moulding conditions for each of the formulation systems studied. Typically, for a 3mm thick plaque (giving approximately a 1kg moulding) and with the densities and mass throughputs of reactants given in Tables I and II, mould filling times of about 1s and plaque demould times of about 60s were used during RIM processing. and toughness result from reducing plaque thickness due to alter-

Unfilled RIM-PU Materials

Initial studies on PU1478 materials showed effects on physical properties of plaque thickness and System Index used during RIM processing. Typical tensile stress-strain data are given in the first 4 columns of Table III. Increases, particularly in modulus, elongation

Table III. Tensile Properties (23°C) of PU1478 Materials, Effects of Plaque Thickness, System Index and Filler (*Filled materials formed using incompatible polyol blend PBA1478 at 104I)

Material	PU1478-97I	PU1478-97I	PU1478-104I	PU1478-114I	PU1478-H18*	PU1478-C5*
	2mm Plaque	← 3mm Plaque →				
Modulus (MN m ⁻²)	296	225	222	289	516	344
Strength (MN m ⁻²)	21	21	24	27	27	20
Elongation(%)	198	171	158	145	120	53
Toughness (MJ m ⁻³)	32	26	27	29	27	8

ations in the proportions of skin-to-core layers clearly visible within the sections of these RIM PUs. As shown by other workers (6-8) the highly exothermic PU reaction causes significant temperature gradients across the RIM mould. A variable thermal profile from the mould surface to centre has been shown to produce differences in gelation behaviour and molar mass, and complex variations in morphological structure of the PU materials (6-8).

Table III also shows the effect on tensile properties of processing RIM PUs with excess polyol (97I) and excess isocyanate (104I and 114I). Generally, as the System Index increases, the decrease in elongation is compensated by concomitant increases in modulus and strength. This combination of tensile properties is reflected in the measured values of toughness, evaluated from the integrated areas under the stress-strain curves. In general terms, these data, together with the flexural modulus-temperature behaviour shown in curves 4, 5 and 6 of Figure 4(b) later, can be interpreted in terms of the influence of reactant ratio on gelation (9) and phase separation during polymer formation, (10) resulting in different morphologies in the final RIM materials (6-8).

The PU1478 materials described were based on the incompatible polyol blend PBA1478. A second series of RIM PUs based on the compatible polyol blends PB821 to PB221 defined in Table 1 were also investigated. Changing the weight proportions of T32/75, LHT240 and EG from 8:2:1 to 2:2:1 in these blends whilst maintaining compatibility produces RIM PUs with increasing potential hard block (HB) contents in the range 34 to 53%. Ideally the HBs in these RIM PUs are dispersed in POE/POP soft blocks (SB) formed from triol mixtures of T32/75 and LHT240 with average molar masses between 2,300 to 1,270g mol⁻¹ over the same polyol composition range. For comparative purposes, an incompatible blend PB401 (containing no LHT240) was used to form PU401 from the triol T32/75 and EG resulting in a 59% HB content.

Tensile Stress-Strain. The curves shown in Figure 3(a) illustrate the progressive change in the second series of RIM materials from a soft, ductile elastomer (PU821) to a high-modulus, yielding plastic (PU221). Preliminary DSC studies indicated that extensive phase mixing or even phase inversion has probably occurred in PU221 (with the highest HB and lowest mixed triol M) and the yielding behaviour may be the result of plasticisation of an essentially continuous hard phase by a well dispersed, low molar-mass, soft phase. It is not possible on the basis of stress-strain behaviour alone to deduce the degree of phase separation resulting from the use of compatible polyol blends since comparison of PU521 and PU621 curves with PU401 (itself similar to PU1478-104I) shows little apparent difference in tensile properties as summarised in Table IV. This is to be expected on the basis of the compensating effects of the reduced molar mass of the triols (2,000g mol⁻¹) and lower HB-content (43%) in PU521 and PU621 compared with 5,300 and 59% respectively for PU401.

Flexural Modulus-Temperature Behaviour. This is shown in Figure 4(a) for various RIM materials PU821 to PU221, compared with PU401, where the effects of polyol compatibility versus incompatibility are more evident. In the compatible polyol-based series, reducing triol M (increasing crosslink density) together with increases in HB

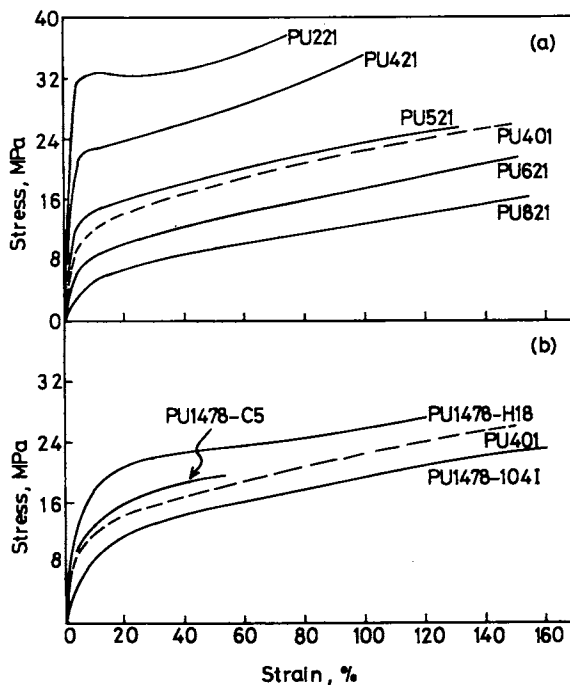


Figure 3. Tensile stress-strain curves (23°C) of RIM PUs defined in Table I. PUs formed from isocyanate VM10 and (a) compatible and incompatible polyol blends (Series II); (b) incompatible polyol blends and slurries based on PBA1478 (Series I).

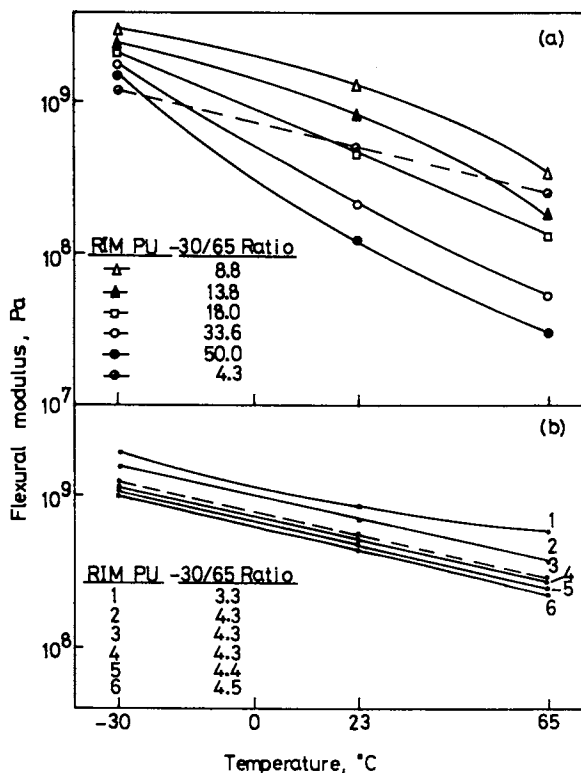


Figure 4. Variation of flexural modulus with temperature (-30°C to 65°C) for the RIM PUs in Series I and II defined in Table I. Curves show the effects on flexural modulus-temperature behaviour and $-30/65^{\circ}\text{C}$ ratios of polyol composition and added fillers. (a) Polyol blend compatibility/incompatibility: Key: Δ , PU221; \blacktriangle , PU421; \square , PU521; \circ , PU621; \bullet , PU821; \ominus , PU401. (b) Reactant ratio (System Index) and glass-fibre: Key: 1, PU1478-H18; 2, PU1478-C5; 3, PU401; 4, PU1478-114I; 5, PU1478-104I; 6, PU1478-97I. (PU401 and all PU1478 materials formed from incompatible polyol blends.)

content significantly reduces the temperature dependence of these PUs as indicated by the decreasing value (50.0 to 8.8) for the ratio of flexural moduli at -30 and 65°C (Figure 4(a)). However, comparison of PU221 with PU401 at approximately equal HB-content (53-59%) shows that despite the domination by crosslinking of the absolute

Table IV. Tensile Properties (23 °C) of RIM PUs Formed as 3mm Plaques Using Either Compatible (c) Polyols or Incompatible (i) Polyols

Material Property	PU821 (c)	PU621 (c)	PU521 (c)	PU421 (c)	PU221 (c)	PU401 (i)	PU1478 (i)
Modulus(MN m ⁻²)	109	221	464	818	1280	325	222
Strength(MN m ⁻²)	16	22	24	35	38	26	24
Yield Stress(MN m ⁻²)	-	-	-	23	33	-	-
Yield Strain(%)	-	-	-	10	13	-	-
Elongation(%)	155	152	130	100	75	147	160
Toughness(MJ m ⁻³)	17	23	23	27	24	28	27

values of flexural modulus, a "flatter" temperature dependence of PU401 is observed. This indicates the effects of good phase separation on temperature dependent properties as evidenced by the lowest flexural modulus (-30/65°C) ratio of 4.3 compared with 8.8 for PU221.

Dynamic Mechanical-Temperature Behaviour. Dynamic properties, derived from torsion pendulum (1Hz) data in terms of shear storage moduli (G' , T) and loss tangent ($\tan\delta$, T) are shown in Figures 5 and 6 respectively. Generally, in the series PU821 to PU221, increasing crosslinking and HB-content shifts the G' , T curves in Figure 5 progressively to higher temperatures. However, PU221 and PU421, despite having higher HB-contents, show no evidence of phase separation and exhibit only a single transition from glassy- to -rubbery state occurring gradually over the entire temperature range investigated (-180 to 200°C). Materials PU621 and PU821 differ slightly in that the transition from glassy- to-rubbery state occurs over a narrower temperature range with a small but distinct rubbery plateau evident at around 70°C. On the other hand, material PU401 shows distinct phase separation with good mixing between soft and hard phases, so that a more gradual transitional behaviour is observed particularly between -30 and 150°C. However, at temperatures approaching 200°C, the effect of higher crosslink densities in PU221 and PU421 become apparent and G' begins to plateau whereas G' for PU401 shows a dramatic decrease as the hard phase begins to melt.

The transitional behaviour shown in Figure 6 divides the materials into three types. PU401 is clearly phase separated showing a distinct soft phase T_g at -60°C and a hard phase T_g at 125°C. By contrast, no phase separation is apparent in PU221 and PU421 which show a single, broad T_g at about 80°C resulting from extensive segmental interaction of the various PU moieties present. For PU821 and PU621, a broader T_g is observed between -30 and 70°C containing two peaks (0°C and 40°C) attributable to phase separation between, respectively, T32/75- and LHT240-dominated PU segments in these

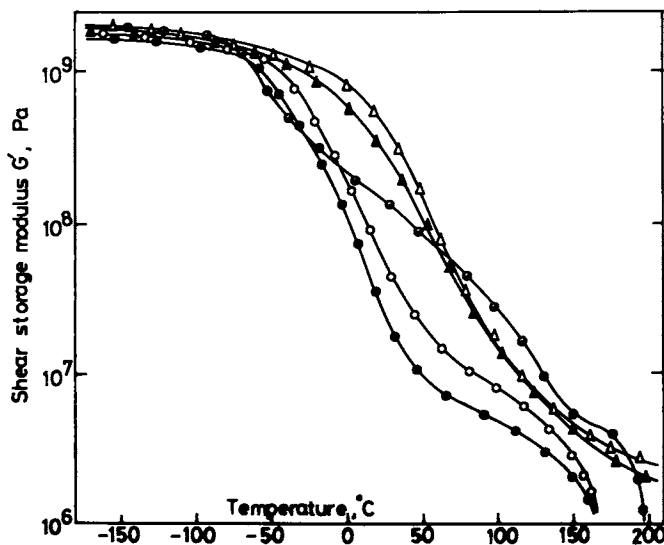


Figure 5. The effect of polyol blend composition on the dynamic storage modulus versus temperature behaviour of the unfilled RIM PUs of Series I defined in Table I. (Key as in Figure 4 (a).)

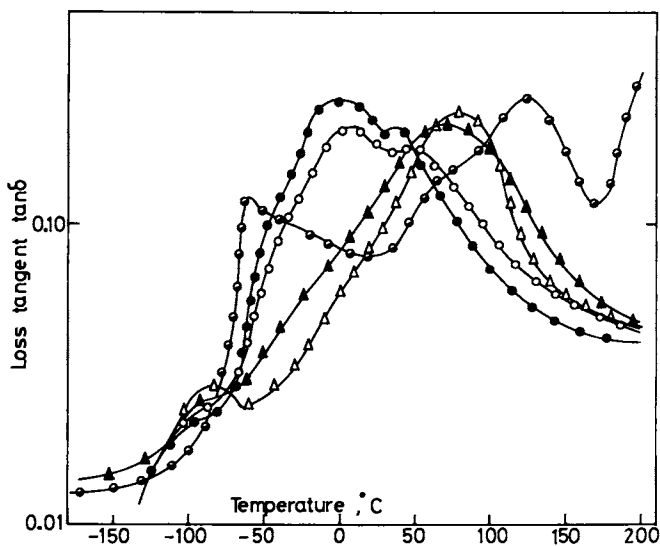


Figure 6. The effect of polyol blend composition on damping versus temperature behaviour for the RIM PUs shown in Figure 5. (Key as in Figure 4 (a).)

materials. The absence of LHT240 in PU401 is clearly evident at temperatures above 180°C where damping increases rapidly as the hard phase melts, whereas in the other PUs, damping is still decreasing as a result of the much higher crosslinking present.

In summary, the results indicate that phase separation in these segmented PUs is influenced by polyol compatibility. However, it should be emphasised that polyol compatibility or incompatibility (on whatever level) is not a prerequisite for forming phase-separated PUs. Phase separation depends mainly on the relative solubility parameters of the initial reactants and of the various PU moieties subsequently formed, and on the competing development of molecular weights of essentially linear HB segments with those of the network forming SB segments, prior to gelation (10). Regarding the advantages of compatible versus incompatible blends, the present studies on glass-fibre slurries showed that compatible polyol blends were more effective in completely filamentising and wetting the glass-fibres to give uniformly dispersed slurries for filled-RIM processing. Uniform slurries aid filled-RIM processing and facilitate rheological measurements and their interpretation, as described in the following paper (3).

Filled-RIM PU Materials

For filled PU1478 materials, changes in tensile stress-strain behaviour are shown in Figure 3(b) and derived tensile properties are summarised in the last two columns of Table III. The greater increase in modulus for PU1478-H18 is a direct result of the higher loading of HMG used (10% w/w) compared with that of CSG (5% w/w). Despite the higher filler loading in PU1478-H18, a much smaller decrease in elongation from that of the unfilled materials is observed which is due to the use of much shorter fibre lengths (70µm) of the HMG compared with the 1.5mm lengths of the CSG.

As expected, the flexural moduli of the filled PUs (PU1478-H18 and PU1478-C5) compared with those of PU1478-104I are higher at all temperatures as shown in Figure 4(b). The temperature dependence of PU1478-H18 is slightly less than for PU1478-C5, as defined by the -30°/65°C flexural modulus ratios (3.3 cf 4.3), which again is the result of using a higher loading of HMG in the former.

Literature Cited

1. Stanford, J.L.; Still, R.H.; Stepto, R.F.T. In "Reaction Injection Molding and Fast Polymerization Reactions"; Kresta, J.E., Ed.; POLYMER SCIENCE AND TECHNOLOGY SERIES Vol. 18, p.31; Plenum, 1982.
2. "Technical Data Sheet PU15", ICI Polyurethanes Group, ICI Europa, Belgium.
3. Cross, M.M.; Kaye, A.; Stanford, J.L.; Stepto, R.F.T. Following
4. Fruzzetti, R.E.; Hogan, J.M.; Murray, F.J.; White, J.R. SAE Technical Paper Series, No. 770839, September 1977, Detroit.
5. Schneider, F.W. In "Reaction Injection Molding and Fast Polymerization Reactions"; Kresta, J.E., Ed.; POLYMER SCIENCE AND TECHNOLOGY SERIES Vol. 18, p.243; Plenum, 1982.
6. Tirrell, M.V.; Lee, L.J.; Macosko, C.W.; ACS SYMPOSIUM SERIES No. 104, American Chemical Society 1979; p.149.

7. Fridman, I.R.; Thomas, E.L.; Lee, L.J.; Macosko, C.W. Polymer 1980, 21, 393.
8. Carmargo, R.E.; Macosko, C.W.; Tirrell, M.V.; Wellinghoff, S.T. Polym.Eng.Sci. 1982, 22, 719.
9. Stanford, J.L.; Stepto, R.F.T. Br.Polymer J. 1977, 9, 124.
10. Manzione, L.T.; Gillham, J.K.; McPherson, C.A. J.Appl.Polym.Sci. 1981, 26, 889.

RECEIVED April 16, 1984

Rheology of Polyols and Polyol Slurries for Use in Reinforced RIM

M. M. CROSS¹, A. KAYE², J. L. STANFORD¹, and R. F. T. STEPTO¹

¹Department of Polymer Science and Technology, University of Manchester, Institute of Science and Technology, Manchester, M60 1QD, England

²Department of Mathematics, University of Manchester, Institute of Science and Technology, Manchester, M60 1QD, England

Measurements with glass fibre/polyol slurries demonstrate that fibre aspect ratio, l/d , is a dominating factor in relation both to attainable fibre loading and to slurry rheology. The fibre packing fraction, ϕ_0 , measured by sedimentation, is shown to be a rapidly decreasing function of weight average l/d . For fibres of different l/d the relative viscosity of the slurry at low rates of shear is a unique function of ϕ/ϕ_0 , where ϕ is the fibre volume fraction. The rheological investigation is based on novel instrumentation and techniques for measuring the viscosity of glass fibre slurries at shear rates from 1 to 10^6 s⁻¹. Measurements up to 10^4 s⁻¹ are based on modified cone and plate geometry, while the higher shear rates are attained with a capillary viscometer attached to a RRIM machine. Measurements on polyol blends with the RRIM viscometer show a slight fall in viscosity as the shear rate is increased to 10^5 s⁻¹, but beyond this point there is a sharp rise in viscosity which is thought to be associated with boundary layer effects.

In the RRIM process rheological behaviour is involved at every stage from the initial dispersion of reinforcing fibre to the final flow into the mould. This calls for a sound knowledge of the rheological properties of glass fibre slurries under widely differing conditions of flow. In the case of spherical particles the packing behaviour and dispersion rheology have been extensively studied but comparatively little has been done for cylindrical particles or fibres, of fibre length l and diameter d . One reason for this may be the practical difficulties associated with rheological measurements on fibre slurries.

In the present investigation it has not been possible to undertake a systematic investigation of all the variables that might affect the viscosity of a glass fibre slurry, but an attempt has been made to identify the more important parameters. Polyol blends as described in a preceding paper in this volume (1) were used. Three specific aspects of rheological behaviour have been investigated.

0097-6156/85/0270-0097\$06.00/0
© 1985 American Chemical Society

1. A study of the packing behaviour of glass fibres, its dependence on fibre dimensions and its influence on slurry rheology.
2. A study, relevant to recirculation behaviour in a RRIM machine, of polyol and polyol slurry rheology at shear rates in the range $0-10^3 \text{ s}^{-1}$. This study is based on viscometry with modified cone and plate geometry.
3. High shear rate viscometry, extending to 10^6 s^{-1} , simulating conditions in the mixing head, using a capillary viscometer attached to a RRIM machine.

Measurements of Fibre Packing Fraction

For particles of a defined shape and size distribution there exists a volume fraction (ϕ_0) corresponding to a state of close packing. For example, for uniform spheres in a condition of hexagonal close packing, $\phi_0 = 0.74$. If the packing fraction is ϕ_0 , the voidage between the particles represents a volume fraction of $1-\phi_0$, and the bulk volume factor is $1/\phi_0$.

For hammer-milled glass (HMG), the bulk volume can be determined by direct measurement in air, and data for HMG of different aspect ratios have been published by Milewski (2) and by Isham (3). However, for chopped strand glass (CSG), where considerably higher aspect ratios occur, there do not appear to be any comparable data. Here it is important that the integral strand material is completely filamentised. Accordingly, in the present work fibres were uniformly dispersed in one of the miscible polyol blends (PB021) detailed previously (1) and ϕ_0 was determined by sedimentation under gravity. The CSG used throughout had a diameter of $17\mu\text{m}$.

A known weight of fibre was dispersed in the medium by hand stirring, and in the case of CSG great care was taken to ensure that filamentation was complete. The slurry was poured into a measuring cylinder. Sedimentation was assisted by vigorous tapping, but became slow in the final stages, particularly with the longer fibres, and several days were allowed for equilibrium to be reached. The volume v_1 corresponding to the equilibrium sedimentation level was noted and also the overall volume v_2 . If w represents the weight percentage of glass fibre in the dispersed slurry, the packing fraction ϕ_0 was calculated from the relation

$$\phi_0 = (v_2/v_1)[1 + (100-w)\rho_g/(\rho_p)]^{-1} \quad (1)$$

where ρ_g and ρ_p are the densities of the glass and the polyol. Measurements were carried out with samples of CSG using essentially mono-disperse materials and also bimodal blends. Other workers (2,4) have contended that ϕ_0 is a function of number average ℓ/d and accordingly the results are represented on this basis in Figure 1. The correlation is poor and it is clear from Figure 2 that in reality ϕ_0 is a function of weight average ℓ/d . ϕ_0 is seen to be a rapidly decreasing function of $(\ell/d)_w$ and can be represented empirically by the equation

$$1/\phi_0 = 1.38 + 0.0376(\ell/d)_w^{1.4} \quad (2)$$

Equation 2 has definite implications for the maximum fibre loadings

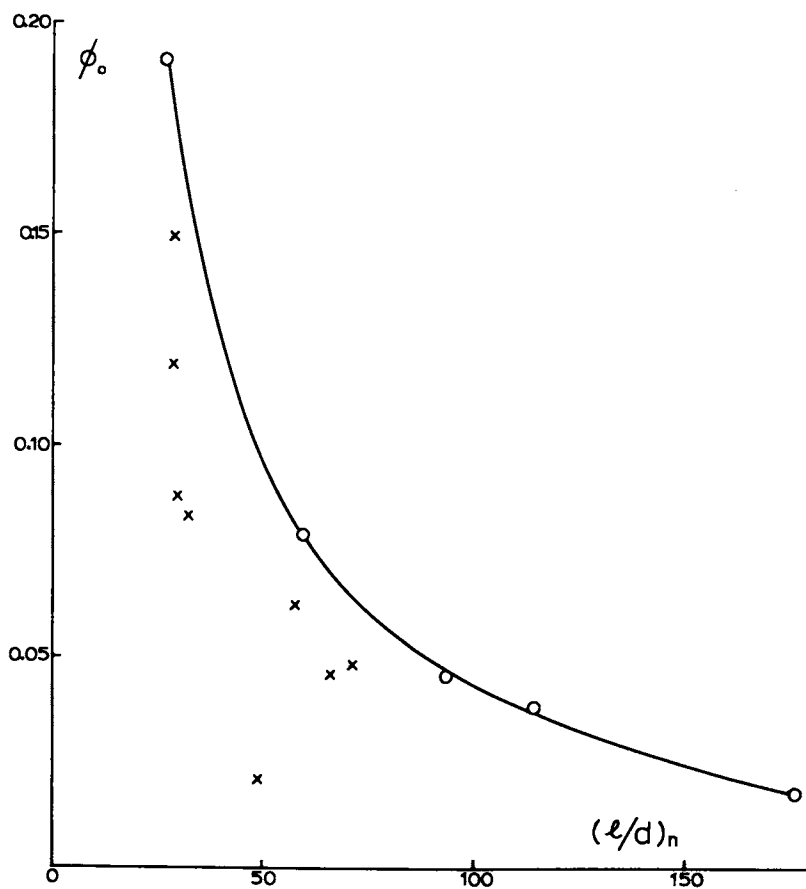


Figure 1. Packing fraction (ϕ_0) of glass fibres as a function of number average l/d . Key: O, monodisperse samples; X, bimodal samples. (The polyol blend used was PB021 (1). 0:2:1 of polyols T32/75: LHT240: EG. The fibres were CSG of $17 \mu\text{m}$ diameter. Bimodal mixtures were obtained by using pairs of monodisperse samples such that the differences between weight and number averages were as large as possible.)

which can be used in RRIM. Thus a fibre with $(\ell/d)_w = 100$ (e.g. $\ell_w = 1.5\text{mm}$, $d = 0.015\text{mm}$) gives $\phi_0 = 0.0398$, corresponding to a weight fraction of 0.092 in the polyol stream. Reducing the fibre length to 0.45mm would give $\ell/d = 30$ (for the same diameter), $\phi_0 = 0.0173$ and a weight fraction of 0.339. It may be noted that equation 2 also gives a good representation of the data of Milewski (2) for mono-disperse wooden rods.

Modified Cone and Plate Viscometry

Preliminary measurements were attempted on glass fibre slurries using two laboratory instruments, a Weissenberg rheogoniometer using a truncated cone and plate geometry, and a Ferranti-Shirley cone and plate viscometer using both standard and particle cones. The particle cone is essentially a truncated cone with a central pip for gap setting purposes. Serious difficulties were encountered with both instruments, particularly with fibres of high aspect ratio and at higher fibre concentrations.

Difficulty was experienced in setting the gap correctly because of the very high resistance to vertical movement of the plate with the test sample in position. It was also often impossible to rotate the cone relative to the plate, and when rotation did take place, the readings were very erratic. Shearing at relatively low speeds sometimes resulted in fibres forming into clumps resembling balls of cotton wool. These difficulties seemed to be associated with the narrow operating gap between the cone and plate, which was not large compared with the size of the suspended particles. Two modifications of the cone and plate geometry were adopted.

The Displaced Cone and Plate. The basic advantage of cone and plate geometry is that it provides a uniform rate of shear within the test fluid. In order to meet this condition the cone is normally set to the theoretical position where its apex is in contact with the surface of the plate. It is also possible to operate with a displaced cone/plate system, i.e. with the cone apex set at a displacement 'c' from the surface of the plate. In this way relatively large gaps can be achieved, but there is the disadvantage that there is no longer a uniform rate of shear within the test sample. Accordingly the computation of rheological data becomes more difficult and normally involves basic assumptions regarding the viscosity/shear characteristics of the test fluid. The present work used a new mathematical approach to the problem which does not involve such assumptions. Details of the mathematical analysis are to be published elsewhere. Essentially, the measured torque is a function of the cone displacement c and its angular velocity ω . Computer programs have been written and used to analyse data. The analysis has also been applied to parallel plate geometry, which can be regarded as a displaced cone system with zero cone angle.

The Annular Cone and Plate. The concept of the annular cone is thought to be new. Figure 3 shows a comparison of truncated and annular cones. With the truncated cone there is a small error associated with the torque developed over the flat surface, and for this reason the truncation is kept small. In turn, this imposes

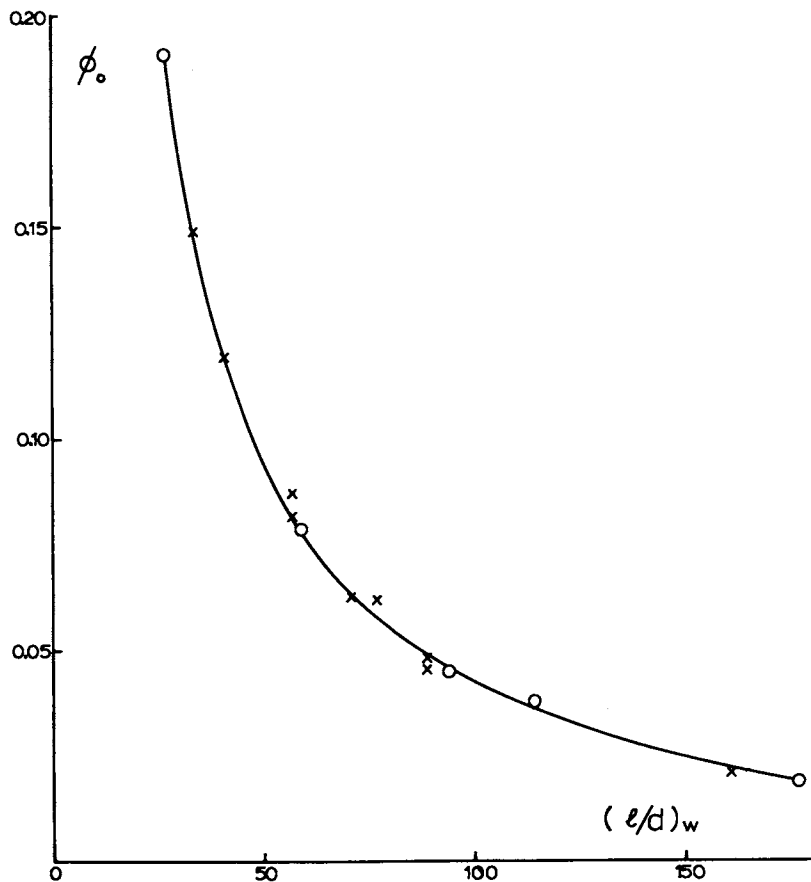


Figure 2. Packing fraction (ϕ_0) of glass fibres as a function of weight average l/d . Key: O, monodisperse samples; X, bimodal samples.

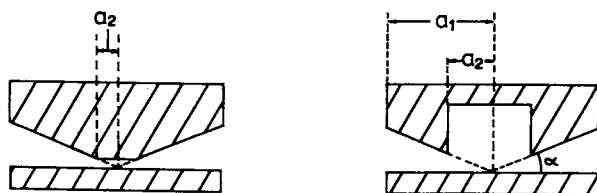


Figure 3. Truncated and annular cones.

a limit to the attainable gap width, $a_2 \tan \alpha$. Gap widths are normally in the range 10 to 100 μm .

With the annular cone there is no comparable error since the whole of the torque is developed over the conical surface bounded by radii a_1 and a_2 . Consequently there is no limitation to the value of a_2 , and the gap width can be comparatively large. As a_1/a_2 approaches unity the system approximates to a ring and plate configuration. The condition of uniform shear rate is maintained and the total torque τ developed over the conical surface is given by

$$\tau = 2\pi\sigma \int_{a_2}^{a_1} a^2 da = \frac{2\pi\sigma}{3} (a_1^3 - a_2^3) = \sigma A \quad (3)$$

where σ is the shear stress. Also

$$\dot{\gamma} = \omega / \tan \alpha \cong \omega / \alpha \quad (4)$$

and the viscosity, η , is given by

$$\eta = \alpha\tau / (\omega A) \quad (5)$$

as for the conventional cone/plate system. A prototype 3° angular cone, with a gap width of 1100 μm was made in aluminium and fitted to a Ferranti-Shirley viscometer.

The displaced cone and annular cone measurements represent new experimental techniques and their validity was checked by comparison with conventional cone/plate geometry using a non-Newtonian solution of polyisobutylene in decalin. Agreement was found to be excellent, and the new techniques were adopted for all subsequent measurements on fibre slurries. With the wide gaps employed, experimental difficulties were largely overcome, although fibre clumping remained a problem with longer fibres.

Results. In general, the glass fibre slurries exhibited slight shear thinning behaviour, which became more marked with increase in fibre length and with concentration. This is illustrated in Figure 4 with a series of flow curves for different w/w concentrations of 1.5mm, CSG dispersed in PBA1478, (see (1)) measured with a 3° annular cone.

Viscosities were measured using 70 μm HMG dispersed in two different polyols differing significantly in both chemical composition and viscosity, one being a diol/triol blend and the other a higher molar mass triol, the viscosities at 25°C being respectively 1.4 and 11.3 Poise. At a given concentration there was no significant differences between the relative viscosities of the two media.

Figure 5 shows a plot of relative viscosity at zero rate of shear against volume concentration, for slurries of CSG of different fibre lengths suspended in the two polyols. Again there is evidence that the relative viscosity is insensitive to the precise nature of the suspending medium. However, it should be emphasised that this will only apply if the fibres are in a well-defined state of dispersion. Figure 5 shows the major influence of fibre aspect ratio on slurry viscosity, and also the influence of packing behaviour. The dotted vertical lines indicate the experimental values of ϕ_0 for the different fibre lengths and it is seen that, in each case, the

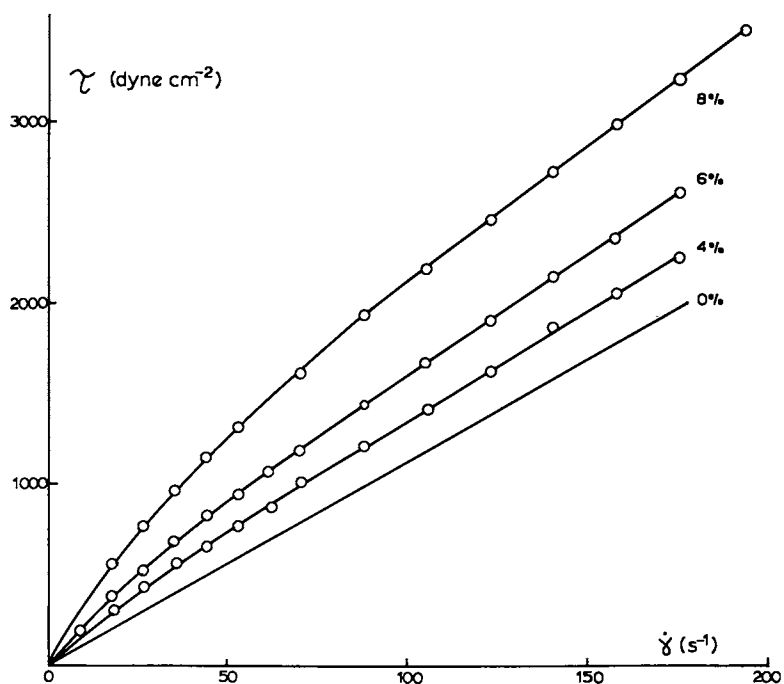


Figure 4. Flow curves for 1.5mm CSG dispersed in PBA1478. See (1) for specification of polyol blend PBA1478.

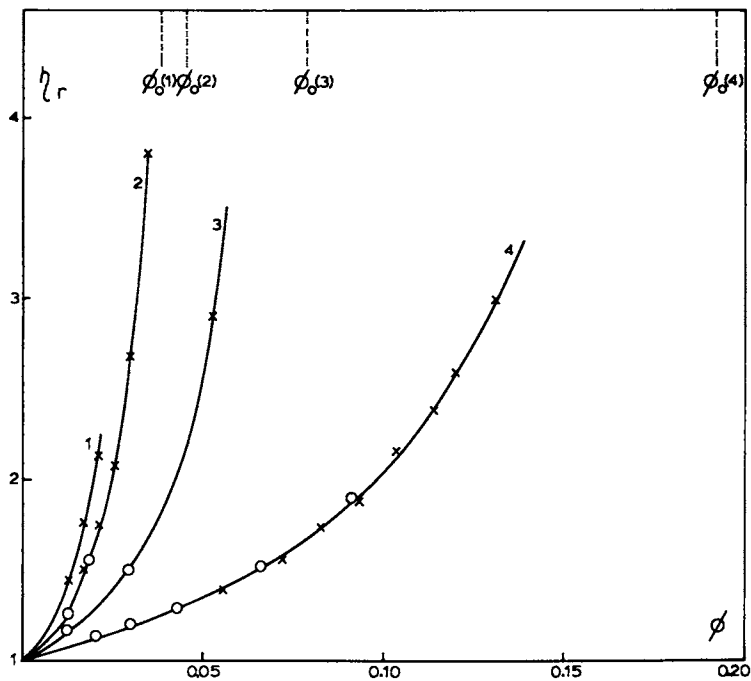


Figure 5. Relative viscosity (η_r) of polyol slurries versus volume fraction (ϕ) of CSG. Polyols: O, PB821; X, PBA1478. CSG: curve 1, $l_w = 1.94\text{mm}$; curve 2, $l_w = 1.5\text{mm}$ (nominal); curve 3, $l_w = 1.0\text{mm}$; curve 4, $l_w = 0.45\text{mm}$. See (1) for specification of polyol blends PB821 and PBA1478.

viscosity is rising asymptotically as ϕ tends to ϕ_0 , i.e. with an approach to conditions of maximum packing.

The viscosity data of Figure 5 can be reduced to a single curve by replotting η_r as a function of ϕ/ϕ_0 , indicating that the relative viscosity at zero shear rate is a unique function of ϕ/ϕ_0 . A relation between dispersion viscosity and ϕ/ϕ_0 , derived by Mooney (5) and modified by Krieger and Dougherty (6), gives

$$\eta_r = [1 - \phi/\phi_0]^{-k\phi_0} \quad (6)$$

where k is called the dimensionless intrinsic viscosity.

In conformity with Equation 6 the data for CSG can be linearised by plotting $\log \eta_r$ against $\log (\phi_0 - \phi)$ using the values of ϕ_0 derived from sedimentation measurements. The gradient of the linear plot gives $k\phi_0 = 1$, i.e. the intrinsic viscosity equates with the bulk volume factor and Equation 6 reduces to

$$\eta_r = [1 - \phi/\phi_0]^{-1} \quad (7)$$

Figure 6 shows the four curves of Figure 5 superposed and linearised in accordance with Equation 7 with a plot of relative fluidity against ϕ/ϕ_0 .

High-Shear RRIM Viscometer

With cone and plate viscometers, the highest attainable shear rate is in the region of $2 \times 10^4 \text{ s}^{-1}$, but with glass-fibre slurries, where large gap dimensions are essential, the practical limit is much lower. This compares with estimated shear rates in the region of 10^6 s^{-1} in the mixing head of a RRIM machine. Accordingly, it was decided to design and construct a high shear rate viscometer attachment for a RRIM machine, simulating conditions in the head.

The viscometer employed a series of interchangeable capillaries based on 1/4 inch outer diameter (o.d.) stainless steel tubing, differing in inner diameter (i.d.) and cut to suitable lengths. These could be rapidly and conveniently interchanged by the use of 1/4 inch Swagelok fittings. Internal diameters were selected on the basis of attainable shear rates and wall thickness requirements at the high operating pressures. However, with available 1/4 inch tubing the highest attainable shear rate was $5 \times 10^5 \text{ s}^{-1}$. The range was extended to 10^6 s^{-1} by the expedient of cementing a short length of narrow bore 3/16 inch o.d. tubing inside a 3/16 inch i.d. tube using an epoxy adhesive. Compatibility with the 1/4 inch Swagelok fittings was thus retained. 0-5000 psi pressure transducers were mounted at each end of the capillary and normally these were used in a differential mode to record the pressure drop along the tube.

The usual volume flow rate for the RRIM machine, and hence for the viscometer, is approximately $500 \text{ cm}^3 \text{ s}^{-1}$. In order to measure this, the liquid emerging from the capillary was collected in a large cylindrical vessel, approximately 35 cms in diameter, where the liquid level was measured by means of a float connected to the armature of a linear displacement transducer. Liquid entered the collecting cylinder through a vertical tube in the centre of the base but in order to minimise any irregularities of the surface it was baffled by a diversion through 6 horizontal channels arranged

radially at 60° angular spacings in a cylindrical block at the base of the vessel.

By connecting the output of the displacement transducer to a pen recorder, the rate of rise of liquid (dh/dt) was obtained, and, if R is the radius of the collecting vessel and Q the volume flow rate,

$$Q = \pi R^2 dh/dt \quad (8)$$

Also, if the capillary radius is r, the shear rate at the wall, assuming Newtonian flow, is given by

$$\dot{\gamma} = 4Q/\pi r^3 = (4R^2/r^3)dh/dt \quad (9)$$

If P is the pressure drop along the capillary of length l , the viscosity η of the fluid is given by the Poiseuille equation

$$\eta = r^4 P / (8R^2 l dh/dt) \quad (10)$$

The capillary diameters were measured by weighing a measured length of the appropriate stainless steel tubing. The mean outer diameter d_1 of the tube was measured with a micrometer and the internal diameter d_2 calculated.

Viscous Heating and Temperature Correction. With viscosities of the order of 10 Poise or more, and shear rates as high as 10^6 s^{-1} , it was anticipated that the measurements would be greatly influenced by viscous heating in the capillary. The problem has been treated mathematically, both for the situation where heat conduction through the walls is negligible, and also for the other limiting case of perfectly conducting walls. In the first situation, where conditions are essentially adiabatic, it can be shown that the total heat dissipation per unit volume depends only on the pressure drop, P, along the capillary, and is independent of other variables such as shear rate, fluid viscosity and capillary dimensions. This result appears to have been first noted by Jakobsen and Winer (7). Under these conditions the mean temperature rise of the liquid is given by

$$\Delta T = P / (\rho s) \quad (11)$$

where ρ and s are the density and specific heat of the liquid.

The mean temperature rise of the liquid was recorded by means of a fast response chromel-alumel thermocouple on the output side of the capillary and could be up to 10°C. For each viscosity measure three quantities were recorded, namely the pressure drop, the volume throughput (height) and the temperature rise. A typical recording for pressure and volume is shown in Figure 7. The pressure pulse is approximately rectangular in form, and viscosity calculations were usually based on the plateau region, where P is essentially constant and the volume-time shows corresponding linearity.

A basic similarity in the form of the pulses for P and T is found. This is consistent with the theoretical relation between P and T for adiabatic conditions Equation 11. Conformity with this equation was also shown by measurements on a polyol blend with two different capillaries, which gave a linear plot of ΔT against P. The gradient indicated a specific heat of 0.45 cal g^{-1} , in reasonable

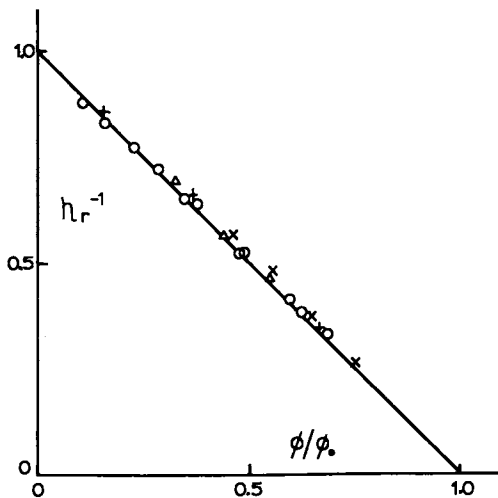


Figure 6. Relative fluidity (η^{-1}) versus ϕ/ϕ_0 , using the data of Figure 5. Key: Δ , 1.94mm CSG; X , 1.5mm (nominal); $+$, 1.0mm CSG; O , 0.45mm CSG.

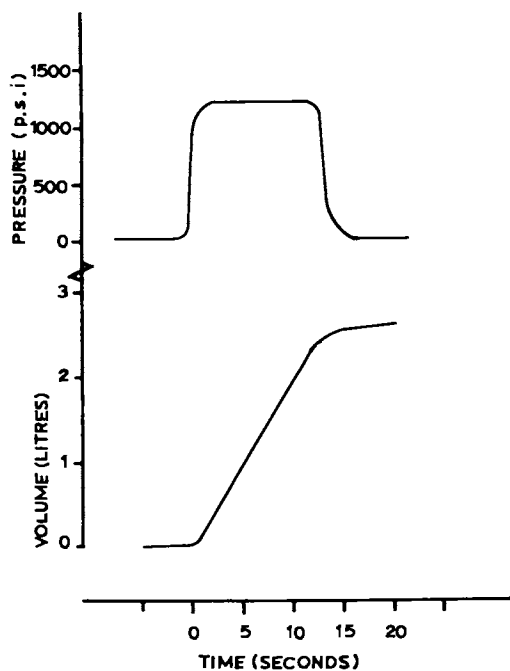


Figure 7. Typical RRIM viscometer traces for pressure and volume throughout.

agreement with an experimental value of 0.50 cal g^{-1} obtained by a conventional method based on the mixing of liquids at different temperatures.

The viscometer could also be used at lower shear rates by employing pressures in the range 0-50 psi from a compressor. By supplementing the high shear rate data in this way the operating range of the viscometer was from 10^2 to 10^6 s^{-1} .

The high shear rate data obtained in the viscometer were built up from a series of individual viscosity data points, each obtained at a known rate of shear and at known input and output temperatures T_1 and T_2 . A simple procedure was adopted for reducing data to a single reference temperature. It was assumed that, over the limited ranges involved, the viscosity showed a linear temperature dependence and that the measured value corresponded to that at the mean temperature $(T_1 + T_2)/2$. Figure 8 shows data for a polyol blend, obtained under different temperature conditions and with different capillaries, reduced in this way to a temperature of 25°C . Data for shear rates up to $2 \times 10^4 \text{ s}^{-1}$ obtained with the Ferranti-Shirley viscometer are included for comparison. At lower shear rates the two instruments show reasonable agreement and both show evidence of shear thinning. In the RRIM viscometer this behaviour is maintained to a shear rate of approximately $3 \times 10^5 \text{ s}^{-1}$, but beyond this point there is a very sharp rise in apparent viscosity. This rise is quite unexpected and requires further investigation but is thought to be associated with boundary layer effects.

Acknowledgments

Financial support by the Polymer Engineering Directorate of the Science and Engineering Research Council is gratefully acknowledged. We also thank Imperial Chemical Industries, Organics Division for some of the polyols used and Pilkingtons Fibre Glass Division and Turner Brothers Asbestos Ltd., for supplies of glass fibre.

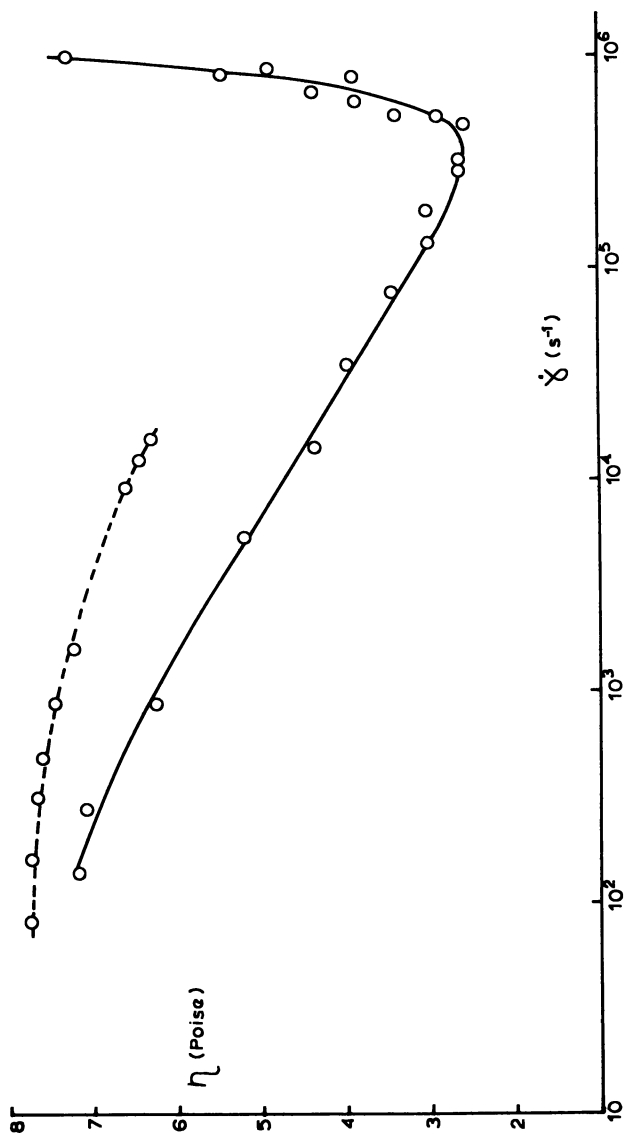


Figure 8. Viscosity (η) versus shear rate ($\dot{\gamma}$) for PB521 at 25 °C. —, RRIM viscometer; data corrected to 25 °C as described in text. ----, cone and plate viscometer data. See (1) for specification of polyol blend PB521.

Literature Cited

1. Barksby, N.J.; Dunn, D.; Kaye, A.; Stanford, J.L.; Stepto, R.F.T., preceding paper.
2. Milewski, J.V. Reinforced Plastics/Composites Institute Soc. Plastics Ind., Inc., Proc. 28th Annual Tech.Conf. 1973, Section 31, pp 1-8.
3. Isham, A.B., Reinforced Plastics/Composites Institute, Soc. Plastics Ind., Inc., Proc. 33rd Annual Tech. Conf. 1978, 14-A.
4. Tucker, C.L.; Suh, N.P. Polymer Engg. and Sci. 1980, 20, 887.
5. Mooney, M.J. J. Colloid Sci. 1951, 6, 162.
6. Krieger, I.M.; Dougherty, T.J. Trans.Soc.Rheol. 1959, 3, 137.
7. Jakobsen, J.; Winer, W.O. Trans.Amer.Soc.Mech.Eng., Series F, J. Lubrication Technol. 1975, 97, 472.

RECEIVED April 16, 1984

Organotin Catalysis in Urethane Systems

K. WONGKAMOLSESH and JIRI E. KRESTA

Polymer Institute, University of Detroit, Detroit, MI 48221

The catalysis of urethane formation reaction by dibutyltin dilaurate (DBTDL) was investigated in the model system isocyanate-n-butanol. It was determined that DBTDL participated in the polarization of the isocyanate group during the catalysis. On the other hand the amine catalyst -1,4 diaza [2,2,2] octane did not polarize the isocyanate group but its catalytic activity was associated with the induced polarization of the hydroxyl group. During the interaction of alcohol with DBTDL no ligand exchange was detectable, but solvation of the tin central ion and separation of the carboxylate amine by the hydroxyl group was observed. The mechanism of DBTDL catalysis based on the interaction of isocyanate with the solvated tin complex is discussed. The effect of a small amount of the hydrolyzable chlorine on the urethane formation reaction, catalyzed by DBTDL was studied.

Catalysis plays an important role in the RIM processing of urethanes. Catalysts not only affect the curing characteristics but also morphology and ultimate properties of resulting urethane elastomers. In the urethane RIM technology, the catalysts most often used are organotin compounds. Many investigators studied the mechanisms of catalysis of urethane reaction and their results were summarized in several reviews (1, 2, 17). Generally, it is accepted that the catalysis of urethane reaction is associated with the formation of complexes between organotin catalysts and reactants. Various complexes between tin catalysts and reactants including the triple complexes were proposed (1-20). The formation of complexes between organotin catalysts and protic reactants was experimentally verified (3, 4, 15, 16). The complex formation between organotin catalysts and isocyanates was not satisfactorily established, because no shifts in IR spectra were observed. Bloodworth and Davis et al. (8) found that trialkyltin methoxide reacted with isocyanate forming trialkylstannyl carbamates which in the presence of alcohol formed urethane and regenerated original catalyst. Based on these results, they proposed mechanism in which the ligand exchange

0097-6156/85/0270-0111\$06.00/0

© 1985 American Chemical Society

between DBTDL and alcohol occurred forming organotin alkoxide as main catalyst.

The kinetic studies of isocyanate-alcohol reactions catalyzed by DBTDL showed that the dependence of the rate constants on the concentration of DBTDL was not linear (14, 18, 20). In order to explain this behavior various mechanisms were proposed based on series of consecutive complexing equilibrium (14), dissociation of a catalyst (18, 19) or dissociation of OH bond in the alcohol-DBTDL complex (20).

At the present time, regardless of a great quantity of experimental data on the tin catalysis, the mechanism is still not fully understood.

In this paper, the results dealing with the complex formation between various catalysts and isocyanates, the ligand exchange and solvation at the tin cation, and effect of hydrolyzable chlorine on the catalytic activity of DBTDL will be presented and discussed.

Experimental

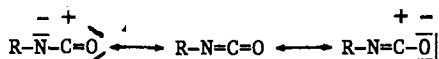
Dibutyltin dilaurate (DBTDL) (M & T Chem. Co.), 1,4-diaza [2,2,2]-octane (Air Products), isocyanatoethyl methacrylate (IEM) and carbamoyl chloride of IEM (Dow Chem. Co.) and hexamethylene diisocyanate were used as supplied. Phenyl isocyanate, p-tolyl isocyanate, p-chlorophenyl isocyanate (all Aldrich Chem. Co.), 2-ethoxyethyl acetate (Eastman Kodak Co.) and n-butanol (Mallinkrodt) were purified by distillation before use.

The catalyzed reactions of isocyanates (0.5N) with n-butanol (0.5N) were carried out in 300 ml three-necked flasks under nitrogen atmosphere. The reaction flask was immersed in a thermostated bath at 25°C. The samples were taken at regular time intervals and the isocyanate contents were determined using the dibutylamine method.

The IR spectra were recorded using Pye-Unicam spectrophotometer, model 3-300. The specific conductivity of catalyst systems was studied using Leed & Northrup conductivity bridge and cell.

Results and Discussion

Interaction Between NCO Groups and Organotin Catalyst. The reactivity of isocyanates in the urethane formation reaction is determined by the structure and the distribution of the electron density in the isocyanate molecule. The isocyanates possess large dipole moments; the nitrogen and oxygen carry fractional negative charges and carbon carries a positive charge. The distribution of the electron density can be depicted by the following resonance formulas:



The size of fractional charges of the isocyanate group is determined by the substituent R in the vicinity of the NCO group. The electron withdrawing substituents attached to the NCO group increase the partial positive charge on the carbon atom of the NCO group, resulting in the increased polarization of the NCO group and increased reactivity of isocyanate with the protic reactants. On

the other hand, the electron donating substituents decrease a partial positive charge on the carbon atom and with the decreased polarization of the NCO group, the reactivity of isocyanate is decreased. These facts explain the differences in reactivities between aromatic and aliphatic isocyanates in the urethane formation reaction.

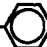


For the non-catalyzed urethane reactions it was established (23) that the relative reactivities (ratios of rate constants) of substituted aromatic isocyanates correlated with the structural parameter σ of the substituent R (measuring the electron withdrawing ability of the substituent R) according to the Hammett equation:

$$\log \frac{k}{k_0} = \sigma \rho$$

where k and k_0 are rate constants for the non-catalyzed reaction of substituted and non-substituted isocyanates. The positive value for ρ (determined by various authors) (23, 13) indicates that the electron withdrawing groups attached to the nitrogen increased the polarization of the isocyanate group.

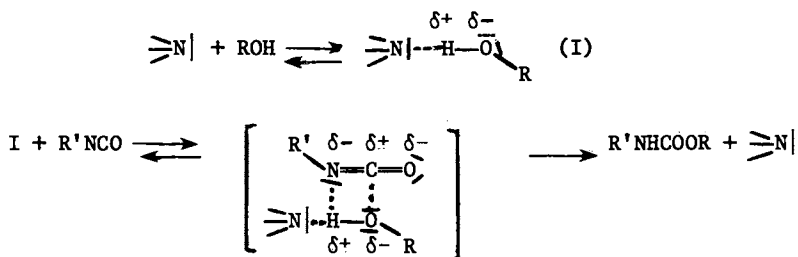
As was mentioned previously, the catalysts accelerate the urethane reaction by the induced polarization of reactants in the transition complex. The formation of polarized complexes between the NCO groups and catalysts (amines, organotins) was not satisfactorily documented. Indirectly, the formation of polarized NCO-catalyst complexes in urethane reaction can be established by studying the dependence of the rate constants on the substitution of phenyl isocyanates in the presence of various catalysts. The magnitude of the reaction constant ρ is essentially a measure of the polarization of isocyanate groups induced by a catalyst. In the case that the catalyst polarizes the NCO group during the reaction, the contribution of the substituent R on the benzene ring to the polarization of the NCO group will diminish resulting in the decrease of the ρ -value. In the opposite case, there will be a small effect of the catalyst on the ρ -value. The data for non-catalyzed and catalyzed urethane reaction by 1,4 diaza [2,2,2] octane (DAO) and DBTDL are summarized in Table I and Figure 1.

TABLE I.

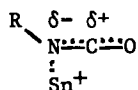
Catalyst		Non-Catalyzed	DAO	DBTDL
Isocyanate	σ	$\log (k_x/k_0)$	$\log (k_x/k_0)$	$\log (k_x/k_0)$
Cl-  -NCO	0.23	0.596	0.562	0.094
 -NCO	0	0	0	0
CH ₃ -  -NCO	-0.17	-0.373	-0.251	-0.0586
ρ		2.45	2.15	0.38

As can be seen from Table I, the ρ -values for uncatalyzed and DAO catalyzed reactions are relatively close, indicating that DAO catalyst does not significantly participate in the induced polarization of isocyanate.

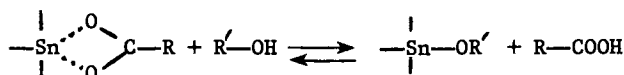
These results support the mechanism proposed previously by Farkas et al. (21). The reaction proceeds via interaction of isocyanate with the polarized amine-alcohol complex (22):



In the case of the DBTDL catalyst, a significant decrease of the ρ -value ($\Delta\rho = 2.07$) was observed. A comparable decrease was also reported by Entelis et al. (13). This indicates that the tin catalyst participates in the induced polarization of isocyanate through complexation with the tin cation during the reaction:

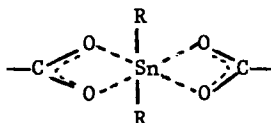


Ligand Exchange in DBTDL and Solvation Effects. Several mechanisms based on the idea of the ligand exchange at the central tin atom were proposed in the literature (8, 20). In those mechanisms an exchange of carboxylate ligands for alkoxy ligands or ionisation of the coordinated hydroxyl (alcohol) groups were suggested:



In order to better understand the catalytic mechanism of organotin complexes, the possibility of the ligand exchange between reactants and DBTDL was studied using IR spectroscopy.

DBTDL is monomeric in a liquid form as well as in solution. It has an octahedral structure and carboxylate groups are coordinated with tin as a bidentate ligands:



In the IR spectrum, the carboxylate anions of DBTDL showed two peaks $\nu_{\text{as}}(\text{CO}_2^-)$ 1600 cm^{-1} (bonded bidentate ligand to tin) and 1565 cm^{-1} (dissociated carboxylate anion as separated in ion pairs). In our model study DBTDL was premixed with n-butanol and n-butyl isocyanate (molar ratios 1:1:1) and urethane was extracted by acetonitrile. The residual DBTDL was investigated by IR spectroscopy. Results are summarized in Figure 2. In the case of the ligand exchange and the

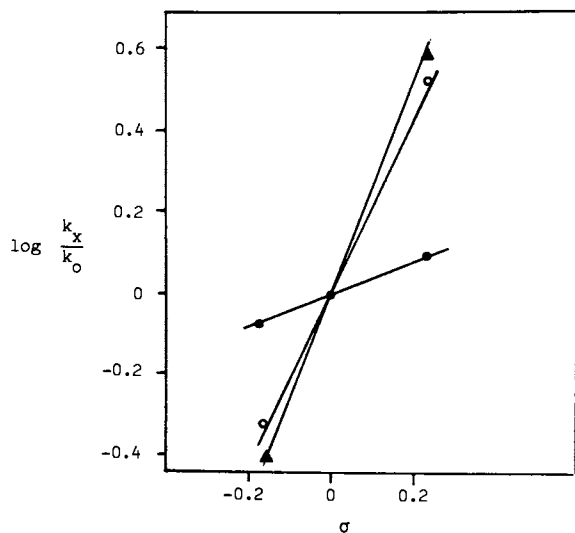


Figure 1. Effect of catalysts on the reactivity of substituted aromatic isocyanates with n-butanol. Dependence of the rate constant ratios on the σ -parameter of substituted isocyanates. \blacktriangle no catalyst, \circ 1,4 Diaza [2,2,2] octane, \bullet DBTDL; $T = 25^\circ\text{C}$ Solvent: 2-ethoxyethyl acetate.

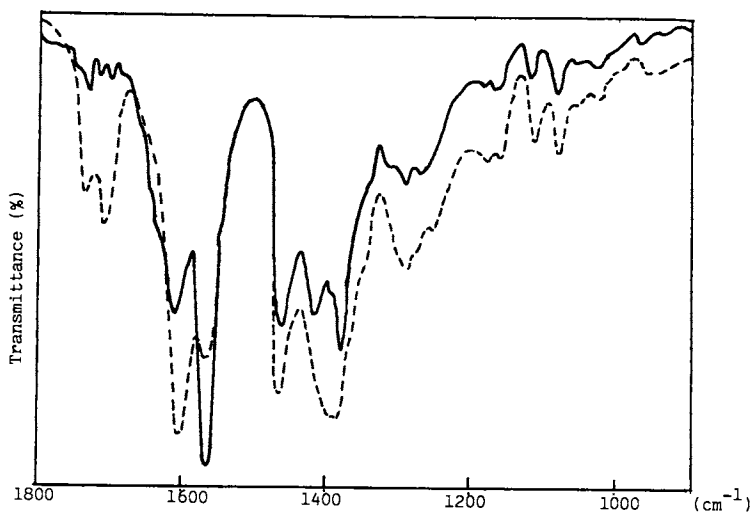


Figure 2. Comparison of IR spectra of extracted DBTDL (—) with a neat DBTDL (----).

formation of alkoxide, there will be a decrease of the $\nu_{as}(\text{CO}_2)$ peak and an increase of $\nu(\text{C}=\text{O})$ at 1710 cm^{-1} and $\nu(\text{C}-\text{O})$ of alkoxide. None of these changes were observed. The comparison of spectra of extracted DBTDL (solid line, Figure 2) with neat DBTDL (dotted line) showed that the extracted DBTDL had increased absorption band at 1565 cm^{-1} indicating increased separation of carboxylate anions from the central atom.

The effect of n-butanol on the IR spectra of DBTDL is depicted in Figure 3. In the presence of n-butanol, an increase of the absorption band at 1565 cm^{-1} and a decrease of a band at 1600 cm^{-1} was observed.

This indicates that the hydroxyl group solvated the tin ion separating the carboxylate anion from the coordination sphere of the tin ion. This coordination of the hydroxyl group created a vacant ligand site on the tin ion suitable to coordinate isocyanate group. In our IR study of the interaction of DBTDL with isocyanates it was determined that no coordination of isocyanates with DBTDL (no shifts of isocyanate absorption band $\nu(\text{NCO})$ at 2280 cm^{-1} and $\nu_{as}(\text{CO}_2)$ of DBTDL) occurred. Therefore it was concluded that the DBTDL has to be first solvated by the hydroxyl of alcohol or polyol in order to be able to form a complex with isocyanate.

Similar solvation effect on DBTDL was observed in the presence of other polar aprotic solvents such as DMF and DMSO.

The dissociation of DBTDL in alcohol was confirmed by the conductivity measurements. The dependence of the specific conductance of DBTDL in ethanol at various concentrations are shown in Figure 4. On the contrary, the dissociation of the DBTDL was inhibited by the presence of lauric acid. This is shown in Figure 5, where the disappearance of the absorption band at 1565 cm^{-1} (solid line) was observed in the system DBTDL-lauric acid.

Based on the presented data, the probable mechanism of the catalysis of urethane reaction by the DBTDL catalyst is depicted in Figures 6 and 7.

Effect of Hydrolyzable Chlorine on Activity of Tin Catalysts. The effect of small amounts of hydrolyzable chlorine on the catalytic activity of DBTDL was studied on the model aliphatic system--isocyanatoethyl methacrylate and n-butanol. The presence of the hydrolyzable chlorine in isocyanate usually decreases the reactivity of isocyanates in the urethane reaction. The results of measurements of the chlorine effect on the change of the rate constant is summarized in Figure 8. It was determined that the very small amounts of the hydrolyzable chlorine, especially in the form of carbamoyl chloride, increased at the beginning the rate constant for the urethane reaction catalyzed by DBTDL and after achieving the maximum at 500 ppm of chlorine the reactivity decreased. This effect was not observed when benzoyl chloride was used in place of carbamoyl chloride. It was assumed that the activation effect of the chlorine was due to the interaction of the carbamoyl chloride with the DBTDL catalyst. In order to understand this effect, the interaction of DBTDL with carbamoyl chloride of hexamethylene diisocyanate (with and without the presence of n-butanol) was studied using the IR technique. Results are summarized in Figure 9.

It was found that the ligand exchange occurred and the rate of this exchange depended on the presence of n-butanol in the system.

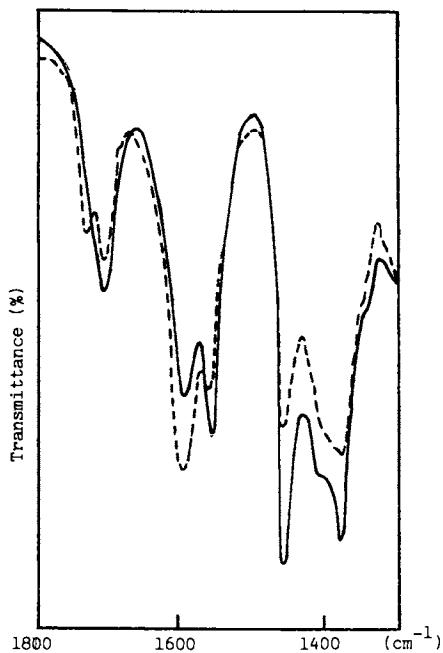


Figure 3. Comparison of the IR spectra of the solvated DBTDL (DBTDL/n-BuOH = 1:5) (—) with a neat DBTDL (---).

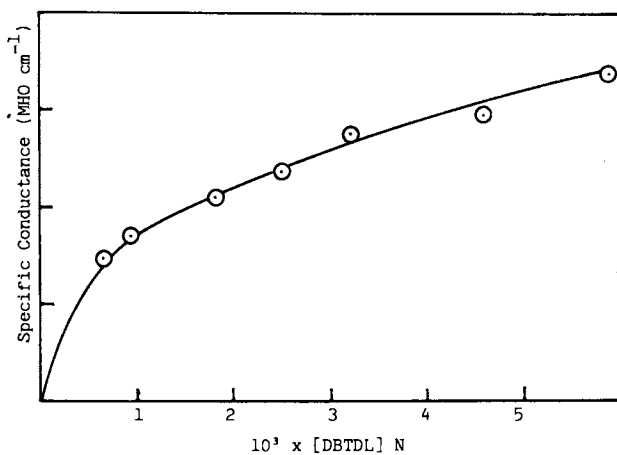


Figure 4. Dependence of the specific conductance of DBTDL solution in ethanol on the concentration of DBTDL.

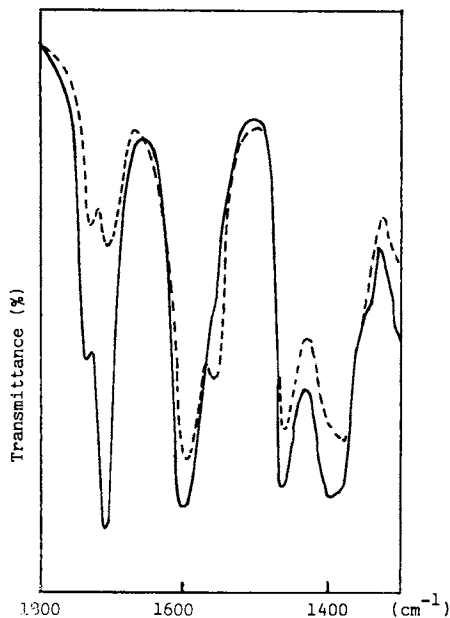


Figure 5. Effect of lauric acid on IR spectra of DBTDL. Mixture of DBTDL and lauric acid (1:1) (—); neat DBTDL (----).

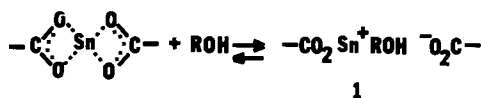


Figure 6. Solvation of DBTDL by alcohol. (Perpendicular butyl groups in DBTDL omitted.)

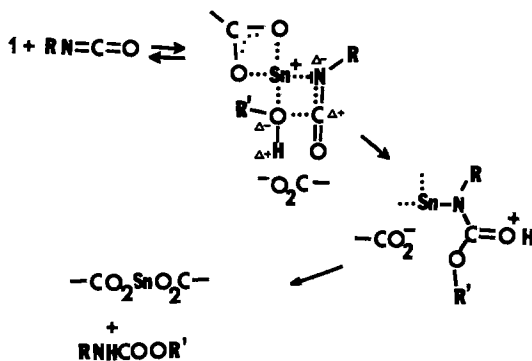


Figure 7. Mechanism of interaction of isocyanate with solvated DBTDL. Formation of urethanes.

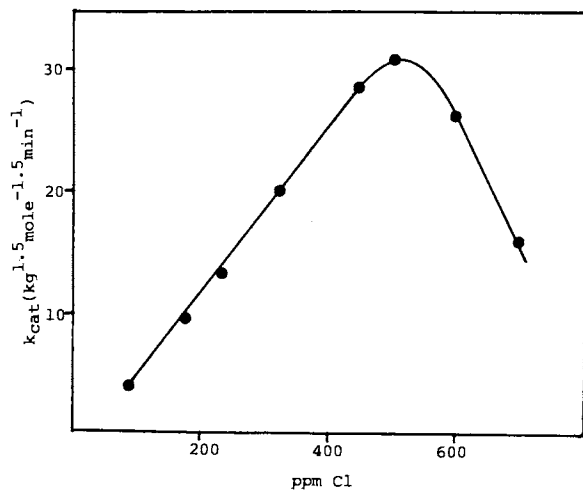


Figure 8. Effect of hydrolyzable chloride on the urethane rate formation constant.

Isocyanatoethyl methacrylate/n-butanol (1:1); DBTDL; solvent: n-butyl acetate, 25°C.

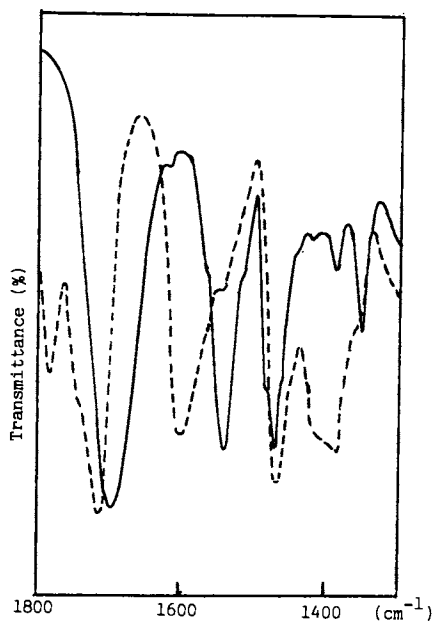
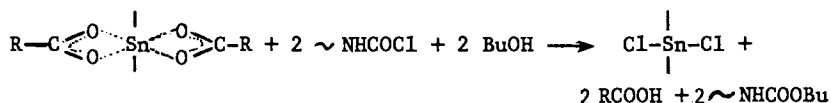


Figure 9. Comparison of the IR spectra of the DBTDL-carbamoyl chloride mixture (1:1) (---) with the DBTDL-carbamoyl chloride mixture in n-butanol (1:1:10) (—).

In the absence of n-butanol, the reaction between DBTDL and carbamoyl chloride was very slow (dotted curve). In the presence of n-butanol (solid curve) the completion of the reaction was very fast as can be seen from the disappearance of dimerized of the carboxylate anion band (~ 1600 cm^{-1}) and the formations of dimerized acid band (~ 1700 cm^{-1}) and urethane bands (~ 1700 cm^{-1} , $\nu(\text{C}=\text{O})$; 1535 cm^{-1} (NH)). This reaction can be depicted as follows:



Similar results were obtained, when HCl was bubbled into DBTDL (Figure 10). Also in this case, the stretching vibrations of the carboxylate ion disappeared and have been replaced by a strong band at 1700 cm^{-1} belonging to the dimerized acid.

The structure of the catalytic species was not established at the present time but indications are that the increased catalytic activity is associated with the formation of chloro complexes of dibutyltin monolaurate. Dibutyltin dichloride is very weak urethane catalyst as was previously established (2).

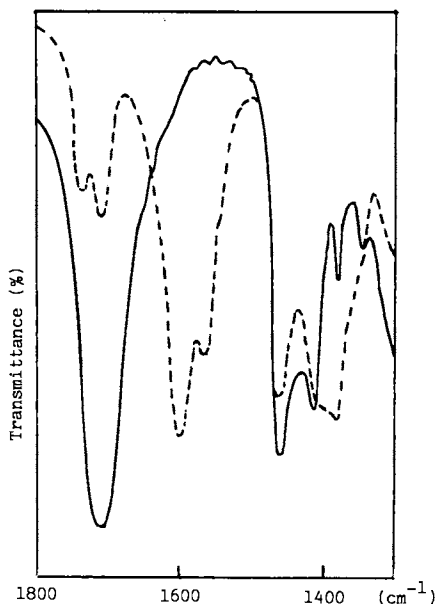


Figure 10. Comparison of the IR spectra of DBTDL reacted with HCl (neat DBTDL ----).

Literature Cited

1. Frisch, K.C.; Rurnao, L.P. J. Macromol. Sci. Rev., Macromol. Chem. 1970, 5, 103.
2. Entelis, S.G.; Nesterov, O.V. Russ. Chem. Rev. 1966, 35, 917.
3. Smith, H.A. J. Appl. Polym. Sci. 1963, 7, 85.
4. Entelis, S.G.; Nesterov, O.V. Kinet. Katal. 1966, 7, 464.
5. Zabrodin, V.B.; Nesterov, O.V.; Entelis, S.G. Kinet. Katal. 1970, 11, 114.
6. Lipatova, T.E.; Bakalo, L.A.; Sirotinskaya, A.L.; Lopatina, V.S. Vysokomol. Soedin. 1970, A12, 911.
7. Thiele, L.; Becker, R.; Frommelt, H. Faserforsch. Textiltechnik 1977, 28, 343.
8. Bloodworth, A.I.; Davies, H.G. J. Chem. Soc. 1965, 5238.
9. Britain, J.W.; Gemeinhardt, P.G. J. Appl. Polym. Sci. 1960, 4, 207.
10. Robins, J. J. Appl. Pol. Sci. 1965, 9, 821.
11. Nesterov, O.V.; Chirkov, Yu N.; Entelis, S.G. Kinet. Katal. 1967, 8, 1371.
12. Zabrodin, V.B.; Nesterov, O.V.; Entelis, G. Kinet. Katal. 1969, 10, 663.
13. Entelis, S.G.; Nesterov, O.V.; Tiger, R.P. DAN USSR 1968, 178, 661.
14. Chirkov, Yu N.; Zabrodin, V.B.; Nesterov, O.V.; Entelis, S.G. Kinet. Katal. 1972, 13, 228.
15. Frisch, K.C.; Reegen, S.L.; Floutz, W.V.; Oliver, J.P. J. Polym. Sci. 1967, Part A-1, 5, 35.
16. Reegen, S.L.; Frisch, K.C. J. Polym. Sci. 1970, A-1, 8, 2883.
17. Thiele, L.; Frommelt, H. Acta Polym. 1979, 30, 353.
18. Borkent, G. Adv. Ureth. Sci. Technol. (K.C. Frisch & S.L. Reegan, Eds.) 1974, 3, 1.
19. Richter, E.B.; Macosco, C.W. Polym. Eng. Sci. 1978, 18, 1012.
20. Van der Weij, F.W. J. Polym. Sci., Pol. Chem. Ed. 1981, 19, 381, 3063.
21. Farkas, A; Strohm, P. IEC Fund. 1965, 4, 32.
22. Kresta, J.E.; Shen, C.S.; Lin, I.S. Polymer Preprints 1978, 19, 21, 631.
23. Kaplan, M. J. Chem. Eng. Data 1961, 6, 272.

RECEIVED August 28, 1984

The Ketene Aminal-Isocyanate Reaction and RIM Systems

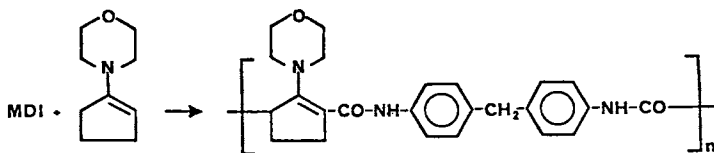
D. F. REGELMAN, L. M. ALBERINO, and R. J. LOCKWOOD

D. S. Gilmore Research Laboratories, The Upjohn Company, North Haven, CT 06473

Improvements to conventional polyurethane RIM technology have given better performing parts, fewer rejects, faster molding cycles, etc. Improvements have been found in formulation changes of existing polyurethane RIM technology. New extenders have broadened the scope of isocyanate-based RIM systems. (1)

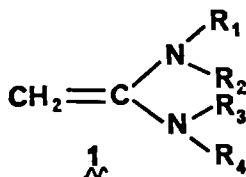
Both step-growth and chain growth RIM polymerizations require rapid, essentially quantitative reactions evolving no volatiles (intentionally foamed parts excluded). The chemistry employed, monomer purity, viability of catalysts if used, etc. must insure that these relatively basic requirements be met.

We have recently been examining chemistry that allows the preparation of RIM derived polyamides from isocyanates. We reported some initial results during a previous RIM symposium held in Atlanta. (2-3) We reported the use of enamine isocyanate chemistry to give amide products (equation 1).



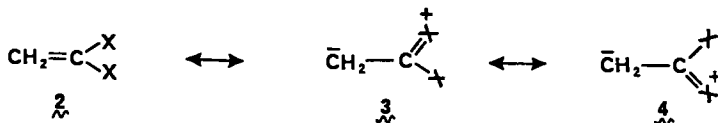
This paper will describe the reactions of ketene aminals, 1, more highly activated electron-rich alkenes, with isocyanates to again afford amide products. We shall initially discuss the chemistry of the ketene aminal/isocyanate reaction, the preparation of these activated monomers and some properties of solution-derived model "hard segments".

0097-6156/85/0270-0125\$06.00/0
© 1985 American Chemical Society



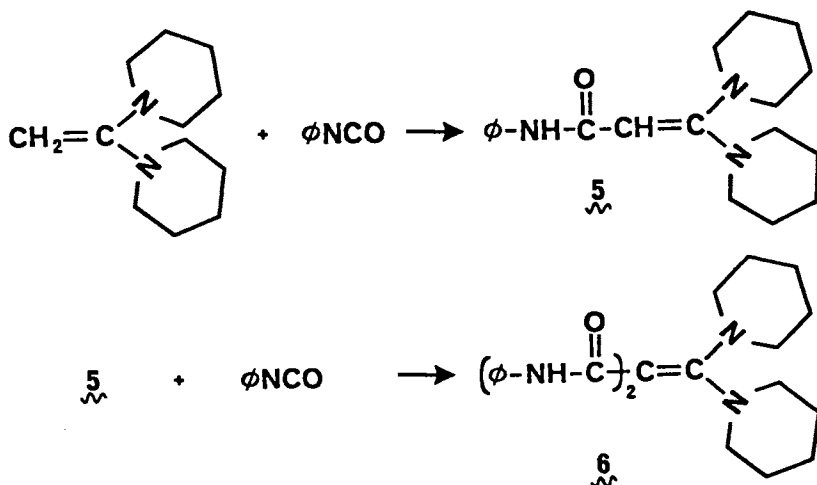
I. Chemistry of the Ketene Amino/Isocyanate Reaction

The reactivity of electron-rich alkenes towards isocyanates is governed by the polarization of the functionality as shown.



The availability of the unshared pair of electrons on the heteroatom(s) dictates the potential reactivity of these compounds. For enamines (vinylamines) or ketene aminals, the more basic $-\text{NR}_2$ groups give more reactive compounds. Secondly, the orbital containing the available electron pair must be coplanar with the pi orbital of the alkene for polarization, 4, to occur. Clearly, greater polarization gives more nucleophilic character to the β -carbon and enhanced reactivity towards isocyanates.

Clemens reported the reaction of 1,1-di(N-piperidinyl)ethylene, 1 ($-\text{NR}_2 = \text{piperidinyl}$), with both one and two molar equivalents of phenyl isocyanate. (4)



Clemens reported additionally that the phenyl isocyanate diadduct 6 was "quite stable towards hydrolysis, being unaffected by refluxing overnight with aqueous sodium hydroxide." (4)

Our investigations have confirmed this earlier work; ^{13}C NMR analysis of the diadduct product is consistent with the formation of 6.

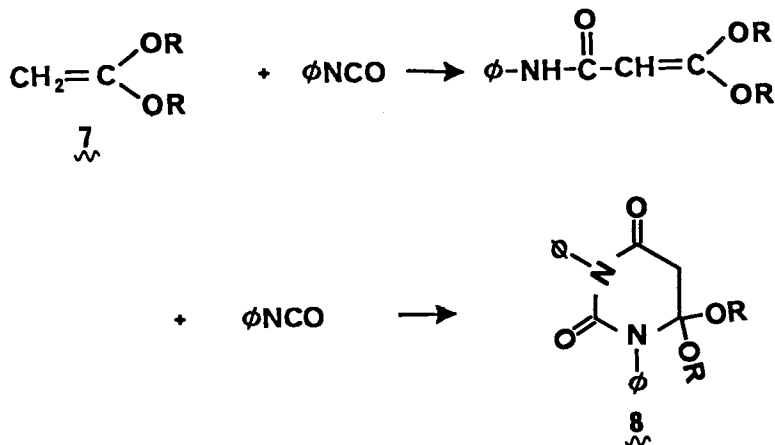
Our investigations have shown additionally that the reaction between various ketene aminals and two equivalents of isocyanate is rapid, exothermic and essentially quantitative with or without the use of solvent. No catalysis is required to achieve quantitative results.

Reactions of these activated alkenes with phenyl isocyanate with or without added solvent were used to gauge the reactivity of various RIM-extender candidates. Compounds which failed to give essentially quantitative reactions were deemed unlikely RIM candidates. Additionally, the melting points of the bis-phenylisocyanate adducts were used to model the melting behavior of the bis-amide hard segments which would result from the use of these compounds as extenders in MDI-based RIM systems.

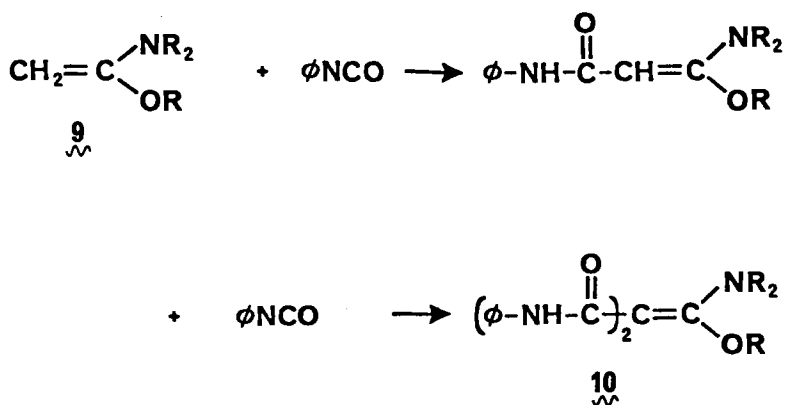
Ketene aminals must be protected from moisture. Water causes a rapid hydrolysis of the ketene aminal giving a substituted acetamide and a mole of secondary amine. Additionally, the preparation of these compounds from triethylorthoacetate at reflux temperatures invariably gives 10 to 20% formation of undesired acetamide side products. The thermal rearrangement of triethylorthoacetate to ethylacetate has been reported earlier. (11)

We have found that the reaction between triethylortho-acetate and excess piperidine or morpholine with acidic catalysis is not an equilibrium reaction. Ethanol generated need not be removed as it forms. Additionally, NMR studies indicate that at 100°C the preparative reaction is complete in 10 to 20 minutes with little or no substituted acetamide side products formed. The stability of these compounds in the presence of alcohol and/or excess amine contrasts the behavior of ketene acetals which revert rapidly to orthoesters in the presence of alcohol. This of course speaks to the utility of these various compounds in the presence of hydroxyl functionalities from either RIM polyols or RIM glycol coextenders.

Variations of the ketene aminal structure were also screened as extender candidates. Ketene acetals 7 give barbituric acid derivatives 8 in less than quantitative yields. (5) Additionally, the instability of ketene acetals in the presence of primary alcohols would limit their RIM utility. (6)

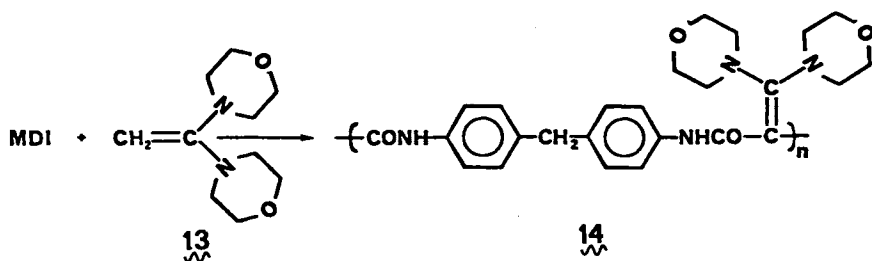


The mixed O,N acetals 9 give better yields in model reactions, 95%, but the bis amide products 10 have rather low melting points (130°C). (5)



II. Solution and Bulk (RIM) Polymerizations Using Ketene Aminoal

A series of polyamides were prepared by reaction of 4,4'-methylene bis(isocyanatobenzene), MDI, with various ketene aminoal. A typical reaction using 1,1 bis(4-morpholino) ethylene, 13, and MDI to give polymer 14 is shown.



A DSC analysis of 14 using a DuPont 910/990 system shows a prominent glass transition of 85°C. A small melt can be seen at 215-220°C. Annealing a DSC sample followed by a rescan did not suppress the observed T_g or give an enhanced melt. Thermogravimetric analysis at 10°C/minute under nitrogen shows polymer degradation occurring after 225°C.

Table I summarizes properties of RIM elastomers obtained at a 40% hard segment level. Several isocyanate indices are given. Systems having a "1" suffix, i.e. A1, were not post-cured. Systems with a "2" suffix were post-cured under conditions given. In general, the higher index systems give higher strength properties and lower elongations at break. Comparison of non post-cured with post-cured systems indicate little property enhancement upon post-cured.

Tables II and III summarize properties of 50% and 60% hard segment systems at different indices. Higher hard segment parts show higher hardnesses and strength properties with lower elongations at break. Heat sags for systems A-I are all relatively poor, actual values are routinely greater than one inch after exposure to 250°F for one hour. DSC studies indicate good phase separation as evidenced by a well defined soft segment glass transition at -55°C. The hard segments appear to be largely amorphous with a prominent hard segment glass transition at 60-65°C with a small broad melt at 160 to 220°C. We were unable to enhance the hard segment crystallinity by annealing.

Table I. 40% Hard Segment Systems

	A1	B1	C1	A2	B2	C2
NCO Index	1.00	1.05	1.10	1.00	1.01	1.10
Density, g/cc	1.14	1.14	1.15	1.15	1.15	1.15
Hardness, Shore D	50	50	50	50	50	50
Flexural, Modulus, psi	18000	22000	25000	18000	21000	27000
Tensile Strength, psi	2300	2400	2600	2500	2600	2600
Elongation at Break, %	490	430	427	450	420	340
Tensile Set, %	50	47	50	50	47	40
Die C Tear, pli	480	476	487	460	479	490
Post Cure	None	None	None	180°F/ 1 Hr.	180°F/ 1 Hr.	180°F/ 1 Hr.

Table II. 50% Hard Segment Systems

	D1	E1	F1	D2	E2	F2
NCO Index	1.00	1.05	1.10	1.00	1.05	1.10
Density, g/cc	1.12	1.12	1.11	1.12	1.11	1.12
Hardness, Shore D	65	65	65	65	65	65
Flexural Modulus, psi	57000	57000	62000	58000	59000	65000
Tensile Strength, psi	2400	2400	2700	2400	2700	2700
Elongation at Break, %	310	323	330	307	297	287
Tensile Set, %	70	73	77	72	70	70
Die C Tear, pli*	594	617	655	639	663	638
Post Cure	None	None	None	180°F/ 1 Hr.	180°F/ 1 Hr.	180°F/ 1 Hr.

* Pounds per linear inch, pli

Table III. 60% Hard Segment Systems

	G2	H2	I2
NCO Index	0.95	1.00	1.04
Density, g/cc	1.12	1.13	1.12
Hardness, Shore D	72	72	74
Flexural Modulus, psi	102,000	114,000	116,000
Tensile Strength, psi	3,400	3,600	3,800
Elongation at Break, %	167	177	157
Tensile Set, %	95	97	98
Post Cure	250°F/1 Hr.	250°F/1 Hr.	250°F/1 Hr.

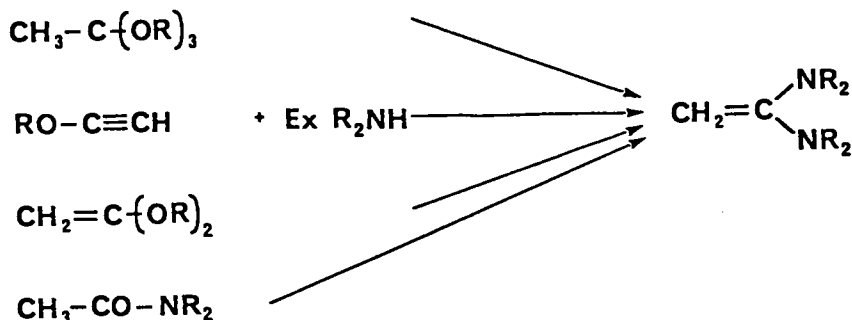
Table IV summarizes properties of isocyanurate systems. Isocyanate indices of 1.11 to 2.00 were molded using an additional catalyst to convert the excess isocyanate into isocyanurate. The basic system is a 50% hard segment level which is progressively overindexed. The 2.00 index system M is a 60% hard segment and 10% isocyanurate hard segment. These systems are crosslinked with the molecular weight between crosslinks lower with higher isocyanate indices. Inclusion of the high melting (triphenylisocyanurate $T_m = 285^\circ\text{C}$) tri-functional isocyanurate structure increases the hardness and strength properties, improves the heat sags and gives lower tensile elongations with increasing crosslink density.

Table IV. Isocyanurate Systems

	J1	J2	K2	L1	L2	M2
NCO Index	1.11	1.11	1.30	1.50	1.50	2.00
Density,g/cc	1.12	1.12	1.12	1.14	1.13	1.13
Hardness,Shore D	65	65	72	74	75	79
Flexural Modulus, psi	60000	65000	91000	103000	117000	138000
Tensile Strength, psi	2200	2900	3200	2800	3400	4400
Elongation at Break, %	207	150	118	97	67	58
Tensile Set,%	78	63	57	42	32	26
Heat Sag- 250°F/1 Hr.		1.00	0.53			0.07
Post Cure, 250°F/1 Hr.	NO	YES	YES	NO	YES	YES

EXPERIMENTAL

Ketene aminoal can be prepared from the reaction of orthoesters, alkoxyacetylenes or ketene acetals with excess secondary amine. (4,7,8)



Treatment of ethoxyacetylene with excess morpholine or piperidine gives the corresponding ketene aminoal in 85% and 78% respectively. (4) Reaction of triethylorthoacetate with either morpholine or piperidine gives the same products in 88% and 68%.⁸ Preparation from substituted acetamides involves either preparation of an intermediate mixed O,N acetal or the use of rather expensive reagents. (9,10)

Solution derived polyamides were prepared as 15% solids in N,N-dimethylacetamide at room temperature under argon. The polyamides were isolated by slowly pouring the polymerization reaction mixtures into methanol and collecting the precipitated polymers.

Ketene aminoal 13 was used in all RIM formulations. Compound 13 is soluble in polyols currently used in urethane RIM technology. Ketene aminoal 13 was used as a urethane chain extender, "hard segment", in concert with higher equivalent weight polyols, "soft segments". Again for ease of comparison, Thanol SF-6503^R a six thousand molecular weight triol supplied by Texaco was used in all formulations discussed. Isonate 181^R was used in systems A-1; Isonate 143L^R was used in the isocyanurate systems J-M. Both isocyanates are supplied by The Upjohn Company. A urethane catalyst, T-12^R, was used in all formulations. Isocyanurate systems utilized an additional isocyanate trimerization catalyst T-45^R. Both catalysts are supplied by M & T Chemical Company

Parts were prepared on an Admiral 2000 HP RIM machine. A flat, plaque mold was used; mold temperature was kept between 175-180°F. Gel times ranged from 0.6 seconds for 60% hard segment parts to 1.2 seconds for isocyanurate systems. Demold times ranged from 0.5 to 1.0 minutes. Post-cure temperatures of 180-250°F were used. Not all parts prepared were post-cured.

Mechanical properties of parts were determined using standard ASTM procedures. Heat sag measurements reflect the verticle drop in inches of a four inch cantilevered specimen after exposure to a given temperature for a given length of time.

Percentage of "hard segment" in the molded part reflects the weight of extender plus the weight of isocyanate reacting with the extender divided by the weight of the total formulation. Hard segment levels of 40-60% are discussed.

Literature Cited

1. L. M. Alberino, "Future of RIM Development in the USA in the 1980s"; Reaction Injection Molding and Fast Polymerization Reactions. J. E. Kresta, ed., Plenum, New York, 1982, p. 1 and references therein.
2. D. F. Regelman and L. M. Alberino, Org. Coatings and Plastics Chem., 44 151 (1981).
3. D. F. Regelman and L. M. Alberino, *ibid.* 157 (1981).
4. D. H. Clemens, J. A. Bell, J. L. O'Brein, *JOC*, 2932 (1964).
5. F. Effenberger, R. Gleiter, G. Kiefer, *Chem. Ber.*, 99 3893 (1966).
6. A. Kankaanpera, et al., *Acta Chemica Scandinavica*, A28, 815 (1974).
7. H. Bohme and F. Soldan, *Chem. Ber.*, 95, 3109 (1961).
8. H. Baganz and L. Domaschke, *Chem. Ber.*, 95, 2095 (1962).
9. H. Ahlbrecht and C. Vonderheid, *Chem. Ber.*, 106, 2009 (1973).
10. H. Weingarten and W. White, *JOC*, 31, 2874 (1966).
11. S. M. McElvain and B. E. Tate, *JACS*, 202 (1945).

RECEIVED May 7, 1984

Nylon 6 RIM

R. M. HEDRICK, J. D. GABBERT, and M. H. WOHL

Monsanto Company, St. Louis, MO 63166

The successful utilization of Reaction Injection Molding (RIM) to fabricate complex polyurethane shapes in a single step from relatively low viscosity streams has led to a search for other chemical systems which can be fabricated by the RIM process. The rapid polymerization of molten caprolactam by anionic catalysis has been utilized to develop attractive nylon RIM systems. The incorporation of a rubber segment in the polymer chain allows the fabrication of high impact or even elastomeric nylon parts. The combination of a rubber phase with the high melting (215°C) crystalline nylon phase provides useful properties at low temperatures as well as at elevated temperatures.

Equipment is now commercially-available for nylon RIM and while process conditions are different from those required for urethane RIM, cycle times are competitive. No postcure is required.

The success of urethane reaction injection molding (RIM) has led to a search for other chemistry with suitable characteristics for RIM which can yield products with useful properties and good economics. Lactams, especially caprolactam, are potentially interesting candidates.

Caprolactam is commercially-available at a reasonable price. Molten caprolactam can be polymerized by anionic catalysis in one to five minutes with low exotherm to produce a solid part. The polymerization is essentially complete in that time, although an equilibrium amount of monomer remains dependent upon the temperature (approximately two percent monomer at 160°C). No postcure is necessary.

The product of the anionic polymerization of caprolactam is nylon 6, a crystalline polymer with excellent mechanical properties, melting at 215°C. The development of nylon block copolymers has permitted the range of properties to be extended from nylon 6 on one extreme through tough engineering-type products to soft elastomeric products on the other extreme. In addition to improved properties for RIM products, these block copolymers offer some process

0097-6156/85/0270-0135\$07.75/0

© 1985 American Chemical Society

advantages over nylon 6 RIM. These advantages include lower mold temperatures, reduced shrinkage in the mold and perhaps faster molding cycles. When compared to urethane RIM systems, these products offer an improved balance of stiffness and toughness, better chemical and temperature resistance, lower toxicity and simpler processing requirements.

Anionic Polymerization of Caprolactam

Joyce and Ritter (1) in 1941 obtained a patent on the base catalyzed polymerization of caprolactam. They described the reaction of a small amount of sodium or other alkali metal in caprolactam to form sodium caprolactam and the rapid, exothermic polymerization of caprolactam above 200°C to form molten nylon polymer. The polymerization reaction is an isomerization of the low viscosity cyclic amide to a high viscosity, high molecular weight polyamide. Although the product of this early technology was a molten polymer, the rapid polymerization and high molecular weight polyamide product are clearly desirable qualities for a reaction injection molding (RIM) system.

The mechanism for the polymerization was not understood and since interest in the anionic system was for its use in the preparation of polymer for melt process application, i.e., fiber or plastic moldings, most of the work during the next decade concentrated on controlling the molecular weight of the polymer produced or reducing it to desired levels after polymerization. Surprisingly, the molecular weight of the nylon 6 prepared by the anionic method was always very high and was not a function of the sodium caprolactam concentration.

In the light of later knowledge, it can be postulated that not only did ring-opening polymerization occur, but that each chain formed had one amino end group and one acyllactam end group (see Figure 1) giving rise to the possibility of combinations of chains by a condensation polymerization mechanism as well.

In 1955, Monsanto Company began exploratory research on the base catalyzed polymerization of lactams. A two-stage mechanism for the thermally-initiated anionic polymerization was postulated as shown in Figure 1. This proposed mechanism was first published in Italian patent 580069 which was issued July 28, 1958. (2) H. K. Hall (3) of DuPont subsequently proposed an identical mechanism which was published in December, 1958. The mechanism was tested by the simple procedure of adding a pre-formed acyllactam to caprolactam containing sodium caprolactam at 160°C. Very rapid polymerization and a solid nylon casting resulted in four to five minutes. In the absence of the acyllactam initiator, polymerization did not occur. The mechanism for the acyllactam initiated caprolactam polymerization shown in Figure 2 produces a nylon chain with an acylamino end group and without the amino end group of Figure 1.

In the absence of impurities, there is no termination reaction. Polymerization stops when the monomer level is reduced to an equilibrium amount which is a function of temperature. The condensation polymerization route which results in very high molecular weight cannot occur with this initiated polymerization. Below temperatures at which the thermal initiation occurs, the initiator concentration controls the number of chains started and thus the molecular weight.

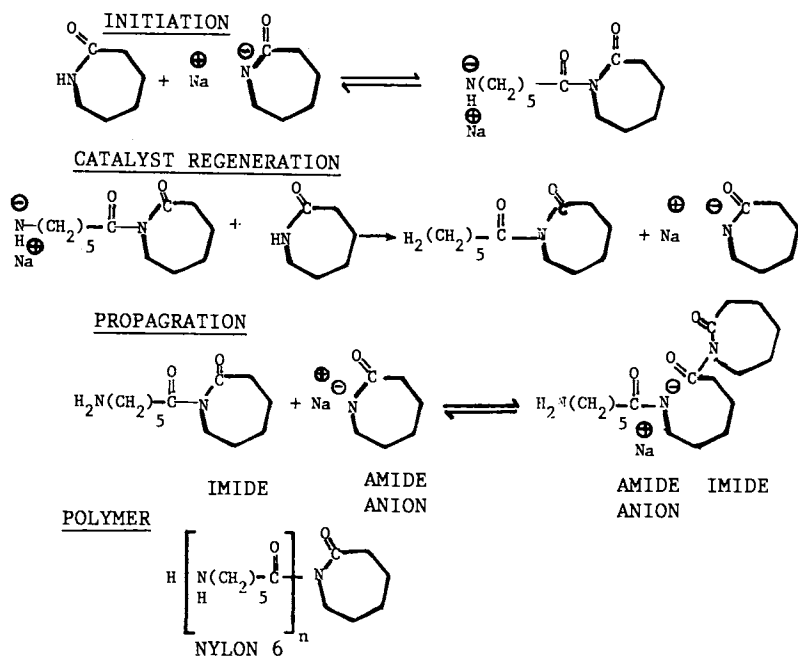


Figure 1. Proposed mechanism for the thermally initiated anionic polymerization of caprolactam.

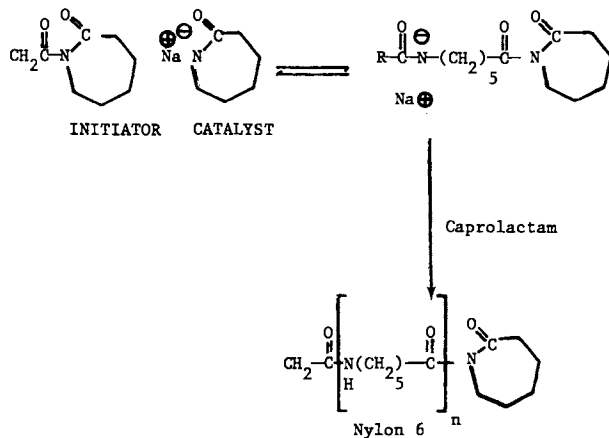
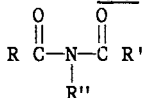
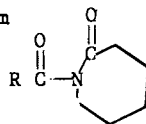


Figure 2. Acylactam initiated anionic polymerization of caprolactam.

A branching reaction results in the combination of chains to give a product of higher molecular weight than predicted by acylactam concentration. The addition of a primary amine such as aniline in an amount equivalent to the acylactam appears to eliminate the branching reaction and linear polymer with a normal distribution of molecular weights can be prepared over a very broad molecular weight range. (4) Since primary amines are known to react with acylactams, the probable reaction is shown in Figure 3. The molecular weight control is achieved by stoichiometric formulation and the product has neither appreciable amine or carboxyl end groups. A number of patents were issued to Monsanto Company which detail the structural requirements for initiators for the anionic polymerization of caprolactam and their use. (5) The most important structure for the initiator is

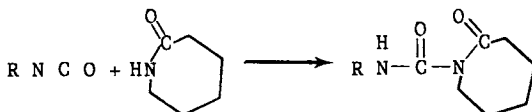


cannot be a hydrogen. The most commonly-used initiators combine R' and R'' and have the structure of an acylactam



Examples of this type are acetylcaprolactam and adipoylbiscaprolactam.

A convenient method for forming an initiator in situ is by reacting an isocyanate with the caprolactam monomer.



Use of diisocyanate produces an initiator molecule capable of growing at both ends, which allows faster polymerization rate for a given molecular weight product. With diinitiators the product is usually lightly crosslinked due to a branching reaction.

The most commonly-used catalysts for caprolactam polymerization are sodium caprolactam and caprolactam magnesium bromide. The latter catalyst can be made by reacting a Grignard reagent with caprolactam.

The anionic polymerization of lactams has been explored in great depth by Wichterle and Sebenda and their co-workers at the Institute of Macromolecular Chemistry in Prague. (6-8)

Nylon 6 Reactive Molding

The use of initiated anionic polymerization to produce cast shapes directly from caprolactam was commercialized in the United States by the Polymer Corporation. The technology was particularly useful for the production of large pieces since the molten monomer is of low viscosity, the initial rate of increase of viscosity of the catalyzed feed is low and the heat of polymerization is low. A similar system was commercialized in Germany by Bayer. (9)

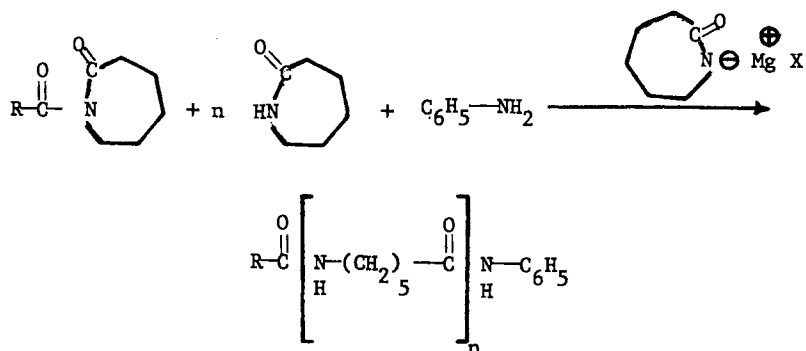


Figure 3. Use of aniline to control molecular weight and distribution.

The adaptation of the anionic polymerization of lactams to casting and reaction injection molding of commercial products has undoubtedly proceeded at several companies. The progress presented here reports the activities at Monsanto Company since that is the work with which the authors are most familiar.

In 1962, work was initiated by Monsanto in the use of particulate reinforcement of polymers. Although particulate or mineral reinforcement does not provide the increase of stiffness obtainable with fibrous reinforcement, it does have some advantages. It is low cost, reduces the multiaxial impact much less than fibrous reinforcement and yields readily pumpable slurries of high loading with low-viscosity monomers such as molten caprolactam. In order to obtain reinforced properties with particulate reinforcement, it is necessary to treat the mineral with coupling agents. For silica or silicates, the organic functional silane coupling agents are very effective. A polyamide such as nylon 6 is a polar polymer and bonds well to a polar silicate mineral as long as the system is completely dry. Moisture which permeates through the nylon readily completely disrupts the adhesion to uncoupled reinforcements and the mechanical properties are severely and irreversibly degraded. Functional silanes, such as 3-aminopropyl triethoxysilane provides an effective bond between the nylon and silicate surface. While the nylon matrix is still plasticized by moisture, the bond between phases is not destroyed and reinforced properties are maintained.

In the 1960's Monsanto developed and commercialized several mineral-reinforced formulations tailored for RIM as well as a mineral-reinforced nylon 6 for injection molding. The product was sold under the trademark Vykan. The range of properties of typical products are given in Table I. Since this was before the development of the impingement mix-head, equipment was designed and built which automatically batch-catalyzed, degassed and injected the charge into the mold. After injection, fresh charge of slurry containing initiator, mineral and molten caprolactam was automatically dispensed into the holding vessel, diluting any remaining catalyzed material sufficiently that polymerization did not proceed until the next catalyst charge was added.

Minerals were used in the range of 30 to 60 percent by weight. The most useful minerals were ground quartz (SiO_2), Wollastonite (CaSiO_3) and calcined clay. Although the silica is very abrasive and could not be tolerated in an injection molding or extrusion resin, the slurries in the low viscosity caprolactam were pumped and cast without excessive abrasion. Calcined clay is much less abrasive than silica and is preferred if the mineral reinforced polymer is to be post-processed by injection molding.

The best combination of properties, especially impact strength, was obtained with very small mineral particles in the range of one to two microns. The acicular shaped Wollastonite particles contributed greater stiffness to a product, sometimes with a sacrifice of impact strength.

Hundreds of thousands of pigmented chair shells were produced for sale by this method. Since all surfaces were appearance surfaces, sink-marks or other surface defects could not be tolerated. Methods were developed which compensated for polymerization

Table I. Mechanical Properties of Vykan A (Mineral-Reinforced Nylon 6)

Property	Units	Dry, as		ASTM Procedure
		Fabricated	~1.3% H ₂ O	
Tensile Strength	10 ³ psi			
Yield		8.70-14.8		D-638
Fail		8.50-14.7	6.90-8.80	
Tensile Elongation	%			
Yield		2-3		D-638
Fail		3-7	6-12	
Tensile Modulus	10 ⁵ psi	8-17	5-8	D-638
Flexural Strength	10 ³ psi	18-25	9-15	D-790
Flexural Modulus	10 ⁵ psi	8-17	3.3-8	D-790
Impact				
Falling Dart	ft-lbs	4-30	4-65	Monsanto
Falling Ball	ft-lbs	8->45	11->45	Monsanto
Deformation under load	%			
2000 psi, 122°F, 24 hrs		0.1-0.8	0.2-0.18	
4000 psi, 122°F, 24 hrs		0.25		
Compressive Stress	10 ³ psi			
@ 1% Strain		16-19	12-14	D-695
Rockwell Hardness				
R-Scale		120		D-785-65
M-Scale		92-100		

shrinkage without defects. Furniture consisting of headboards, desks, and chests and luggage racks was produced for a twelve-hundred room motel. Castings as large as thirty-five pounds were produced for a variety of individual parts.

The total cycle time for the mineral-reinforced nylon 6 casting process was three to four minutes. While details of this system have not been published, the technology is contained in a number of patents. (10)

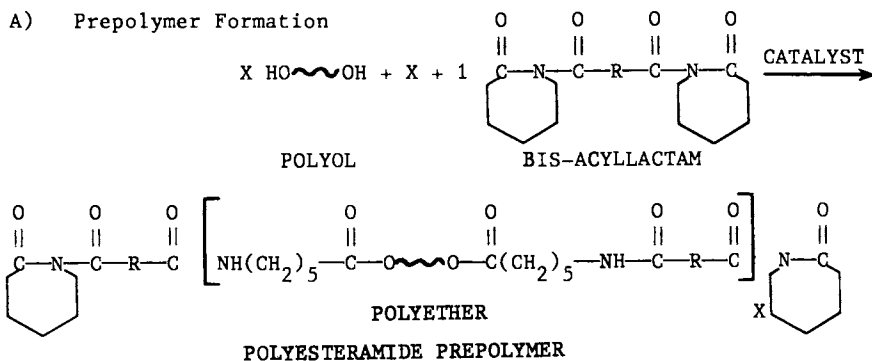
The production of cast mineral-reinforced nylon 6 products was terminated in 1971. Research was then directed at expanding the range of properties obtainable from the anionic polymerization of caprolactam through nylon block copolymers and their fabrication by reaction injection molding.

Nylon Block Copolymers

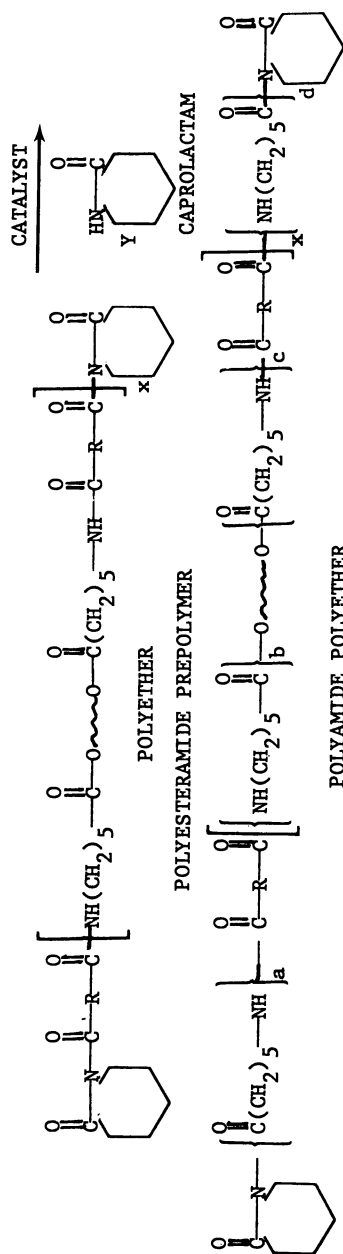
Chemistry

Nylon block copolymers were previously synthesized from the anionic polymerization of caprolactam in the presence of polyurethane prepolymers. (11) The prepolymers, prepared from the reaction of diisocyanates with polyether glycols, contained isocyanate end groups which initiated caprolactam polymerization. Sodium caprolactam was used to catalyze the reaction. This copolymer system is the basis for some current areas of nylon 6 RIM research. (12)

NYRIM nylon block copolymers are formed from stoichiometric mixtures of polymeric polyols and caprolactam using poly acyllactam initiation which was described previously. The reactions are as follows:



In the prepolymer reaction, the multifunctional acyllactam which normally acts as initiator for caprolactam polymerization, also functions to combine the polymeric polyol moieties. An excess of acyllactam is used so that the resulting prepolymer is terminated by acyllactam. The reaction occurs slowly with heat (13), but in the presence of an alkaline catalyst is completed within seconds. The prepolymer may be prepared in mass or in the presence of inert organic solvents, or in caprolactam as part of the total copolymerization reaction. See Reaction B.



In the anionic polymerization to form nylon block copolymer, the acyllactam initiates caprolactam polymerization from the ends of the prepolymer.

At the same time, the ester linkages along the prepolymer backbone act as weak initiation or transfer sites so that polycaprolactam may insert at these points throughout the prepolymer chain. The result is an alternating block copolymer or A(BA)_x instead of ABA which would occur if caprolactam polymerization occurred only from the acyllactam initiating end groups. The structure is presented more clearly in schematic. See page 147.

The amount of caprolactam available for copolymerization is equally divided between the active prepolymer ester and acyllactam groups so that the resulting nylon blocks are all the same molecular weight within the normal distribution curve for condensation polymers (i.e., $M_w/M_n = 2/1$). The elucidation of the alternating structure is described more fully by J. E. Kurz. (14) Kurz used a method of selective degradation of the polyol blocks of nylon block copolymer and analyzed the resulting nylon residues.

The molecular weight of polyol and the ratio of polyol to bisacyllactam determine the molecular weight of resulting prepolymer. These parameters in addition to the amount of polyol in the final resin determine the molecular weight of the final nylon block copolymer product. The molecular weight of the individual nylon blocks are determined by polyol molecular weight and by percentage of polyol in the final polymer. Thus, very good control can be exercised over molecular weight and properties of the copolymers.

The alkaline catalyst systems used for caprolactam polymerization are suitable for both the prepolymer and copolymerization reactions. The preferred catalyst is caprolactam magnesium bromide, prepared by reaction of Grignard reagent with caprolactam. With NYRIM copolymers, a two-package system is used—reactive prepolymer and catalyst concentrate. These are dissolved in caprolactam to make up the two reactive streams.

Most glycols or polyols such as polyether or hydrocarbon diols may be used in the reaction to give block copolymers. Other types of polyols such as polyester polyols may be used in the reaction to yield useful resins, but these will not give block copolymers. The multiple ester linkages in polyester act as multiple transfer sites so that a random copolymer is obtained.

Properties

The properties of nylon block copolymers are determined to the greatest extent by the ratio of polyol to polyamide. Other factors which play an important role are polyol type, polyol molecular weight, coupler-activator type and reactant ratios as well as the polymerization conditions.

A typical range of nylon block copolymer properties is illustrated in Table II. The effect of rubber phase concentration is seen when the polyol content is varied from 0 to 60%. For these data, polypropylene glycol of 2000-molecular weight was used. The expected changes occurring with increased polyether soft block phase are decreased hardness, tensile strength, tear strength and flexural modulus accompanied by increases in tensile elongation,

recovery and impact strength. The five-fold decrease in tensile strength is accompanied by an eighteen-fold increase in elongation—an effect which is reflected in the impact strength. Incorporation of small amounts of polyol result in a dramatic decrease in notch sensitivity for increased Izod as well as multiaxial impact strength. At low levels of polyol a modified nylon 6 is obtained which has a combination of high modulus and high impact strength.

In general, higher molecular weight polyols contribute to a better balance of impact strength and flexural modulus, particularly in the lower polyol, higher modulus end of the physical property spectrum. Molecular weights of at least 2000 are required, with further improvements as polyol molecular weight is increased beyond that level. Multifunctional polyols also contribute to better properties through crosslinking.

Table II. Effect of Polyol Content on NBC

Property Dry as Molded	Percent Polyol				
	0	10	20	40	60
Shore D Hardness	84	83	78	62	37
Tensile Strength PSI	10,800	7,800	6,400	5,300	2,100
% Elongation	30	35	285	490	530
% Recovery	30	30	30	60	80
Tear Strength PLI	1,800		1,300	800	410
Flexural Modulus PSI	390,000	280,000	220,000	31,000	
Notched Izod Impact Ft Lbs./In.	0.6	1.6	5.7	N.B.	N.B.

The effects of polyether content on the impact strength/stiffness balance for a different polyether copolymer are illustrated graphically in Figure 4. Flexural modulus and Izod impact strength are shown as a function of polyether content. As polyether content is increased, flexural modulus exhibits an expected decrease. This occurs linearly up to 30% polyether. At the same time, Izod impact strength increases. The increase is also linear in the low polyether range. But starting at about 14% polyether, the impact curve shows an increase in impact occurring at a much higher rate than the decrease in flexural modulus. Thus, at 14% and higher polyether, the copolymers have a much better balance of impact strength and stiffness. This phenomenon occurs with other polyol nylon block copolymers as well as other rubber-reinforced resins.

Structure and Morphology

While the polyether rubber phase results in higher impact strength and greater tensile elongation, the high melting nylon blocks continue to provide crystallinity for the hard block phase resulting in high polymer melting points and high resistance to heat sag. Differential scanning calorimeter and torsion pendulum studies on linear nylon block copolymers show transitions at -60 to -70°C (polyether) and at 45 to 50°C (nylon 6). These transitions occur in all copolymers for the entire range of polyether content. Melting temperatures range from 195° for 65% polyether copolymer to 216°C (nylon 6 T_m) for 20% polyether.

The dynamic modulus curves from torsion pendulum data (14) are reproduced in Figure 5 and show complex modulus (G^*) as a function of temperature for a series of NBCs ranging in polyether content from 0 to 66%. The curves representing 9 and 18% polyether copolymers are quite similar to, but not identical with nylon 6, which is shown in the dashed curve. The copolymer curves show a deflection at -60°C , the t_g for polyether. This deflection becomes much more pronounced while changes in the nylon t_g region at 45 to 50°C are not apparent.

From the same data, the loss modulus (G'') is plotted as a function of temperature in Figure 6. The curves for 9 and 56% polyether were deleted for clarity. In Figure 6 the damping peaks for nylon t_g are more clearly shown. As polyether content is increased from 37 to 66%, the -60°C polyether peaks become more pronounced, while the change due to nylon 6 in these regions becomes more diffuse. This may be explained in part by the nylon crystallinity which tends to broaden the transition region and also to decrease the amount of amorphous material which give rise to the transition. Another reason is the changes in morphology occurring in the copolymer with changes in polyether content. In the range 0 to 20% polyether, nylon is the continuous phase. In the mid-range of 37%, the polymers are becoming more elastic and at higher polyether concentration, nylon becomes the dispersed phase with the nylon crystallites acting as crosslinks to stiffen the polyether rubber phase.

Heat Resistance

Table III shows the effect of temperature on flexural modulus for copolymers with polyol contents in the mid-range 20-40%. The low modulus ratio at $-29/70^{\circ}\text{C}$ shows only slight change over the polyol range even though the modulus shows an eighteen-fold decrease as polyol is increased from 20-40%.

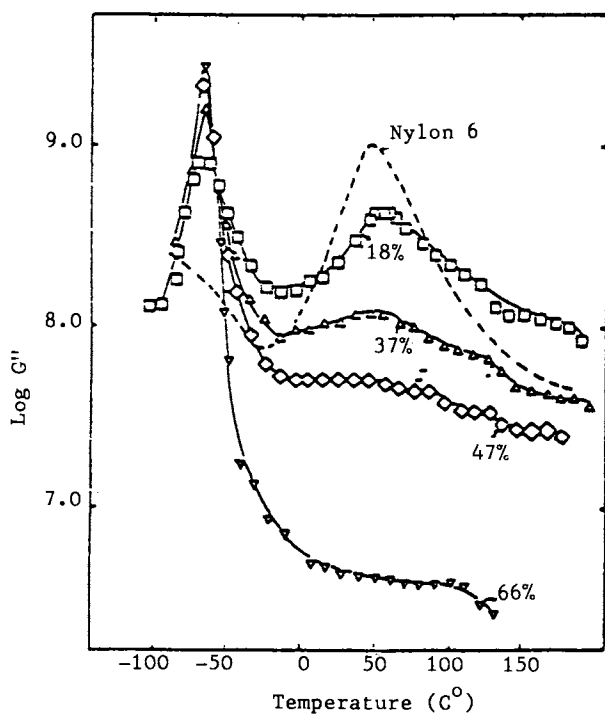


Figure 6. Loss modulus versus temperature for nylon block copolymer.

Table III. NBC Temperature-Modulus Response

	Polyol Content			
	20	30	35	40
Flexural Modulus				
@ -20°C	296,000	80,000	54,000	28,000
23°C	197,000	42,000	22,000	11,000
70°C	71,000	21,000	17,000	9,000
Modulus Ratio				
-29°/70°C	4.2	3.8	3.2	3.1

The contribution of the crystalline high melting nylon 6 blocks and soft-block hard-phase separation are also reflected in the resistance to heat sag exhibited by NBC. Table IV shows the heat sag at 163°C as these values are related to the flexural modulus. Even at the very low end of the modulus spectrum, sag values were quite low.

The low heat sag values relate to the ability of fabricated parts to withstand automotive assembly line paint bake-oven cycles—an ability which could eliminate the requirement for a separate off-line painting operation and permit use of the same paints used for steel components.

Table IV. NBC Heat Sag/Flexural Modulus

Flexural Modulus PSI @ 23°C	Heat Sag 163°C - in.
169,000	0.1
115,000	.06
60,100	0.15
33,500	0.15
24,700	0.2
11,000	0.34

.125" thick specimen 4" overhang - 60 minutes

Moisture Effect

The effect of moisture on nylon 6 resins is well-known and well-documented. (15) Because of this, the susceptibility of nylon block copolymers to moisture absorption was expected. Evaluation of requirements for exterior automotive body panels and other applications requiring dimensional stability indicated that early nylon block copolymer formulations would not meet specifications

with regard to expansion due to moisture absorption. The decrease in expansion resulting from the use of glass fiber reinforcement was not sufficient to give the required dimensional stability.

The use of polyol rubber blocks in NBC gave unexpected increase in moisture absorption over that of nylon 6. The effect of absorption on linear expansion is shown in Figure 7 for three types of polyol blocks. Polyol level was 20% of copolymer. Polyols A and B not only increased the total moisture absorption, but greatly increased the rate of absorption as well. Reinforcement with glass fiber will give further improvement in dimensional stability, as illustrated below, but the degree of improvement is insufficient to meet specifications for critical applications.

A third polyol variation (Curve C) gave a further significant decrease in moisture expansion. Use of Polyol C not only decreased the amount absorbed, but the rate of absorption as well. The absorption rate of Polyol C copolymer was identical to nylon 6. The dimensional stability of this copolymer appears to be sufficient for most applications, when reinforced with glass fiber.

The effect of relative humidity on the three copolymers is shown in Figure 8. Under the conditions of relative humidity typical of the end-use, Polyol C gave almost 30% improvement in expansion over the original NBC formulation while Polyol B gave nearly 60% improvement. The added improvement of milled glass fiber reinforcement with Polyol C is illustrated in the immersion growth data of Figure 9. The range of values for reinforced resin reflects orientation of glass fiber. Expansion is reduced to a maximum of 0.3% by reinforcement with 25% 1/16" milled glass fiber. These values appear to be well within parameters for exterior automotive applications or other areas requiring dimensional stability.

Molding Processes

Anionic polymerization of nylon-based polymer systems to produce finished parts directly from monomers or prepolymers can be carried out by several processes; e.g., reaction injection molding, low-pressure casting, resin transfer molding, rotational casting.

For our purposes, reaction injection molding is defined as a process in which two or more reactive streams are combined and mixed with an impingement mixing device and injected into a closed mold where they polymerize to rapidly form a plastic part. To compensate for polymerization shrinkage, RIM parts are foamed to some degree.

In low-pressure casting, static or dynamic mixers are employed and the pumping systems are set up to compensate for polymerization shrinkage by packing the mold with additional material. Thus, a solid part can be produced.

In resin transfer molding, a preformed reinforcing mat is placed into the mold and the reacting liquid stream is injected so as to fully impregnate the reinforcement. This permits the use of large percentages of heavy continuous fiber or long fiber reinforcement so as to impart maximum stiffness and toughness to the molded part, much higher than is possible with the short fiber reinforcements required for the RIM or casting processes.

In rotational casting, the reactant mixture is introduced into a closed mold which rotates around one or more axes so as to produce

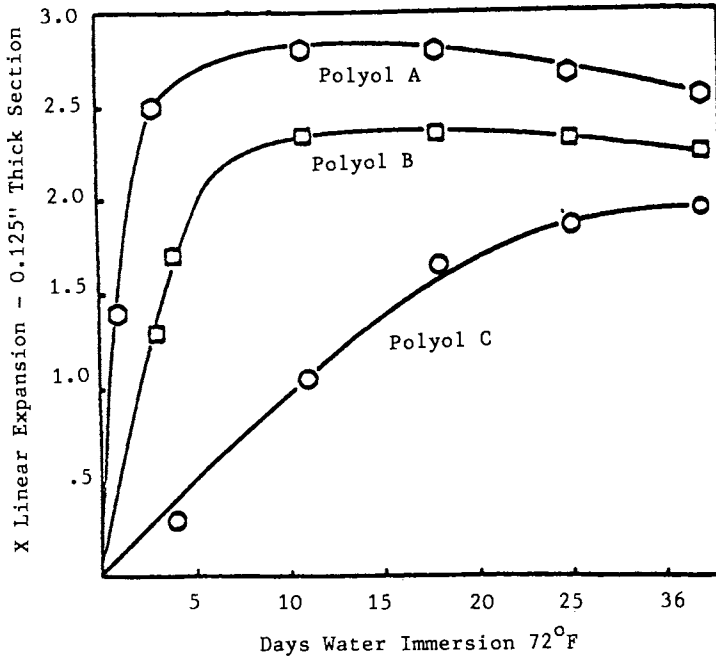


Figure 7. Effect of water immersion on expansion of nylon block copolymer.

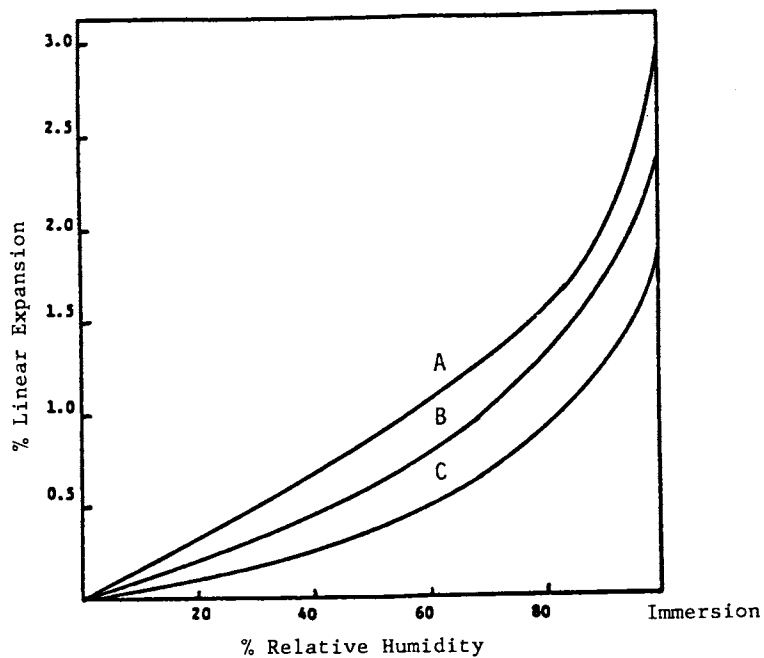


Figure 8. Effect of relative humidity on expansion of nylon block copolymer.

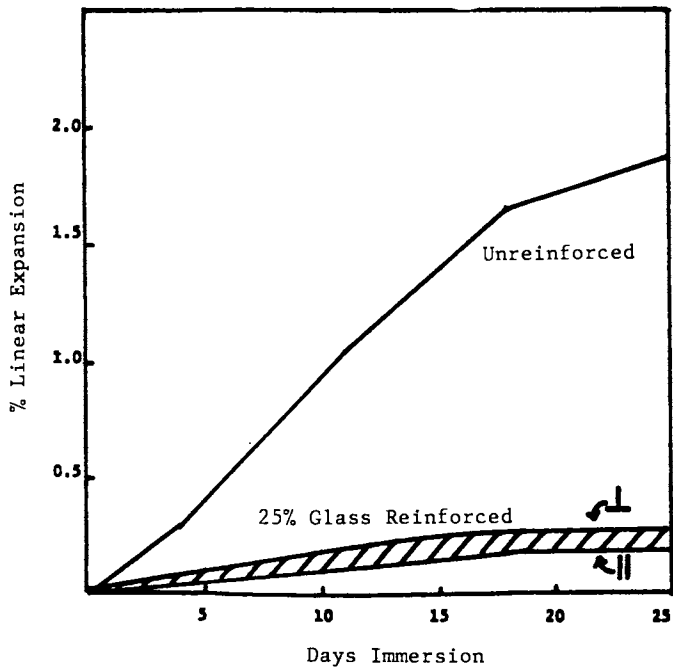


Figure 9. Effect of water immersion on reinforced and unreinforced nylon block copolymer (Polyol C).

a uniform layer of polymer on the inner surface of the cavity. A hollow part is produced.

The last two processes are not practiced with urethanes.

Reaction Injection Molding

Nylon-based RIM systems differ from urethane RIM systems in several important aspects which impact the design of RIM equipment and the molding process conditions.

First, the monomers found most useful for nylon RIM systems are ϵ -caprolactam and lauryl lactam. Unlike the liquid polyol and isocyanate materials in common use in urethane RIM, these materials have melting points of 158°F and 320°F respectively, making them solids at room temperature. Thus, nylon RIM equipment must have heated tanks, pumps, lines and molds. In commercial practice, this is accomplished by jacketing the equipment with circulating hot oil or water systems, by enclosing the hardware in temperature-controlled ovens or by electrically tracing the equipment with resistance heating bands and tapes. The first two methods are preferred because of their uniformity of control and lack of hot spots.

Second, the two reactive streams, whether they contain rubber modifiers or not, are very low in viscosity compared with typical urethane streams. See Figure 10 for a comparison of the viscosities of a typical urethane system, RIM 2700 from Union Carbide, and NYRIM 2000 nylon block copolymer from Monsanto, over their normal ranges of operating temperatures. Additionally, since both streams in nylon-based RIM systems are solutions in lactam monomer, they are chemically quite comparable. Thus, the required energy of mixing is quite low and so low impingement mixing head pressures are used, typically in the 150-300 psig range. This is one-tenth of that required for urethane systems. This allows for use of low-pressure lines and valves and lower horsepower hydraulic systems.

Third, the gel times of nylon systems are much longer than those of urethanes, typically on the order of 45 to 120 seconds, versus 5 to 30 seconds for urethanes. There are several reasons for this. First, the polymer is soluble in the monomer until very high molecular weights are attained. Second, the reactants are typically held at temperatures 30 to 90°F lower than the mold temperatures for reasons of energy conservation and product stability. At these temperatures, polymerization rate is low and pot life of the mixed stream is on the order of 5-10 minutes. For optimum physical property generation, part surface quality and release from the tool, nylon RIM molds are normally run at temperatures between 250 and 325°F. At these temperatures, gel times are typically 30 to 60 seconds for parts of about 1/8-inch thickness. Thus, part of the gel time difference is the time required for the reactants to rise to mold temperature by conductive heating. This longer time is also a result of the very low heat of reaction of caprolactam, only 3-4 kcal/mole versus 18-20 kcal/mole for urethanes. A typical reaction exotherm is shown in Figure 11 for NYRIM 2000 nylon block copolymer.

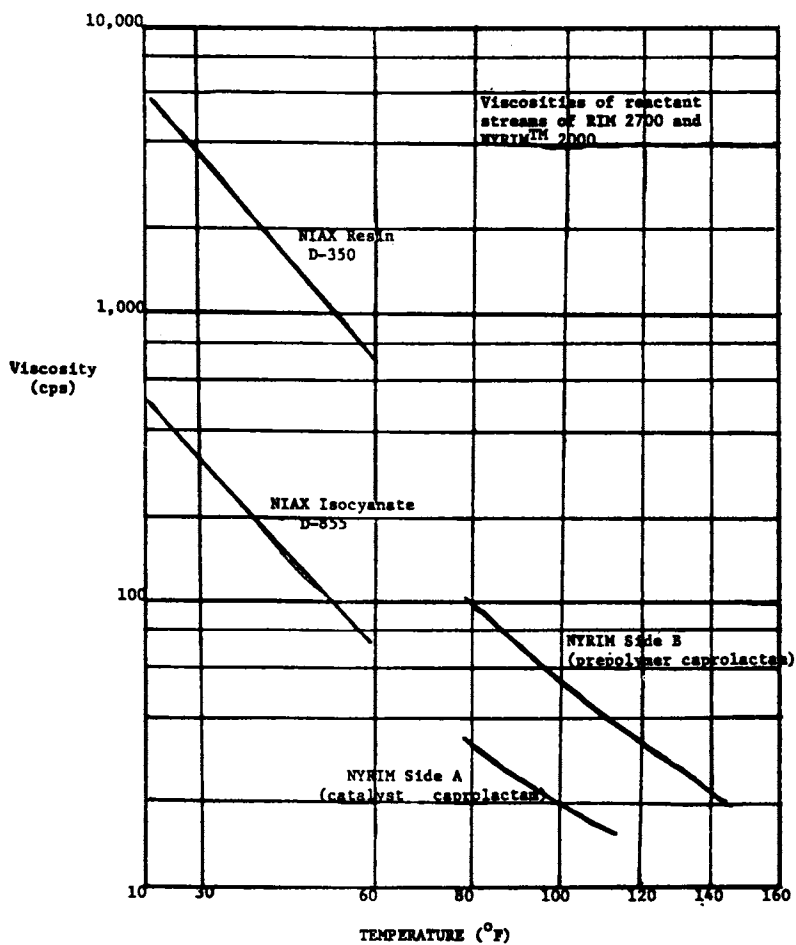


Figure 10. Viscosity of urethane and NYRIM raw material streams.

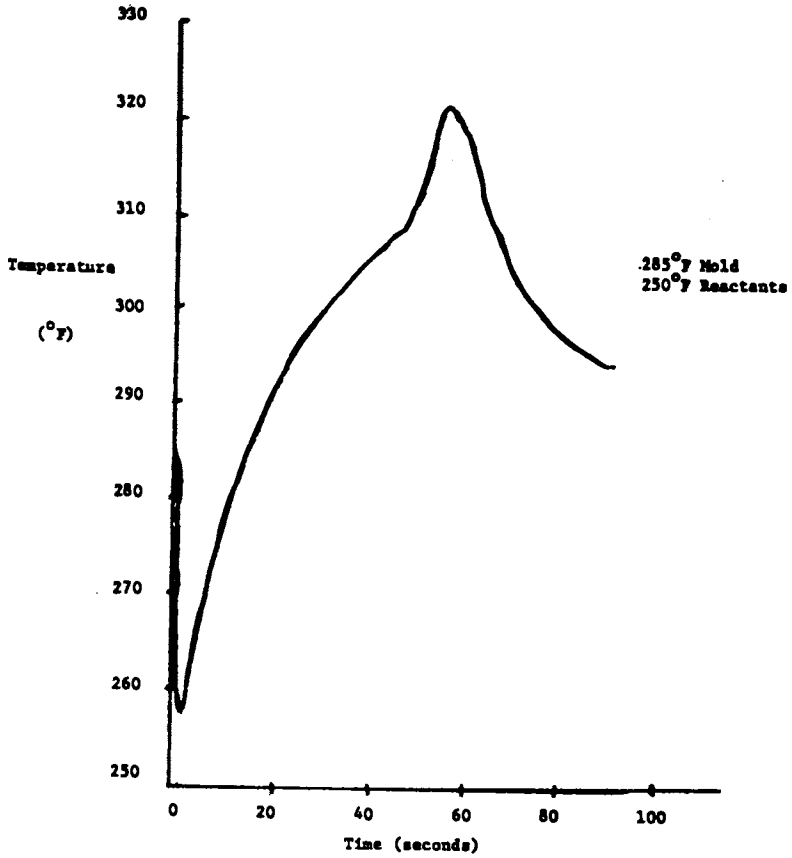


Figure 11. In-mold reactant temperature during cure of a part made from NYRIM 2000.

The net effect is to permit lower injection rates to be used in nylon RIM. This permits use of smaller pumping units and produces less part anisotropy when fiber-reinforced systems are used. Injection rates as low as 0.1 lb/second are common on 3-4 lb parts, although rates as high as 1.0-1.4 lbs/second can be used.

A fourth difference between nylon and urethane systems is the method of foaming. In urethanes, the reactant streams are typically nucleated with nitrogen by frothing in the tanks by means of high-speed agitators or by use of external pipeline mixers in recirculation systems. For optimum control of microcellular foams, nuclear density gauges are used to measure and control the froth density in the tanks. Blowing agents, such as Freon chloro-fluorocarbons, are also frequently added to control density and shrinkage values of urethanes.

Nylon RIM systems are also nitrogen-blown but control of nitrogen content is provided by setting the pressure of the nitrogen blanket used to inert the material hold tanks. Nitrogen is quite soluble in the caprolactam monomer and so no frothing is required. The nylon foam is produced by gas which comes out of the reactants upon throttling through the impingement mixer orifices and during polymerization, as nitrogen is much less soluble in the polymer than in the monomer. The fact that the nylon RIM streams are liquids, not froths, makes accurate metering simpler. Chemical blowing agents and solid nucleating agents have also been successfully used in nylon RIM systems.

Accurate metering is less important with nylon systems as well. Urethane stream ratios must typically be held to within 0.5% of target in order to achieve the desired finished part physical properties, these being very sensitive to isocyanate ratio. All of the physical properties of nylon RIM materials are essentially determined by the blend of materials made in the stream which contains the initiator and rubber modifier components. The second stream contains only catalyst solution. Thus, being off-ratio will affect only reaction rate, not physical properties. Nylon systems can be formulated so that ratio changes as high as 5% do not show any effect on either kinetics or properties.

Internal mold release technology is well developed for nylon RIM systems while it is being developed for urethanes. Most urethanes require application of a mold release agent, a wax, a soap or a silicone, after every shot. Many mold releases cannot be added to the urethane reactant streams or the tanks because they react with the urethane chemicals. These reactions have caused problems of build-up in the mold, even with spray-on mold releases, necessitating periodic shutdowns to scrub the mold surfaces. Some newer systems use a third component stream to introduce mold release at the mix head. Newer internal mold release systems permit from 0 to 50 urethane shots to be made between applications of external mold release spray to the tool. Monsanto's nylon RIM system contains an internal mold release that is paintable. In certain applications where a high quality smooth show surface is required on a part, a

thermosetting mold release is used on the tool surface that produces the reverse or unseen surface of the part. This provides differential release from the tool surface, allowing the show surface of the part to preferentially adhere to the tool surface, maximizing surface quality and fidelity of tool surface replication. A similar result can be obtained by maintaining a 5°F lower reverse surface temperature in the tool. Silicone mold releases may also be used.

The last major difference between urethane and nylon RIM systems lies in the extent of cure obtained in the mold. Many urethanes are polymerized just far enough in the mold to generate sufficient green-strength for demolding and handling the part. Parts are then oven post-cured to complete the reaction before atmospheric moisture reacts with the residual isocyanate in the part. Nylon RIM parts are fully cured in the mold.

The state of cure of the urethane results in flash which is fairly weak and brittle, which breaks off and must be manually removed from the tool after each shot. Nylon RIM flash is much tougher and typically comes out completely with the part. This difference in operation, and the need for mold release application between urethane shots, means that cycle times for nylon and urethane parts are quite comparable, in spite of the shorter closed-mold time used for urethane RIM. Commercial cycles of 2.5 minutes are common.

Equipment Requirements

As a result of the system differences previously outlined, nylon RIM machines can be simpler and lower in cost than urethane machines.

The nylon machines, of course, must be well heated and insulated, but they can be lower pressure units, have lower injection rates and have less need for accurate ratio control.

The tanks for nylon machines should be agitated with slow speed anchor-type agitators if reinforced systems are to be used. Additionally, the bottom valves should be of the flush type to avoid valve plugging should any settling of reinforcement occur. Tank lids should also be heated to avoid sublimation of lactam monomer which might plug pressure relief valves or pressurization/degassing ports. Agitator and lid seals should be of Teflon resin or ethylene-propylene rubber to avoid attack by the monomer. Tanks should be both pressure and vacuum-capable.

The tanks and lines should be set up to allow recirculation. This improves temperature control of the material in the lines and avoids settling of reinforcing materials when they are used. All lines should be designed to be self-draining to simplify machine clean out. Smooth inside surfaced flexible hoses lined with Teflon are preferred where flexible lines are required. Where these lines are jacketed, it is preferred that the jackets be coupled to the suction side of the recirculating oil pumps to keep the oil pressures low. Should leakage occur between the jacket and the reactant streams, then it is more likely that the reactants will leak into the oil than visa versa. Oil contamination will adversely affect nylon RIM reaction speed and physical properties. Many manufacturers of RIM equipment recommend that all tanks, valves and fittings for nylon RIM machines be made of stainless steel. Mild steel and

galvanized steel tanks have been successfully used, however, as have copper and brass lines and fittings in applications where the color of the material was not an issue because the parts were to be ultimately painted.

Both rotary pump and piston-type metering units are suitable for nylon RIM. Displacement lance piston units are best for reinforced systems.

Provision must be made for dry gas inerting of all storage and hold tanks. Nitrogen with a moisture content of less than 5 ppm is suitable. Tank pressures from 0 to 30 psig are used, depending upon the foam density to be produced.

Vacuum degassing of the mix tanks is required when fiberglass reinforcement is used as its incorporation tends to carry large volumes of gas into the mix. Following degassing, the dissolved nitrogen in the tank is adjusted by control of nitrogen pressure.

Molds for nylon RIM systems can be made from a wide variety of materials including steel, aluminum, kirksite and nickel. Chrome and nickel plating has also been widely used to improve the scratch resistance of molds made of softer materials. At this writing, no epoxy tooling system has been demonstrated that will produce more than a few parts before failing. Development work continues in this area.

In most respects, molds for nylon RIM are identical to those used for urethanes. Clearances on internal slides and on parting lines should be $< .002$ " to avoid excessive flash. Gating should be done at the lowest part of the tool, venting at the highest. This means building the tool with the part at an angle to the horizontal or using a clamp with a tilting feature.

Gating and venting must be done with an eye to the effects of reinforcement orientation and bubble track formation downstream of flow obstructions. The size and number of vents required depends upon the volume of the part and the rate of fill used in addition to the shape of the part itself. Preferred vent geometry is a groove .003-.005 inches deep and 3/8 inches wide. This does not permit excessive flash and polymerizes closed rather quickly. As many as 5 or 6 vents may be cut into a large tool. Fan or weir-type gates like those used for urethanes are preferred, particularly when reinforced systems are used. This minimizes any tendency to part warping caused by radial orientation of fibers.

After-mixers are also generally built into RIM tools upstream of the gate. By producing some back pressure on the mixhead, they tend to provide better control of bubbles in the molding as well as a more uniform part.

Because of the lower viscosities of nylon systems and their longer gel times, more care must be taken in making a good seal between the mixhead and the tool to avoid leakage during injection and polymerization.

The surface temperature of each mold half should be held within $\pm 4^{\circ}\text{F}$. At the high temperatures at which nylon RIM tools are operated, this requirement necessitates the use of more coring than is sometimes used for urethane tools. In steel tools .75 inch diameter circulating oil core holes, spaced at 2.5 inches on centers and located roughly 2-inches from the cavity surface have worked quite well. An average temperature difference of about 50°F can be

used to provide differential release from the mold halves, forcing any sink marks that do tend to form, in spite of the foaming of the part, to occur on the cooler side of the part.

Molds are designed where possible with the show side down so that any rise of bubbles during the cure cycle will be to the reverse side of the part.

Molds should be well-insulated to reduce energy costs. Insulating hardboard should be put between the mold and the clamp platens and the sides of the mold and the circulating oil hoses should be insulated as well. A typical 15-ton steel automotive fender tool, properly insulated, required 20 kw to maintain its temperature during production.

Because nylon RIM systems are low in viscosity and tend to polymerize first at the hot tool surface, they reproduce the condition of the tool surface very faithfully. Very high gloss parts can be produced. On the negative side, however, scratches or contamination on the tool surface will show up clearly on the part. Hard surfacing with chrome or nickel will minimize problems from tool damage, as will use of a hardened tool steel. Where parts are not to be painted, a textured surface or an SPE 2 finish on the tool also minimized these effects.

Low-Pressure Casting

In many instances, one wishes to produce solid parts so as to maximize the toughness of the product. In some cases, the economics of the business will not permit the high cost and process sophistication of reaction injection molding equipment. Low-pressure casting is then the process of choice. Casting machine prices are usually 20 to 50% of those of RIM machines. They are typically smaller and simpler machines. They use static or dynamic mixers rather than impingement mix heads.

Nylon-based reactive resin systems differ from urethanes in the way in which they cure in the mold. The high exothermic heat of reaction of urethanes typically causes them to polymerize in the center of the mold first and last at the cooled mold surface. Nylon reactions proceed in just the opposite way. This means that in a properly designed tool, the nylon part will have a liquid core for most of the polymerization cycle. This allows for the packing of the mold with fresh material as polymerization occurs, thereby compensating for polymerization shrinkage and producing parts free of sink marks. This is similar to the packing carried out in thermoplastic injection molding to compensate for thermal shrinkage.

Polymerization of caprolactam produces about 15% volume shrinkage. Since most nylon casting or RIM systems contain fillers, elastomeric impact modifiers and/or plasticizers, and because some thermal expansion takes place in the mold as the reactants heat to mold temperature or beyond, the net volume shrinkage is typically on the order of 6 to 10%. The long gel times of the mixed nylon reactants at the usual stream temperature of 150°F for caprolactam-based systems makes mold packing possible. Either the primary pumping system, as in piston-type machines, or a separate packing piston built into the injection line between the mix head and the mold, as in gear pump-type machines, can be used for packing. Gear pumps are not suitable for packing for several reasons. First, with low viscosity liquids, like nylon reactants, gear pumps do not meter

accurately against pressure heads because of leakage flows. Second, most gear pump drives cannot be switched from a speed-controlled mode, used for injection metering, to the torque-controlled mode needed for packing. The mixed material remaining in the pistons or lines downstream of the mixer after packing is injected into the next part at the start of the next shot. The time between making the shot and carrying out the packing depends upon the shape of the part and the design of the vents. Sufficient time must elapse for the vents to polymerize shut before packing is initiated, typically 20 to 30 seconds. Packing pressures of 150 to 200 psig are sufficient.

To produce solid parts, the nitrogen blanketing on the tanks is kept at as low a pressure as possible and no foam stabilizer is used in the formulation. Some machines which require high tank pressures to fill pumping pistons or to avoid cavitation at gear pump inlets may require the operator to periodically degas the system to avoid bubbles in the parts.

In almost all other respects, the low-pressure casting process is the same as the RIM process for nylon systems.

In contrast to urethane casting systems, open-topped molds cannot be used for all parts. Inhibition of polymerization at the exposed surface of the nylon reaction mix by moisture in the air will produce a tacky surface. If this is to be machined off to produce a finished part, open topped molds may be used.

Molds with open-topped risers and vents, like those used for casting of metals, may be used for certain thick parts. Makeup for polymerization shrinkage comes from the volume of material in the vents and risers which are eventually machined off.

Because of the comparatively low exotherm of nylon systems, quite thick parts can be produced by casting processes. Castings 10-12 inches in diameter and 10 inches thick have been made in times as short as 10 to 15 minutes with no evidence of adverse thermal effects at the core of the part.

Literature Cited

1. Joyce, R. M. and Ritter, D. M., U.S. Patent 2,251,519, Aug. 5 1941.
2. Italian patent to Monsanto Company filed Nov. 15, 1957, issued July 28, 1958.
3. Hall, H. K., J. Am. Chem. Soc. 80 5404 (1958).
4. Mottus, E. H., Hedrick, R. M. and Butler, J. M., Polymer Preprints [1] 390, (1968).
5. Mottus, E. H., Hedrick, R. M. and Butler, J. M., U.S. Patent 3,017,391, January 1962.
Butler, J. M., Hedrick, R. M., and Mottus, E. H., U.S. Patent 3,018,273, January 1962.
Butler, J. M., Hedrick, R. M. and Mottus, E. H., U.S. Patent 3, 028,369, April 1962.

- Mottus, E. H., and Hedrick, R. M. U.S. Patent 3,086,962, April 1963.
- Hedrick, R. M., Mottus, E. H., U. S. Patent 3,320,355, May 1967.
6. Wichterle, O., Sebenda, J., and Kralicek, J. Adv. Polym. Sci. 2 578-95 (1961).
 7. Sebenda, J., J. Macromol. Sci. Chem. A6 1145 (1972).
 8. Sebenda, J., Prog. Polym. Sci. 6 123-168 (1978).
 9. Friedrich Fahnler, Plastics and Rubber International 5 251-5 (19).
 10. U.S. Patent 3,341,501 R. M. Hedrick and W. R. Richard, September 12, 1967.
U.S. Patent, 3,418,268 R. M. Hedrick and P. A. Tierney, December 24, 1968.
U.S. Patent 3,419,517 R. M. Hedrick and W. R. Richard, December 31, 1968.
U.S. Patent Re 28,646 R. M. Hedrick and W. R. Richard, December 9, 1975.
U.S. Patent 3,833,534 P. A. Tierney, R. M. Hedrick and J. D. Gabbert, September 3, 1974.
U.S. Patent 3,843,591 R. M. Hedrick and W. R. Richard, October 22, 1974.
 11. R. M. Hedrick and E. H. Mottus, U. S. Patent 3,320,335 to Monsanto Company.
 12. J. L. M. van der Loos and A. A. van Geenan. "Properties and Morphology of Impact Modified RIM Nylon. Paper presented at 186th National Meeting, American Chemical Society, Washington, D.C. September 1, 1983.
 13. P. J. Flory, U.S. 2,682,526.
 14. J. E. Kurz "Block Size and Distribution in Nylon 6 RIM." Paper presented at AIChE meeting, Washington, D.C., November 1983.
 15. Melvin I. Kohan, Editor. Nylon Plastics SPE Monographs. John Wiley and Sons, New York 1973.

RECEIVED July 5, 1984

Activated Anionic Polymerization of ϵ -Caprolactam for RIM Process

GIOVANNI CARLO ALFONSO, CARMEN CHIAPPORI, SANDRO RAZORE,
and SAVERIO RUSSO¹

Centro Studi Chimico-Fisici di Macromolecole Sintetiche e Naturali, C.N.R., Corso Europa 30,
16132 Genoa, Italy

The role of initiator and activator concentrations on the whole process of ϵ -caprolactam anionic polymerization has been explored, with the aim of selecting the most suitable experimental conditions for the RIM process. The effects of the active species on high polymer yield, residual monomer content, higher oligomers and side products have been evaluated. It has been found that polymer molecular masses and their distributions are related to both active species in a complex manner. Under specific experimental conditions, it is however possible to predict their values in a relatively large range of average masses. Side reactions and structural irregularities in the polymer chains have been correlated to the absolute and relative concentrations of activator and initiator, in order to minimize their extent. The effect of active species on the overall polymerization time as well as on the initial and maximum rates of polymerization has been evaluated.

In recent years the activated anionic polymerization of ϵ -caprolactam (CL) in bulk, in the presence of some inorganic salts, has been the subject of a thorough investigation by our research group (1-6). Indeed, some

¹ Author to whom correspondence should be addressed.

0097-6156/85/0270-0163\$06.00/0

© 1985 American Chemical Society

halides such as lithium and calcium chloride are able to modify and improve many bulk properties of the resultant poly(ϵ -caprolactam) (PCL). For instance, they can induce an increase of polymer density, glass transition temperature, Young's modulus and melt viscosity, as well as a decrease of its melting temperature, degree of crystallinity and crystallization rate.

At present, attempts to polymerize CL added with various fillers, reinforcing agents and property-modifiers are explored by us in great detail (7,8). The aim is to synthesize polymer blocks where the additive, dissolved or finely dispersed in the monomer medium, remains homogeneously distributed throughout the polymer matrix. Indeed, if the polymerization kinetics is not adversely affected by the additive, the very short polymerization time and the rapid increase of the medium viscosity prevent any coarse aggregation of the additive and the consequent phase separation in large domains.

Therefore, at least in principle, the above process may represent a very easy way to produce polymer mixtures, blends and composites based on PCL, with some peculiar morphologies and properties.

Quite recently, the activated anionic polymerization of CL has been found suitable for the reaction injection molding (RIM) technology (9-12) and has prompted some new studies (13-15) devoted to update the classical picture of the reaction kinetics (16), mostly in terms of potential industrial applications of the RIM process (13-15,17-20). Successful attempts by Hedrick et al. (11,12) to anionically synthesize a series of PCL block copolymers has led to impact-modified RIM nylon (Monsanto's NYRIM).

The possibility to utilize the RIM technology for the synthesis of PCL-based materials requires a careful control of many reaction parameters, which strongly affect the whole kinetic course of the polymerization as well as the properties of the resultant material.

It is well known, indeed, that the anionic polymerization of CL is constituted of a complicated set of main and side reactions, giving rise to a variety of active species and irregular structures in the polymer chains (16). Our study has been focused on the role played by activator and initiator concentration in determining the optimum conditions for the polymerization of CL in the mold. To our knowledge no such study has been published so far, at least under experimental conditions suitable for RIM. We report here the first part of our study, related to the

polymerization of neat CL. The effects of various additives on the polymerization kinetics at 'optimum' conditions are in progress and will be given elsewhere (21).

We have carried out a series of polymerization runs in quasi-adiabatic conditions, as described in Ref. 3, at different concentrations of both initiator and activator, so that not only their absolute amounts but also their relative ratios were widely modified.

Experimental

Sodium caprolactamate (prepared in situ from sodium metal and CL) and N-acetyl caprolactam were chosen as initiator and activator, respectively. The starting temperature of polymerization was 155°C. A double-walled glass reactor, of about 60 cm³, equipped with mechanical stirrer, inert gas inlet and outlet and thermocouple lodging was used (3). The polymerization products were fractionated following the published literature (5) into high polymer, residual monomer, higher oligomers and low molecular mass side products, and their respective yields were determined. Monomer content has also been evaluated by g.l.c.

A thermokinetic analysis of the polymerization runs has enabled us to evaluate both enthalpy and instantaneous rate of polymerization, following the procedure described in Ref. 3.

Molecular mass distribution of PCL has been determined by GPC of the corresponding trifluoroacetyl derivatives by using the method described in Ref. 22. A solution of N-TFA derivatives at c=0.2 g/dl was prepared, adding o-dichlorobenzene as internal standard (1 μ l/ml solution). 25 μ l of the solution were injected in a Waters High Pressure Liquid Chromatography apparatus (pump 6000 A, injector U6K, UV detector 440, μ -styragel columns set: 10⁵- 10⁴- 10³- 500 Å), λ =254 nm, flow rate: 1 ml/min).

UV absorption spectra of 1% (w/w) PCL solutions in anhydrous formic acid have been recorded with a Cary UV spectrophotometer mod. 219. For all samples, band maximum at 275-277 nm has been found, at variance to previous analyses of PCL samples synthesised under different experimental conditions (1).

Results and Discussion

Mass balances of the polymerization products have been performed for the whole set of polymerization reactions, where both the initiator and activator concentrations have been varied from 0.3 to 1.5 moles over 100 moles of CL. In Table I the data related to the maximum monomer conversion and the high polymer yield are given as functions of the active species concentration (initiator and activator), which are present in equimolar amount in the polymerizing mixture. For almost all systems, monomer conversion and polymer yield are higher than 98 and 95%, respectively. In such concentration range of active species, yield fluctuations are less than 1.5% in terms of monomer conversion and less than 2.0% for the high polymer yield.

Also for activator concentrations higher than those of initiator, the yield data are close to the above values, as evidenced in Table II. Only for very low initiator concentrations (less than 0.3%) there is a dramatic decrease of the high polymer yield.

Very few runs have been performed using activator concentrations lower than those of the initiator (see Table III), because of the claimed adverse effects, caused by the strong basicity of the medium, on the structural homogeneity of the polymer. It is well known, indeed, that Claisen-type condensation reactions on the performed polymer are induced by a strong base and are responsible for the formation of structural irregularities along the chain, i.e. of groups which are able to strongly absorb in the UV region (16) and represent preferred degradation sites. We will discuss the behaviour of our PCL samples in this respect later on. It can be noticed, nevertheless, that even in excess initiator concentrations both monomer conversion and high polymer yield show values only slightly lower than those quoted in the previous tables. In crude terms of conversion, therefore, it can be inferred that a rather large range of active species concentrations can be explored without any significant worsening of the attainable conversion values.

Molecular Mass Distribution

The molecular mass evaluation of aliphatic polyamides as well as the determination of their molecular mass distribution are relevant problems which only very

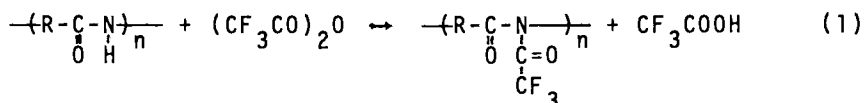
Table I. Monomer Conversion and High Polymer Yield in Polymerization Runs with Equimolar Concentrations of Initiator and Activator

[A] = [I] (mol/100 mol CL)	Monomer Conversion (λ) %	High Polymer Yield %
0.3	97.9	95.0
0.5	98.6	95.7
0.6	98.2	95.6
0.7	98.2	95.6
0.9	98.2	95.6
1.2	98.3	95.5
1.5	98.2	95.4

Table II. Monomer Conversion and High Polymer Yield in Polymerization Runs Where $[A]/[I] \geq 1$

[A] / [I] (mol/100 mol CL)	Monomer Conversion (λ) %	High Polymer Yield %
0.6/0.1	-	76.3
0.6/0.15	-	85.6
0.6/0.2	-	93.7
0.6/0.3	-	96.2
0.6/0.4	98.2	95.3
0.6/0.6	98.2	95.6
0.7/0.4	96.7	94.1
0.7/0.6	98.4	96.1
0.7/0.7	98.2	95.6
0.8/0.4	96.6	93.5
0.8/0.6	98.4	96.1
0.8/0.7	98.8	96.1
0.9/0.6	97.8	97.3
0.9/0.7	98.5	95.2
0.9/0.9	98.2	95.6
1.0/0.6	98.5	96.2
1.0/0.7	98.1	95.6
1.2/0.6	-	96.0
1.2/0.9	98.7	95.7
1.2/1.2	98.3	95.5
3.0/0.6	-	88.3

recently have been satisfactorily solved(22-25). The aforementioned N-trifluoroacetylation reaction runs as follows:



Complete substitution of the nitrogen-bonded hydrogen and easy reproducibility are the most relevant aspects of the above reaction.

The N-trifluoroacetylated derivative of PCL is quickly soluble in many solvents (such as acetone, THF, dioxane, chlorinated hydrocarbons, etc.) and can easily be analyzed by conventional GPC apparatus.

Preliminary data on MMD of our samples are given in Table IV. It is evident that equimolar concentrations of activator and initiator produce PCL polymers characterized by a regularly decreasing polymolecularity index Q , from ca. 2.6 to 2.0. In Figure 1 the number of polymer molecules formed per acyllactam molecule is plotted as a function of initiator concentration. The actual values should be compared to the 'theoretical' value of 1, which corresponds to the assumption that the number of macromolecules would be equal to the number of acyllactam molecules (26), as in the ideal case of a step-addition of lactam anions to a constant number of growth centers.

It is evident that, by increasing $[I]$ at equimolar concentrations of active species, there is a regular decrease in the number of polymer molecules N per activator molecule. Moreover, all experimental values of $[N] / [A]$ are lower than 1, in the $[I]$ range from 0.5 to 1.5 mole %. Extrapolation to infinite dilution of caprolactam anions shows a consistent coincidence with the calculated value of 1, in full agreement with theory. From the above data it is evidenced that, in the experimental range of initiator concentrations we used, polymer molecular masses are higher than expected. Indeed, additional growth centers, i.e. new polymer chains, can be produced by disproportionation reactions such as the following one, induced by strong bases:

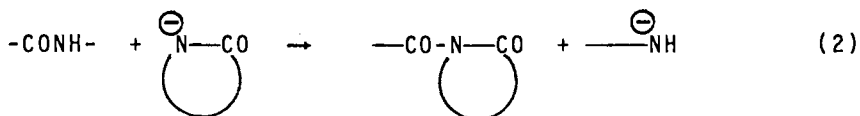


Table III. Monomer Conversion and High Polymer Yield in Polymerization Runs where $[A]/[I] \leq 1$

[A] / [I] (mol/100 mol CL)	Monomer Conversion (λ) %	High Polymer Yield %
0.6/0.6	98.2	95.6
0.6/0.9	-	94.9
0.6/1.2	-	94.9
0.6/1.8	-	93.6
0.7/0.7	98.2	95.6
0.7/0.9	98.2	95.2

Table IV. GPC Data on PCL Samples

[A] / [I] (mol/100 mol CL)	$\bar{M}_n \cdot 10^{-3}$	$\bar{M}_w \cdot 10^{-3}$	Q
0.5/0.5	27.04	70.63	2.61
0.7/0.7	19.74	46.09	2.33
0.9/0.9	{ 16.77 17.42	{ 39.32 38.37	{ 2.34 2.20
1.2/1.2	14.40	32.42	2.25
1.5/1.5	14.34	29.25	2.04

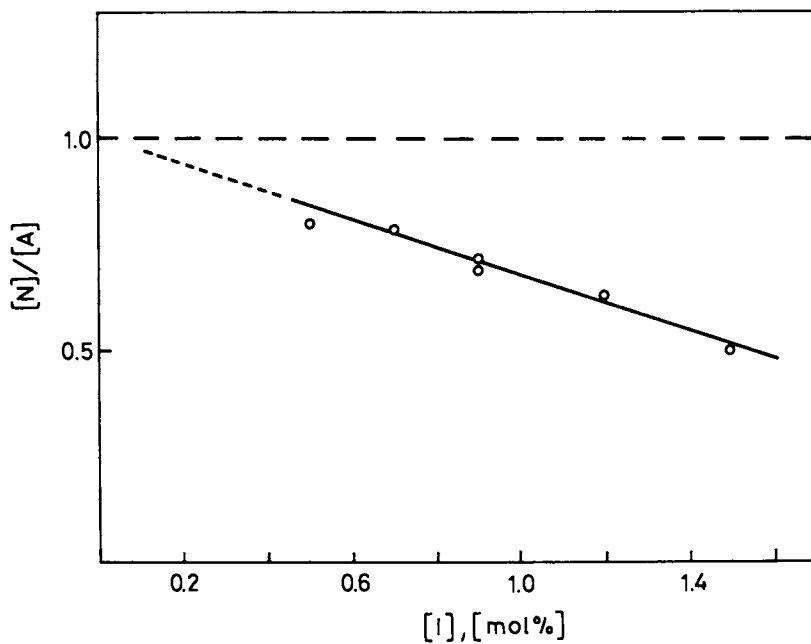
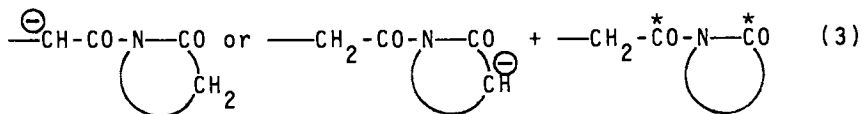


Figure 1. Number of polymer molecules formed per acylactam molecule, as a function of initiator concentration in the case $[I] = [A]$.

whereas Claisen-type condensation reactions, such as those involving the following species (16), are responsible for an increase of molecular masses:



Actual balance between the two opposite effects determine the average value of polymer molecular mass and its distribution.

From our data it seems that the prevailing effect is caused by type (3) reactions, which are more and more relevant as basicity of the medium is increased.

Side Reactions and Structural Irregularities

As already mentioned, the active species (imide groups and lactam anions) undergo a series of side reactions, which induce the formation of irregular units along the chains. Not only the regularity of the chains is affected, but also the whole polymerization process as well as the polymer end properties are markedly modified (16). The structures, arising from the aforementioned Claisen-type condensation reactions, are very reactive: on one hand, they re-create growth centers and, on the other, they are responsible for the formation of heterogeneous groups, such as derivatives of isocyanates, uracil, malonamide, etc., which act as color centers and inversion points of chain regularity.

As a consequence, together with linear chains, branched and crosslinked structures are also formed. They strongly affect molecular masses, MMD, and solution properties. Moreover, these non-crystallizable units cause a decrease of both the polymer melting temperature and the crystallization rate, as well as a poorer thermo-oxidative stability (16).

In order to minimize these effects, which may be relevant also to RIM technology, we have studied the role of active species concentration on the UV absorption spectra of the resultant polymer. The data are given in Figures 2 and 3, where the effects of equimolar and non-equimolar concentrations of active species, respectively, are shown.

In Figure 2 the UV absorption coefficient of PCL samples appears to be a linear function of each active species

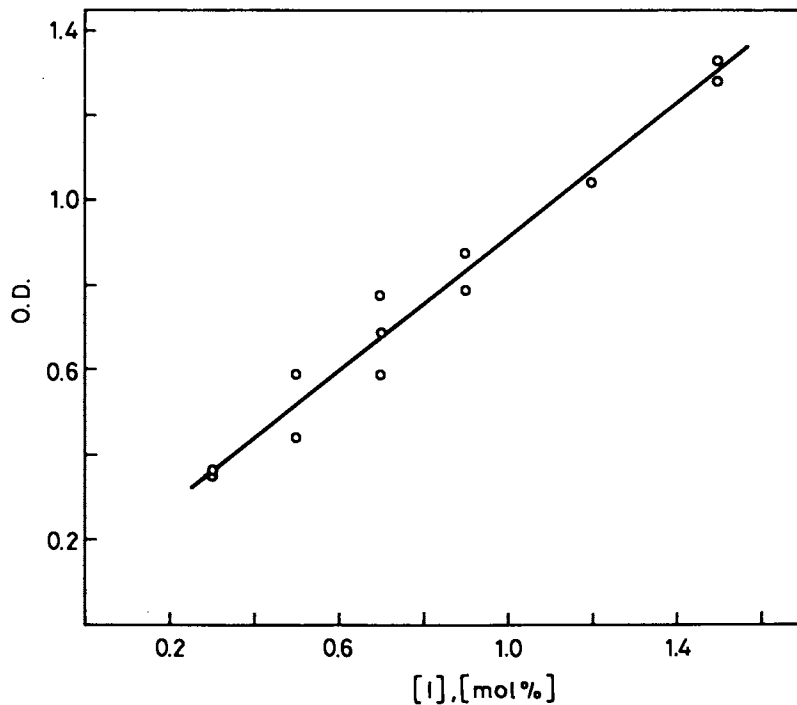


Figure 2. Optical density of PCL samples at $\lambda = 276$ nm as a function of initiator concentration, in the case $[I] = [A]$.

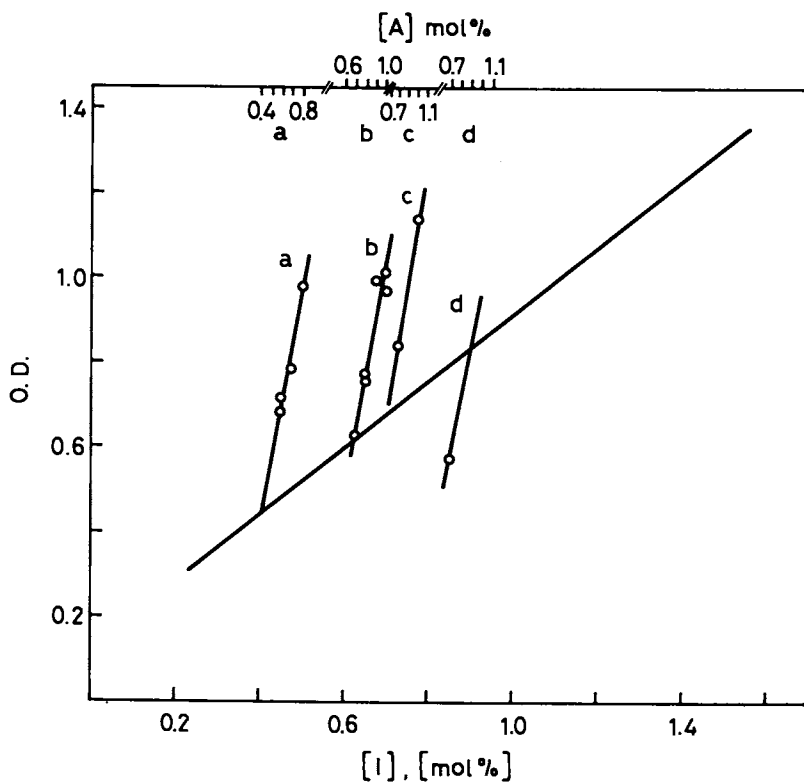


Figure 3. Effect of activator concentration, as constant $[I]$, on polymer optical density at $\lambda = 276$ nm. a) $[I] = 0.4$; b) $[I] = 0.6$; c) $[I] = 0.7$; d) $[I] = 0.9$.

concentration in the range between 0.3 and 1.5 mole %. It is reasonable to assume that the UV absorption is directly proportional to the total amount of side products arising from the Claisen-type condensation reactions, which are catalyzed by strong bases. Thus, the abscissa is formally expressed in terms of initiator concentrations.

In Figure 3 the effect of activator concentration on the UV absorption coefficient of our polymer samples, at constant $[I]$, is given. Almost parallel lines, well joined to the interpolated values on the equimolar concentration line, have been found.

From the whole set of above data it can be inferred that, by suitably playing with appropriate concentrations of the active species, it is possible to reduce the amount of structural irregularities along the chain.

Polymerization Kinetics

The whole polymerization kinetics has been followed by means of the adiabatic reactor method (3,6), which allows to simultaneously determine polymerization times and rates. In Table V data, related to the overall polymerization time, t_p , as well as to the initial and maximum rates of polymerization, are given. All these parameters are, of course, very relevant to RIM technology.

In Figure 4 the overall polymerization time is plotted as a function of one or the other active species concentration. A hyperbolic type dependence of t_p on [active species] is evident, with a very sharp decrease of t_p in the concentration range between 0.3 and 0.7 mole %, and a much slower decrease at higher concentrations. At the highest levels of active species concentrations, t_p is very low (ca. 3 min) and this value compares rather well with the usual reaction times for the RIM technology. Non-equimolar concentration conditions roughly follow the same pattern, as evidenced from the data quoted in Table V, and allow to underline the prominent role of $[I]$ on t_p , whereas $[A]$ has a much lower relevance on it.

The initial polymerization rates show a dependence on the first power of $[A]$ and 0.9 power of $[I]$, as evidenced in Figure 5. With only a few exceptions almost all the experimental points are well aligned on the straight line, passing through the origin. The 0.9 exponent indicates an almost complete dissociation of the

Table V. Overall Polymerization Time, Initial and Maximum Polymerization Rates in Runs with Different Amounts of Activator and Initiator

[A] / [I] (mol/100 mol CL)	Overall Polym. Time, t_p (min)	Initial Rate $(d\lambda/dt)_0 \cdot 10^2$ (min^{-1})	Maximum Rate $(d\lambda/dt)_m \cdot 10^1$ (min^{-1})
0.3/0.3	12.05	1.95	3.38
0.3/0.3	11.05	1.41	3.74
0.5/0.5	8.10	3.39	5.17
0.7/0.7	4.90	6.98	8.01
0.7/0.7	5.40	7.40	8.28
0.9/0.9	3.80	9.41	10.04
1.2/1.2	3.70	19.28	13.64
1.5/1.5	3.15	23.63	15.82
0.6/0.4	6.50	3.69	5.69
0.7/0.4	9.30	3.37	4.30
0.8/0.4	7.85	4.54	5.06
0.7/0.6	6.05	5.61	6.77
0.8/0.6	5.60	7.10	7.90
0.9/0.6	5.40	4.78	8.21
1.0/0.6	3.95	8.64	9.43
0.8/0.7	5.15	7.49	9.90
0.9/0.7	5.70	6.11	7.77
1.0/0.7	4.70	11.12	10.96
0.7/0.9	5.15	8.57	8.48
1.2/0.9	5.40	9.77	7.96

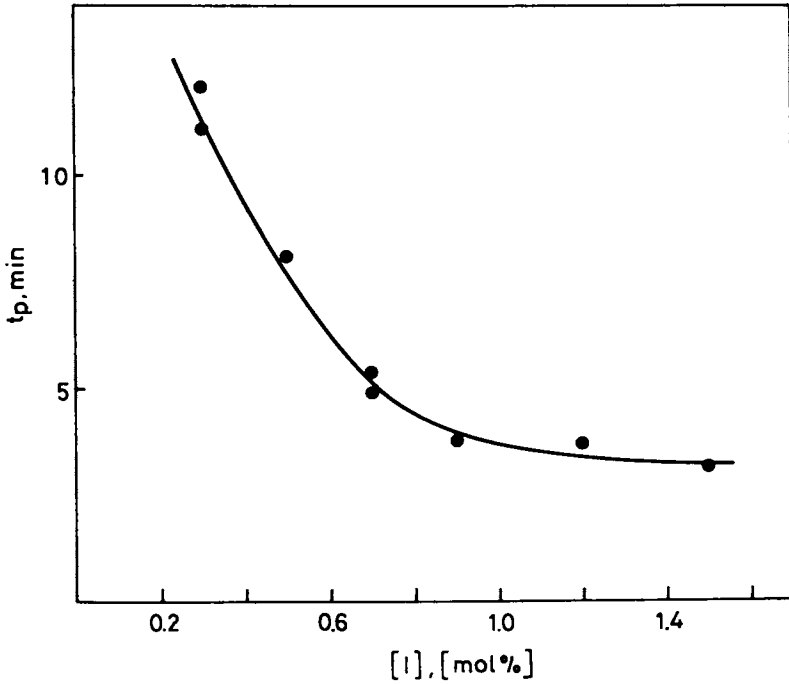


Figure 4. Overall polymerization time as a function of initiator concentration, for $[I] = [A]$.

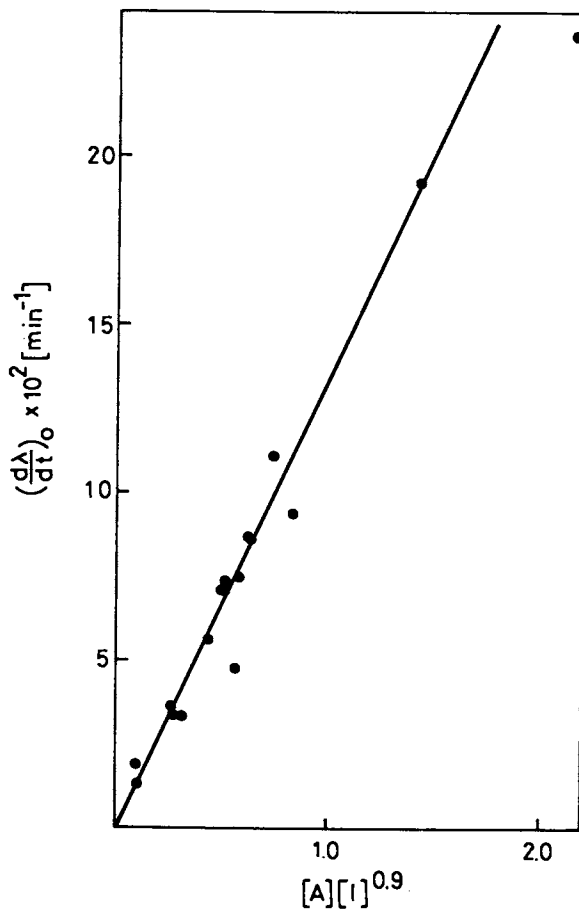


Figure 5. Initial polymerization rate as a function of active species concentration.

caprolactamate salt in our experimental conditions, at variance with previous findings (16).

From the data of Table V it is also evident that the maximum polymerization rates in quasi-adiabatic conditions are 10-20 times higher than the initial reactions rates. At increasing concentrations of the active species, the ratio between the two rates regularly decreases.

Conclusions

The RIM process for materials based on PCL requires a stringent control of the many reaction parameters which strongly affect the whole pattern of the activated anionic polymerization.

Among these parameters, initiator and activator concentrations play a very relevant role. The present study underlines their influence on the polymerization kinetics and polymer properties.

'Optimum' conditions for each of the following aspects have been found: high polymer yield, maximum monomer conversion, initial and maximum rate of polymerization, overall time of polymerization, polymer molecular mass and its distribution, side reactions and irregular structures.

Other relevant parameters, such as viscosity raise and crystallization rate, which are currently explored by other research groups (13,15), will be the subject of future studies on our experimental system, in the presence of various added substances.

Research under Contract C.N.R. - ANJC S.p.A. reg. 22.12.82

Literature Cited

1. Bonta', G.; Ciferri, A.; Russo, S. "Ring Opening Polymerization"; Saegusa, T.; Goethals, L., Eds.; ACS SYMPOSIUM SERIES No. 59: Washington, D.C., 1977; p. 216.
2. Costa, G.; Pedemonte, E.; Russo, S.; Sava', E. Polymer 1979, 20, 713.
3. Alfonso, G. C.; Bonta', G.; Russo, S.; Traverso, A. Makromol. Chem. 1981, 182, 929.
4. Alfonso, G. C.; Pedemonte, E.; Russo, S.; Turturro, A. Makromol. Chem. 1981, 182, 3519.
5. Biagini, E.; Pedemonte, B.; Pedemonte, E.; Russo, S.; Turturro, A. Makromol. Chem. 1982, 183, 2131.

6. Alfonso, G. C.; Cirillo, G.; Russo, S.; Turturro, A. Eur. Polym. J. 1983, 19, 949.
7. Alfonso, G. C.; Costa, G.; Pedemonte, E.; Russo, S.; Turturro, A. Proc. 5th AIM Meeting, Milan, 1981.
8. Russo, S. Proc. IUPAC 28th Macromolecular Symp., Amherst, 1982.
9. Kubiak, R. S.; Plast. Engng. 1980, 36, 55.
10. Kubiak, R. S.; Harper, R. C. Reinf. Plast./Composites Inst., 35th Annual Conf., 1980, Sec. 22-C, p. 1.
11. Hedrick, R. M.; Gabbert, D. A. I. Ch. E. Symp., Detroit, 1981.
12. Gabbert, D.; Hedrick, R. M. A. I. Ch. E. Symp., Detroit, 1981.
13. Sibal, R. E.; Camargo, R. E.; Macosko, C. W. Int. J. Polym. Techn. Eng. Polym. Process. Eng., in press.
14. Russo, S. Proc. 5th AIM Summer School on Polymer Processing, Gargnano, 1983; p. 289.
15. Camargo, R. E.; Gonzales, V. M.; Macosko, C. W.; Tirrel, M. Rubber Chem. Techn. 1983, 56, 774
16. Šebenda, J. In "Comprehensive Chemical Kinetics"; Bamford, C. H.; Tipper, C. F., Eds.; Elsevier: Amsterdam, 1976; Vol. XV, Chap. 6, 'Lactams', p. 379ff.
17. Alfonso, G. C.; Russo, S.; Pedemonte, E.; Turturro, A.; Puglisi, C. Italian Pat. 21912A/83 (to C.N.R.).
18. Russo, S.; Alfonso, G. C.; Pedemonte, E.; Turturro, A.; Martuscelli, E. Italian Pat. 21950A/83 (to C.N.R.).
19. van der Loos, J. L. M.; van Greenen, A. A. ACS PMSE Proc. 1983, 49, 549.
20. Biagini, E.; Razore, S.; Russo, S.; Turturro, A. ACS Polymer Preprints, 1984, 25 (1), 208.
21. Russo, S.; et al., to be published
22. Biagini, E.; Gattiglia, E.; Pedemonte, E.; Russo, S. Makromol. Chem. 1983, 184, 1213.
23. Schuttenberg, H.; Schulz, R. C. Angew. Chem. 1976, 88, 848.
24. Jacobi, E.; Schuttenberg, H.; Schulz, R. C. Makromol. Chem. Rapid Comm. 1980, 1, 397.
25. Weisskopf, K.; Meyerhoff, G. Polymer 1983, 24, 72.
26. Šebenda, J.; Kouřil, V. Eur. Polym. J. 1971, 7, 1637.

RECEIVED June 14, 1984

Properties and Morphology of Impact-Modified RIM Nylon

J. L. M. VAN DER LOOS and A. A. VAN GEENEN

Polymer Chemistry Department, DSM. Research and Patents, PO Box 18, 6160 MD Geleen, The Netherlands

RIM nylon is a new development in the long-established technique of anionic polymerization of ϵ -caprolactam. For most applications the toughness of dry non-modified nylon is insufficient. By dissolving an impact modifier (a rubber-like material, such as a polyol, with low T_g) in the caprolactam melt before polymerization the impact strength can be improved, though with a decrease in flexural modulus. The various kinds of morphology which can occur with rubber-toughening and the relation between morphology and mechanical properties will be discussed. For the ABA type block copolymers the postulated morphology is that of a continuous rubber network extending through a nylon phase, which would explain the high toughness and the low flexural modulus of these block copolymers.

The anionic polymerization of caprolactam (CL) is a fairly old polymerization technique by which molten caprolactam is polymerized in a mould by means of an accelerator and a basic catalyst at a temperature lower than the melting point of the polymer to be formed. With a correct choice of polymerization system and by optimization of the polymerization conditions the polymerization can be completed in about 3 minutes so that the reaction can be carried out in a specially adapted RIM machine.

For most applications, in particular in the automotive industry, the toughness of nylon is insufficient. The most successful method developed for modifying brittle polymers is rubber-toughening. By incorporation of a minor amount of a dispersed rubber phase (impact modifier) the fracture resistance is improved significantly and the impact strength can be increased severalfold. There is an unavoidable decrease in flexural modulus and tensile strength, but the balance of properties of the rubber modified nylon is much better than that of unmodified nylon. Several kinds of morphology which

0097-6156/85/0270-0181\$06.00/0

© 1985 American Chemical Society

can occur with rubber-toughening and the relation between morphology and mechanical properties will be discussed.

Experimental

The polymerization runs were carried out in a flat aluminium mould. At a temperature of about 100 °C, the initiator was dissolved in one half of the caprolactam while the catalyst and the impact modifier were dissolved in the other half. The two solutions were mixed and the mixture was poured into the mould, which had a temperature of 130-160 °C. After about 10 minutes the finished plate was taken from the mould no mould release agent was used.

In this study a diisocyanate or the product of the reaction between a diisocyanate and the impact modifier was used as accelerator. The polymerization was catalysed with common basic catalysts such as potassium lactamate, sodium lactamate and/or bromomagnesium lactamate.

The Izod notched impact strength (ASTM D-256) and the flexural modulus (ASTM D-790) of the obtained products were measured. For a number of specially selected samples, the dynamic mechanical properties were determined.

The rubber distribution was studied by means of electron micrography (EM). Fracture surfaces for scanning electron micrography (SEM) were obtained by breaking the samples after cooling in liquid nitrogen. They were sputter-coated with an Au/Pd alloy. The microscope used was a Philips SEM 505, maximum resolution 7 nm. For transmission electron micrography (TEM) a carbon-replica shadowed with Pt/Pd alloy was used, the microscope being a Philips EM 300.

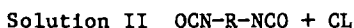
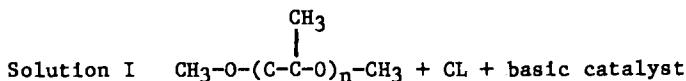
A large number of polymers with a low glass transition temperature, which are soluble in molten caprolactam, but not compatible with nylon, were tried out. The best polymerization results were obtained with polyols.

Morphology

Depending on the interaction of the impact modifier with the accelerator, three different morphologies can occur (see "Figure 1"). Intermediate forms are of course also possible.

System 1 This morphology is produced when no reaction can occur between the impact modifier and the accelerator. This can be achieved by using as impact modifier a methoxylated polypropylene glycol (PPG) ("solution I").

"Solution II" contains the accelerator.



After mixing and polymerization only a homopolymer is formed. Because there is no interfacial adhesion the rubber segregates as

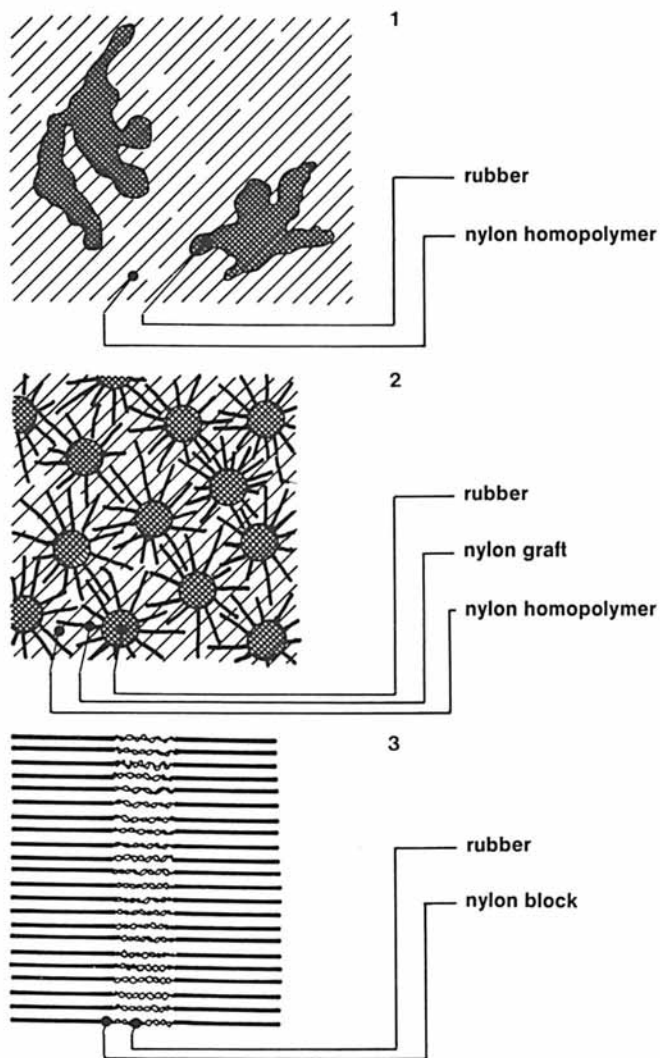
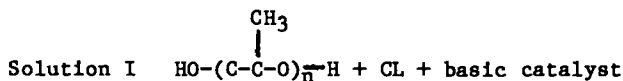


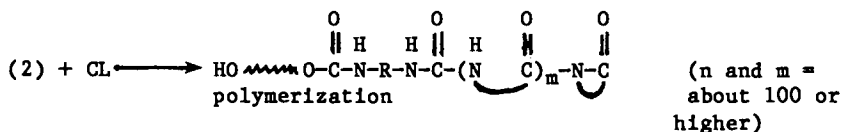
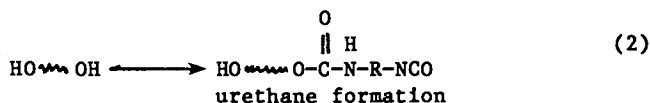
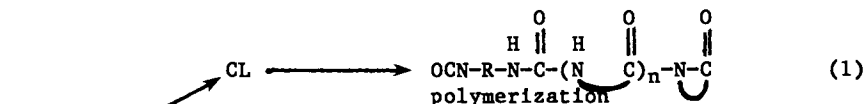
Figure 1. Morphology of the various polymerization systems described.

shapeless patches and is poorly distributed in the nylon phase. This procedure was already described in 1965 (1).

System 2 By application of an impact modifier containing groups which are reactive to the accelerator ("solution I"), graft polymers (block copolymer) can be formed. In this case polypropylene glycol with terminal-OH groups was used.



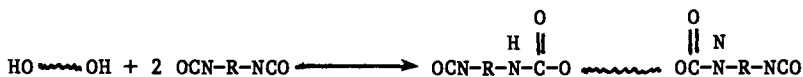
The isocyanate accelerator ("solution II") can react in either of the following ways:



Because "reaction (1)" is considerably faster than "reaction (2)", only a minor quantity of block copolymer is formed. The impact modifier segregates as fine spheres homogeneously distributed in the nylon phase. The block copolymer concentrates at the interface, acting as an emulsifier for the two incompatible polymers (2). In this polymeric 'oil in oil' emulsion the interfacial adhesion is good.

A disadvantage of the polymers prepared by systems 1 and 2 is that the rubber phase can be extracted and, if the molecular weight of the rubber is low, can even exude. System 2 is described in several patent applications (3-5).

System 3 This morphology occurs in the case of complete interaction between the rubber and the nylon phase. Separately, a prepolymer is prepared consisting of a rubber segment with terminal accelerator groups.

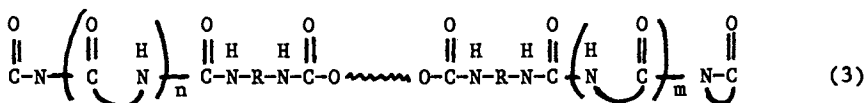


This prepolymer is dissolved in CL and mixed with a catalyst solution in CL.

Solution I Prepolymer + CL

Solution II Catalyst + CL

In this case an ABA block copolymer is formed. The chemical structure of such a polymer is represented by formula (3)



(n and m = about 100 or higher).

In this system the interfacial adhesion is optimum; the rubber phase cannot exude or be extracted.

The new developments in RIM nylon, also by DSM, are based on this last postulated mechanism (6-8) but in some older patents block copolymers are already mentioned (9-13).

Results and discussion

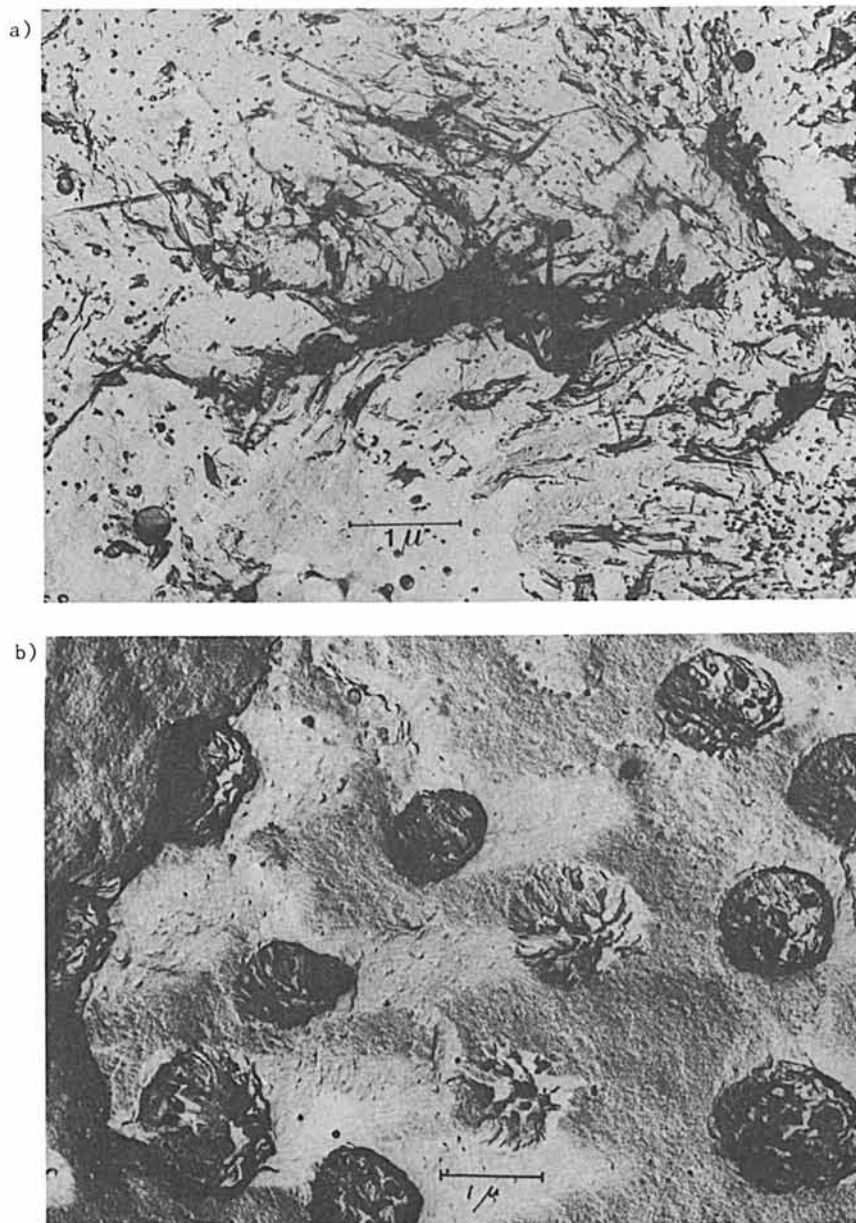
EM micrographs of the polymers prepared by the systems 1, 2 and 3 are given in "Figure 2".

"Figure 2A" clearly shows that the rubber distribution in a polymer made according to system 1 is very poor.

The rubber is segregated as big shapeless patches in a continuous nylon phase (the black domains in the micrograph). When the polymerization conditions are not optimum this can also occur in system 3. "Figure 2D" shows a polymer made according to this system where as a result of premature phase separation the polymer has segregated as big particles (about 3 μ) and quite a few active groups have not reacted to form nylon blocks. The interfacial adhesion is very small and the mechanical properties of this polymer are equal to those of a polymer prepared according to system 1. The micrograph of system 2 ("Figure 2B") shows a very regular distribution of small rubber particles (about 1 μ) in a continuous nylon phase.

In the block copolymers prepared according to system 3, the rubber segments may be arranged in thin layers, in thin cylinders or as a nearly continuous network (14). The thickness of the rubber phase can never be greater than the end-to-end distance of the stretched rubber sequence. In the case of a polyol with a molecular weight of 4000, this end-to-end distance is at most about 200 Å. Because the rubber chain will not be fully stretched, the thickness of the rubber phase will even be smaller, viz. about 100 Å. Because the resolution of SEM is also about 100 Å, the rubber phase in system 3 is hardly distinguishable ("Figure 2C").

However, with dynamic mechanical relaxation domains of about 100 Å can be detected. The dynamic mechanical spectrum of a polymer prepared by system 3 ("Figure 3") indeed displays two separate loss peaks; one at about -62 °C owing to the glass transition of polyol

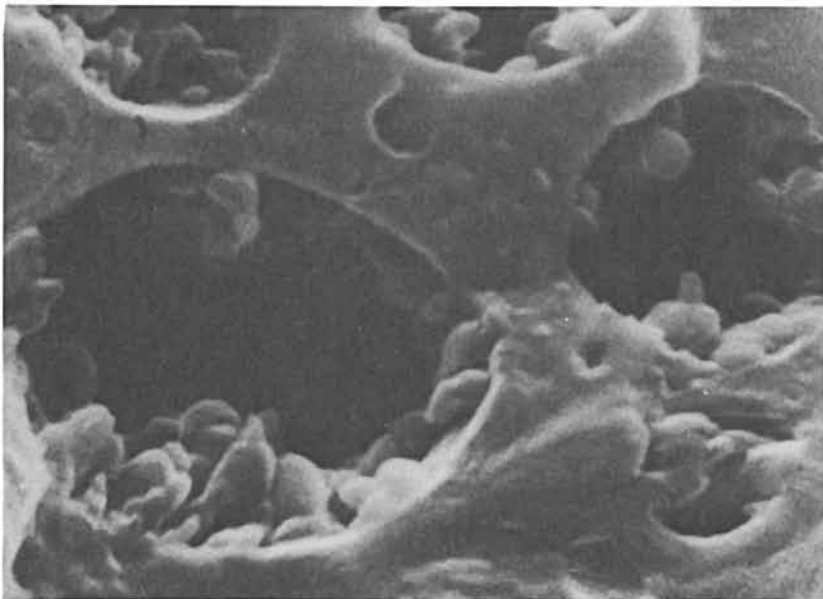


Figures 2a and b. Electron micrographs of fracture surfaces of polymerization system 1 (a) and 2 (b). Figures a and b were examined in TEM.

c)



d)



Figures 2c and d. Electron micrographs of fracture surfaces of polymerization system 3. Figures c and d were examined in SEM.

and one at about 70 °C owing to the glass transition of the nylon. Apparently, even in a block copolymer the bonded polyol is present as a separate phase.

An overview of the mechanical properties is given in Table I.

Table I. Mechanical Properties (Measured Dry as Made)

	Polyol % (wt)	Izod (notched) kJ/m ²	Flexural modulus N/mm ²
AP nylon	-	4	3250
System 1	20	5	2420
System 2	10	9	2700
	20	12	2310
System 3	10	26	1850
	20	54	1370
	30	60	420

From the table it appears that the Izod impact strength improves as the interfacial adhesion increases. This is also concluded in a recent publication about nylon 6.6 compounded with polyethylene-g-maleic anhydride polymer (15). Addition of more rubber in system 3 (30 %) affords hardly any additional improvement in toughness, but the flexural modulus, which in ABA block copolymers is already lower than in a dispersed rubber system, is more than halved.

Several authors have given a basic theory for the prediction of the modulus of a composite (16-18). The line in Fig. 4 shows the theoretical curve for the reduction of the modulus (E/E_0) due to incorporation of a soft rubber phase in a hard matrix at a temperature above the transition region of the soft phase and below the transition region of the hard phase (E = flexural modulus of the modified nylon and E_0 = flexural modulus of the unmodified nylon). The experimental points of systems 1 and 2 fit fairly well onto the theoretical curve. This proves that they are well-dispersed systems without inclusions. The difference in impact strength between system 1 and system 2 is mainly due to the better interfacial adhesion of system 2, by which crazes are stabilized and/or the formation of small shear bands is initiated. The points of system 3 deviate widely from the theoretical curve. This is an indication of an anomalous structure, for example interlocking networks or, in the case of a higher rubber content, an intermediate state of phase reversion. Therefore, we postulate that the morphology of system 3, with about 20 % impact modifier is that of an almost continuous rubber network extending through a nylon phase ("Figure 5"). By increasing the rubber fraction the network will be more perfect. More nylon is included and therefore less nylon can contribute to the modulus.

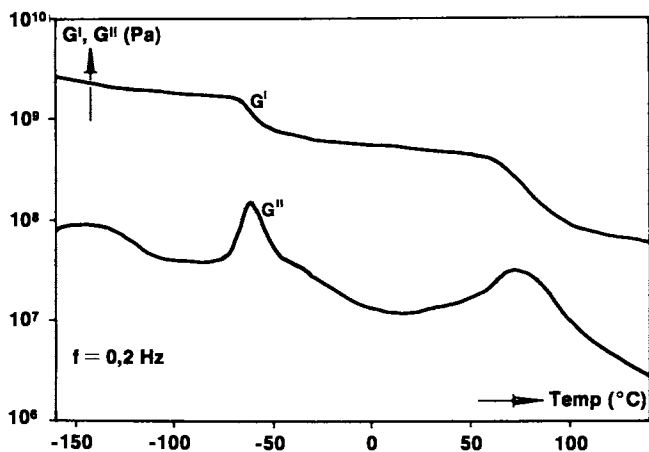


Figure 3. Shear modulus G' and loss modulus G'' of an ABA block copolymer (system 3).

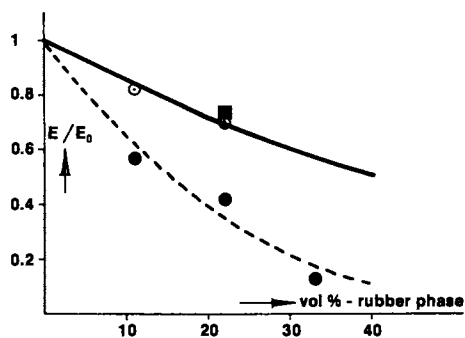


Figure 4. Modulus reduction as a function of the soft rubber phase volume (temperature 23 °C). Key: ■, system 1; O, system 2, and ●, system 3.

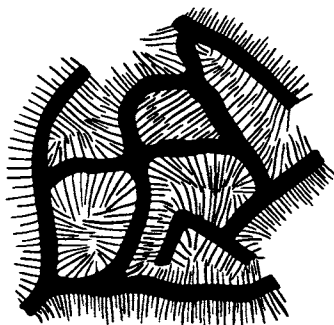


Figure 5. Postulated morphology of ABA block copolymers (system 3).

The net effect is a sharp drop in modulus. Furthermore, the deformation behaviour will be largely determined by the rubber properties. If this is true, the deformation mechanism will be that of the rubber phase, so one would expect that plastic deformation will take place mainly by shear flow. This was verified by analysing the deformation mechanism by means of volume monitoring during tensile testing (19,20). From these experiments it was concluded that in products of system 3 with 20 and 30 weight % polyol the plastic deformation was completely due to shear flow; no crazing was observed, which is in accordance with the morphology postulated.

Another consequence of this morphology is that the ultimate properties of the system are largely determined by those of the rubber. Consequently, a high elongation at break will be attained. This is in accordance with the high Izod values of the ABA block copolymers obtained experimentally.

Conclusions

- Improvement of the impact strength of RIM nylon can be achieved by incorporation of a polyol. Of the various kinds of morphology shown, the ABA block copolymers possess the highest toughness, although this is accompanied by a great loss in flexural modulus.
- It is postulated that the morphology of ABA type block copolymers with 20 % or more polyol is that of a continuous rubber network extending through a nylon phase, the deformation behaviour and ultimate strength being determined by the rubber phase. Improvement of impact strength is due to shear flow.
- Application of a high polyol content (30 %) is not interesting, because further perfection of the rubber network yields little additional improvement in impact strength, while the modulus decreases sharply.

Acknowledgments

The authors wish to express their appreciation to Mr. J. Bongers for his experimental work, to Dr. F. Maurer and Dr. S. Sjoerdsma for their interest and helpful discussion, to Mr. S. Nadorp for his electron-microscopy studies and to Mr. C. Vrinssen for the examination of samples under his guidance.

Literature Cited

1. Courtaulds, G.B. Patent 1126211 pr. date 1-14-1965
2. G.E. Molau, J. Polym. Sci A3, 1965, 4235
3. DSM/Stamcarbon, US Patent 3704280 pr. date 3-25-1969
4. DSM/Stamcarbon, US Patent 3770689 pr. date 1-24-1970
5. DSM/Stamcarbon, US Patent 3793399 pr. date 9-23-1970
6. Monsanto, European Patent 67694, pr. date 6-16-1981
7. Monsanto, European Patent 67695, pr. date 6-16-1981
8. DSM/Stamcarbon, patent applications to be published
9. ICI, GB Patent 1.067.153, pr. date 5-17-1963
10. British Celanese, GB Patent 1099265, pr. date 5-11-1964
11. Toyo Rayon, Japanese Patent 16028/69, date 7-15-1965

12. Monsanto, US Patent 3862262, pr. date 12-10-1973
13. Monsanto, US Patent 4031164, pr. date 8-25-1975
14. M.J. Folkes and A. Keller, *Physics of Glassy Polymers*, Appl. Science Publishers, 1973, Ed. R.N. Haward Chapter 10
15. S.Y. Hobbs, R.C. Bopp and V.H. Watkins, Polym. Eng. Sci. 1983, 23, 380
16. E.H. Kerner, Proc. Phys. Soc. London 1956, B69, 808
17. C. van der Poel, Rheol. Acta 1958, 1, 198
18. L. Bohn, *Copolymers, Polyblends and composites. Advances in chemistry series no. 142*, 1975, Ed. N.A.J. Platzter, Chapter 6
19. C.B. Bucknal and D. Clayton, Nature (Phys. Sci.) 1971, 231, 107
20. D. Heikens, S.D. Sjoerdsma and W.J. Coumans, J. Mater. Sci. 1981, 16, 429

RECEIVED April 16, 1984

Self-Releasing Urethane Molding Systems: Productivity Study

LOUIS W. MEYER

The Dow Chemical Company, Freeport, TX 77541

This review identifies the primary reason for utilizing self-releasing urethane molding systems: increased productivity. In achieving this goal, however, the practical issues of various performance features, which may be critical to overall results, must be recognized, understood, and dealt with.

For example, the need to paint parts is most often a very real and critical issue which must be effectively worked out when using self-releasing systems.

Theory relates release in terms of the equations defining adhesion, especially work of adhesion, W_a . What is sought is minimum adhesion and this is achieved by an IMR agent acting as a low energy film barrier between the mold metal high energy surface and the moderate (polar) energy surface of the urethane system itself.

To date self-releasing systems have not provided infinite cycles of release, yet the number of consecutive releases for molds of differing degrees of complexities result in significantly improved productivity - the range being between 25% to 140% increased production yield.

Cost reductions in manufacturing operations using IMR systems should be coupled to productivity increases. Typically, a 50% increase in productivity should show a cost reduction on the order of between 15% and 20%.

The technology of self-releasing systems based on IMR agents is both new and incomplete in total development. Probably much needs to be done in terms of refinement and further extension of use, yet the overall benefits of a system which can be termed "effective" are of considerable practical value, even now.

0097-6156/85/0270-0195\$06.00/0

© 1985 American Chemical Society

Mold release agents have always been an important and critical requirement of any type of urethane molding process. RIM molded parts cannot be removed from their molding tools without effective release agents. Likewise, foam molded articles such as seat cushions, cannot be removed from their tools without the aid of such agents. The need for mold release compounds is brought about by the fact that urethanes, because of their chemical composition, are adhesive in nature. Thus, urethanes like to stick to the molds in which articles are formed. The common practices of overcoming the "sticking" problem of urethane is to apply an external mold release agent to the mold surface. This is normally done by a press operator who applies it in the form of a spray between every one or molding cycles. This method of achieving release is effective in a technical sense, but it has numerous draw backs. The spray operation is both messy and wasteful. Its use is not without cost - as much as \$.05 per part. The time required to apply external spray release is wasted efficiency in cycle time, and this in turn is negatively reflected in curtailed productivity. For example, if in a 120 second molding cycle, it requires 30 seconds to apply an external release agent, a 25% reduction in productivity would be observed. It is not uncommon to observe even higher productivity losses because of time devoted to spot cleaning of the mold and application of external release waxes and sprays on the mold during the production cycle. In addition, excessive use of sprays leads to "dirty" mold build-up conditions, necessitating total mold clean up. This may have to be done as often as every four hours, although once a shift is more common. This additional "time-out" condition to make the process operational again, cuts out a portion of otherwise available production time. If this lost time is 1 hour out of each 8 hour shift, which is typical, it represent 12.5% machine utilization loss. Combining this 12.5% loss with the previous 25% loss results in a total loss of 37.5% productivity overall, a value that cannot be easily ignored.

Production efficiency and manufacturing costs are directly and indirectly related. When productivity increases, costs go down. The relationship between these two important variables is further discussed in the subject section of Production Optimization.

The problems surrounding part quality, while not always identified in a quantitative way, are certainly inherent in the use of external mold release sprays. A self-releasing system, made possible by the incorporation of an internal mold release agent in polyurethane chemicals offers a possible way of eliminating, or at least, minimizing the problems akin to external release methods. The gains which can be realized are distinct and real. The benefits derived from of a self-releasing system based on effective internal mold release agents are:

1. Increased production efficiency,
2. Reduced manufacturing cost,
3. Improve part quality.

All of which adds up to optimizing production performance.

Commercial IMR Products and Self-Releasing Systems

It appears that the first commercial promotion of an effective IMR agent came about through the introduction of a product chemically defined as a carboxy-functional dimethylsiloxane fluid (1). Although this product is an effective release agent, it is prone to have deleterious effects on tin catalysts. Practical use has thus been limited to increasing the amount of tin catalyst in the B-side of the system, and adding a third stream to the process equipment through which this agent is introduced. The introduction of other commercial products - as IMR agents - has to date, not been evident.

In an abstract of an unpublished paper, Dominquez (2) approached the question of internal mold release by making use of an all - polyurea system. Specifics are not available on either the system or IMR agent employed. Further information may be gleaned, however, from the work of Plevyak and Sobieski (3). They show the utilization of the carboxy-functional dimethylsiloxane fluid in a two stream process operation in conjunction with a system which is all polyurea.

A self-releasing system based on an amine modified polyol to which had been added a proprietary IMR agent when formulated with the aromatic amine chain extender diethyltoluendiamine (DETDA) and MDI quasi-prepolymers demonstrated exceptional process and molded product attributes. The formulated systems is shown in "Table I".

Table I. Formulation for Internal Mold Release System (4)

Item	Generic Type	Designation	Quantity (PBW)
Polyol + IMR-II	Amine Modified	XA-10888.00L	100
Chain Extender	Aromatic Amine	DETDA	18-24
Isocyanates	Quasi-prepolymers	Isonate (1) 191	1.03 Index
		Mondur (2) PF	
		Rubinate (3) LF-179	
Catalysts	Amine	Dabco (4) 33LV	0.10%
	Tin	Fomrez (5) UL-28	0.15%

1Trademark of Upjohn Chemical Company

2Trademark of Mobay Chemical Company

3Trademark of Rubicon Chemical Company

4Trademark of Air Products Chemical Company

5Trademark of Witco Chemical Company

(Reproduced with permission from Ref. 4. Copyright 1983, SPI.)

Particular attributes include, for example, these outstanding characteristics; stable physical properties retention, stable tin catalyst reactivity, stable nucleation, and most importantly, exception release - between 25 and 300 RIM parts for metal molds which had no prior wax base coat.

Performance Features

In addition to release per se, there are other features which are often crucial to the adaptability and usefulness of a fully formulated self-releasing system. A brief review of these characteristics are important to assessing the value or worthiness of the self-releasing system as a whole.

Compatibility: It is highly desirable and often mandatory that IMR agents be compatible, both physically and chemically with the chemicals of the urethane system. This means that the IMR agent should be compatible with either the B-side components (polyols plus chain extenders), or the A-side isocyanate. Obviously, the reactive nature of isocyanates with compound having an active hydrogen, limits the choice of compounds to those which are non-reactive, that is, chemically inert toward isocyanates. Polyol and isocyanate manufacturers who are active in IMR technology supply their products with the IMR agent in a totally compatible and stable form.

Reactivity: In a two stream molding operation catalysts are normally added to the B-side components. If the IMR agent is also incorporated in the B-side it's important to make certain that catalytic reactivity is not seriously reduced. Not all IMR compounds induce this problem on tin catalyst, but some do. For example, the carboxy-functional dimethylsiloxane fluids tend to bring about this degrading effect. A possible way of minimizing this problem (although this is not always true) is through the use of third stream addition of either the catalyst or IMR agent. By adding a third stream to the equipment the catalyst and IMR agent remain separate until they reach the mixing head. Ideally, however, a two stream operation, free of this "catalyst kill" problem remains preferable.

Exudation or Bleed-Out: Freedom from exudation or bleed-out of the IMR agent in the molded article is also be a critical factor to overall performance.

This phenomena, if present in the molded part, will usually be self-evident. Adhesive qualities to materials such as scotch tape and paint, for example, will be very poor. For the most part, however, this undesirable feature can be controlled or avoided. Raw material manufacturers will usually select only those IMR compounds which are either; (1) isocyanate reactive, or (2) have polymer solubility characteristics which are free of this problem.

Physical Property Retention: IMR agents in self-releasing systems should not adversely affect the the physical properties of the urethane polymer. There must be no evidence of either plasticization or embrittlement in molded parts. Plasticization is usually evident by a reduction in flexural modulus, while embrittlement is most often seen through a significant reduction in elongation. Comparative physical property data for three low modulus RIM systems is shown in "Table II". These results show that changes in physical properties by the addition of the release agent IMR-II were essentially non-existent - a good indication of product property stability.

Table II. Physical Property Comparison of Systems With and Without IMR (4)

Formulation	A	B	C
Type Polyol, 100 pts	Conventional	Amine Modified	Amine Modified + IMR-II
DETDA, pts	21	18	18
Mondur PF 1.03 Index, pts	53	60	60
Property			
Flexural Modulus, psi	28,650	30,000	30,800
Tensile Modulus, psi	3,600	2,800	2,900
Elongation, %	265	280	290
Tear Strength, pli	280	480	490
Heat Sag, in.250 ^o F/ 60 min.			
6 in. overhang	0.57	0.51	0.53
4 in. overhang	-	0.29	0.31
Specific Gravity, g/cc	1.01	1.00	1.02

(Reproduced with permission from Ref. 4. Copyright 1983, SPI.)

Many RIM formulated systems also incorporate milled glass fibers, or other kinds of fillers to bring about a reduction in linear thermal expansion and contraction, and increase part rigidity. When this is done, some reduction in elongation is always evident. This is expected. The reduction, however, should not be drastic. Therefore, any combination of filler plus IMR agent in a formulated self-releasing system should not bring about additional loss in toughness as evidenced by further reduction in elongation. In other words the bond strength between fiber and polymer should not be critically lowered by the presence of IMR agents. For example, when formulation B of "Table II" was modified by a 10% addition of 1/16 inch milled fiber glass the flexural modulus nearly doubled, and the reduction in elongation was only slightly more than 30% as shown in "Table III".

Table III. Effect of IMR Plus Milled Glass Fiber Reinforcement on Physical Properties

Formulation	B	C
Glass Loading*	10	10
Neat Flexural Modulus, psi	30,000	30,800
Flexural Modulus, psi	54,200	53,800
Tensile, psi	2,750	2,800
Elongation, %	198	200
Tear, pli	511	532
Heat Sag (250°F/60 min), in.		
6 inches overhang	0.30	0.20
4 inches overhang	0.25	0.21
Specific Gravity, g/cc	1.09	1.11

*737 AA Owens Corning 1/16" milled glass properties of RRIM parallel to flow.

Likewise, when formulation C was also modified by 10% milled glass fiber, the toughness of the polymer remained intact, as evidenced by low loss of elongation and retention of tear strength - a good measure of retained bond strength. These results are also shown in "Table III".

Nucleation: Most urethane RIM processed systems are nucleated. The reasons for this include such things as; reduced density to lower cost, increased ease of mold filling, and improved part surface appearance. The microcellular structure which makes these benefits realizable is achieved by nucleation, either with a gas such as air or nitrogen, or by incorporating a blowing agent in the system formulation. An IMR agent must, therefore, not affect the cell structure or the stability of the nucleated froth: it must neither subtract or hinder the emulsified stability of the nucleated system.

Painting: The elusive problems of painting described in terms such as orange peel, fish eyes, and the like are always of great concern. Painting difficulties can usually be related to one of two things relative to the presence of IMR agents; wet-out and adhesion. Poor wet-out brings about fish eye, and orange peel paint problems. It can also lead to poor paint adhesion as well. The phenomenon of wet-out is related to the property of surface tension - of the solid (molded part surface), and of the liquid (paint). Wet-out difficulties tend to occur when a liquid will not effectively spread on a surface. Zisman and co-workers (5) related the ability of a liquid to spread on a surface (thus wet it effectively) to the property he defined as the critical surface tension of the solid γ_{sc} . This is an empirical parameter usually obtained by plotting the cosine of contact angle of various liquids on the surface of the solid in question against the surface tension of those liquids. Extrapolation of this plot to the value $\cos = 1$ ($\theta = 0^\circ$) yields γ_{sc} , which is the liquid vapor surface tension γ_{lv} value a liquid must possess to spontaneously spread on that

surface. An example of this relationship is shown in Figure 1. Paint problems, therefore tend to occur when the liquid vapor surface tension γ_{lv} of paints are near or less than the critical surface tension γ_{sc} of the surface of the molded part.

For self-releasing systems the presence of an IMR agent on the surface of the part, which makes it self-releasing, also lowers the value of the solid's critical surface tension, making it less wettable by the paint, than if it were free of the IMR surface coating. This problem, however, can be solved by either one of two ways: (1) by the addition of solvent to the paint formulation that will solubilize the IMR agent on the part surface, or (2) by washing the part (after post cure) to remove residual surface IMR agent. Typical methods of cleaning include; solvent wiping, vapor degreasing, and water power wash systems which utilize both solvent and emulsion cleaners.

Paint adhesion although a factor of wet-out, is also controlled by solvent "bite", and post molded freedom from IMR exudation or bleed out, a topic previously reviewed. Obviously, the selection of a solvent system for a paint formulation must be properly addressed in order to eliminate, or, at the very least, minimize this type of paint adhesion deficiency. Some of this topic is further discussed under the section titled Theoretical Considerations.

From each of the foregoing topics, it is quite obvious that the ease by which IMR agents are selected is greatly curtailed. Finding a compound which can be "dumped" into any and all systems to provide the property of self-release is perhaps realistically impossible. Each and every system must have its own "right" formulation - a task so far accomplished only by a limited number of suppliers of urethane raw material chemicals.

Theoretical Considerations

When a molded part doesn't release, the essential problem (the fact that it sticks to the mold) is one of adhesion. Thus, if release is to be achieved, adhesion must be prevented. For most molded urethane systems there are four factors which can affect adhesion, thus release:

1. Wetting (5) - The ability of the liquid polymer to "wet" the mold.
2. Spreading (5-6) - Complete "wetting"; the ease or degree the liquid polymer spreads in "wetting" the mold.
3. Covalent Bonding (7) - Bonding by direct chemical reaction of the liquid system to the mold surface.
4. Hydrogen Bonding (8) - Bonding by association of the highly polar polymer to the mold surface.

Of these phenomena, two are physical in nature - wetting and spreading, and two are chemical - covalent bonding and hydrogen bonding. The two broad characteristics, physical and chemical adhesion, are best examined separately.

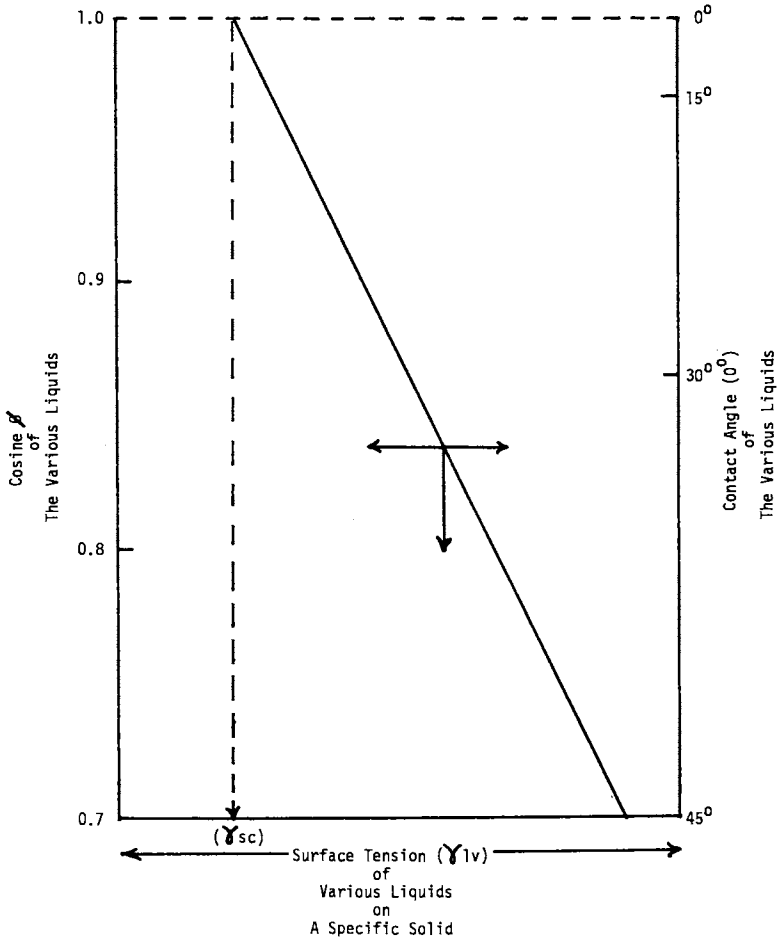


Figure 1. Method to determine the critical surface tension of solids.

When a liquid material like a reactive urethane system enters a clean mold and contacts its surfaces, all of the previously mentioned adhesive forces quickly develop. The liquid urethane chemicals, all of which are fairly high polar compounds tend to very easily "wet" metal molds, be they steel, aluminum, nickle plate, or other metallic surfaces, because they are high energy surface materials. Not only are they easily "wet", but the ease with which the initial wetting "spreads" to the point of complete wetting (a spreading of the film interface to a nearly molecular level of thickness) substantially promotes adhesive characteristics at the metal/liquid interface. With these physical characteristics now established in an optimum condition at film interface, the reactive chemistry, which then occurs to cure the part, is maximized to bring about excellent adhesion via chemical bonding - both direct and indirect. Thus, to reduce adhesion to the point of non-sticking, the properties of wetting and spreading must be altered or otherwise controlled so that they are no longer a detriment, and instead are an aid to ease of release.

In general, external mold release agents form a physical barrier (a new film interface), which is essentially impervious to being "wet" by the liquid chemicals of the system. In addition this new film barrier is chemically non-reactive with the system chemicals, thus bond energy is very low, i.e. brought a point of minimum value. Internal release agents, however, not only act as a physical barrier, but they alter the wetting and spreading properties of the system as well.

The forces responsible for adhesion/release are intermolecular, and are usually referred to as secondary valence forces. In many cases, however, they can also be primary, that is, those of direct chemical bond. In any event, the force of separation F_s is shown to be a function of two factors; work of adhesion W_a , and the distance of bond separation d . Taylor and Rutzler (9) have shown that the force of separation is also complicated by the practical fact that only about 1% of the surfaces are in a bond condition, because of geometrical imperfections. These variables are related by "Equation 1":

$$F_s = \frac{W_a (.01)}{d} \quad (1)$$

Further refinement of this equation was made by Kraus and Mansar (10). They showed that for thin layer adhesive systems the force of release passed through a maximum value where $F_{max} = 1.46 F_s$. Under this condition:

$$F_{max} = 1.46 \frac{W_a (.01)}{d} \quad (2)$$

Direct measurements on the work of adhesion W_a have also been summarized by Krauss (11). Values of W_a are also calculatable with reasonable accuracy for systems free of direct chemical bond as is shown later in "Equation 3". The separation distance d for high energy systems where F_{max} exists has been estimated by McKelvey

(12) at about 4°A . Estimation of d for different film interface condition to calculate F_s are also possible. The range for these is probably on the order of 20A° to 100A° . For many high energy solid-liquid systems the values of W_a are on the order of 200 to 300 ergs/cm², and can be as high as 400 ergs/cm², or more under condition of high hydrogen bonding, as for example, with metal oxide surface in conjunction with high hydroxyl functional (OH) liquid systems. On the other hand, W_a for low energy surfaces, can be nearly as low as the liquid systems surface tension value, i.e. on the order of 30 to 50 ergs/cm² of surface energy. Calculation of the force of separation for two cases, good adhesion and poor adhesion, yield these results;

Case 1. High energy (metallic) surface, no mold release. (Good adhesion, poor release)

$$F_{\max} = (1.46) \frac{(300)}{4 \times 10^8} (.01) = 1.095 \times 10^8 \text{ dynes/cm}^2$$

$$= 1,588 \text{ psi}$$

Case 2. High energy surface with mold release, which is also approximately equivalent to low energy surface, no mold release. (Poor adhesion, good release)

$$F_s = \frac{30}{20 \times 10^8} (.01) = 0.00150 \times 10^8 \text{ dynes/cm}^2$$

$$= 2.17 \text{ psi}$$

The difference is significant. By making use of a mold release agent (Case 2) the high energy surface has been altered to that of a low energy surface, and the high bond intermolecular distance increased, thus both factors contribute to a much lower release value. The values of W_a used are confirmable through the use of the Young - Dupree (5) equation for high energy surfaces. It relates W_a as follows:

$$W_a = \pi_e + \gamma_{lv} (1 + \cos \theta) \quad (3)$$

where, γ_{lv} = liquid vapor surface tension
 θ = contact angle of the liquid to the solid
 π_e = spreading factor (degree of complete wetting)
 $\gamma_{lv}(1 + \cos \theta)$ = wetting factor

The work of Bangham and Rozouk (6) also showed that π_e always has a value, $\pi_e \geq 0$. The studies by Harkins (8) and co-workers showed that π_e always exceeds the liquid-vapor surface tension by a factor of about 3 to 4, and that the contact angle tended to approach zero ($\cos \theta \approx 1.0$). This being so:

$$W_a = (3 \text{ to } 4) \gamma_{lv} + \gamma_{lv} (1 + \cos \theta)$$

$$= \gamma_{lv} (3 \text{ to } 4) + 2 = \gamma_{lv} (5 \text{ to } 6)$$

If γ_{lv} is say 60 dynes/cm, then $W_a = 300$ to 360 ergs/cm².

Further, if the mold surface is not metal, but rather a low energy one instead, olefinic for example, the spreading factor θ would be zero, therefore:

$$W_a = \gamma_{lv} (1 + \cos \theta) \quad (4)$$

Which is the Young - Dupree relationship for low energy surfaces.

It has generally been observed that urethane systems, which are cured on the surface of some low energy materials, are also free from adhering to them, i.e. they are self-releasing. Materials which show this characteristic relative to urethanes in a very effective way include at least three different types of plastics; polytetrafluoroethylene, polyethylene, and polypropylene. These materials all have a defined critical surface tension σ_c less than about 30 dynes/cm. Assuming that this value is near, the liquid vapor surface tension γ_{lv} value of an effective IMR urethane systems, then the work of adhesion as given by Equation 4 is as follows:

$$\begin{aligned} W_a &= \gamma_{lv} (1 + 0) = \gamma_{lv} \\ &= 30 \text{ ergs/cm}^2 \end{aligned}$$

the value used in the example of Case 2.

The problems of adhesion viewed from a chemical bonding standpoint are similar. Typical metal mold surfaces have been shown by Kaelble (7) to have a surface hydroxide layer of about (40-80) Å^o. Such a surface provides two possible modes of chemical bonding, reaction of the ionic metal - hydroxide directly with the isocyanate, not too likely, or via hydrogen bonding with hydroxyl or other functions of either the chain extender and/or polyol. Thus, to eliminate or minimize chemical adhesion the metal mold surfaces must be protected from polar materials such as polyurethanes by an interface which not only avoids the physical problems of adhesion, but those which are of a reactive chemical nature as well, i.e., a non-wetable, non-polar, non-reactive boundary layer or film. In terms of releasability, therefore, such a boundary between the metal mold surface and the polyurethane must be present. It makes no difference whether this is achieved by the application of an external mold release (EMR) agent, or though the incorporation of an internal mold release (IMR) agent.

Production Optimization

Increased efficiency starts with the molding cycle. It must be reduced if gains are to be made in production optimization. A shorter molding cycle is the place where optimization starts. What automatically follows as a consequence of this is, increased

productivity - the yield factor, followed by cost reduction - the economic factor, and, most often, better surface appearance of the part - the quality factor.

Cycle Efficiency: The number of consecutive self-releasing cycles which should be attained to reach a practical yet efficient molding cycle is readily calculable. This may be done by the "Equation;

$$t_a = t_o - t_s + \frac{t_s}{n} \quad (5)$$

where: t_a = average cycle time for n consecutive releases,
 t_o = original cycle time, ($n=1$),
 t_s = time required to apply external mold release spray,
 n = number of consecutive release between external mold release spray.

This equation expresses the relationship between the averaged effective molding cycle t_a , which is obtained by eliminating the time required to apply EMR spray t_s , derived as a benefit from a system containing an IMR agent for n consecutive self-releasing molding cycles. A generalized relationship between t_a and n is shown graphically in Figure 2. Typically, only about 10 consecutive releases are needed to dramatically improve the molding cycle as can be seen in "Table IV".

Table IV. Relationship of the Average Cycle Time for n Consecutive Releases t_a , and the Number of Releases Between External Mold Release Spray n

TIME (SECONDS)				
Time (Sec.)			Releases Between Spray	
t_o	t_s	t_a	n	
120	30	120.0	1	
120	30	93.0	10	
120	30	90.3	100	
120	30	90.0	∞	

In a paper by Taylor (13), et. al. this type of relationship has been extended to reflect productivity improvements in a similar manner. Increased cycle efficiency alone, however, is not the whole answer to improved productivity, yet it is fundamental to the reason for wanting systems containing IMR agents. Ideally, a self-releasing system which would provide an infinite numbers of releases ($n = \infty$) is a valid but difficult target. On a more practical level, however n releases between 30 and 300 are attainable.

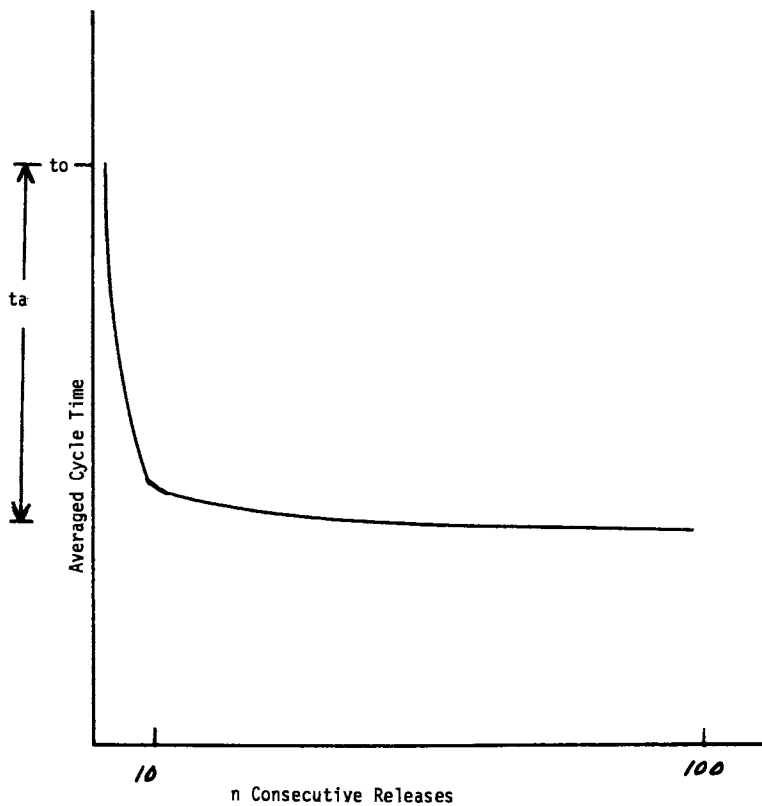


Figure 2. Averaged cycle time for n consecutive releases obtained as a result of eliminating the time necessary to apply external mold release spray.

Productivity: The primary reason for wanting a self-releasing system is increased productivity. In its simplest form productivity is a function of three factors: cycle time, machine utilization, and scrap rate. In the terms of Equation 5 the percent cycle reduction and percent productivity increase as a result of the cycle reduction may be expressed as follows:

$$\% \text{ Cycle Reduction} = 100 \frac{t_o - t_a}{t_o} \quad (6)$$

$$\% \text{ Productivity Increase (Cycle Basis Only)} = 100 \frac{(t_o - t_a)}{t_a} \quad (7)$$

Using the cycle times of Table 1 for the value $n = 100$,

$\% \text{ Cycle Reduction} = 25\%$ and,

$\% \text{ Productivity Increase} = 33\%$ (machine basis only).

To this productivity gain, must be added the gains of improved machine utilization and of reduced scrap rate. The actual results of these combined effects as determined by an extensive production trial of fascia manufacture is tabulated in "Table V". The total gain realized (60.5%) is significant. It is typical of the increased productivity an effective self-releasing system can provide to a RIM process manufacturing operation.

Table V. Fascia Productivity with and Without an IMR Agent

	Without IMR	With IMR
Productivity Features		
Cycle Time, sec.	120	90
Utilization, %	75 (6/8 Shift)	87.5 (7/8 Shift)
Parts/Hr (8 hr shift)	22.5	35.0
Scrap, %	5	2
Parts/year, M	76,950	123,480
Increase, %	-	+60.5

*Two 8 hr shifts/day 6 days/week; 45 weeks/year

How much productivity might be expected from a wide range of tool designs? This question was answered by evaluating a number of different commercial molds under both laboratory conditions, and actual industrial production conditions. To maintain account confidentiality the molds used are identified by group characterization only. A summary tabulation of these trials is shown in "Table VI".

Table VI. Production Performance Results Summary

Generic System Components: Polyol-Amine Modified + IMR-II
 Chain Extender - DETDA
 Isocyanate - Quasi Prepolymer
 Fascia or Fascia-like

Mold	Simple	Simple	Complex	Complex
Description	Simple Rear	Front	Rear	Front
Original Cycle, sec.	150	150-180	200-275	240-300
New Cycle, sec.	85-95	85-90	150-200	100-200
No. of cycles w/o EMR				
Best case	325+*	160	186+*	50
Worst case	100	125	25	25
Cycle Reduction, %				
Best	43	50	38	58
Worst	37	43	25	33
Production Increase, %				
Best	76	100	38	140
Worst	58	76	33	50

*Run stopped end point was not determined.

External mold release was still necessary, but only every so often - as little as once every 300 cycles or so, or as often as once every 25 cycles. All in all, not often enough to be a factor in cycle efficiency. For this series, productivity improvements ranged from a worst case of 33% to a best case of 140%, with the range 50% to 75% being typical. The values are significant.

Cost Reduction: As productivity increases, cost reduction should automatically follow. By how much? Although an exact answer can't be given unless actual accounting figures are obtained, it is possible to get a reasonable idea of what the reduced cost might be. One approach to this economic question can be made by equating unit cost to both variable and fixed costs in a simplified way. With reasonable assumptions of basic inputs on such things as molded part weight, raw material cost, tooling cost, and production volumes, values for production increase versus cost reduction can be determined. The following sensitivity study is used to illustrate and relate this inverse relationship:

Assumed Basis:

Part Weight = 8.90 lbs
 Urethane System = \$1.00/lb
 Tooling = \$250,000
 Annual Production = 200,000 units
 Variable Costs = Raw Material costs + Tooling Costs
 Fixed Costs = (1.2) (Initial Variable Costs)

Cost Equation:

$$\frac{\text{Total Cost}}{\text{Unit}} = \frac{\text{Variable Cost}}{\text{Unit}} + \frac{\text{Fixed Cost}}{\text{Unit}} \quad (8)$$

Therefore:

$$\begin{aligned} \frac{\text{Total Initial Costs}}{\text{Unit}} &= \frac{\$8.90}{\text{Unit}} + \frac{\$250,000}{200,000 \text{ Units}} + 1.2 \text{ } \$ (8.90 + 1.25) \\ &= \$10.15 + \$12.18 = \$22.33 \end{aligned}$$

Employing this initial unit cost as a base value of manufacturing cost the value of percent cost reduction for given values of percent production increase can be determined. These are shown in "Table VII".

Table VII. Economic Sensitivity Study: Production Increase vs. Cost Reduction

Production Increase (%)	Raw Material \$/Unit	Tooling Amount \$/Unit	Fixed Cost \$/Unit	Total Cost \$/Unit	Cost Reduction (%)
0	8.90	1.25	12.18	22.33	0
25	8.90	1.00	9.74	19.64	12.0
50	8.90	.83	8.12	17.85	20.0
75	8.90	.71	6.96	16.57	25.8
100	8.90	.63	6.09	15.62	30.0
150	8.90	.50	4.87	14.27	36.1

A separate study based on capital investment requirements comparing RIM without IMR and RIM with IMR showed similar cost savings benefits, "Table VIII". In this particular example, a 27% reduction in cycle increased productivity by 63%. The combined effects of these benefits yielded costs saving on the order of 17%, which is significant.

Table VIII. Capital Investment Economic Comparison of RIM Without IMR vs. RIM with IMR

Process/Product	RIM	RIM + IMR	% Change		
Unit Weight (#)	7.00	7.00			
Unit Thickness (In.)	0.150	0.150			
Raw Material (\$/#)	1.00	1.00			
Cycle (Min.)	2.50	1.83	-27		
Parts/Hour	24.00	34.7			
Operating Hours	6,000	6,000			
Clamps	2	2			
Capacity Utilization	0.90	0.90			
Efficiency	0.75	0.87			
Scrap (%)	5	2			
Actual Production (Units)	184,680	301,380	+63		
Capital Equipt. (\$M)	950	950			
Costs					
	<u>\$M/YR</u>	<u>\$/Unit</u>	<u>\$M/YR</u>	<u>\$/Unit</u>	
Raw Material		7.00		7.00	
Utilities		.18		.22	
Tooling	225	1.23	225	.75	
Variable		8.41		7.97	
Fixed Costs*	2,000	10.82	2,400	7.96	
Total Mfg. Costs		19.23		15.93	-17

*Estimated at \$2,000 M/YR for RIM and \$2,000 + 20% for RIM + IMR due to increased labor.

Conclusions

Self-releasing systems based on "effective" IMR agents can typically increase productivity by about 50% to 75%. In conjunction with this increase, a cost reduction of between 12% to 20% should be expected.

Practical problems such as the need to paint molded parts, can be dealt with in a realistic way.

This product technology although quite new in both development and commercial introduction, still holds great promise in radically improving the value of the RIM process itself.

Literature Cited

1. J. E. Plevyak, L. A. Sobieski, Proceedings of the ACS Division of Polymeric Materials Science and Engineering, Vol. 49, p. 619-624 (1983).
2. R. G. Dominquez, SPE NATEC '83 Conference Proceedings, p. 52.
3. J. E. Plevyak, L. A. Sobieski, Proceedings of the SPI - 6th International Technical/Marketing Conference, p. 365-369 (1983).
4. L. W. Meyer, Proceedings of the SPI - 6th International Technical/Marketing Conference, p. 372 (1983).
5. W. A. Zisman, "Adhesion and Cohesion", P. Weiss Ed. Elsevier Amsterdam, 1982.

6. D. H. Bangham, R. I. Razouk, *Trans. Faraday Soc* V. 33, 805, (1937).
7. D. H. Kaelble, "Physical Chemistry of Adhesion"; Wiley Interscience, New York, NY (1971).
8. W. D. Harkins, "The Physical Chemistry of Surfaces", Reinhold, New York, (1952).
9. D. Tayler and J. Rutzler, "Industrial Engineering Chemistry", 50, 904 (1958).
10. G. Kraus and J. Manson, "Journal of Polymer Science", 6, 625 (1951); 8, 448 (1952).
11. G. Kraus, "Adhesion and Adhesives", John Wiley, p. 45 (1954).
12. J. McKelvey, "Polymer Processing", John Wiley, p. 161 (1962).
13. R. Taylor, *Proceeding of the ACS Division of Polymeric Materials Science and Engineering* Vol. 49 p. 625 (1983).

RECEIVED October 5, 1984

Improved RIM Processing with Silicone Internal Mold Release Technology

JOSEPH E. PLEVYAK and LORETTA A. SOBIESKI

Dow Corning Corporation, Midland, MI 48640

Since its commercial introduction in 1974, reaction injection molding (RIM) of elastomeric polyurethane has proven to be a cost-effective and energy-saving process to produce large and intricate parts with good impact strength. Government legislation promoting safety and damage resistance has been one key factor that helped open the American automotive market for elastomeric polyurethane fascia manufactured by the RIM process. In fact, the use of elastomeric RIM fascia is expected to reach a 50% penetration level in North America by 1985. Although the automotive market is the largest user of the RIM process, non-automotive uses of polyurethane RIM are also beginning to show much promise. From the early RIM process in 1974 to current processing techniques, chemical and mechanical improvements have been made which have decreased cycle times from five and one-half minutes in 1974 to current cycle times of two to two and one-half minutes. Although these improvements have been substantial, RIM processors still expect shorter cycle times.

Presently, elastomeric polyurethane molded using the RIM process must rely on the use of external mold release agents in order to facilitate part removal from the molds. These external mold release agents must be applied before each part is made, making this application step extremely time and labor intensive. The application of external mold release agents have shown to consume 25-33 percent of the RIM cycle. An alternative to the present mold release situation, is the development of internal mold release agents which would work in conjunction with external release agents. This synergism allows the molder to produce multiple parts before the external release agent must be reapplied.

0097-6156/85/0270-0213\$06.00/0

© 1985 American Chemical Society

This paper will discuss silicone internal mold release as a major contribution towards increased RIM productivity. The value of these internal release agents together with the necessary developmental parameters of such agents will be detailed. The paper also presents details of internal mold release agents developed by Dow Corning for polyurethane RIM. Field trial results including paint aging data will be presented. Finally, an update on more-recent commercial and experimental Dow Corning internal release agents, including two stream additives will be given. This paper should enable RIM processors to see how useful internal mold release agents can be in their polyurethane RIM process and the benefits they can realize by incorporating internal release agents into their systems.

Background Of The RIM Process

In 1974, the first commercial urethane part was molded by a newly developed process known as reaction injection molding or RIM. Today, RIM is a leading plastics process developed for high delivery and low rejection rates, thereby meeting current product design, production, and performance challenges. Reaction injection molding is defined as a plastics manufacturing process in which two reactive liquid chemicals are forced at high pressure to impingement mix in a small chamber and instantly dispense into a closed mold at relatively low molding pressure where part curing and solidification occurs. RIM gave the plastic manufacturer a new molding method with great tooling variety and process versatility. This has allowed RIM processing to maintain a healthy annual growth rate over the past several years (1).

Synonymous with RIM is the chief classification of elastomer that is currently being produced by reaction injection molding -- namely, polyurethane. This material, as molded using RIM techniques, has advantages of excellent flexural strength, low weight and good dimensional stability with excellent chemical resistance. The largest current use of RIM produced polyurethane is automotive front and rear fascia.

Major RIM Developments

The cycle in a reaction injection molding process can be described by these six operations: (1) press movement, (2) cylinder pressurization, (3) injection, (4) curing, (5) part removal and (6) external mold release application. Figure 1 represents the relative percentage of time that each of these operations consumes of the total RIM cycle. Data shown here were obtained during actual molding operations of a glycol-extended RIM system on an Admiral 9000 3HP machine equipped with an automotive fascia tool. This molding operation is typical of the cycle times seen with most current production RIM equipment.

An emphasis on "fast-cycling RIM" reduced cycle times from 340 seconds in 1974 to approximately 150 seconds by 1981 (1,2). This represented a 55 percent reduction in overall cycle time. Much of

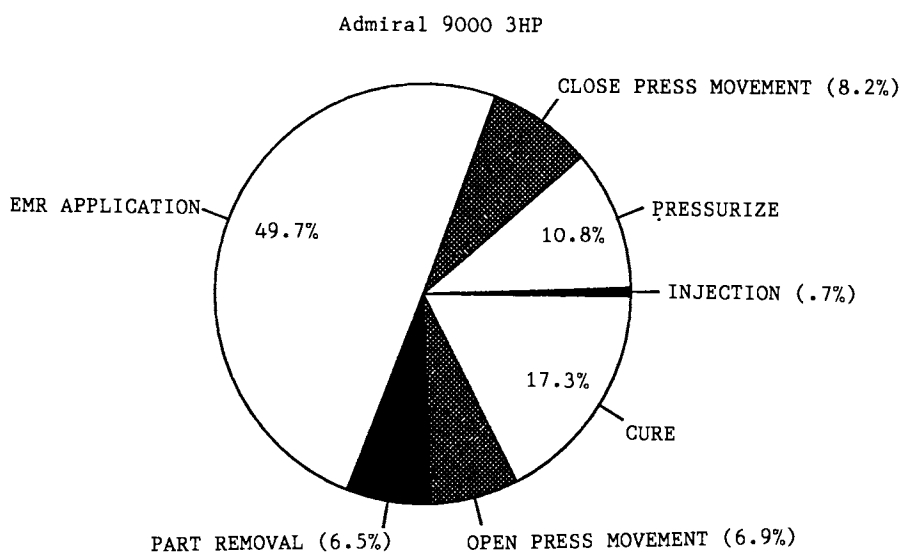


Figure 1. Typical RIM cycle.

the improvement in cycle time that has been seen during this time has developed from improvements in the injection and cure steps. Introduction of the fast cure amine extended systems (3) and today's faster reacting glycol systems have reduced polymerization cure time by an astounding 75%. These systems react and develop green strength faster, thus allowing for shorter cure time, expediting demolding. In addition, equipment modifications allow faster closing and opening of RIM clamps.

Need For Internal Mold Release

Efforts continue towards improvements and modifications for faster-curing chemistry and faster-moving equipment. In addition, much current interest is focused around improvements in the mold preparation operation in the RIM cycle. Presently, elastomeric polyurethane, molded using reaction injection molding techniques, must rely on the use of external mold release agents in order to facilitate part removal from the molds. These wax or fatty ester-soap based external mold release agents are typically applied before each part is made. This application step is extremely time and labor intensive. The application of external mold release agents can consume 25-50 percent of the RIM cycle depending on mold design and complexity of the molded part. An alternative to the present mold release situation is the development of internal mold release (IMR) agents which work in conjunction with external release agents. Such synergism allows the molder to produce multiple parts before the external release agent must be reapplied. In the industry this is frequently referred to as "multiple release from an external mold release basecoat." One mathematical model of the RIM process (2) suggest that the vast majority of the benefits of using IMR are realized by a system which allows a minimum of twenty parts to be molded before basecoat reapplication. However, future generations, including bare metal release, are being evaluated.

The use of IMR as an alternative to the reapplication of an external mold release agent has some significant economic advantages. With internal release, the cost of the external release agent will be reduced, as well as the time consumed during each cycle for application. Average improvements in cycle time of 38 percent have been observed (1,2,4). Reduced cycle times means less labor and utility cost per part. Productivity increases will also extend capacity limits on existing equipment. This may delay or eliminate the need for further capital expenditure at that point in the future when demand exceeds current production capacity. In addition, the use of IMR technology will reduce the number of parts that must be rejected due to poor surface quality. Since less external mold release per mold cycle would be applied with IMR incorporation, part cleaning cost and mold stripping times will be reduced. Finally, reduced spraying of external mold release may improve air quality. All these result in overall improved operating efficiency of a RIM molding plant. The economic benefits must be balanced with the additional cost of an IMR system. Too costly of a system would technically succeed but fail as a marketable system. Several economic studies have been done to indicate the economics of current systems to be favorable.

Requirements Of An Internal Release Agent

For internal mold release to be a viable processing alternative, it must fulfill a number of demanding requirements:

Release: Rather obviously, the IMR must provide release. The ability for an IMR agent to impart release to a given urethane system is a difficult property to quantify and compare. This requirement becomes dependent upon many processing and chemical factors, such as:

- 1) the urethane system's kinetics and reactivity;
- 2) the external basecoat;
- 3) the model configuration and complexity.

Therefore, it is important that a comparison of the release characteristics of IMR systems be performed on an equal basis with regard to factors which would affect release.

Paintability: Of equal importance in automotive applications is the need to mold parts which are paintable after normal cleaning. Following standard cleaning and painting procedures, a painted part should pass aging in Florida exposure without cracking, peeling, fading, or loss of paint adhesion.

Reactivity: Faster processing of urethane systems has been obtained by improvements in the development of green strength or cure rate, allowing quicker part removal from the mold (3). IMR additives should not significantly reduce reactivity. The effects that internal mold release agents might exhibit on the reactivity of a given RIM urethane system can be determined through measurement of the cream (gel) times of systems with and without the IMR.

Nucleation: Most elastomeric urethane systems are molded to a reduced density to lower cost, to allow complete mold filling which yields better surface quality, and to provide optimum physical properties. A microcellular structure is achieved by nucleating with a gas or incorporating a blowing agent. An internal release agent should not affect the cell structure or froth stability, as these could result in a change in physical properties.

Physical Property Retention: Another consideration with the use of internal mold release agents is that they should not adversely affect the performance of the finished part in its application. This can be tested for by comparing physical properties of parts molded with and without the internal release agent. No significant differences should be observed.

In the development of release agents for RIM molding, one or more of these requirements can appear to be in opposition with one another. Materials which might be excellent release additives become commercially ineffective because of a possible lack of paintability. Obviously, as the number of requirements increases, the number of fluids which meet all these requirements becomes limited.

Organic-Silicone Hybrid Technology

Current technology allows the synthesis of hybrid molecules that are part silicone and part organic. Materials can be designed that have the good release properties of a silicone combined with various types of organic reactivity. The ability to vary not only viscosity, but also the reactive group, and the number and position of reactive

groups (i.e., AB, ABA, rake structures) allows an infinite possibility of materials and adds a unique dimension of versatility. Examples of these structures are shown by the following formulas:

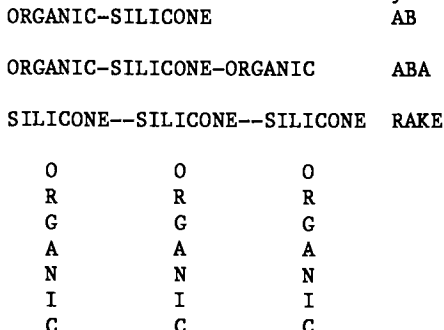


Figure 2 illustrates how the tailor-made silicones function as IMR agents in RIM molding. Due to the known surface tension reduction phenomenon of silicone fluids in urethanes and the differences in surface tension at the urethane/mold interface, internal mold release agents based upon silicone molecules can be developed to selectively migrate at different rates to the urethane/mold interface. There, it will orientate itself to build a protective layer which decreases the ability of the urethane to wet-out the mold surface. The inability of the urethane to wet-out the mold surface will facilitate release.

Although many fluids can be developed to act as IMR for RIM, many would fail as commercial products due to their inability to impart paintability to the resulting molded part. In order to rectify this paintability concern with the use of silicone internal mold release agents, a functional moiety is designed into the silicone. This functionality, when correctly specified, reacts into the urethane matrix once the IMR has migrated to the urethane/mold interface. This reactivity causes the IMR to be immobilized in the urethane matrix, thus allowing paintability.

Silicone organic hybrids play a critical role as surfactants in the formation of polyurethane foam (5). These surfactants are tailored to provide the balance of reactivity and compatibility required for proper foam stabilization. Similarly, silicone fluids designed for RIM release must also adequately stabilize the cell structure of the faster RIM-processed polyurethanes.

First Successful Silicone-Organic Hybrid IMR

Dow Corning has introduced DOW CORNING Q2-7119 Fluid (hereafter known as Q2-7119) as an IMR agent commercially available to the RIM industry. Field evaluations of Q2-7119 in amine and glycol extended systems demonstrated the ability of this functional silicone fluid to act as an internal release agent. Table I shows results of this material as an internal mold release agent in an amine extended system.

In both trials, the J-car fascia were molded using 1-2 parts of Q2-7119 per hundred parts of B-side resin in conjunction with an

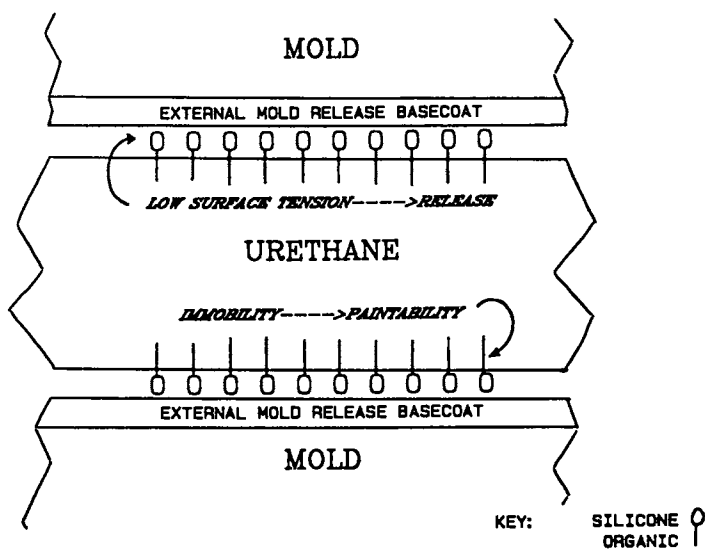


Figure 2. How silicone-organic hybrid fluids function as internal mold release agents.

external mold release agent. The trials were stopped after 20 pieces were molded without a reapplication of the external release. The release was still excellent at the time the trial was terminated. The control fascia (molded without Q2-7119 had to rely on respraying of the mold after each cycle. As noted in the table, the silicone IMR had no detrimental effects on the overall physical properties of the resulting RIM parts.

Table I. Dow Corning Q2-7119 Fluid in Three Stream Amine Extended Trials

Bayflex 110-35 System Admiral 3-stream Machine	Chemtrend XMR-136 J-car Rear Fascia			
	2.0 PHR Q2-7119			
Unfilled	5% 1/16 Inch Milled Fiberglass			
	Control	With IMR	Control	With IMR
Additional T-12 (PHR)	0	0.45	0	0.50
Parts Released	1	20+	1	20+
Physical Properties:				
Density (G/CC)	0.99	1.00	1.04	1.01
Flex Modulus (PSI)	39,000	38,900	52,400	50,300
Tensile (PSI)	3,600	3,000	2,400	2,500
6" Heat Sag, (inch)	1.20	0.89	0.48	0.40
Elongation (%)	350	240	190	200
Two Year Florida Exposure	Excellent	Excellent	Not Run	Not Run

Table II, depicting trial results of Q2-7119 as an IMR in a glycol system, shows similar success with release and physical property retention to what was shown with the amine system. Eighteen consecutive cycles were obtained with the IMR before the trial was stopped.

In order to check the paintability of parts molded with Q2-7119, test panels molded with and without silicone fluid were post-cured, solvent wiped with toluene, primed with PPG Durethane 600 Primer and then top coated with Durethane 300 blue metallic flake or white. Painted samples were exposed for 2 years in Florida Direct Black Box 5° South and then evaluated for appearance and adhesion. Results of these tests showed no difference between control and IMR-containing panels. Paint adhesion was excellent.

In all the trials discussed thus far, the typical RIM process was modified to necessitate the successful use of Q2-7119. Currently, the majority of the urethane molded by the RIM process is by a two stream approach in which the isocyanate and resin sides are introduced into the mixhead as separate streams. This requires that the IMR agents be masterbatched into either or both streams.

Q2-7119 is reactive towards the isocyanate side and the catalysts that are typically used in RIM systems. If placed on either side, some gellation can occur which will result in plugged filters or molded parts which paint poorly due to the exposed gels. In addition, due to the interaction of the IMR with the catalyst, cure times are lengthened and green strength is reduced. An approach which allows for the successful use of this silicone-organic fluid is known as the three stream approach, in which three streams impingement mix at the mixhead. The third stream contains the IMR, which has been diluted with uncatalyzed polyol to aid in ratio control. Additional amounts of catalyst may be necessary in the resin components to compensate for any possible green strength reduction brought about by the reactive silicone internal mold release.

Table II. Dow Corning Q2-7119 Fluid in Three Stream Glycol Extended Trials

RIM 121 System Admiral 3-stream Machine		Chemtrend XMR-136 Bathtub Type Mold	
2.0 PHR Q2-7119			
	Control	With IMR	
Additional T-12 (PHR)	0	0.2	
Dabco 33 LV (PHR)	0	0.2	
Parts Released	1	18	
Physical Properties:			
Density (G/CC)	1.00	1.04	
Flex Modulus (PSI)	101,650	110,200	
Tensile (PSI)	4,300	4,200	
4" Heat Sag (inch)	0.08	0.08	
Elongation (%)	135	123	

Advances In Silicone-Organic Hybrid IMR Agents

Although Q2-7119 is considered a three stream IMR agent for RIM, several two-stream approaches have been identified and are currently being pursued. Several highly reactive RIM urethane systems are being currently introduced to RIM molders. These systems are inherently fast reacting, and do not require tin catalyst. Q2-7119 has been showed to provide excellent internal release capability to those systems as a two-stream release agent. One such system is being introduced by Texaco Chemical Company. The silicone fluid is blended into the resin side of the system and does not adversely react due to the absence of tin compounds. Multiple release with good paintability and processing has been observed with this two-stream approach. Table III shows the excellent release results and retention of physical properties with this Texaco system. Other unique systems which are not tin catalyzed can utilize Q2-7119 as an IMR agent.

Table III. Dow Corning Q2-7119 Fluid in Two Stream Texaco Jeffamine System

	Control	With IMR
IMR Concentration (% Part)	0	1.0
Parts Released	20	120+
Physical Properties:		
Density (G/CC)	1.00	1.00
Flex Modulus (PSI)	32,000	35,000
Tensile (PSI)	3,400	3,500
6" Heat Sag (inch)	0.60	0.40
Elongation (%)	240	230
Tear (PLI)	410	370

Estimates (4) show that only 18% of the present RIM machines have multiple-stream capability. Although success has been demonstrated with the three-stream IMR approach, the auto industry expressed a desire to obtain a two-stream release agent. This two-stream approach would allow the RIM molder to gain release by a simple addition of the IMR agent into the A or B side. A fluid had to be found which would have the proper balance of incompatibility and reactivity in order to obtain the desired release and paintability, yet not impair the urethane cure. Several experimental fluids which have shown promise for release, paintability, processability and physical property retention as two stream candidates have been developed.

Table IV shows results from an experimental trial using a Dow Corning experimental IMR agent in an amine extended system. As seen, unlike the three stream trials previously discussed, no additional catalyst needed to be used to produce good RIM parts. The internal release was added directly to the resin side. Forty releases were obtained before the trial was stopped. Release was still good at the time the trial was terminated. Also of note is the excellent retention of physical properties. In addition, initial results with new experimental silicone IMR fluids showed paint adhesion and retention to be good. Table V similarly illustrates results of an experimental two stream fluid in a glycol-extended RIM system. Again, excellent release and physical property retention were observed. With similar levels of this experimental fluid, twenty-five releases have been obtained.

Summary

IMR will be a wide spread reality in the very near future of the RIM industry, due primarily to the reduction in cycle time and resulting increase in productivity that are apparent through the use of internal mold release agents. Although the requirements are rigorous, versatile silicone/organic hybrid products can satisfy all the requirements in many systems. Research efforts are well on the way towards successfully commercializing silicone internal mold release agents for urethane reaction injection molding.

Table IV. Dow Corning Experimental Fluids in Two Stream Amine Extended Trials

Dow Amine System Admiral 9000 3HP	Chemtrend XMR-136 '80 Mustang Front Fascia	
	Control	With IMR
IMR Concentration (% Part)	0	3.1
Parts Released	2	40+
Physical Properties:		
Density (G/CC)	0.99	1.02
Flex Modulus (PSI)	36,000	34,000
Tensile (PSI)	3,900	3,700
4" Heat Sag. (inch)	0.3	0.2
Elongation (%)	310	320

Table V. Dow Corning Experimental Fluids in Two Stream Glycol Extended Trials

Union Carbide Glycol System Admiral 9000 3HP	Chemtrend XMR-136 '80 Mustang Front Fascia	
	Control	With IMR
IMR Concentration (% Part)	0	4.0
Parts Released	4	25+
Physical Properties:		
Density (G/CC)	0.90	0.95
Flex Modulus (PSI)	39,000	31,500
Tensile (PSI)	3,500	3,100
4" Heat Sag (inch)	0.60	0.40
Elongation (%)	150	190

Literature Cited

1. Von Hassell, A. "RIM Machinery and Materials Evolve Towards Higher Productivity," Plastics Technology, November, 1981, pg. 69.
2. Cekoric M.E., Taylor R.P. and Barrickman C.E., "Internal Mold Release The Next Step Forward in RIM Productivity," Paper 830488, SAE Automotive Engineering Congress and Exposition, Detroit, MI, February 28 - March 4, 1983.

3. Ludwico W.A. and Taylor R.P., "The Bayflex 110 Series - The New Generation of RIM Materials," Paper 770836, SAE Automotive Engineering Congress and Exposition, Detroit, MI, September 26-29, 1977.
4. Von Hassel A., "RIM Materials Take Quantum Leap Forward," Plastic Technology, March, 1983, pg 37.
5. Kendrick T.C., Kingston B.M., Lloyd N.C., and Owen M.J., "Surface Chemistry of Polyurethane Foam Formulation, Part I", Journal of Colloid and Interface Science, Volume 24, pg. 135, 1967.

RECEIVED April 16, 1984

Fiberglass Reinforcements in RIM Urethanes

MIKHAIL M. GIRGIS

PPG Industries, Inc., Fiber Glass Research Center, Pittsburgh, PA 15230-2844

Applications for high modulus Reaction Injection Molding Urethane parts require the addition of short glass fibers to increase stiffness and dimensional stability and to reduce heat sag during painting cycle. Fiber glass reinforcements can, however, reduce the impact resistance of these materials and introduce anisotropy in their composites. The effects of fiber glass reinforcements on RRIM urethane panel properties were investigated and compared. The fiber glass reinforcements evaluated include: milled fiber glass 1/16 in., integral chopped fiber glass strands 1/8 in., and a hybrid of milled fiber glass and chopped strand. Six major panel properties were examined for: surface quality, flex modulus, Izod impact strength, tensile strength, heat sag, and tensile elongation. Results indicate that integral chopped strand have limitations in surface quality, tensile strength, and tensile elongation, and have significant advantages over milled fiber glass in impact strength and in thermal stability (less heat sag and less anisotropy).

The current strong interest in RRIM is due mainly to the U.S. automobile industry's efforts to reduce auto weight. The involvement of such a huge volume industry geared to high-speed production has dominated the thinking of all facets of RRIM technology. It has led to a search for very fast polymerization systems and the upgrading of manufacturing technology and processing machinery. Attention has been focused, at the present time, on RRIM urethanes using fiber glass as the main reinforcing element. However, it is clear that there is great potential for the wider application of RRIM in the nonautomotive market, such as in the production of furniture, appliance housings, building cladding panels, sporting goods, and others.

A schematic diagram of the RIM process is shown in Figure 1.

0097-6156/85/0270-0225\$06.00/0
© 1985 American Chemical Society

The basic principle of RIM is simple. Two liquid reactants or prepolymers are mixed rapidly by high-speed impingement. The mixture then passes into a closed mold where a major part of the polymerization process occurs to produce a finished solid part in a single step.

One of the main features of the RRIM process is the low energy requirement which results from the relatively small energy needed in pumping low viscosity reactants. A recent estimate indicates that the energy used in a RRIM part is considerably lower than that of a typical metal or thermoplastic part as shown in Figure 2.

The U.S. automotive industry developed a soft front end fascia using a RIM urethane elastomer which provides the low speed impact resistance required by law. In addition, American car manufacturers continue to face legislative mandates on fleet average fuel economy which may require further reduction in the average car weight. This implies lighterweight materials such as synthetic organic polymers which have relatively low density. Therefore, attention has been focused on weight savings by replacement of external body parts (which are nonload-bearing components), such as hood and deck lids, doors, fenders, quarter panels, and roof sections.

The soft, elastomeric urethane cannot, however, be used for large auto body parts because of its low rigidity and high thermal expansion. Changes in resin chemistry (polyol) can provide flexural moduli of over 4×10^5 psi and possibly acceptable impact properties. However, no modification in resin formulation appears capable of bridging the order of magnitude difference in thermal expansion between the urethane part and the steel framework to which it is attached. Similar part distortion, due to creep and low modulus at high temperature (325°F), is observed after 30 minutes' residence time in the paint bake oven. Reinforcement with temperature insensitive and high modulus material such as glass fibers is therefore considered essential in auto body and other large, rigid part applications.

Milled glass fibers and/or glass flakes are currently the preferred RIM reinforcement due to their compatibility with appropriate RIM machines (which are equipped with displacement metering cylinders, wear-hardened critical parts, and relatively straight material flow lines), and to their lesser degradation of impact properties relative to other inorganic fillers and surface appearance. Milled glass fibers are glass filaments processed through a hammermill with discharge screens of a specific opening size. The screen opening size determines the length and/or the type of milled glass. The 1.6 mm (1/16") milled glass fiber is the most popular reinforcing material in RRIM today. Milled fibers have a much shorter fragment length. The upper size limit is defined roughly by the screen size used in the mill.

Glass flakes consist of very thin, essentially rectangular-shaped flakes made by shattering a thin glass bubble and passing the pieces through a sieve 1/64". Although passed through a smaller sieve than milled glass fiber, the flaked glass gives at least equivalent (1) reinforcement, because essentially all of the flakes have an aspect ratio greater than one.

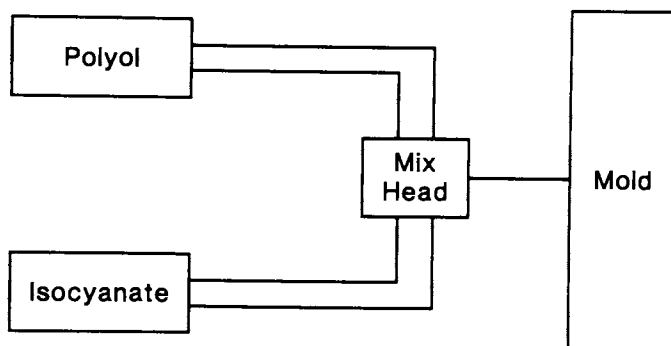


Figure 1. RIM urethane process.

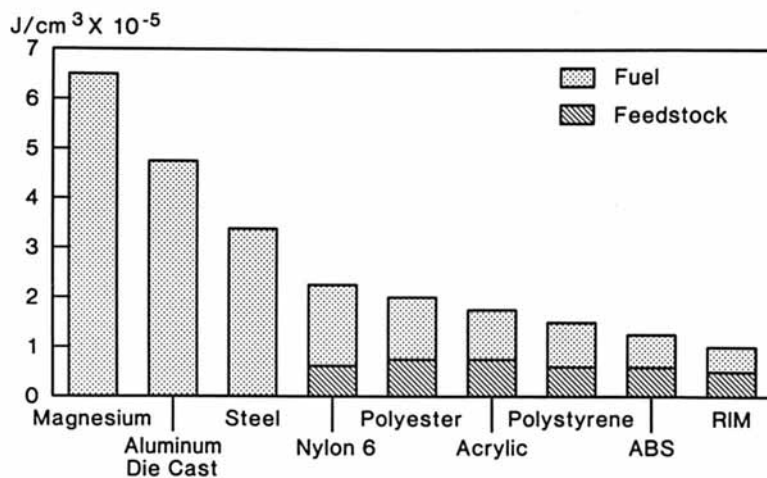


Figure 2. Energy requirements to produce and form various materials.

Reinforced RIM urethane using milled glass fibers (1/16") at 25% loading or more is now the "state of the art" reinforcement. In a "high" modulus urethane resin (100 to 150 x 10³ psi), such milled fiber loadings produce composites with a modulus of 300 x 10³ psi, an elongation of 20%, an Izod impact of 5.0 ft-lb/in., a sag at 325°F for 30 minutes of 0.2" for a 4" specimen, and a thermal expansion coefficient of 20 x 10⁻⁶/°F, with all properties measured along the flow direction. It has been found that there is a considerable degree of fiber orientation along flow lines leading to roughly a 2:1 enhancement of properties along the flow direction (2).

In order to obtain maximum reinforcement and impact strength, it is necessary to use fibers with a length of at least 0.02" (the calculated critical length for reinforcing a high modulus RIM system). ICI and Pilkington Glass Ltd. have developed 1.5 mm (1/16") chopped fibers (3) coated with a coating agent which dissolves in urethane polyols, thus allowing fiber bundles to disperse into individual filaments. This results in high levels of reinforcement. However, it also results in preferential flow orientation of the reinforcement during molding, resulting in anisotropic properties in composites. One of the results of this anisotropy is warpage of RRIM parts when cooling. The anisotropy and the resultant warpage are greatly reduced (1) by the use of plate-like reinforcements such as flaked glass or mica.

A disadvantage of flaked glass is the significant reduction of the impact resistance of the composite. Milled glass fibers at 22% by weight loading normally reduce the Izod impact strength of the original urethane matrix by 50%, but use of flaked glass at the same level of loading lowers the Izod value by 90%.

The use of chopped strand bundles as the reinforcing elements in a RIM urethane system has not been fully explored. Some work was done using integral strands chopped to 3 mm lengths coated with a coating which was not resistant to dissolution by warm polyols (2). This produces panels with varying degrees of filamentization and varying levels of physical properties. Therefore, in order to evaluate the integral chopped strands concept as RIM urethane reinforcement, a proprietary coating system which does not dissolve in the polyol at 120°F was developed. Coating, drying, curing, and chopping processes were done directly in one step as illustrated in Figure 3.

This paper reports the effects of loading level of integral chopped strands mixture of milled fibers and integral chopped strands on physical properties and surface quality of reinforced RIM urethane composites.

Experimental

The VR-75 RRIM machine made by Accuratio Systems, Inc. (ASI) was used in this study, and a chromium polished steel mold (220 x 293 x 3 mm) with an aftermixer section was also used. It was equipped with cores for hot water circulation and was controlled at 60°C-70°C. The clamping force was supplied by a simple air bag press. The resin used consisted of a polyurea dispersion in a blend of

polymeric and short chain diols ("B" side), with a specific gravity of 1.02 at 30°C and a viscosity of 800 MPAs (cp). An MDI 4,4-diisocyanato biphenyl methylene type isocyanate having a specific gravity of 1.20 at 30°C and a viscosity of 350 MPAs was used for the "A" side at a volumetric ratio B:A of 2:1 for the unfilled system. The liquids were kept between 35°C-50°C depending on the fiber glass loading. A simplified piping diagram of the VR-75 machine is shown in Figure 4.

The fiber glass used consisted of a high integrity strand chopped to 3 mm lengths. The glass coating had been designed to provide excellent resistance to mechanical shearing to produce excellent finely integral chopped strands.

The evaluation of panel physicals was carried out as follows: The fiber glass reinforcement was preblended into the B-component (polyol side) on a high shear mixer and the slurry was charged to the machine. The panels were postcured for one hour at 250°F and conditioned in the Instron Lab for at least 12 hours before testing. Tests were performed according to ASTM standards (4). Specimens for each test were cut both parallel and perpendicular to the direction of the flow in the mold; five specimens per direction were cut from each of two panels (a template was used to ensure good run-to-run comparison).

Results and Discussion

Surface Quality. Class "A" surface (after painting) is considered by the automotive industry as their first requirement for an exterior part. Comparing the surface quality of several reinforcements in RRIM urethane panels, it was found by visual examination that the best surface quality was the glass flakes and the worst was the integral chopped strands. Milled fiber is slightly worse than glass flakes, but it is still considered a "Class A" surface.

Two techniques have been reported in the literature to judge surface quality: surface gloss and surface roughness. Several attempts were made to improve the surface quality of integral chopped strands, such as nucleating agents and decreasing composite density by mixing dry air in the polyol slurry, but without success.

It was noticed from the limited number of molded panels that the following factors have significant effects on surface quality: (1) amount of glass loading in the panel and (2) length of the integral chopped strand. Surface quality decreased by increasing the percent loading and strand length of the integral chopped strand. More work needs to be done in this area.

Flexural Modulus. Figure 5 shows flex modulus values at 23 °C measured parallel and perpendicular to flow. The nonreinforced urethane polymer has a value of about 50,000 psi. Columns B and C show the results obtained with 8.5% and 20% loadings of milled glass fibers, respectively. Column D shows results obtained with 3.5% loadings of 1/8" chopped integral strands. The flex modulus increased by about 20%. Column E shows data for 13.4% integral chopped strands; the increase was more than 240% of the original

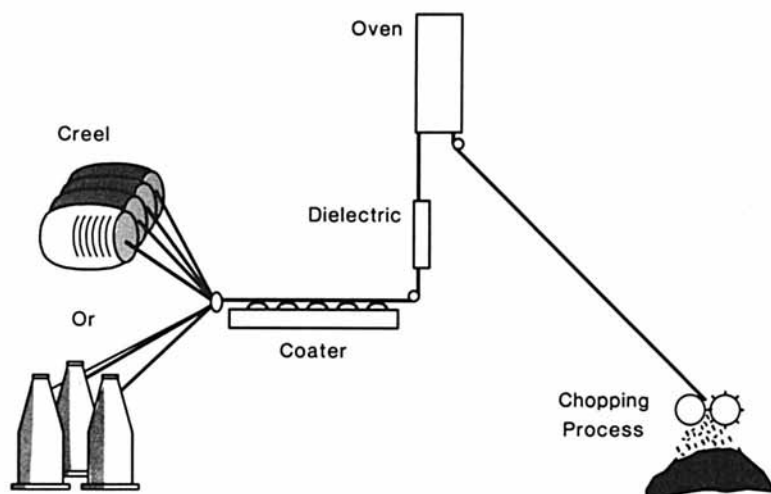


Figure 3. Schematic of integral chopped strands coating and direct chopping process.

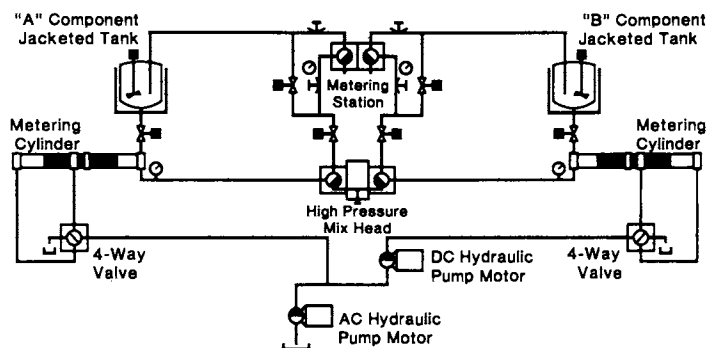


Figure 4. Simplified piping diagram of the VR-75 RRIM machine.

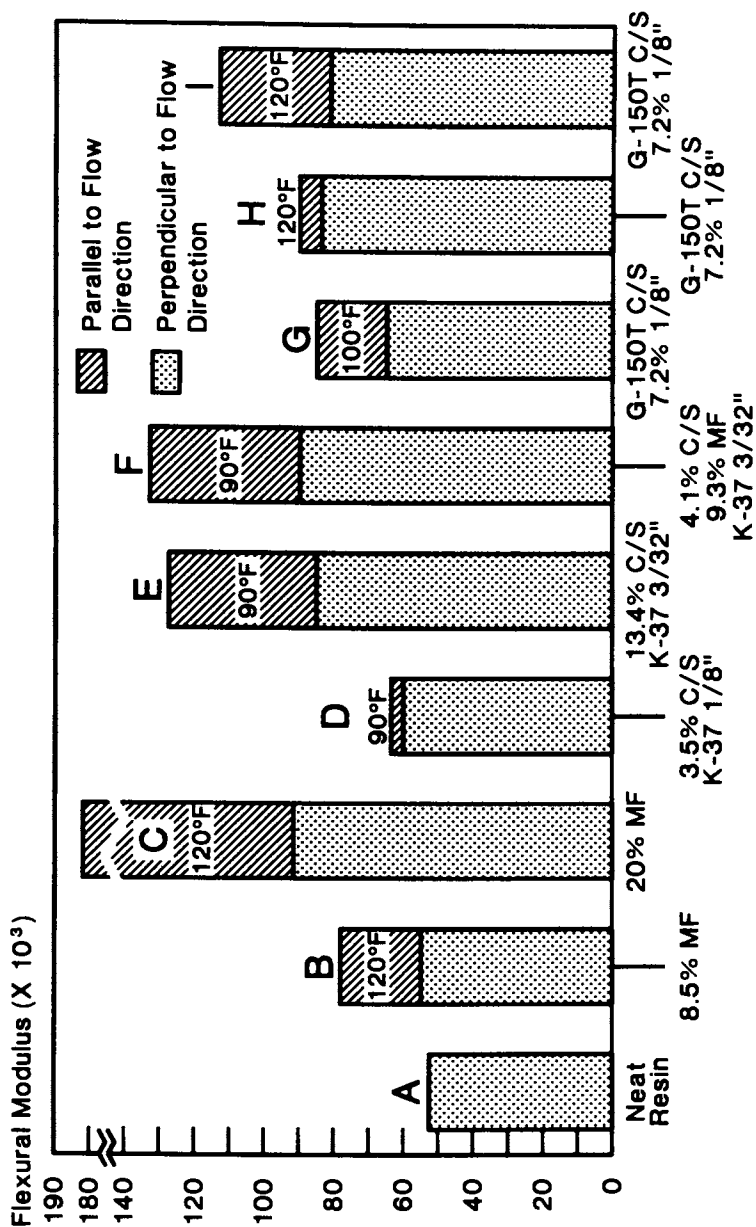


Figure 5. Flexural modulus.

value. Column F is for the 1:2 chopped integral strands:milled glass fiber combination at 13.4% overall. An average value of 133,000 psi is obtained vs. a value of about 182,000 psi for 20% milled fiber. Columns G, H, and I are for the same reinforcement (7.2% of chopped strand and 1/8" long) run at two different processing temperatures (100°F vs. 120°F) and on two different RRIM machines. These data show that by increasing the process temperature of the polyol from 100°F to 120°F, the viscosity of the system decreases and strand orientation (orientation index) also decreases. If the level of chopped strand increases to about 10% or higher, the flex modulus value may reach the target value of about 150,000 psi.

The flex modulus values of Figure 5 give an excellent illustration of the level of orientation obtained from various reinforcements. Milled glass fiber (20% loading) gives an "orientation index" (parallel/perpendicular) of about 2.0. A mixture of chopped strands and milled fiber (Column F) has an index of about 1.5, which is substantially lower than that of milled fiber only. Chopped integral strands give an orientation index in the range of 1.1 to 1.5 depending on the nature of chopped strand (its aspect ratio) and the level of chopped strand loadings; the higher the loading the higher the index.

Impact Strength. Figure 6, notched Izod impact strength, shows one of the main reasons for the interest in chopped integral strands (c/s) as RRIM urethane reinforcement. The nonreinforced urethane polymer used in this study had an impact value of approximately 12 ft-lb/in. Reinforcement with 20% milled glass fibers lowers this value to about 5 ft-lb/in. (Column B).

The best impact values are obtained with the integral chopped strands, apparently because of a combination of factors. These composites contain only 13.4% reinforcements vs. 20% for milled fiber, therefore it retains more of the impact resistance of the nonreinforced urethane polymer. Another contributing factor to the improved impact resistance of the integral chopped strand-containing composite may be the nature of the interface between the treated glass bundles and the urethane polymer (glass/coating/urethane). Also milled fibers dispersed easier in the system than chopped strand, and the probability of fiber attrition and the earlier failure of milled fibers during impact is higher than that of chopped strands. Fiber or strand length, also, plays a role in impact strength; Composite D contains a 1:2 blend of chopped strand and milled fiber and has higher impact strength (25%) than that of milled fibers only.

It must be noted that there is almost no orientation effect on the notched Izod impact values of these composites. The differences between the parallel and perpendicular directions are within the experimental error of the test.

Tensile Strength. Tensile strength data (Figure 7) indicate that the highest value was obtained with milled glass fiber (20% loading) and the relatively low value obtained with chopped integral strands. This may be related to the aspect ratio of dispersed milled fiber in the composite compared to chopped

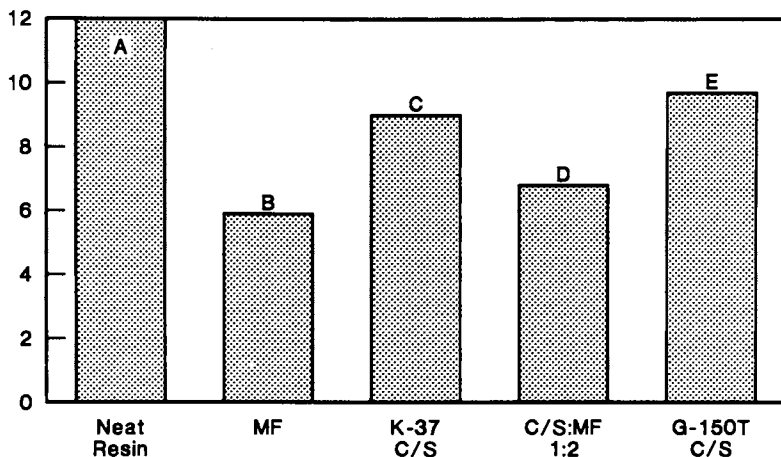
Impact Strength,
Foot-Pounds/Inch

Figure 6. Notched Izod impact strength.

Tensile Strength, PSI

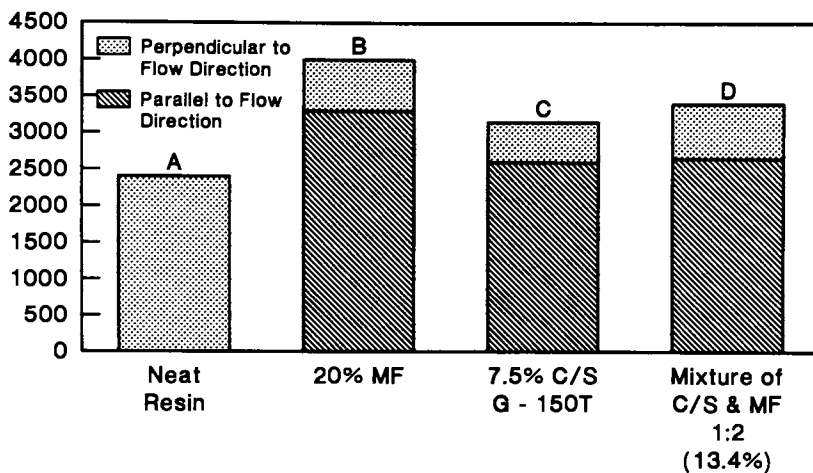


Figure 7. Tensile strength.

strand. Milled fiber is about 10-20, but chopped strand is about 8-12. However, both are significantly higher than that of nonreinforced urethane polymer. The integral chopped strand and milled fiber combination (1:2 ratio) improved tensile strength over that of chopped strand alone, but it also decreased its value from that of milled fiber. Apparently, when chopped strand is used, there is less glass overall which may explain the drop in tensile values between Columns C and B or Columns D and B. However, this cannot be the complete story because the chopped strand has relatively longer fibers than milled fiber (1/8" vs. 1/16" or less). Another important factor is the nature of the interface between the soft elastomeric coating on the fiber glass bundles and the stiff urethane polymer in the composite. This area needs to be studied further to shed some light on the effects of coating chemistry, strand length, and glass loading on the tensile strength of the urethane composite.

Heat Sag. The heat sag test was run according to ASTM Method No. D-3769-79. The results of this test (Figure 8) show that chopped integral strands at 7.5% loading give essentially the same heat sag values parallel to flow direction and substantially lower values (approximately 40%) than milled fiber in the perpendicular direction. The mixture of milled fiber and chopped integral strands (Column D) gives lower values in both directions than those of the milled fiber only or the chopped strands alone; it seems that this hybrid has unique characteristics which should be further investigated.

Tensile Elongation at Break. The effects of the type of reinforcements on tensile elongation values (Figure 9) are similar to those for tensile strength. It is interesting to compare the tensile elongation results (Composites B, C, and D in Table V) with the notched Izod values of the same composites (B, C, and D) in Figure 6. By comparing milled fiber composites (Column B) and hybrid (milled fiber/chopped strand) composites (Column D), it is clear that the hybrid composite has higher impact value but lower tensile elongation than milled fiber composites. Also, if chopped integral strands and milled fiber composites are compared, similar results are obtained. These discrepancies from the known fact that elongation at break correlates with and predicts the impact strength suggest that other factors, such as strand dimension, aspect ratio, and adhesion level to the urethane matrix, play a role in determining the Izod impact resistance of the composite.

Conclusions

1. Urethane RIM panels reinforced with chopped integral strands have better impact strength, less heat sag, and less anisotropy than those reinforced with milled fiber, at the same loading level or higher.
2. Tensile strength, elongation, and impact properties of chopped strand RRIM urethane panels increased with increased integral strand aspect ratios; flex modulus was not affected.

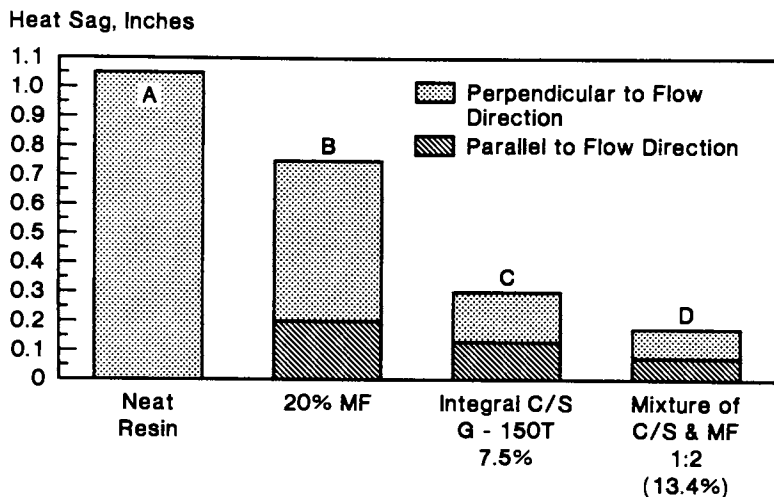


Figure 8. Heat sag.

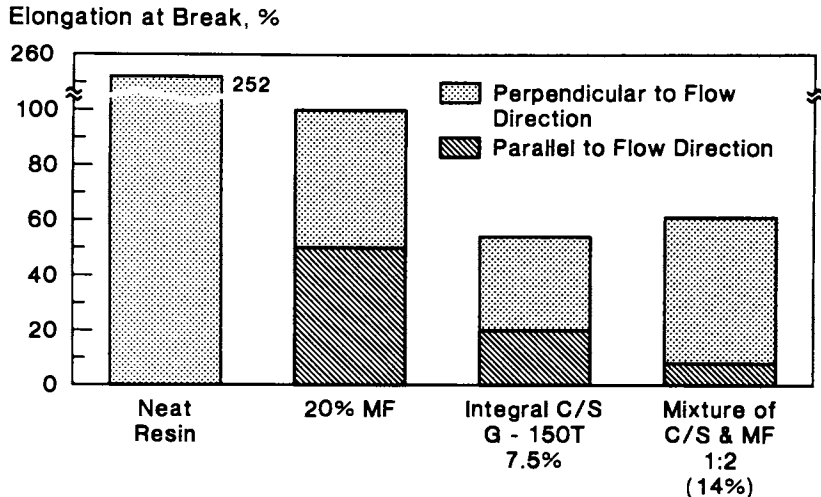


Figure 9. Tensile elongation.

3. Anisotropy increased with increasing integral chopped strand content for tensile strength and flex modulus of RRIM urethane panels. Higher glass content results in higher viscosity which causes well-defined flow and hence well-defined orientation.
4. Elongation and Izod impact strength decreased with increasing chopped strand content, but flex modulus increased; this finding follows the "rule of mixture" of composites.
5. Hybrid reinforcement of integral chopped strand and milled fiber improved flex properties but hurt impact strength and heat sag. This could be due to the amount of milled fiber in the mixture. The hybrid contained about 70% by weight of milled fiber. The overriding properties were that of milled fiber composites.
6. Surface quality of panels reinforced with integral chopped strands are inferior to that reinforced with milled fiber. Nucleating agents slightly improved the surface quality of the chopped strand panels, but a Class A surface could not be achieved with the use of chemical nucleating agents. An in-line, automatic nucleating process using dry nitrogen gas may improve the surface quality of chopped strand reinforced automotive parts.

Acknowledgment

I would like to express my appreciation to John Maaghul, Director, Fiber Glass Research Center, PPG Industries, Inc., for his permission to publish this paper.

Literature Cited

1. Ferrarini, J.; Cohen, S. "Reinforcing Fillers in Polyurethane RIM"; Proc. Annual Conference of the Reinforced Plastics/Composites Institute, 1982, p. 37.
2. Girgis, M. M.; Harvey, J. A.; B. Das. "Fiber Glass Reinforced RIM Urethanes: Chopped Strands vs. Milled Fibers"; Proc. Annual Conference Reinforced Plastics/Composites Institute, 1981, p. 36.
3. Chisnall, B. C.; Thorpe, D. "RRIM-A Novel Approach Using Chopped Fiberglass." Proc. Annual Conference Reinforced Plastics/Composites Institute, 1980, p. 35.
4. "Standard Test Method for High-Temperature Sag of Microcellular Urethanes," (ANSI/ASTM D 3769-79), Annual Book of ASTM Standards. American Society for Testing and Materials: Philadelphia, 1979.

RECEIVED April 30, 1984

Mold Filling with Polyurethane

H. MÜLLER, W. MROTZEK, and G. MENGES

Institut für Kunststoffverarbeitung, RWTH Aachen, Ponstrasse 49, D-5100 Aachen, Federal Republic of Germany

Even today, the production of polyurethane by the impingement mixing principle still involves high reject rates and/or high finishing costs. This is due mainly to the complexity of the process, which people often failed to recognize in the past. The process must therefore be seen as a linking together of a number of individual processes of varying complexity. Each of these separate processes - particularly achieving an adequate mixing quality and filling the mix into the mold - must be optimized if a good-quality molding is to be ensured. There has, however, always been a large amount of uncertainty with regard to the latter operation, filling the mold, as there was no way of describing the processes taking place inside the mold. The consequences were - and still are today - defects in the molding due to the entrapment of air bubbles. In order to examine this subject more closely, the relevant parts of the mold (flow restrictor, gate, mold cavity) were made of transparent plastic (PMMA) so that the injection process and the flow conditions could be observed and recorded with a video camera. With the aid of these tests, it was then possible to evaluate the influence of some flow-restricting and gating systems commonly used in practice with regard to air entrapment. In addition to this, there is a simple method - the filling pattern method - with which the mold designer can, as early as the development stage, obtain a visual idea of the mold-filling process. This method enables major errors in mold design to be eliminated at a relatively early stage.

In industry, polyurethanes are frequently referred to as "tailor-made plastics". Despite this very promising description, the proportion of polyurethanes in the total plastics consumption is at present well below 10 %. If we also consider that the majority of this is made into foam slabs for processing in the upholstered furniture

0097-6156/85/0270-0237\$06.25/0
© 1985 American Chemical Society

industry and in the insulating sector, it becomes apparent that there is a considerable amount of reticence towards this material. Really, far greater use ought to be made of polyurethanes for the manufacture of high-quality technical mouldings since they have favourable properties and allow considerable scope in production. One of the major reasons why this is not the case is, without doubt, the highly complex processing technique which, even today, is not always fully understood in practice.

This processing technique, which is characterized by the exceedingly fast formation - often in the space of seconds - of the actual "polyurethane" material in the mould, must be viewed as a series of individual processes that take place one after the other or parallel with one another. For the manufacture of perfect mouldings, it is essential to ensure that each one of these separate processes is performed entirely free of faults. This applies not only to a constant metering and homogeneous mixing of the components needed for producing the material, but also in particular to the subsequent processes of feeding the final mix into the mould and ensuring that the expanding material properly fills out the mould cavities.

It is precisely with these two steps, which have a major influence on the quality of the subsequent moulding, that a large number of problems arise, since any errors made during these parts of the process can no longer be corrected in view of the enormous speed of the chemical reaction.

Filling the mix into the mould

In impingement injection mixing, the two or more components needed for producing the material are injected at high energy into a relatively small mixing chamber. The idea is that, through impingement of the jets of liquid and the complex flow conditions that subsequently form (swirling), a homogeneous mix is produced within extremely short periods of time. The material then flows at very high speed (≥ 2 m/s) out of the mixing head and, with direct feed into a mould cavity, would result in serious defects in the final moulding, such as entrapped air and flow lines. It is therefore necessary to provide an element between the mixing head and the mould cavity in which the flow of mix is slowed down so that it can subsequently flow homogeneously into the mould without taking up any air. From this objective, we can derive a variety of demands made on the design of the gate of a polyurethane mould with regard to the flow behaviour. The most important of these is that inconstant or large changes in cross-section should be avoided and that the mix should flow through the gate into the mould at as low a speed as possible and in a laminar manner.

However, adhering to these criteria, which are very necessary from the point of view of flow behaviour, tends to conflict with a number of solid economic arguments, so that they are often almost incompatible. Of these, we are thinking above all of the necessary low production costs, which permit only a gating geometry that is simple to design or simple to manufacture, a small volume to avoid excessively high material losses and good deformability. The compromise between the gate form necessary from the point of view of flow behaviour and desirable from economic aspects is thus also reflected in the gate concepts most commonly being used at present: the direct gate and the film gate /1 - 3/.

Direct gating

With the direct gate (Figure 1), the flow of mix does not have to pass through any changes in direction or cross-section on its way to the mould cavity and, because the material is expelled from the gating zone by means of a cleaning piston, also works completely free of loss. From an economical point of view, this gate variation has to be regarded as the most ideal solution, but more widespread usage is excluded as it has certain serious disadvantages as regards the flow behaviour. Application of this gate design requires the generation of a purely radial flow in the mould cavity - something which it is only possible to even closely achieve in the case of thin-section mouldings (Figure 2). At wall thicknesses of more than approx. 6 mm, on the other hand, there is a risk that the flow front on the wall opposite the gating point will break up and lead to turbulence and, in critical cases, to the entrapment of air (Figure 3) /3/. Although the formation of a perfect radial flow is made easier by the use of higher-viscosity systems due to the much higher viscosity forces, the problem is that the systems being used in recent years are having shorter and shorter cream times, which means that higher metering rates are also being called for. Consequently, any possible advantage brought about by a higher viscosity becomes lost again. In addition to this, the use of a direct gate means that a number of other points also have to be observed, without which perfect moulding production is not possible either. In particular, attention has to be paid to using a mixing head that works absolutely free of prefeed and overrun and conveys the mix into the mould cavity completely free of turbulence. And yet it is above all these problems of prefeed and overrun which have still not been very satisfactorily solved today, continually resulting in moulding defects under production conditions.

$$\frac{\pi d^2}{4} \geq \pi d s \Rightarrow s \leq \frac{d}{4}$$

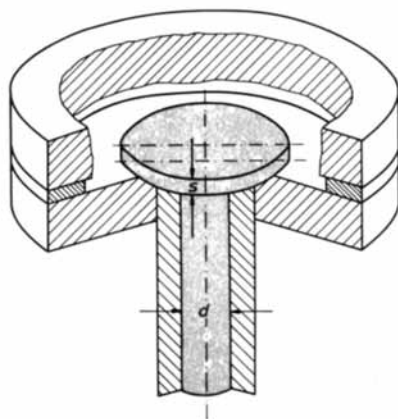


Figure 1. Direct-gate.

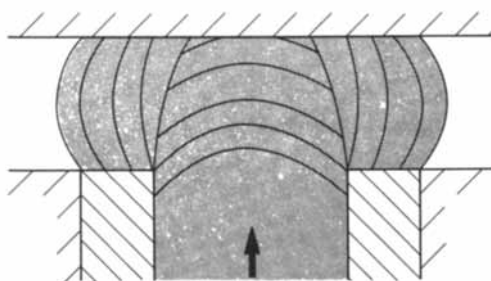


Figure 2. Direct-gate (source-flow).

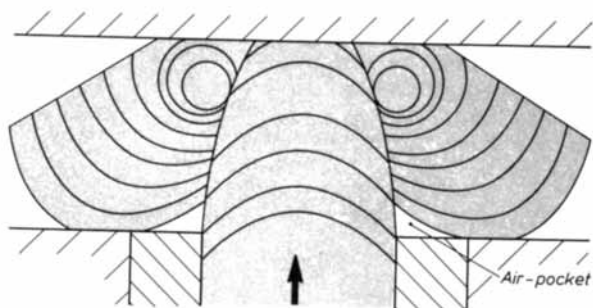


Figure 3. Direct-gate with vortex-formation and disturbed flow-front.

Film gating

Because of these problems with direct gating, much more frequent use is made in practice of the so-called "film gate". This second gating concept can be divided according to the design into the "fan gate" and the "sprue gate" (Figure 4 - 5).

A fan gate converts the circular flow channel at the outlet to the mixing head into a rectangle with a high length to thickness ratio (Figure 4) while maintaining a constant cross-section, with the result that the flow of mix leaves the gate as a kind of film with a maximum thickness of 2 mm. Because the free flow cross-section remains constant, the fan gate does not cause any change in the mean flow rate and thus has a purely distributing function. The requirement that none of the flow should become separated in the gating zone and the requirement that the material loss through the gate should be as small as possible combine, however, to restrict the possibility of a very broad distribution of the flow of mix in the mould. This is because, in order to prevent turbulence and parts of the flow breaking away, an opening angle of approx. 20° must not be exceeded for an enlargement of the cross-section, which means that, with a wide gating surface, a correspondingly long and uneconomical design would have to be selected. On the other hand, a narrow gate and a wide mould involve the risk of entrapped air or that the mix will contain air when entering the mould, from which the air bubbles can no longer escape and consequently lead to defects in the moulding (Figure 6) /4/. If it is not possible for economic reasons to put the gate across a whole or almost whole side of a moulding (long design), then this gate design must be regarded as highly problematical and should be avoided wherever possible.

Improved fan gate (IKV version)

A fundamental improvement to this gate design is the fan type developed at the IKV on the basis of experience gained from other processing operations (Figure 7), which guarantees unproblematical distribution of the mix across the width. The basic idea of this principle is that approximately the same pressure drop should be achieved along each strand of the flow. The consequence of this is that the mould is filled simultaneously over its entire width and the flow front subsequently spreads out almost linearly in the mould. This means that entrapped air, as can result, for example, from a circular movement of the flow front (direct gate or narrow fan gate, Figure 6), can be avoided. The decisive factors for the pressure drop along a strand of the flow are simply its path length and its velocity, if we assume that the viscosity of the mix remains constant. Tests with this gating principle

Inlet-length in the laminar flow-area
of a pipe: $l_e = 0,03 \text{ Re} \cdot d_H$

$$d_H = \frac{4 \cdot A}{U} = \frac{4 \cdot b \cdot s}{2(b+s)}$$

$$b \gg s \Rightarrow d_H = 2s$$

$$l_e = 0,06 \text{ Re} \cdot s$$

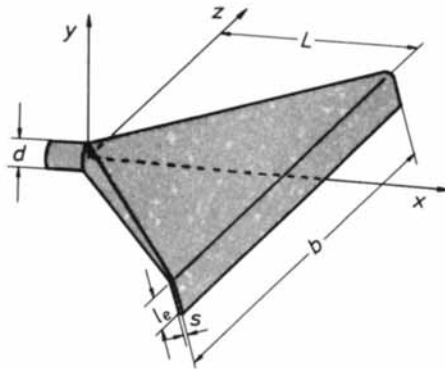


Figure 4. Fan-gate.

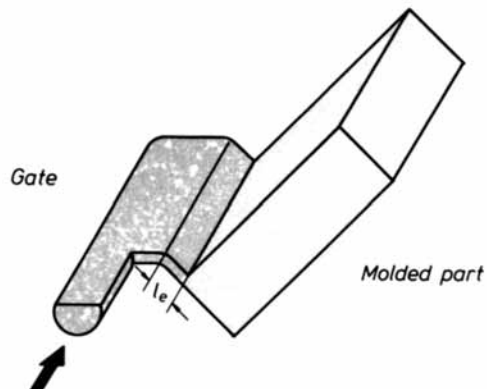


Figure 5. Sprue-gate.

have shown that, as in other areas with similar runners, the viscosity can be regarded as being independent of the shear rate (and there is thus Newtonian behaviour). The pressure drop along any strand of the flow can then be given as

$$\Delta p_{ges} = \Delta p_{R(l)} + \Delta p_{S(l)} \quad (1)$$

It is thus made up of the pressure drop in the runner itself and the pressure drop in the runner slot. For the pressure drop in a runner, we get, with laminar flow

$$\Delta p_R = \frac{8\dot{V}\eta l_R}{\pi R^4} \quad (2)$$

and in a runner slot

$$\Delta p_S = \frac{12\dot{V}\eta l_S}{L_o h^3} \quad (3)$$

where \dot{V} = volume throughput h = height of the slot
 l_R = length of the runner R = radius of the runner
 l_S = length of the slot η = viscosity of the mix
 L_o = half width of the slot

Because of the symmetry of the runner, only half of it is shown in Figure 8 and further calculation need therefore also only be carried out for this half. Regarding this illustration we get:

$$\begin{aligned} \text{film width } L_o &= B/2 \\ \text{throughput } \dot{V}_o &= \dot{V}_{ges}/2 \\ \text{slot length } l_S &= Y \quad (1) \end{aligned}$$

In view of the requirement that the mean velocity in the gate is the same at all points l in the mould, the flow volume in the runner decreases linearly with the longitudinal coordinate l .

$$\dot{V}(l) = \dot{V}_o \frac{l}{L_o} \quad (4)$$

We can then derive the following equation for the pressure drop along a strand of the flow:

$$\Delta p(l) = \frac{12\dot{V}_o\eta}{L_o h^3} y(l) + \int \frac{8\dot{V}_o\eta l}{L_o\pi R(l)^4} dl \quad (5)$$

If $p(l) \neq f(l)$, i.e. $p = \text{const.}$ for any strand of the flow, then the following must apply

$$\frac{\partial}{\partial l} \Delta p = 0 \quad (6)$$

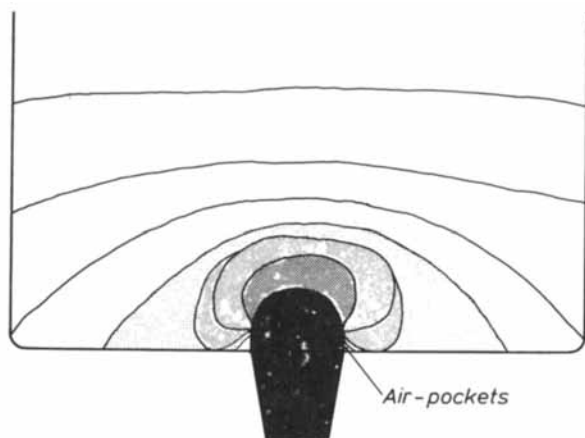


Figure 6. Fan-gate. Material-flow into the mold.

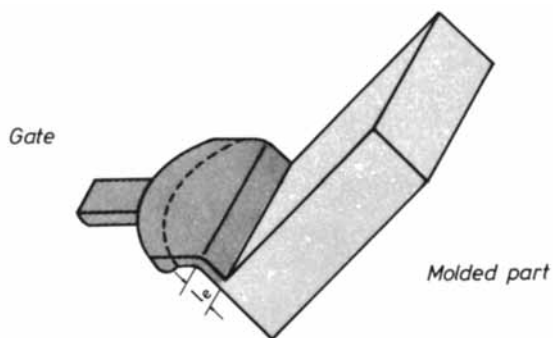


Figure 7. Fan-gate (IKV-version).

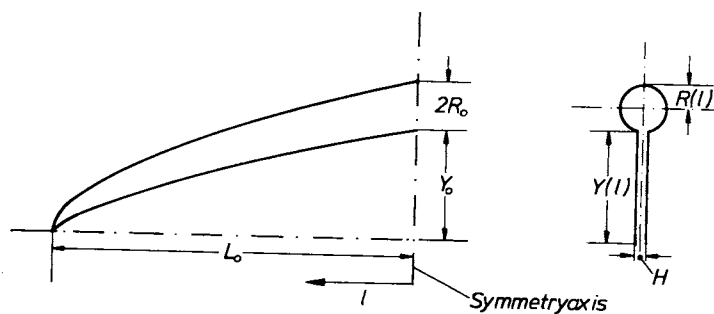


Figure 8. Fan-gate (IKV-version).

From this it follows that

$$\frac{\partial}{\partial l} \Delta p = \frac{12 \dot{V}_0 \eta}{L_0 h^3} \frac{\partial y}{\partial x} + \frac{8 \dot{V}_0 \eta l}{L_0 \pi R(l)^4} = 0 \quad (7)$$

All invariables can be shortened, so that we get

$$\frac{3\pi}{2h^3} dy = -\frac{l}{R(l)^4} dl \quad (8)$$

This equation represents the general relationship between the slot height h , the local (island) length y , the width parameter l and the runner radius R (see Figure 8) and can be integrated when R and h exist as a function of y and l . By ingeniously varying the boundary conditions, we can obtain solutions that are also easy to realize from a production point of view, for example by taking the runner radius R and the slot height h as being constant:

$$R(l) = R = \text{const.} \\ h^0 = \text{const.}$$

From this we get

$$y = -\frac{2h^3}{3\pi R_0^4} \int l dl \quad (9)$$

$$y = -\frac{2h^3}{3\pi R_0^4} \frac{l^2}{2} + C \quad (10)$$

$$y = \frac{h^3}{3\pi R_0^4} (L_0^2 - l^2) \quad (11)$$

This gives us the profile of the "island" geometry and of the runner. A particularly surprising point in this connection is that this is a solution which is very close to the "Staubalken" gates with film gate that are often used. From the point of view of industrial production, this solution is nevertheless still very complicated, since the runner would have to be made in an ellipse. It would be far more favourable if, instead of the elliptical form, it could be made in a circular form. With the aid of an error calculation, which uses the distance of the elliptical path from a corresponding circular path as the criterion for evaluation, it can be shown that this is satisfied with sufficient accuracy for the industrial scale if the L_0/y_0 ratio is approx. 3 or above (Figure 9) /5/. This has also been demonstrated in the tests performed with a gate manufactured accordingly. For this purpose, the gate module and the mould were made of PMMA, so that the flow processes could be recorded with a video camera and subsequently evaluated at a slower speed. In all the tests that were carried out in which the viscosity and the volume throughput were varied, the material nevertheless entered the mould cavity simultaneously at all

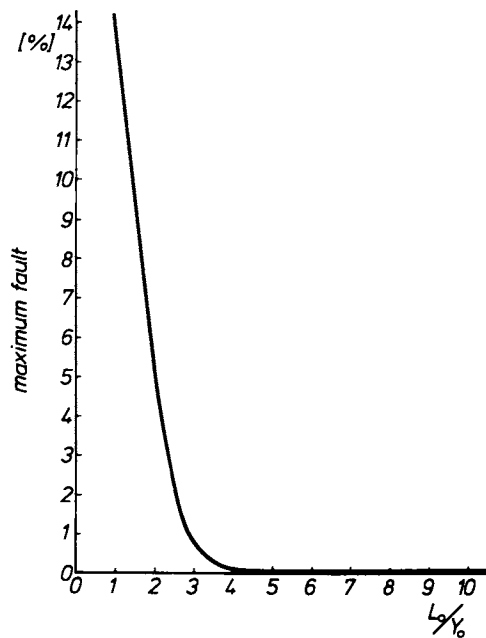


Figure 9. Fault-diagram.

the different points and produced a perfectly straight flow front. Thus one of the essential conditions has been fulfilled for avoiding defects such as entrapped air in the mould, namely the possibility of predicting how the flow front is formed in the mould. This point will be dealt with again in more detail later. This gating principle, notwithstanding its outstanding advantages, is frequently said to have economic disadvantages, since the gating module has to be relatively large and thus results in a very large loss of material. However, with the high reject rates that polyurethane processing is at present having to contend with and which are largely attributable to an incorrect design of the gate, this is an argument which needs thorough examination. On the contrary it would seem that such assessments are made all too prematurely and that savings are being made at the wrong place. By doing this, the manufacturer is landing himself with unpredictable finishing costs or a high reject rate.

Sprue gate

One example of a principle which is nowadays in widespread use, but is nevertheless regarded very critically from the point of view of flow behaviour, is the so-called "sprue gate". With this variation (Figure 10), the flow of mix is first conveyed in a type of runner along one side of the mould cavity and then enters the cavity via a film gate whose length may vary. This, however, produces a number of problems that can cause major defects in the moulding. These problems consist essentially in the fact that the mix, because of its impulse content, flows into the mould cavity in two major areas (Figure 11), which means firstly that there is no predictable formation of flow front and that secondly air becomes entrapped in various sections of the mould (see Figure 11) /4/. It is this entrapped air in particular, because it is in the lower part of the mould cavity and can no longer be expelled via a vent generally situated in the upper area, that causes a large amount of finishing work. This gating variation should therefore be regarded as highly critical and avoided where possible.

After-mixers

The gate module is a necessary element for conveying the mix produced in the mixing head into the mould cavity under controlled conditions. In practice, however, other elements are also inserted between the mixing head and the actual gate (runner), which are said in particular to have the job of "after-mixing". A typical element such as this is the so-called "fir-tree mixer" shown in Figure 12. It is, however, a fallacy that this element could make a mixture that had previously not been sufficiently homogenized into one that was adequate for good-quality

**American Chemical
Society Library
1155 16th St. N. W.
Washington, D. C. 20036**

In Reaction Injection Molding; Kresta, J.;

production. The effect of this component is more to throttle the flow of mix and thus increase the mixing effectiveness of the mixing head by making turbulences produced in the mixing head recede more slowly due to the higher level of pressure /6/. In addition, the gating volume, i.e. the amount of scrap is increased. A similar pressure effect can also be achieved without disadvantages by reducing the outlet pipe diameter of the mixing head. The mixing effectiveness is in this case increased even further by the fact that the injection nozzles come closer together and thus a higher energy is available at the point of impact for the mixing. However, when reducing the diameter of the outlet pipe, we very soon reach a limit, since it considerably increases the speed at which the mix emerges and it would be very complicated to slow it down again sufficiently for it to enter the mould cavity without taking up any air. It is therefore a good idea to provide a local throttling arrangement, the effect of which is greater the closer it is placed to the actual mixing chamber. The MQ mixing head from the firm Hennecke, St. Augustin, for example, is a very good example of this. Using an adjustable throttle slide valve, it enables the flow of mix to be restricted relatively soon after the injection point. With most of the other high-pressure mixing heads at present on the market, there is no provision for throttling the flow in this way, which means that, in these cases, a throttling device must be provided in the mould area. As has already been said, the "fir-tree mixer" shown in Figure 12 is the most unfavourable solution conceivable for this purpose. It is true that it does its job of throttling the flow of mix and thus ensures better mixing of the individual components, but it involves a number of disadvantages in view of the fact that absolutely no attention is paid to the flow behaviour. This results first of all in large dead spots (Figure 12), which are likely to have an effect particularly if the material being used has a very short cream time, as, for example, with flexible polyurethane foams. The danger here is that the mix in these dead spots begins to react and expand before the filling process has finished /4,7/. As a result, the flow channel becomes narrower and, due to the very high build-up of pressure in this area, there is a risk that the mould will open in the gating zone and lead to the formation of flash. The second disadvantage of this element is that very large air bubbles are introduced into the mix, firstly at the beginning of a shot when this element is filled - though these bubbles can generally still escape from the mix - and secondly, something which is far more critical, that air bubbles remain stationary in this element and are only released when the shot is over, when they are driven into the mould cavity through the movement of the cleaning piston (Figure 12). Generally speaking, these bubbles can no longer get out of the material.

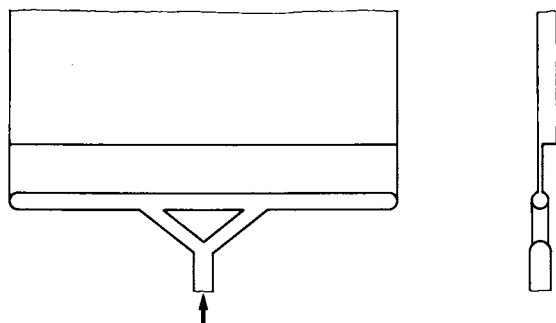


Figure 10. Sprue gate.

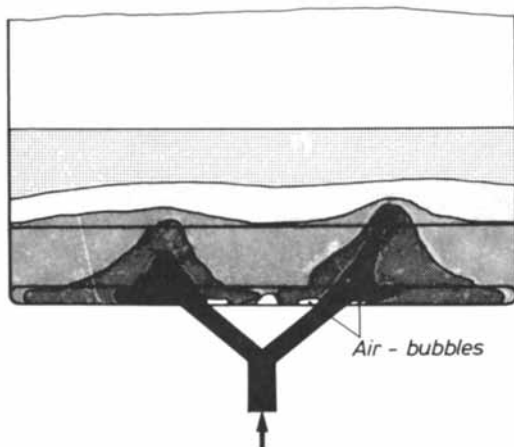


Figure 11. Streaming relationship in a sprue-gate.

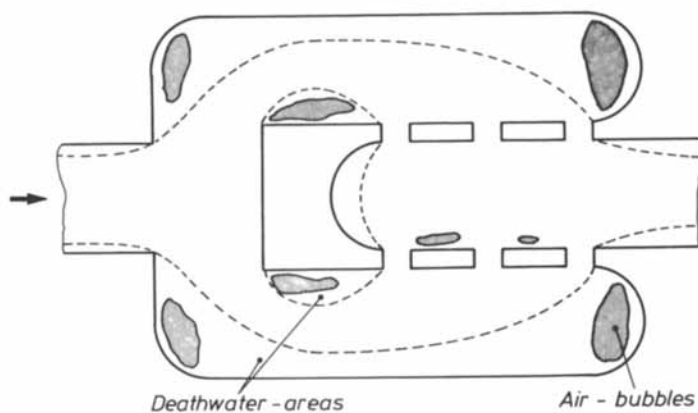


Figure 12. "After-mixer".

Spreading out of the mix in the mould cavity

Alongside the sources of defects through the choice of an unfavourable gate or an unsuitable throttling element, the problems of "mould design" in polyurethane processing have only been partly dealt with. In the same way as problems arise in the section we could term the "runner system", most of which involve the flow behaviour, so similar problems also occur in the mould cavity. A first source of defects can be underflow occurring in the gate section. This phenomenon is essentially due to the mix being injected against the direction of gravity (Figure 13) and even if the gate has been designed to permit favourable flow behaviour, it can still lead to considerable air entrapment. A reaction mix entering a mould that is inclined upwards against the direction of gravity is slowed down by the effects of gravity and friction at a certain distance from the gate, depending on the flow velocity. It then endeavours to flow back to the lowest point in the mould cavity. The reaction mix still coming out of the gate nevertheless prevents any backflow on the lower mould wall, with the result that, on the flow front, the thickness of the fluid film first increases before any flowing back occurs. The underflow that occurs can, however, cause a considerable amount of air to become entrapped in the material. Where the mix enters the mould in the direction of gravity, the material collects at the lowest point of the mould cavity and pushes the air ahead of it during filling of the mould so that it can be released from the last filled areas via the mould parting line or through special venting elements. These vents do not necessarily have to be situated at the highest point of a mould; this will be dealt with later in more detail. In order to be able to efficiently dispose of the air in the mould cavity, it would nevertheless be desirable if, at the mould design stage, know-how were available on the expected formation of the flow front in the mould cavity. Since, however, an analytical description of the mould filling process appears almost impossible in the foreseeable future, there are a number of simplified methods for estimating the spreading out of the flow front in the mould cavity, and these offer the only possibility of achieving efficient mould venting during PUR processing.

Filling pattern method

One method which, according to experience gained so far, is able to predict with sufficient accuracy the movement of the flow front during the production of large-area polyurethane mouldings is the "filling pattern method", which has already been successfully used for describing the mould-filling process in the injection moulding of thermoplastics /8,9/. For the processing of polyurethanes, too, this method enables a simple graph to be

drawn up of the spreading out of the flow front in the mould, so that the designer can obtain a picture of the material flow in the mould back at the planning stage.

The filling pattern method is based on the assumption that the flow front in the mould advances in line with the Huyghens' wave propagation theory, according to which each point on a wave front is regarded as the starting point for a new elementary wave. The enveloping line for all the elementary waves again provides a wave front, which, in the filling pattern method, corresponds to the flow front profile at a later point in time. The change in pressure Δp occurring with a flow front movement of the distance Δl is, according to the Hagen- Poisseuille principle for the wall-sticking laminar turbular flow

$$\Delta p = \Delta l \left(\frac{32 \bar{v} \eta}{d^2} - \rho g \sin \alpha \right) \quad (12)$$

Applying this principle to any desired flow cross-section necessitates, instead of the pipe diameter d , the use of the hydraulic diameter d_h

$$d_h = \frac{4A}{U} \quad (13)$$

which, due to the laminar form of flow, also has to be multiplied by a geometric coefficient φ . With large-surface area mouldings, the width b considerably exceeds by definition the height h ($b \gg h$), which means that under these conditions the hydraulic diameter becomes simplified as

$$d_h = 2h \quad (14)$$

and φ assumes the constant value of 1.5. Since the changes in pressure occurring during the spreading out of the flow front in the mould cavity must furthermore be independent of direction, $\Delta p_1 = \Delta p_2$, we get, on neglecting the influence of gravity

$$\bar{v}_1 \frac{\Delta l_1}{h_1^2} \eta_1 = \bar{v}_2 \frac{\Delta l_2}{h_2^2} \eta_2 \quad (15)$$

Assuming constant fluid viscosities on the flow front during filling of the mould leads finally, together with the definition for the flow front velocities to a simple relationship

$$\boxed{\frac{\Delta l_1}{h_1} = \frac{\Delta l_2}{h_2}} \quad (16)$$

According to this equation, the ratio of flow length to mould cavity height is constant at every moment of the mould-filling process, which means that the flow front profile in large-area mouldings can only be determined from their geometrical dimensions. Assuming equal fluid viscosities is, however, only permissible to a limited extent in the case of polyurethanes, since, with major differences in cross section, the viscosity also changes with the influence of the wall on the curing reaction. In a large number of cases, the mould-filling process in polyurethane processing can nevertheless be followed with sufficient accuracy using the filling pattern method. Figure 14 shows the flow front profiles for a centrally gated cylindrical mould (360 mm dia., $h = 10$ mm), which were determined by experiment and constructed in accordance with this specification. The differing amount to which the material spreads out within one time-step results, in certain areas of the mould, in a meeting up of two or more individual flow fronts, something which always involves the risk of entrapped air in the mouldings /10/. This is also clearly illustrated with the example of a RIM moulding for exterior application in automotive construction (Figure 15), which contains a metal strip in the middle for fastening purposes. The moulding has an air bubble entrapped near the top and has been short-moulded at another point. Both of these defects are caused by inadequate venting of the mould cavity, as is shown by the flow front profile in the mould produced by the filling pattern method and ignoring the moulding ribs (Figure 16). The flow front, which enters the lower area of the mould via a sprue gate across the entire width of the mould, is slowed down slightly on reaching the insert on the left-hand side of the mould cavity because of the lower height of the flow channel, whereas it moves forward at a constant speed in the right-hand half. The reaction mix therefore flows over the upper end of the insert on one side and joins up at some distance from the edge of the mould with the slower rising flow front. However, this contact between the two flow fronts prevents the air inside the mould from escaping via the parting line and it becomes fixed in the moulding with the subsequent gelation of the reaction mix. The differences between the filling pattern method and the actual mould-filling process are due to the fact that the influence of gravity on the spreading out of the flow front is ignored. On reaching the upper edge of the insert, the reaction mix runs, under the influence of gravity, into the thinner, as yet unfilled area of the mould cavity and therefore meets the rising flow front at a lower point than was to be expected by the filling pattern method. In addition, when calculating the mould-filling process, no account was taken of the moulding ribs - another factor which can explain certain differences from the true flow front movement. On the other hand, this simplified application of the filling

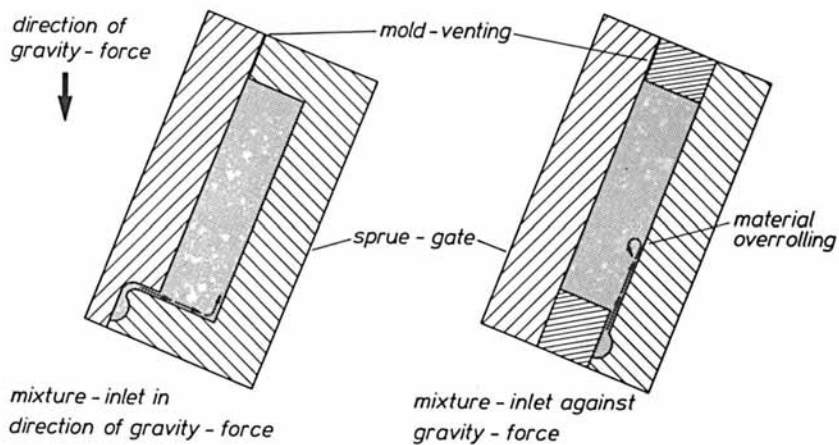


Figure 13. Possibilities of the mixture-inlet.

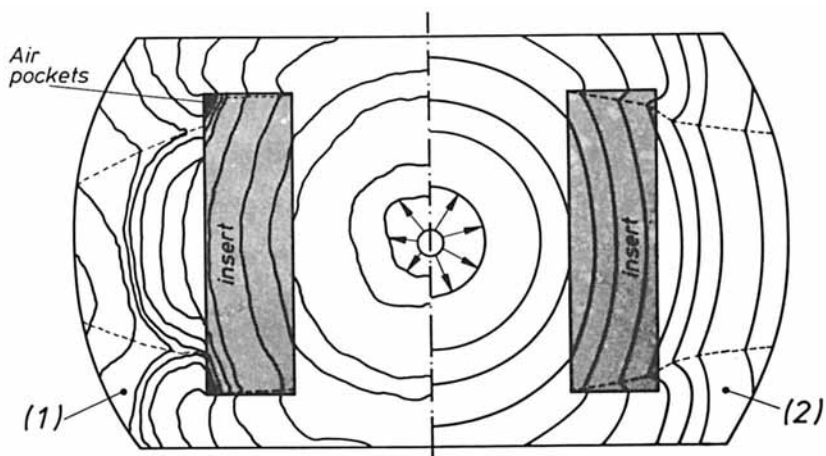


Figure 14. Experimental (1) and theoretical (2) mold filling.

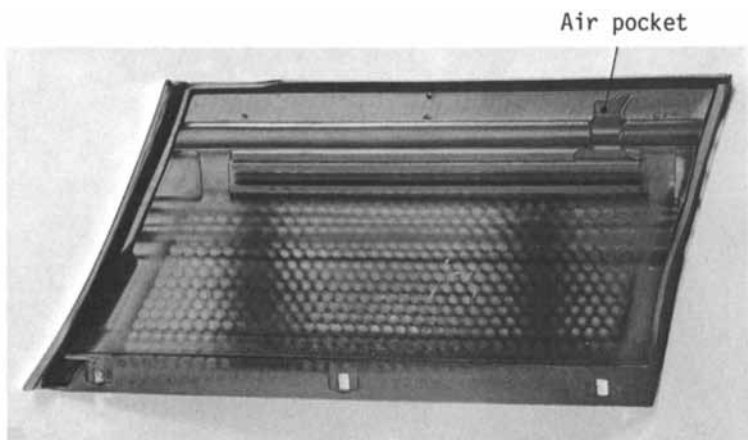


Figure 15. Original fender of an automobile showing insufficient molded areas.

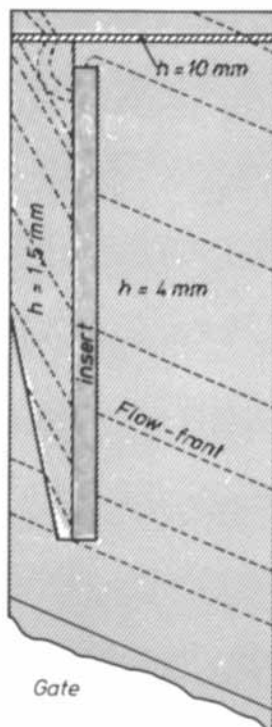


Figure 16. Theoretical constructed flow front.

pattern method clearly illustrates in advance which areas of the mould are at risk from air bubbles and thus enables the mould designer to take effective measures to prevent it. Determining the mould-filling operation in polyurethane foam moulding necessitates a slightly modified application of the filling pattern method, depending on the position of the mould. In the foam moulding of polyurethane, filling of the mould cavity can be subdivided into three individual stages: injecting the flow of mix into the mould, calming of the material and expansion of the material in the mould, as is shown in Figure 17 for a bottom-filled, angled mould of constant geometry. The compression and hardening phase following the expansion stage is, however, of no significance for filling the mould, since compression of the material merely brings about the final formation of the density profile that is then fixed in the hardening phase. The flow front profile forming in the mould cavity during injection of the mix can basically be determined for polyurethane foam moulding in just the same way as in the production of solid polyurethane mouldings (Figure 18). However, when the mould is inclined at an angle, there is, during the calming phase after the injection phase has finished, an equalization of the flow fronts due to gravity as a result of the mould cavity being only partly volumetrically filled. This equalization involves the reaction mix, which has already moved on into the thicker areas of the cavity, flowing back, whereas at the same time the flow front in the other areas is continuing to advance until the surface of the liquid becomes smooth. This leveling out process is not, however, covered by the filling pattern method, since it is controlled purely by gravity. For describing the mould-filling process during the expansion stage, the filling pattern method should therefore be based on the flow front profile at the beginning of the expansion. As long as there are no geometric conditions in the mould cavity below the surface of the liquid which might encourage entrapped air, application of the filling pattern method in polyurethane foam moulding in a mould inclined at an angle is restricted merely to the actual expansion process.

On the other hand, if the mould is in a level position - as is generally the case for centrally gated polyurethane mouldings - there is no equalization of the flow fronts even if the material expands during the calming phase, which means that the filling pattern method can always be applied from the gate onwards (Figure 14). As shown by a comparison between the flow front profile determined by experiment and one calculated by theory based on this cylindrical mould of 360 mm diameter, the filling pattern method is nevertheless also able to correctly describe the areas at risk from air bubbles and the position of the weld lines for a centrally gated moulding with local

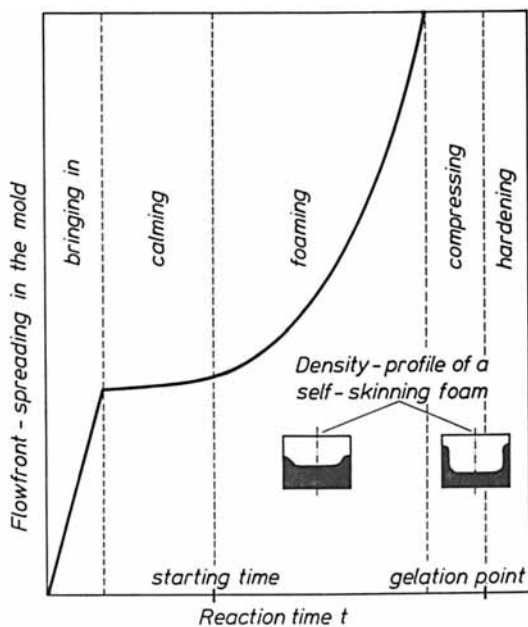


Figure 17. Schematical mold filling in the PUR-foaming technology.

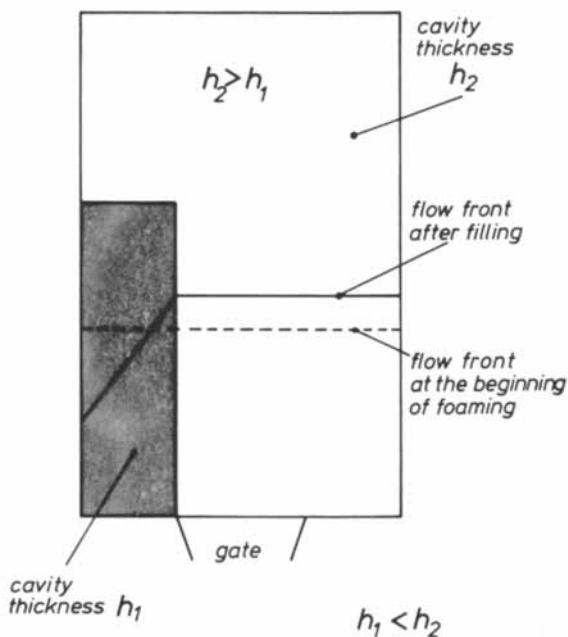


Figure 18. Change of the flow front.

change in cross-section. Unlike the injection moulding of thermoplastics, weld seams in polyurethane processing do not necessarily form zones of reduced strength in the material, but, above all, they impair the optical quality of the moulding and generally represent an aggregation of entrapped air bubbles.

A knowledge of the mould-filling process in polyurethane processing thus makes it possible to recognize back at the mould design stage areas of the mould that are at risk from air bubbles and to do something about it by

- altering the position of the gate,
- varying the thickness of the moulding and
- providing special venting elements,

and thus largely avoid subsequent modifications to the mould. Successful application of the filling pattern method nevertheless requires not only that the mould is gated at its lowest point, but also that jetting is avoided under all circumstances at the beginning of the mould-filling process, otherwise the air bubbles that get into the reaction mix in the gating area cannot be removed even by careful venting of the mould.

Thus, designing the gate to suit the moulding also gains additional significance, since in this case the formation of the flow front is virtually given in advance. A combination of these two elements - gate design and filling pattern method - should, however help in many applications to eliminate back at the mould design stage, serious defects in moulding production.

Literature Cited

1. Mrotzek, W.; Auslegung von Formwerkzeugen für die PUR-Verarbeitung; Promotionsvortrag, 1982; IKV-Archiv-Nr. P-10-1982
2. Becker, E.; Reaction Injection Molding; Van Nostrand Reinhold Company, New York 1979
3. Schneider, W.; PUR-Angußsysteme In: Wirtschaftliches Herstellen von PUR-Formteilen; VDI-Verlag, Düsseldorf 1981
4. Kuchenmüller, K.; Untersuchungen zur Optimierung der Formteilmfertigung beim RIM-Verfahren; Diplomarbeit am IKV, Aachen; IKV-Archiv-Nr. D8347; Betreuer: H. Müller
5. Döring, E.; Hiemenz, C.; Mathematische Beschreibung sowie Versuche mit den aufgrund der Ergebnisse gefertigten Angußsysteme; Nichtveröffentlichte Arbeit am IKV, 1979; IKV-Archiv-Nr. B7931

6. Mrotzek, W.; Gegenstrominjektionsvermischung niedrigviskoser Reaktionsharze; Dissertation an der RWTH Aachen, 1982; IKV-Archiv-Nr. DS 8210
7. Jung, D.; Einfluß der Angußgestaltung auf die Qualität von PUR-Formteilen; Diplomarbeit am IKV, Aachen; IKV-Archiv-Nr. D 8301; Betreuer: H. Müller
8. Menges, G.; Lichius, U.; Bangert, H.; Eine einfache Methode zur Vorausbestimmung des Fließfrontverlaufs beim Spritzgießen von Thermoplasten; *Plastverarbeiter* 11 (1980) 671-676
9. Napp-Zinn, G.; Werkzeugfüllung bei der PUR-Verschäumung; Studienarbeit am IKV, 1982; Archiv-Nr. S 8206; Betreuer: W. Mrotzek
10. Niemöller, B.; Methoden zur Vorherbestimmung der Werkzeugfüllung bei der PUR-Verschäumung; Diplomarbeit am IKV; IKV-Archiv-Nr. D 8238; Betreuer: W. Mrotzek

RECEIVED October 5, 1984

New Developments in RIM Equipment

FRITZ W. SCHNEIDER

Martin Sweets (PTI) Company, Inc., Louisville, KY 40201

The RIM and RRIM technology, using high pressure metering and impingement mixing of the liquid reactants, is widely used for the production of parts from unfilled and filled polyurethane formulations. Its applications are manifold. The better understanding of the mixing requirements, improvements in the design of mixing devices and detail engineering, as well as more sophisticated process controls, led to machines of high reliability and ease of operation and maintenance.

Newer developments include also RIM and RRIM machines for the processing of polyamide and epoxy formulations.

The design and operational parameters of medium to high capacity RIM machines is, in the meantime, well established. The wish of the industry to use the more economical and environmentally friendly RIM process for small part production, has some limitations. These are based on the basic hydrodynamic requirements for impingement mixing, and the design and manufacturing problems associated with small size impingement mixing devices. In cases of processing of solid filled systems, the size, shape and concentration of the solids suspended in the liquid reactants must be considered.

In the following, the main aspects for low capacity impingement mixing and small parts production are discussed.

Impingement Mixing

For good mixing results, it is required to achieve adequate turbulent mixing conditions in the mixing chamber.

0097-6156/85/0270-0259\$06.00/0
© 1985 American Chemical Society

The mixing efficiency can be predicted, to some degree, by comparison of the critical Reynolds' number of a certain mixing system to the actual Reynolds' number of the process conditions in question. The actual Reynolds' numbers have to be larger than the critical Reynolds' number for turbulent flow conditions and satisfactory mixing results.

It was found, by experience, that in case of using mixing devices featuring countercurrent impingement of the two components in cylindrical mixing chambers, sized properly for the capacity requirements, the critical Reynolds' numbers are in general $Re_{crit} = \text{approx. } 50$ for formulations with good mixing affinity - as for example nylon formulations - and $Re_{crit} = \text{approx. } 100 - 200$ for polyurethane RIM systems requiring higher turbulence for a good mix (ref. 1, 2). The borderlines are floating and accurate numbers can only be achieved by the testing of the materials in question in a certain mixing device.

The actual Reynolds' numbers of mixing systems having circular, unobstructed flow areas of the nozzle orifices can be calculated by the following terms:

$$Re = d \cdot v \cdot \rho / \mu = 4 Q / (\pi \cdot d \cdot \mu) \quad (1)$$

with d = diameter of nozzle orifice (m)
 v = flow velocity (m/sec)
 ρ = density (kg/m³)
 μ = dynamic viscosity (kg/m sec)
 Q = flow capacity through nozzle (kg/sec)

The Reynolds' number can also be expressed, as explained earlier (Ref. 2), by substitution with the relationships between capacity, nozzle diameter, flow speed and impingement pressure according to the following terms:

$$Re = 2 \cdot 10^3 / \mu \cdot (\sqrt{Q \cdot k / \pi} \cdot \sqrt[4]{20 g \cdot \rho \cdot \Delta p}) \quad (2)$$

with ρ = density (g/cm³)
 μ = dynamic viscosity (cP)
 Q = flow capacity (g/sec)
 k = nozzle factor - 0.7 to 0.8
 g = earth gravity - 9.81 (m/sec²)
 p = impingement pressure (kg/cm²)

The minimum capacity which may be run successfully can then be gained by the relationship:

$$Q_{\min} = Re_{\min}^2 \cdot \pi \cdot \mu^2 / (4 \cdot 10^6 \cdot k \sqrt{20 \text{ g} \cdot \rho \cdot \Delta p}) \quad (\text{g/sec}) \quad (3)$$

with $Re_{\min} \rightarrow Re_{\text{crit}}$

The viscosity of the fluid has a main influence being directly proportional to the capacity by its square, whereas the impingement pressure is reversed proportional by its square root. The maximum operation pressure of today's production machines is, for practical reasons, usually limited to approximately 200 kg/cm² (approx. 3000 psi). However, higher pressures may be utilized if required.

A practical example may further explain the situation:

For a certain material combination, it was found that a minimum Reynolds' number of $Re_{\min} = 100$ was required for providing good mixing results. The dynamic viscosity of the B component was $\mu = 600$ cP, the A component had $\mu = 400$ cP, the nozzle factor was assumed to $k = 0.7$, the density was $\rho = 1.1$ g/cm³ and the impingement pressure was chosen to $p = 200$ kg/cm². The ratio of the flow streams was A:B - approx. 1:1.

The values according to the B component entered in the term (3) allowed the prediction, that the minimum capacity for this component essential for successful mixing was approximately 20 g/sec. The total minimum capacity was then approximately 40 g/sec.

By lowering the viscosity of the B component to approximately 400 cP (increase of temperature) and otherwise equal conditions, the corresponding total minimum capacity could be lowered to approximately 20 g/sec. On the other side, a viscosity increase to 800 cP would increase the minimum capacity to approximately 70 g/sec.

The described approach for estimating the possible minimum capacities at the impingement mixing of two components, was deducted from theoretical considerations. These results were backed by tests and observations and analysis of a larger number of production and demonstration runs with different capacities and chemical systems. The method was found useful as a guideline for the prediction of the limits of low capacity impingement mixing for small part production, for the interpretation of test results, as well as for the evaluation and development of RIM processable chemical systems.

Small Size Rim Mixing Head

In anticipation of the above considerations, a small size RIM mixing head was developed, suited for small capacity operation.

The mixing head features countercurrent impingement of two components and is self-cleaning by a hydraulically operated piston rod, running in the cylindrical mixing chamber at close tolerances. The mixing chamber and the

cleaning rod have a nominal diameter of only 1/8" (3.175 mm). This design became stresswise possible by using an ungrooved cleaning rod of high material quality, in combination with an automatic valving system allowing switch over from high pressure recirculation to mix and dispense, and vice versa, on stream, without shutoff of the supply lines and related pressure changes (Ref. 3).

Figure 1 shows a photograph of this mixing head type "A/2". The lower part is the mixing head housing incorporating the mixing chamber and the automatic valving system with its connections of the feed and recirculation lines of the chemicals. Fixed on its upper end, is the hydraulic cylinder for the operation of the cleaning rod.

With this design, for the first time, shots of only a few grams could be achieved at accurate shot repeatability using shot times in the 1/10th second range.

One of the first industrial applications of this mixing head was to fill a relatively small amount of flexible foam material in the cavity of aluminum baseball bats.

Figure 2 shows the specifically developed small size custom RIM machine for this application, including the metering unit, electrical controls, fixture for the vertical arrangement of the baseball bats to be filled, and also an up and down moving support on which the mixing head is installed. The operation of the machine is semiautomatic.

Figure 3 shows a photograph of two baseball bats. The lower one is cut open for the display of the arrangement of the flexible foam in its cavity. For getting the desired distribution of the foam, the dispense flow stream from the mixing head has to be smooth and laminar, not touching the small diameter inside surface of the tubular handle part. This is achieved by proper selection of the mixing chamber geometry in regard to capacity.

Other uses of the new mixing head include the production of small size test samples on laboratory RIM machines for the development and evaluation of foam and non-foam RIM materials of different nature, encapsulation of electronic components, production of small size technical parts and the fill of small quantities of insulation foam in plastic picnic jars.

Minimum Capacity For The Processing Of Solid Filled System (RRIM)

For the investigation and prediction of the mixing efficiency at the processing of solid filled systems, as well as for the interpretation of test results, the same approach is useful as described earlier for the processing of unfilled systems.

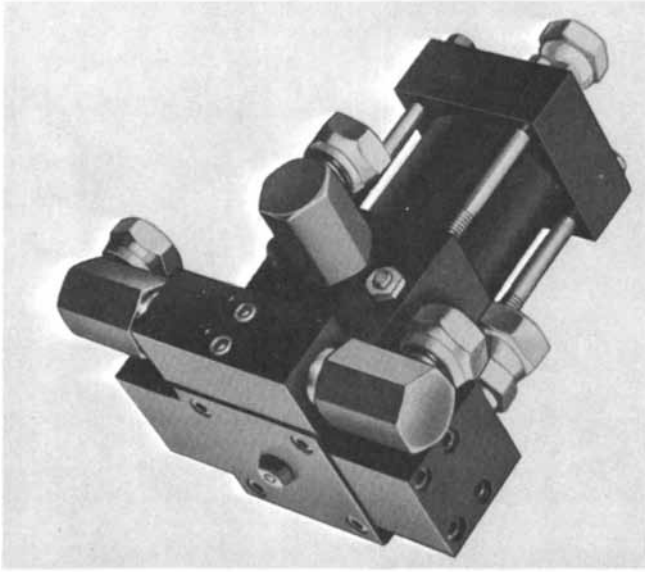


Figure 1. Small size RIM impingement mixing head type "A/2". Diameter of mixing chamber 1/8" (3.175 mm).

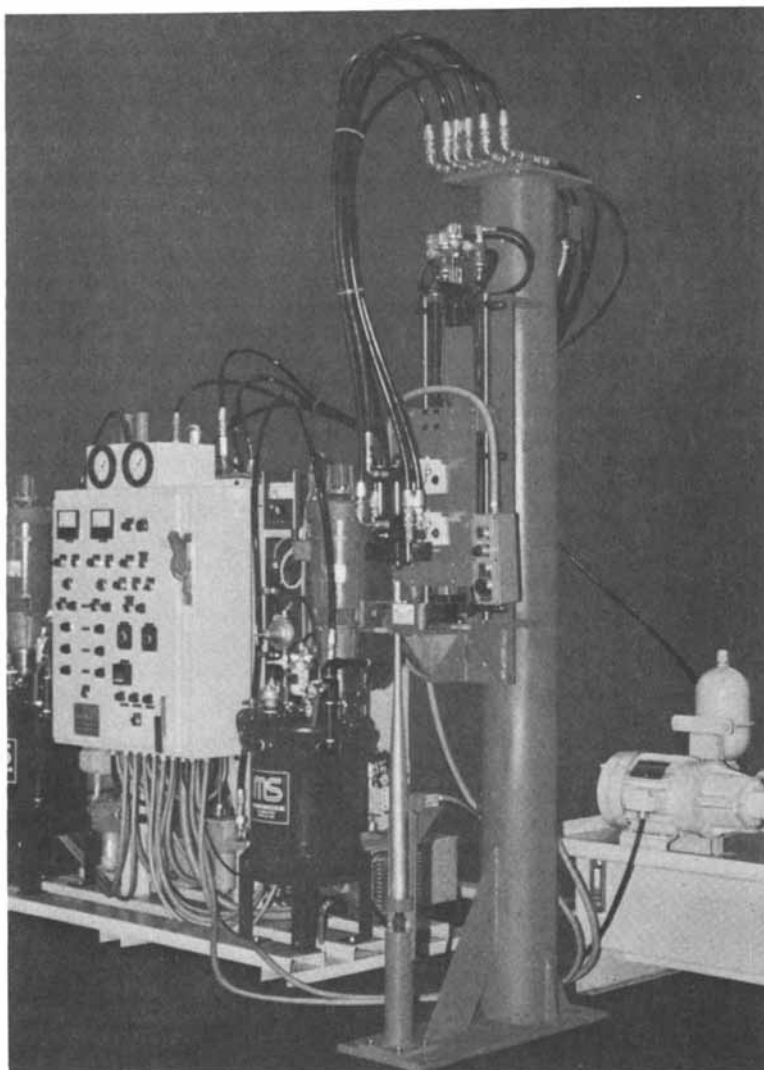


Figure 2. Custom RIM metering and mixing machine with fixture, for the fill of aluminum baseball bats with a small amount of flexible foam.

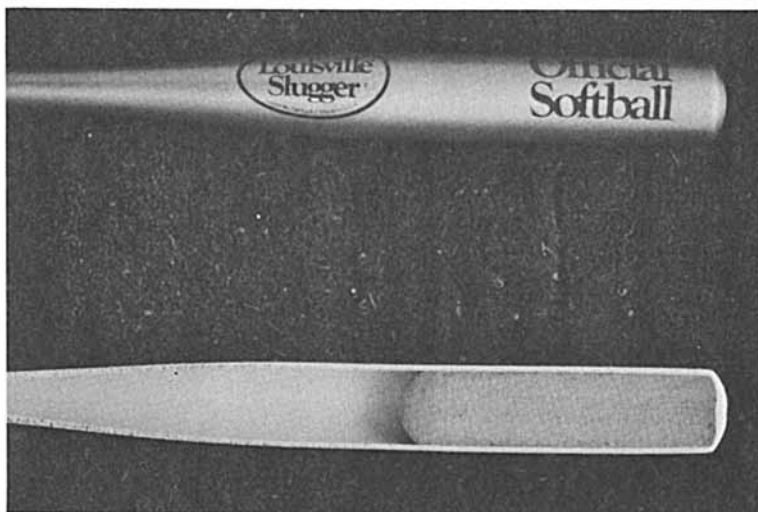


Figure 3. Aluminum baseball bats. Cavity partially filled with flexible foam.

In regard to the viscosities entered in equation (2), the values of the unfilled liquids may be used, as long as no better information is available. This is possible because the high shear forces encountered in the impingement nozzles, dramatically dropping the apparent high viscosities of the suspensions at rest.

For the processing of suspensions with larger size solid fillers, as for example glass fibres etc., the minimum capacity limitations of the equipment are usually decided by the size, shape and volume concentration of the fillers, as well as by the flow characteristics of the suspensions. Efficient mixing of solid filled systems is, according to experience, seldom a problem, as long as the suspensions are able to pass, without clogging, through the impingement nozzles.

The minimum capacity required to avoid clogging effects can be estimated to some degree by the relationship:

$$Q_{\min} = d_{\min}^2 \cdot \pi / 4 \cdot (k \sqrt{20 g \cdot \rho \cdot \Delta p}) \quad (\text{g/sec}) \quad (4)$$

with: d_{\min} = minimum nozzle diameter (mm)
 K = nozzle factor - approx.
 0.7 to 0.8
 g = earth gravity = 9.81 (m/sec²)
 ρ = density (g/cm³)
 Δp = impingement pressure (kg/cm²)

As an example, the knowledge of the minimum capacity for the impingement mixing of a system containing non-agglomerated, free flowing particles of a maximum size of 1/32" (approx. 0.8 mm) is desired, for predicting the size of the process equipment required. The density of the suspension is $\rho = 1.25 \text{ g/cm}^3$, the nozzle factor is assumed to $k_2 = 0.7$ and the impingement pressure is chosen to $\Delta p = 180 \text{ kg/cm}^2$.

In accordance to previous experience with similar materials, the nozzle diameter d_{\min} should be at least 20% larger than the maximum particle size for allowing the free pass of the solids through the nozzles without clogging effects. This requires a minimum nozzle diameter of $d_{\min} = \text{approx. } 1.0 \text{ mm}$.

It can be predicted, by entering these values in (4), that a minimum capacity of $Q_{\min} = 115 \text{ g/sec}$ per flow stream may be satisfactorily realized. The total minimum capacity, according to restriction by solid fillers, at an assumed ratio of A:B = 1:1 can then be expected to be approximately 230 g/sec (Variations in the ratio alter the result accordingly).

A cross-check for the actual Reynolds' number at these values and with a dynamic viscosity of the suspension in question, under the effect of high shear forces, of $\mu = 1000 \text{ cP}$, provides us in regard to (2) with $Re = 147$.

This results allow the conclusion, that efficient mixing and satisfactory processing of the materials should be possible.

The corresponding values for a maximum particle size of 1/16" (approx. 1.6 mm), requiring a minimum nozzle size of approximately 2 mm, result in a minimum capacity of approximately 460 g/sec per flow stream or a total minimum capacity of about 920 g/sec.

The above considerations were found useful as guideline for the minimum requirements for the layout and selection of metering and impingement mixing equipment for the processing of solid filled systems. They do not replace the actual testing of the flow characteristics of solid filled systems, for which no previous experience is available, through impingement nozzles, as well as of their mixing behaviour.

Low And Medium Capacity RIM and RRIM Machines

Typical examples of low and medium capacity machine for RIM and RRIM applications are represented by the "RHP" type series. These machines were first introduced about 3 years ago. They represent an advanced and improved design in regard to their forerunners. Based on experience, their design and engineering was consequently executed for ease of operation and high reliability.

The simplified flow diagram, Figure 4, shows the principle of these machines.

Main components are the material tank stations, lance cylinders, hydraulic systems for operating the lance cylinders, hydraulically operated mixing head, temperature control systems, line and valving system and process controls.

For operation, prepressure is provided in the run tanks by dry pressure air or nitrogen for positive feed pressure of the chemicals to the lance type cylinders acting as metering devices. The tanks are fitted with agitators. The feed outlets of the tanks are connected to the lance cylinders by short lines of relatively large diameter for low flow restriction during the fill strokes. In low pressure mode, the lance pistons are oscillated slowly back and forth. The speeds of the forward and backward strokes are individually adjustable by the hydraulic drive systems. The low pressure recirculation valves, located close to the mixing head, remain open. The valves in the feed lines from the tanks to the lance cylinders are automatically closed when the direction of the lance pistons is reversed to forward and opened for the backward strokes. This procedure provides the required recirculation and movement of the chemicals or the liquid/solid suspensions through the line systems for temperature conditioning, and to prevent settling effects.

For a mix and dispense operation, the feed valves and the low pressure recirculation valves are closed and the lance pistons, starting simultaneously, are moved forward at selected higher speeds, in accordance to the desired capacity and ratios.

At the beginning of the stroke, the displaced volumes of chemicals, according to the stroke length "A" of the total stroke, are used for the build up of pressure in the line systems to the mixing head by passing the materials in total through the impingement nozzles. After completion of pressure buildup, controlled by pressure switches, the mixing head is opened and the material streams are impinged in the mixing chamber, mixed and dispensed. The dispense or shot volumes are in accordance with the stroke length "B" of the lance pistons. After the closing of the mixing head, the displaced volumes according to the stroke length "C" are used for post high pressure recirculation for the purging and cleaning of the entrance ports to the mixing chamber for preventing clogging of these ports by accumulated reactive materials. Then the machine is switched back into low pressure recirculation mode for standby operation or the next dispense operation may be initiated. The total dispense cycle time may be as short as 2 seconds, allowing the processing of rapidly reacting chemical formulations at actual shot times below 1 second.

The "RHP" system requires a minimum amount of elements and process control equipment for reliable operation. Booster pumps for the recirculation of the chemicals and for providing positive feed pressure to the lance type cylinders, as used on earlier models, are eliminated. This results in reduced maintenance.

Standard sizes of the "RHP" series cover machines with flow rates from 43 to 300 lbs/min and for maximum shot weights from 2 to 20 lbs. (See table Figure 5).

Custom machines are available in addition to meet special requirements and larger outputs.

RIM And RRIM Machines For The Processing Of Nylon And Epoxy Formulations

Nylon, epoxy and other formulations using reactive liquid resins for part production can be successfully processed in accordance to the RIM method. Efficient mixing is achieved by utilizing the same basic parameters as established for the impingement mixing of polyurethane systems. The general layout of the machines is similar to the design principles as described in the previous chapter. The detail engineering and design focuses on the control of the elevated process temperatures required for the processing of the chemicals.

	<u>RHP-1</u>	<u>RHP-2</u>	<u>RHP-3</u>	<u>RHP-4</u>
Flow Rate, #/min.	43	68	126	300
Max Shot Wt. Lbs.	2	4	8	20
Residual Volume, in ³	45	70	130	260
Hydraulic Cyl. Base, in.	5	6	8	10
Lance Dia., in.	3	3-1/2	4-1/2	6
Stroke	7	8	12	16
Pump Horsepower	7-1/2	15	25	50
Elec. Power Req'd.	240/3/60	480/3/60	480/3/60	480/3/60
Theoretic Max Filler Size, in.	.040	.050	.069	.109
Approx. Floor Space	7 x 5	9 x 5	10 x 5	11 x 6
Hydraulic Tank, Gal.	40	60	120	250
RIM Head Size	A	B	C	D
Material Tank Size, Gal.	3	2	10	10

Figure 5. Main data of RIM/RRIM machines of "RHP" series.

Several approaches were used for the temperature control, for example, heating of the lines, pumps, valves mixing head, etc., by electrical resistance heating by means of heating cartridges and tracing lines, as well as by the recirculation of heated oil through jacketed tanks and lines. The methods used depend on the specific requirements of the application and the complexity of the machines.

A very feasible and promising approach was to arrange the hot process parts of the machine in total in an oven enclosure provided with means for controlled hot air recirculation. The process parts, including tanks, chemical lines, metering cylinders or pumps, valves, mixing head and mold, can be arranged in different compartments of the oven enclosure for the individual temperature control of the chemicals.

Figure 6 shows a laboratory machine built in accordance with this principle. The unit is used for the production of test samples made from polyurethane, polyamide and polyimide formulations at adjustable process temperatures of up to 240°C.

The temperatures in the different sections are kept in close tolerances (approx. $\pm 2^\circ\text{C}$) with a minimum of control elements and without danger of local over or under heating. The plaque mold for the production of test samples and valves for ratio calibration are arranged in the front part of the oven, accessible by a large door opening.

The oven enclosure is arranged on casters, allowing an unrestricted forward movement of the oven, after the backwall is unlocked, for easy access to the process parts for maintenance.

Figure 7 shows the oven in forward position. All process parts in contact with the chemicals exposed to the hot environment are manufactured from stainless steel. The gear drives for the tank agitators and the hydraulic actuators for the mixing head and for the metering cylinders are arranged outside of the enclosure in ambient environment. The drive parts are coupled to the hot parts by insulated connections for preventing heat transfer.

The machine is designed for the easy cleanout of the chemicals at the change of formulations.

The design principle of this machine can essentially also be used for larger size machines for industrial parts production.

Free Pour Impingement Mixing Head

A further new development consists of an impingement mixing head design with an integrated aftermixer device and a transfer cylinder for low speed dispense for the processing of difficult to mix formulations, requiring prolonged mixing time for the stabilization of the initial mix (Figure 8).

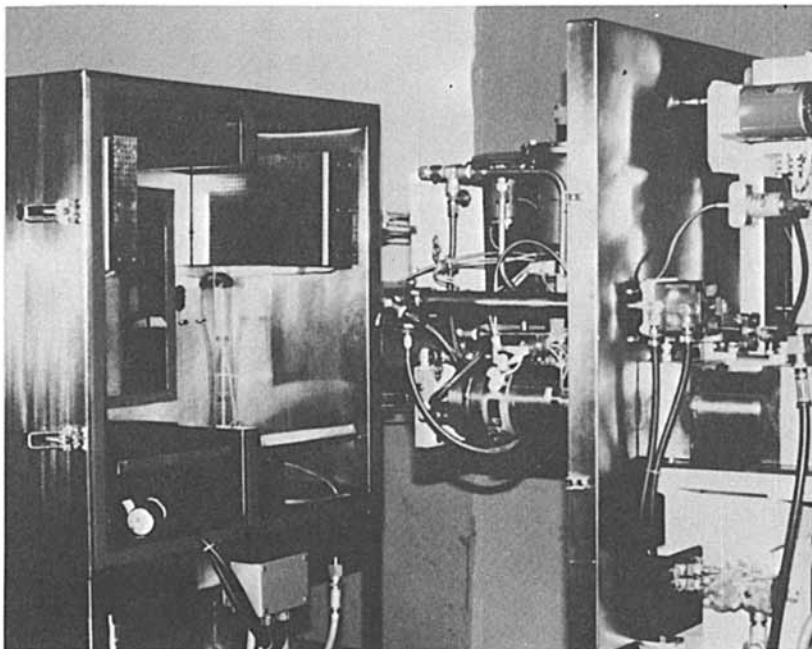


Figure 6. Laboratory RIM/RRIM machine for the production of test samples at elevated process temperatures. Process parts, including mold, in oven enclosure.

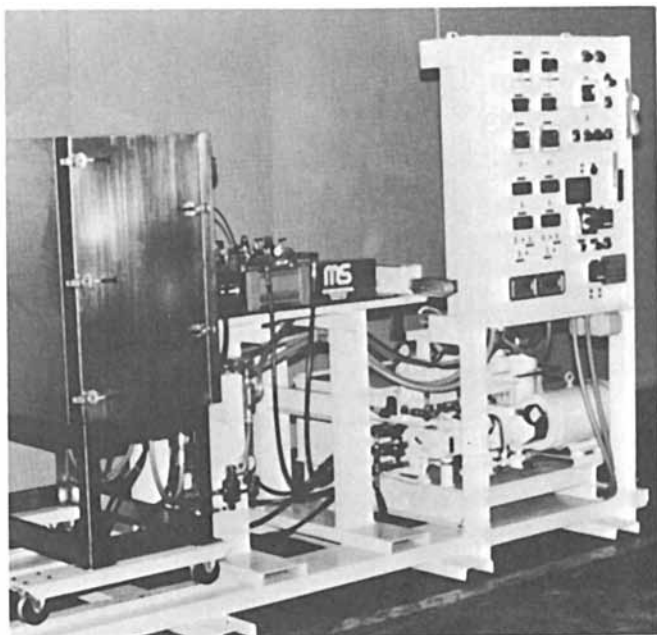


Figure 7. Laboratory RIM/RRIM machine as in Figure 6. Oven enclosure opened for free access to the process parts.

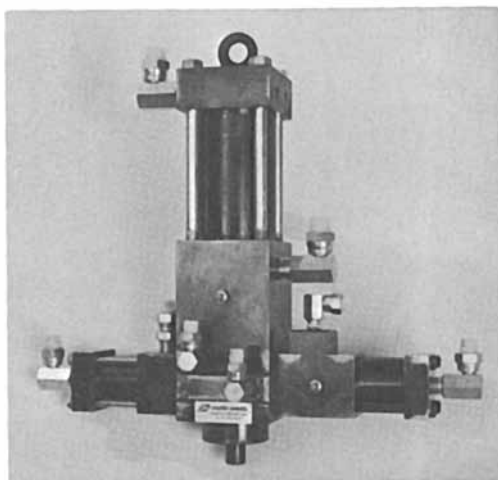


Figure 8. Free pour impingement mixing head with integrated aftermixer chamber.

The mixing head is suited for free pour applications for the dispense of the mixed chemicals in open molds, as well as through fill holes or mold gates, in similar ways as at operation with low pressure mixing devices, but without the necessity for solvent cleaning and restrictions on the positioning of the mixing head and cycle times. All cavities of the new mixing head are cleaned mechanically by cleaning rods actuated hydraulically.

Figure 9 shows schematically a cross section. The movements of the actuators take place with minimum delay. For a dispense operation, the transfer dispense cylinder and the aftermixer chamber are opened in sequence, followed by the opening of the impingement mixing device. In accordance to the relatively small diameter of the main mixing chamber, the mixture passes with relatively large flow velocity through the perpendicular arranged transfer dispense hole into the lower part of the cylindrical aftermixer chamber located oppositely. The aftermixer chamber is of larger diameter than the mixing chamber and has a slightly offset axis. This geometrical arrangement creates a largely upward, 180 degree deflection of the mixture on the rear wall of the aftermixer chamber and a turbulent flow pattern (Figure 10). A liquid particle passes statistically several times through the aftermixer area until it enters finally into the dispense outlet of the transfer cylinder. Here, the flow speed is slowed down in accordance to the increased flow area and the mixture leaves the dispense outlet in a laminar, non-splashing manner.

At the end of the mix operation, which may be in total 1 second and less, the cleaning rod of the mixing chamber is moved into the closed position, and in sequence also the rods of the aftermixer chamber and of the transfer cylinder for complete mechanical cleaning.

Lead-lag effects, due to off-ratio flows and inadequate mixing at the opening of the mixing head, were not observed. This is mainly the result of the proven automatic valving system incorporated in the impingement mixing device.

This patented valving system provides switch-over from high pressure recirculation to impingement, and vice versa, without interruption of the flow streams preventing related pressure changes in the material supply lines.

The design of the mix section of the free pour mixing head is similar to the type "A/2" head as discussed in an earlier chapter. The mixing chamber of the mixing head as shown, having nominal capacities of approximately 30 to 150 g/sec, has, for example, a diameter of only 1/8" (3.175 mm). The transfer cylinder has a diameter of 3/8" (9.525 mm).

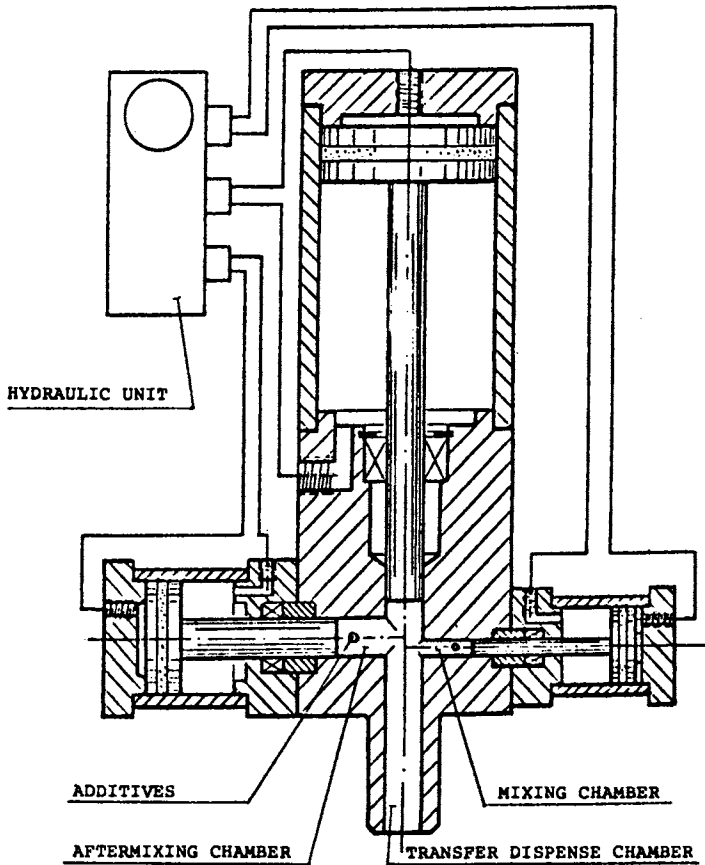


Figure 9. Cross section of free pour impingement mixing head in open position.

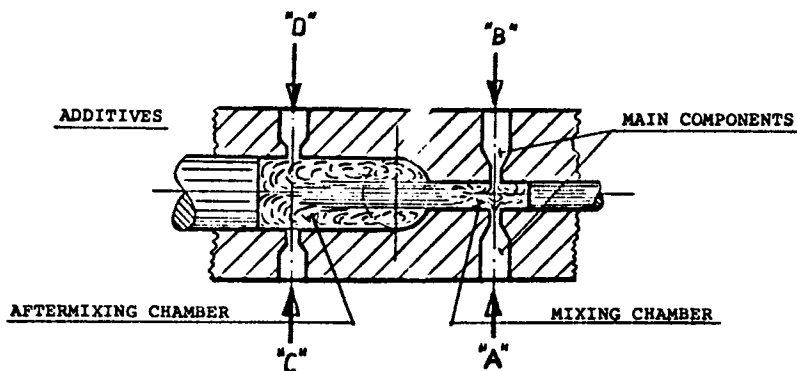


FIGURE 10.1

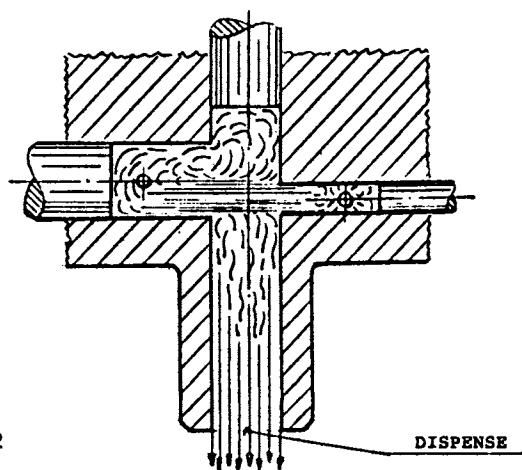


FIGURE 10.2

Figure 10. Schematic drawing of mixing area of free pour impingement mixing head. 10.1 top view, 10.2 side view.

The new free pour mixing head system can also be used for the addition of separate color streams, or other liquid additives, as third components. They are introduced in the turbulent section of the aftermixer chamber as indicated in the upper part of Figure 11.

The new free pour mixing head was tested with good results with a number of self-skinning flexible and rigid foam systems, including shoe sole formulations, which could formerly not be processed in free pour mode using conventional impingement mixing devices.

The principle of its design can be applied for any capacity requirements by according sizing.

The further development of the new mixing head is still in progress for optimizing its performance for different application and formulations.

It can be expected that the performance of the new mixing device is opening new applications for high pressure impingement mixing as well as its use for replacing conventional low pressure metering and mixing equipment on existing production lines because of its more economic and environmental friendly, solvent free operation.

The principle of the new mixing head is covered by a patent application (Ref. 4).

Acknowledgments

Photographs courtesy of Martin Sweets PTI.

Literature Cited

1. "Preliminary Model For RIM Impingement Mixing" by Lee, Ottino, Ranz, Macosko; SPI, 37th Annual Technical Conference, 1979.
2. "Metering and Mixing of RIM Reactants", by Schneider; "Reaction Injection Molding and Fast Polymerization Reactants", Polymer Science and Technology - Volume 18.
3. U. S. Patent No. 4,239,732.
4. U. S. Patent Application Serial No. 390,777.

RECEIVED September 12, 1984

Profiles of Temperature and State of Cure Developed Within Rubber in Injection Molding Systems

A. SADR, R. GRANGER, and J. M. VERGNAUD

Laboratory of Materials and Chemical Engineering, University of Saint-Etienne, U.E.R. of Sciences 23, Dr. Paul Michelon, 42023 Saint-Etienne Cédex, France

To reduce the time of cure cycle in processes of rubber injection molding, higher temperatures for vulcanization as well as for storage bulb are being used. Our purpose in this work was to determine the profiles of temperature gradients and state of cure developed through rubber sheets by using the kinetics of the cure reaction, the thermal properties of rubber and a convenient model. The kinetics of the overall cure reaction could be described by a single first-order reaction with a single activation energy, although vulcanization is a complex series of reaction. The calculation was solved applying an explicit method with finite differences, by taking into account the heat of the cure reaction and the heat transfer by conduction through the rubber and the mold-rubber interface. The effect of the values of the temperature of the mold and storage bulb on the profiles of temperature and state of cure developed within rubber was studied by considering rubber sheets of different thicknesses.

Up to now the rubber industry has shown great interest in the development of processes for faster vulcanization. Accordingly, higher temperature (1-2) for the mold and also the storage bulb are being used to reduce the time cycle of cure in injection molding processes for rubber. However, we believe that the best method of reducing the cure cycle without detriment to quality is to ensure that the process is properly carried out and stopped at the right time (3-4). Obviously, a sufficient knowledge on the time-temperature relation at any point within the rubber mass is required to attain this purpose.

Some early works (5-7) have shown that the temperature gradients developed in the rubber mass during vulcanization could be predicted by using the data of the cure kinetics and heat transfer. The extent of cure reaction could be determined by the balance of internal heat generation from the cure reaction, conduction through the rubber mass and the mold rubber interfaces.

0097-6156/85/0270-0279\$06.00/0
© 1985 American Chemical Society

The purpose of this work is to show that the values for temperatures of mold and storage bulb are important parameters in injection molding process of rubber. The study was performed by using two different thicknesses for rubber sheets and two values for the cure enthalpy. The problem was solved by applying an explicit numerical method with finite differences (6). Although rubber vulcanization consists of a complex series of reactions (8), the overall cure heat could be described by a first-order reaction with a single activation energy, as shown previously (6).

THEORETICAL

Mathematical Treatment. The unidirectional heat flow through the rubber sheet of thickness ℓ was expressed by the general equation of transient heat conduction

$$\frac{\partial T}{\partial t} = \frac{\partial}{\partial x} \left(\frac{\lambda}{\rho C} \cdot \frac{\partial T}{\partial x} \right) + \frac{1}{\rho C} \cdot \frac{dQ}{dt} \quad (1)$$

conduction heat reaction heat

by taking into account the internal heat generation from the cure reaction.

Initial and boundary conditions were as follows :

$$t = 0 \quad 0 \leq x \leq \ell \quad T = T_0 \quad \text{rubber space} \quad (2)$$

$$t \geq 0 \quad x < 0 \quad T = T_c \quad \text{mold space} \quad (3)$$

$$x > \ell$$

$$t > 0 \quad 0 < x < \ell \quad T = T_{xt} \quad \text{rubber space}$$

Although the sulfur vulcanization of the rubber was a complex chemical process "Equation 3", we found that the overall rate of cure was given by a single first-order reaction :

$$\frac{dQ(x,t)}{dt} = k (Q_\infty - Q_t) \quad (4)$$

the constant k having an Arrhenius form with a single activation energy (1, 6).

$$k = k_0 \cdot \exp - \frac{E}{RT} \quad (5)$$

where Q_t was the heat of cure reaction evolved up to time t , and Q_∞ the total enthalpy of this reaction, in the rubber volume unit.

Numerical Calculation. The problem was solved by using an explicit numerical method with finite differences.

According to our model (3) considering the section of the rubber sheet, the sheet was divided into n equal finite slices of thickness Δx . The heat balance was written on the plane n as follows :

$$T_{i+1,n} = \frac{1}{M} \left[T_{i,n-1} + (M-2)T_{i,n} + T_{i,n+1} \right] + \frac{1}{\rho C} \cdot \frac{dQ}{dt} \cdot \Delta t \quad (6)$$

where the dimensionless ratio M was

$$M = \frac{(\Delta x)^2}{\Delta t} \cdot \frac{\rho \cdot C}{\lambda} \quad (7)$$

and $T_{i+1,n}$ was the temperature at plane n and at time $(i+1)\Delta t$.

The heat generated by the cure reaction during the incremental time Δt by using the following equations, was calculated at the time $i \cdot \Delta t$.

$$Q_i = Q_\infty \left[1 - \exp(-S_i) \right] \quad \text{where } S_i = \int_0^{i\Delta t} k \cdot dt \quad (8)$$

$$\frac{dQ}{dt} \cdot \Delta t = Q_\infty \left[\exp(-S_i) - \exp(-S_{i+1}) \right] \quad (9)$$

and the approximative recurrent relation

$$S_{i+1} = S_i + k_{T_i} \cdot \Delta t \quad (10)$$

The two slabs of materials, steel mold and rubber, were assumed to be in perfect contact at the interface. We desired to employ the same modulus and the same incremental time Δt for both materials, so the thickness of the slices had to be different for the mold and the rubber. The heat balance at the interface led to the conclusion that the ratio of the thicknesses of the slices had to be taken as equal to the square root of the thermal diffusivities α_{mold} and α_{rubber} . The temperature is constant inside the mold at Δx from the interface.

$$\frac{\Delta x_{\text{mold}}}{\Delta x_{\text{rubber}}} = \left(\frac{\alpha_{\text{mold}}}{\alpha_{\text{rubber}}} \right)^{\frac{1}{2}} \quad (11)$$

EXPERIMENTAL

Vulcanizate Components. A rubber powder (50-100 micron grain size) recovered from old tires was used. The composition of this material was : 55 percent rubber hydrocarbon, 14 percent acetone extractables

and 25 percent carbon black. This commercial rubber powder was a mixture of NR and SBR in a ratio of about 2/3. Ultrafine powder of sulfur (2 % of the total weight) was used as vulcanizing agent.

Vulcanization Kinetics Studies. These studies were performed using a microcalorimeter (SETARAM=DSC111) working in isothermal conditions. About 100-150 mg of the compound encapsulated in the holder was introduced into the sensitive zone (1,6). The response of the DC is directly related to the rate of enthalpy change with the time.

The data concerned with kinetics parameters and heat transfer were shown in "Table I".

Temperature Measurement at the midplane of Rubber Sheet. Three series of temperature measurements were of interest in this work : the temperature of the mold ; the difference between the temperature of the mold and that measured at the midplane of rubber sheets ; the temperature of the rubber just before its introduction into the mold.

Table I. Thermal Properties of Rubber

Sample 1	: $Q_{\infty} = 10$ cal/g of total rubber mixture
Samples 2	: $Q_{\infty} = 12$ cal/g of total rubber mixture
Samples 4 and 5	: $Q_{\infty} = 18.1, 14.5$ cal/g of total rubber mixture
$\alpha = \lambda / \rho C = 3.1 \times 10^{-3} (1 - 10^{-3} T)$ (cm ² /s)	
$\rho.C = 0.41 [1 + 2.5 \times 10^{-3} (T - 293)]$ cal/cm ³ . K	
$E = 25.4$ kcal/mole $k_0 = 3.10^9$ (s ⁻¹) (eq. 5)	
λ : thermal conductivity	ρ : density C : heat capacity
E : energy of activation	T : (K) k_0 : reaction constant

RESULTS

Several parameters of interest were considered in this work : the one concerned with the operational conditions of the rubber in the storage bulb as time and temperature, the other with the working conditions in the mold as mold temperature, cure time, thickness of rubber sheets, cure enthalpy (or % vulcanizing agent).

State of cure of rubber in the storage bulb as a function of time and temperature. In order to reduce the cure time, higher temperatures are being desired for the rubber in the storage bulb. But too high a temperature might be responsible for an intempesive reaction of vulcanization in the storage bulb. So it is necessary to have a sufficient knowledge on the rate of the cure reaction as a function of temperature and time, in order to be able to predict the right time at which the rubber may be stored without detriment to the working of injection process.

The results from calorimetric experiments are expressed by the ratio Q_t/Q as a function of time and temperature in "Figure 1".

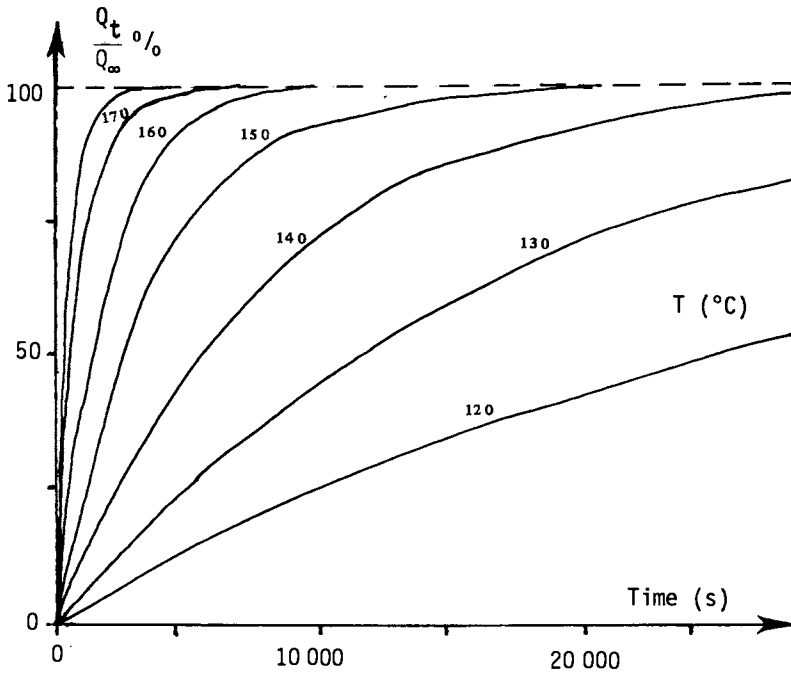


Figure 1. Extent of cure heat vs. time for different storage bulb temperatures.

These results depend only on the kinetics parameters as the reaction constant and activation energy ; they do not depend on the value of the cure enthalpy. The effect of temperature on the state of cure is clearly shown. So, half an hour heating in the storage bulb sets to a state of cure of 20 % when rubber is at 140°C, and 35 % at 150°C.

Variation of midplane temperature with time for different values of the temperature of the injected rubber. Effect of rubber sheet thickness. The temperature of rubber sheet at the midplane is of interest. As shown in previous studies (3) on the profiles of temperature developed through rubber sheets, the highest temperature is obtained at the sheet midplane because of the cure enthalpy. It is easy to make measurements at this place.

The midplane temperature of rubber sheet in the mold rises from the initial temperature T_{ir} (temperature of the injected rubber) to the mold temperature T_m , by reaching peak as shown in "Figure 2" for a thickness of 1 cm and "Figure 3" for 2 cm. Different values were selected for the temperature of the injected rubber within the 20-140°C range. A good correlation was found between the experimental values and the calculated ones.

The increase in the temperature of the injected rubber T_{ir} is responsible for two effects worth noticing :

- The maximum values obtained by the midplane temperature are about the same when the injected rubber temperature is varied.
- The maximum value of the midplane temperature is reached at a shorter time when the temperature of the injected rubber is increased.
- The effect of the thickness of the rubber sheet is of importance. The time necessary for the midplane temperature to reach its maximum value is about proportional to the sheet thickness as shown in "Table II".

Table II. Maximum Value of the Midplane Temperature

Temperature of injection rubber	20	100	140
1 cm thick Time (s)	630	570	480
2 cm thick Time (s)	1 400	1 200	1 040
1 cm thick Max. Temperature (°C)	182.8	182.8	182.8
2 cm thick Max. Temperature (°C)	184.8	184.8	184.9

- The temperature-time curves can be obtained from one another by a translation time as shown in "Table III".

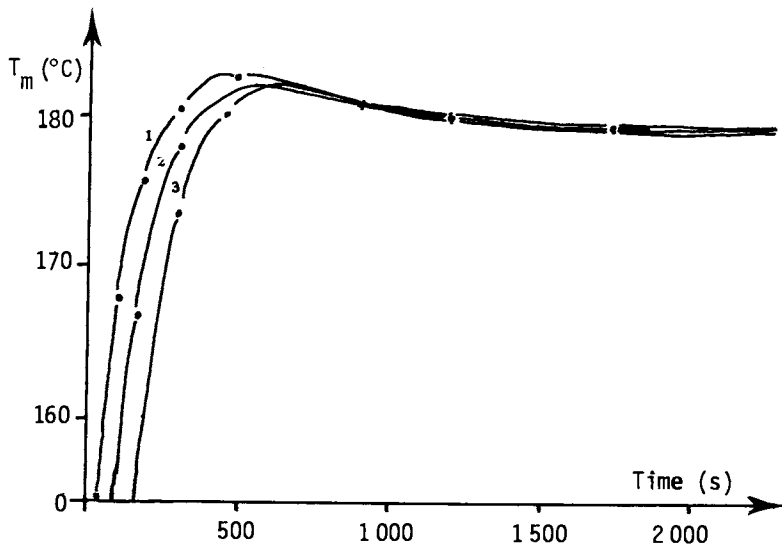


Figure 2. Midplane temperature vs. time for several rubber temperatures at injection. 1:140°C 2:100°C 3:20°C
1 cm thick sheet Cure enthalpy:10 cal/g $T_m = 180^\circ\text{C}$

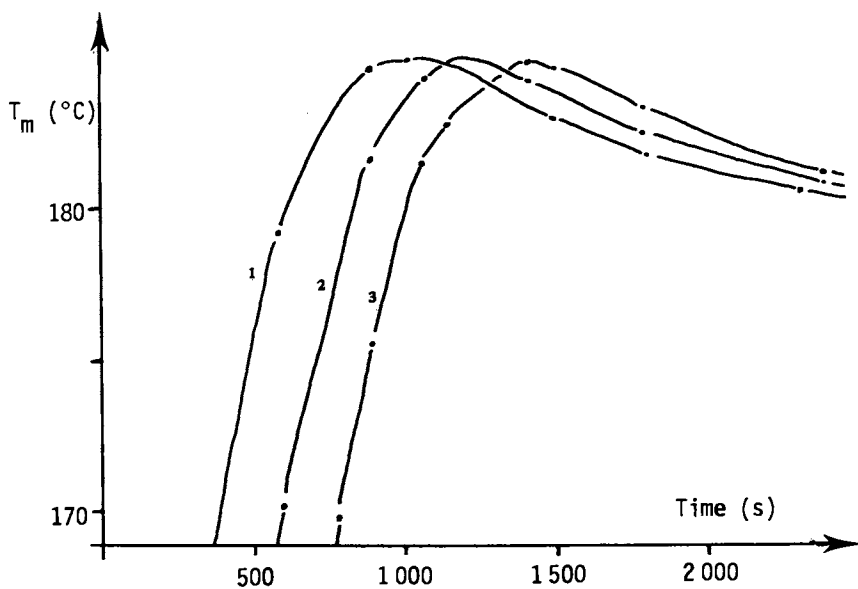


Figure 3. Midplane temperature vs. time, for several rubber temperatures at injection. 1:140°C 2:100°C 3:20°C
2 cm thick sheet Cure enthalpy:10 cal/g $T_m = 180^\circ\text{C}$

Table III. Translation Time for Midplane Temperature-Time Curves

Midplane temperature	180	T_{\max}
1 cm thick $T_{ir} = 20$ $T_{ir} = 100$	70	70
$T_{ir} = 100$ $T_{ir} = 140$	60	60
2 cm thick $T_{ir} = 20$ $T_{ir} = 100$	190	190
$T_{ir} = 100$ $T_{ir} = 140$	210	200

Variation of the state of cure with time for different values of the temperature of injected rubber. Effect of sheet thickness. One of the most interesting applications of temperature calculation during the vulcanization is the estimation of the state of cure. In this work, the state of cure is expressed by the ratio Q_c/Q_∞ and it corresponds to the extent of the heat of cure evolved at time t (6).

The state of cure obtained at the midplane of rubber sheets is plotted as a function of time, for three values of the temperature of injected rubber, for a thickness of 1 cm (Figure 4) and 2 cm (Figure 5), while the mold temperature is kept constant at 180°C.

The temperature of injected rubber and the sheet thickness are found to be parameters of interest :

- An increase in the temperature of injected rubber produces a reduction in the time necessary for the state of cure to reach any selected value. Moreover, the state of cure-time curves are similar for the different values of T_{ir} and are displaced from one another by a translation along the time axis, as shown in "Table IV".

Table IV. Decrease in the Cure Time(s)

State of cure	25	50	75	90
1 cm from $T_{ir} = 20$ to $T_{ir} = 100$	55	58	55	55
$T_{ir} = 100$ to $T_{ir} = 140$	70	65	70	65
2 cm from $T_{ir} = 20$ to $T_{ir} = 100$	200	190	196	190
$T_{ir} = 100$ to $T_{ir} = 140$	200	200	196	200

- The reduction in the cure time due to the increase in the temperature of injected rubber in the mold is found to vary largely with the thickness of rubber sheets. The interest of the use of a high temperature for the storage bulb is clearly shown in "Table III" and "Table IV", especially for thick rubber sheets.

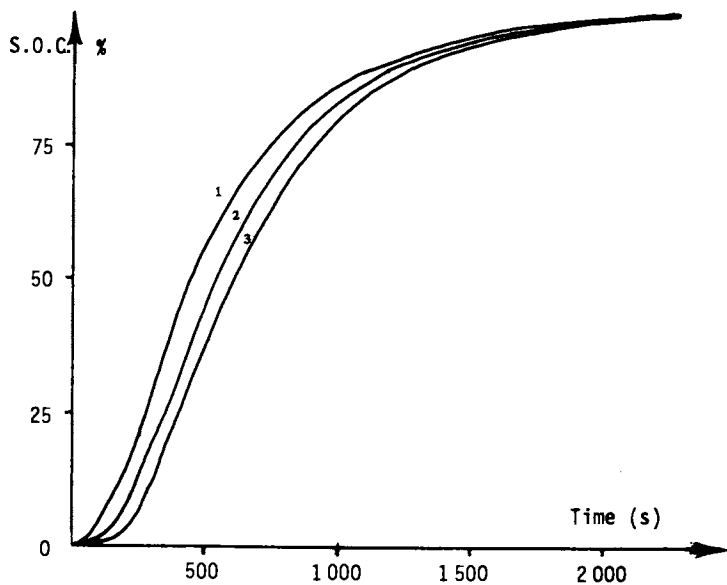


Figure 4. S O C at the midplane vs. time, for several rubber temperatures at injection. 1:140°C 2:100°C 3:20°C
1 cm thick sheet Cure enthalpy:10 cal/g $T_m = 180^\circ\text{C}$

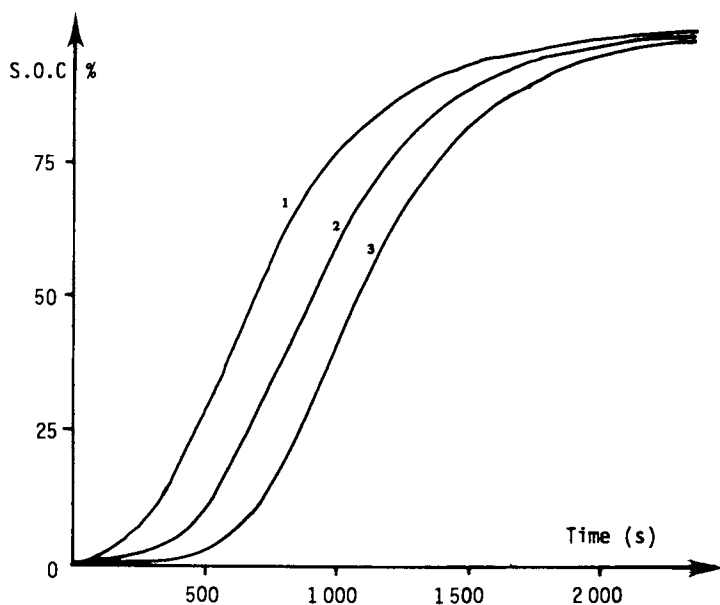


Figure 5. S O C at the midplane vs. time, for several rubber temperatures at injection. 1:140°C 2:100°C 3:20°C
2 cm thick sheet Cure enthalpy:10 cal/g $T_m = 180^\circ\text{C}$

Table V. Maximum Temperature at the Midplane as a Function of Enthalpy

Cure enthalpy (cal/g)	10	12	14.5	18.1
Max. temperature (°C)	184.9	186.6	188.9	192.8
2 cm thick $T_{ir} = 140^{\circ}\text{C}$ $T_m = 180^{\circ}\text{C}$				

Variation of the midplane temperature with time for different values of cure enthalpy. "Figure 6" shows the variation of the midplane temperature with the time obtained by using different values of the cure enthalpy (10, 12, 14.5, 18.1 cal/g), while the temperatures of the mold and the injected rubber were kept constant. Higher is the value of cure enthalpy and higher is the maximum value reached by the midplane temperature.

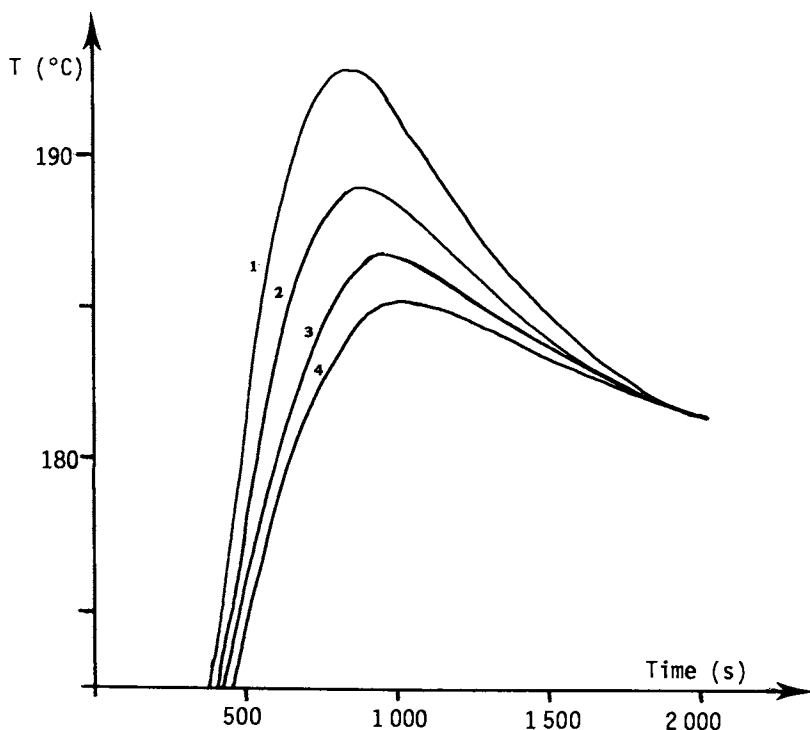


Figure 6. Effect of cure enthalpy on the temperature-time curves at the midplane of 2 cm thick sheet. Cure enthalpy (1 = 18.1 ; 2 = 14.5 ; 3 = 12 ; 4 = 10 cal/g.) $T_m = 180^{\circ}\text{C}$
 $T_{ir} = 140^{\circ}\text{C}$

The time at which the midplane temperature reached its maximum value is reduced when the cure enthalpy is increased.

Variation of state of cure-time curves with the cure enthalpy. As shown in "Figure 7" for 2 cm thick sheets, the effect of a little variation in the cure enthalpy on the profiles of the midplane temperature-time curves is very important. The slope of these curves is increased notably when the cure enthalpy is higher.

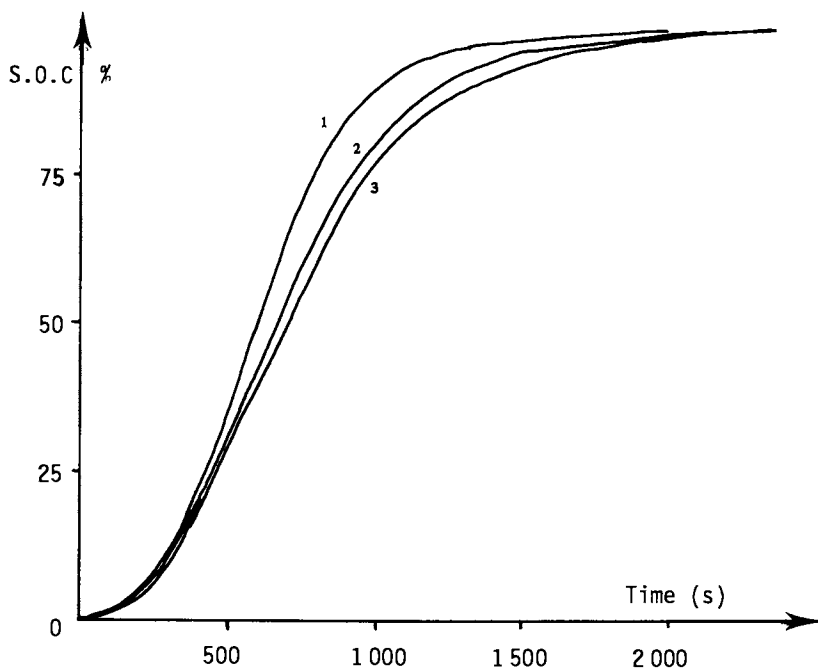


Figure 7. Effect of cure enthalpy on the S O C-time curves at the midplane of 2 cm thick sheet. Cure enthalpy (1 = 18.1 ; 2 = 14.5 ; 3 = 12 ; 4 = 10 cal/g.) $T_m = 180^\circ\text{C}$ $T_{ir} = 140^\circ\text{C}$

CONCLUSIONS

Calorimetry was proved to be an interesting technique for studying the kinetics of the reaction of vulcanization. Our model for the heat transfer and cure reaction was very useful for calculating the values of the temperature and state of cure at the midplane of rubber sheets. The effect of some parameters as the temperature of injected rubber, sheet thickness and cure enthalpy on the profiles of temperature and state of cure at the midplane was considered, by studying the injection molding process. An increase in the temperature of injected rubber is responsible for a time translation of midplane temperature-time curves and state of cure-time curves by shortening the cure time. A limitation in the value of the temperature of injected rubber was found by calculating the rate of cure for the rubber in the storage bulb. The effect of the sheet thickness on the profiles shown above was found of great importance, while the effect of a variation in the cure enthalpy on these profiles was secondary.

NOMENCLATURE

$T_{i,n}$	Temperature at time $i\Delta t$ and space n
Δt	Increment of time
Δx	Increment of space
Q_t	Heat of cure reaction evolved up to time t
Q_∞	Total heat of cure reaction
M	Modulus, dimensionless number
λ	Thermal conductivity of rubber
ρ	Density of rubber
k_0	Constant of cure reaction
E	Activation energy of cure reaction
C	Heat capacity of rubber

LITERATURE CITED

1. Mukhopadhyay, R. ; De, S.K. ; Rubber Chem. Technol., 1978, 51, 704.
2. Khowmick, A.K. ; Mukhopadhyay, R. ; De, S.K. ; Rubber Chem. Technol., 1979, 52, 725.
3. Accetta, A. ; Vergnaud, J.M. ; 122 nd Rubber Div. Meet., Am. Chem. Soc. , Chicago, 1982.
4. Accetta, A. ; Vergnaud, J.M. ; Rubber Chem. Technol., 1983, 56.
5. Accetta, A. ; Vergnaud, J.M. ; Internat. Rubber Conf., Paris, 1982.
6. Accetta, A. ; Vergnaud, J.M. ; Thermochemica Acta, 1982, 59, 149.
7. Accetta, A. ; Gangnet, G. ; Vincent, L. ; Vergnaud, J.M. ; 3rd Internat. Congress on Computers and Chem. Engng., Paris, 1983.
8. Coran, A.Y. in "Science and Technology of Rubber", Eirich, Ed. ; Academic Press ; New York, 1978, 7.
9. Sadr, A. ; Granger, R. ; Vergnaud, J.M. ; J. of Appl. Polymer Sci., in press.

RECEIVED April 30, 1984

Author Index

- Alberino, L. M., 3,125
Alfonso, Giovanni Carlo, 163
Barksby, N. 83
Blackwell, John, 53
Camargo, R. E., 27
Chiappori, Carmen, 163
Cornell, M. C., 15
Cross, M. M., 97
Damusis, A., 65
Dunn, D., 83
Gabbert, J. D., 135
Girgis, Mikhail, 225
Granger, R., 279
Hedrick, R. M., 135
Kaye, A., 83,97
Kresta, J. E., 111
Lee, Chun Dong, 53
Lin, T. B., 65
Lloyd, E. T., 15
Lockwood, R. J., 125
Macdonald, Christine E., 53
Macosko, C. W., 27
McClellan, T. R., 3
Menges, G., 237
Meyer, Louis W., 195
Mrotzek, W., 237
Müller, H., 237
Plevyak, Joseph E., 213
Quay, Jeffrey R., 53
Razore, Sandro, 163
Regelman, D. F., 125
Russo, Saverio, 163
Sadr, A., 279
Schneider, Fritz W., 259
Sobieski, Loretta A., 213
Stanford, J. L., 83,97
Stepto, R. F. T., 83,97
Tirrell, M., 27
Turner, Robert B., 53
van der Loos, J. L. M., 181
van Geenen, A. A., 181
Vergnaud, J. M., 279
Wellinghoff, S. T., 27
Wohl, M. H., 135
Wongkamolsesh, K., 111

Subject Index

A

- Acetylcaprolactam, 138
Acylactam(s), 142
 nylon copolymer formation, 144
 reaction with primary amines, 139f
 structure, 138
Adiabatic reaction(s), 67
Adiabatic reactor data, urethane
 elastomers, 71-73f
Adipoylbiscaprolactam, 138
After-mixers, 247-48
Agglomeration(s), in straight-line
 dependence deviations, 65
Alkene(s), reactivity toward
 isocyanates, 126
Alkoxyacetylene(s), formation of
 ketene animals, 133
Amine(s), primary, reaction with
 acyllactams, 139f
3-Aminopropyl triethoxysilane, 140
Amorphous systems, polyurethane
 elastomers, 33
Anionic polymerization,
 caprolactams, 136-38
 initiation, 138
 thermal initiation, 137f
 termination reaction, 136
Annular cone and plate, 100-102
Annular vs. truncated cones, 101f
Aromatic diisocyanate(s), RIM
 elastomers, 81
Arrhenius equation, second-order
 reaction, 67
Automotive industry, operating
 efficiencies, 18
Automotive RIM, 4t

Author Index

- Alberino, L. M., 3,125
Alfonso, Giovanni Carlo, 163
Barksby, N. 83
Blackwell, John, 53
Camargo, R. E., 27
Chiappori, Carmen, 163
Cornell, M. C., 15
Cross, M. M., 97
Damusis, A., 65
Dunn, D., 83
Gabbert, J. D., 135
Girgis, Mikhail, 225
Granger, R., 279
Hedrick, R. M., 135
Kaye, A., 83,97
Kresta, J. E., 111
Lee, Chun Dong, 53
Lin, T. B., 65
Lloyd, E. T., 15
Lockwood, R. J., 125
Macdonald, Christine E., 53
Macosko, C. W., 27
McClellan, T. R., 3
Menges, G., 237
Meyer, Louis W., 195
Mrotzek, W., 237
Müller, H., 237
Plevyak, Joseph E., 213
Quay, Jeffrey R., 53
Razore, Sandro, 163
Regelman, D. F., 125
Russo, Saverio, 163
Sadr, A., 279
Schneider, Fritz W., 259
Sobieski, Loretta A., 213
Stanford, J. L., 83,97
Stepto, R. F. T., 83,97
Tirrell, M., 27
Turner, Robert B., 53
van der Loos, J. L. M., 181
van Geenen, A. A., 181
Vergnaud, J. M., 279
Wellinghoff, S. T., 27
Wohl, M. H., 135
Wongkamolsesh, K., 111

Subject Index

A

- Acetylcaprolactam, 138
Acylactam(s), 142
 nylon copolymer formation, 144
 reaction with primary amines, 139f
 structure, 138
Adiabatic reaction(s), 67
Adiabatic reactor data, urethane
 elastomers, 71-73f
Adipoylbiscaprolactam, 138
After-mixers, 247-48
Agglomeration(s), in straight-line
 dependence deviations, 65
Alkene(s), reactivity toward
 isocyanates, 126
Alkoxyacetylene(s), formation of
 ketene animals, 133
Amine(s), primary, reaction with
 acyllactams, 139f
3-Aminopropyl triethoxysilane, 140
Amorphous systems, polyurethane
 elastomers, 33
Anionic polymerization,
 caprolactams, 136-38
 initiation, 138
 thermal initiation, 137f
 termination reaction, 136
Annular cone and plate, 100-102
Annular vs. truncated cones, 101f
Aromatic diisocyanate(s), RIM
 elastomers, 81
Arrhenius equation, second-order
 reaction, 67
Automotive industry, operating
 efficiencies, 18
Automotive RIM, 4t

B

Barbituric acid derivative(s),
 formation, 128
 Base-catalyzed polymerization of
 lactam(s), 136
 Baseball bats, foam-filling
 equipment, 264f,265f
 Benzoyl chloride, effect on tin
 catalysts, 116
 Bimodal distributor(s), high,
 rationale, 42
 Bisacyllactam, structure, 142
 Bis(4-morpholino)ethylene, 133
 reaction with MDI, 129
 Block copolymer(s)
 nylon, 142-58
 See also Nylon block copolymers
 dynamic modulus curves, 147f
 effect of polyol content, 145t
 heat sag values, 149
 moisture effect, 149
 polyether effects on impact
 strength/stiffness, 147f
 prepolymer formation, 142
 properties, 144-45
 reaction exotherm, 156f
 viscosity comparison, 155f
 phase mixing effects, 45
 Body panel(s), polyurethane-RRIM,
 thickness, 18
 1,4-Butanediol, 68
 n-Butanol effect, DBTDL, IR
 spectra, 116

C

Calcined clay, 140
 Caprolactam(s), 154
 acyllactam-initiated
 polymerization, 137f
 anionic polymerization, 136-38
 initiation, 138
 thermal, 137f
 termination reaction, 136
 polymerization, 135
 preferred catalyst, 144
 reaction with isocyanates, 138
 Caprolactam magnesium bromide,
 preferred catalyst, 144
 Carbamoyl chloride, effect on tin
 catalysts, 116
 CaSiO₃--See Wollastonite
 Catalysis, 111
 polyurethane elastomers, 45
 Chopped integral strands
 heat sag effect, 234,235t
 notched Izod impact strength,
 effect, 232,233t

Chopped integral strands--Continued
 packing fraction, 99f
 reinforcement
 flexural modulus, 231t,232
 surface quality, 229
 Class A surface
 definition, 229
 obtaining, 21
 Clogging effects, solid filled
 systems, avoidance, 266
 Compression molding, estimated
 capital, 21t
 Cone and plate viscometer(s)
 annular, 100-102
 displaced, 100
 shear rate, highest attainable, 105
 viscosity determination, 102
 Cone and plate viscometry, 100-105
 Consumer application(s), 4,5t
 Cross-link(s)
 fringed micelle crystallites, 66
 physical
 decay, temperature effects, 76-80
 density and plasticizer
 effects, 78
 Crystalline aggregate(s),
 formation, 81
 CSG--See Chopped strand glass
 Cure cycle, time reduction, 279
 Cylindrical mold, flow front
 profiles, 253f

D

DAO--See 1,4-Diazo 2,2,2 octane
 Dashboard--See Fascia
 DBTDL--See Dibutyltin dilaurate
 Densitometer scans, MDI, 57,58f
 Diazo 2,2,2 octane, catalysis of
 isocyanate groups, 113t
 Dibutyltin dilaurate
 catalysis of isocyanate groups, 113t
 dissociation, lauric acid
 effects, 118f
 interaction with carbamoyl chloride,
 IR spectra, 119f
 IR spectra, 115f
 n-butanol effect, 116,117f
 ligand exchange, 114-16
 specific conductance, 117f
 structure characteristics, 114
 urethane reaction, catalysis
 mechanism, 118f
 Differential scanning calorimetry
 polyurethane
 elastomers, 32,38,40f,41f
 urethane elastomers, 75,80
 Diisocyanate(s), aromatic, RIM
 elastomers, 81

Direct gate, 240f
 Direct gating, 239
 Displaced cone and plate, 100
 DSC--See Differential scanning calorimetry
 Dynamic mechanical spectroscopy, polyurethane elastomers, 32

E

Economic advantage(s), 15
 Efficient mixing, achieving, 88
 EG--See Ethylene glycol
 Elastomer properties, hard segments, 130t, 131t
 Enamine(s), reactivity, 126
 Energy balance equation, 67
 Engineering plastic(s), development, 8t
 Engineering rubber(s), features, 7t
 Epoxy formulations, processing equipment, 269, 271
 Epoxy RIM material(s), 9
 Equipment, 259-78
 flow diagram, 85f
 operation, 84-89
 special needs, 9
 usage, 5t
 Ethoxyacetylene, ketene aminals, formation, 133
 Ethylene glycol, 56
 External mold release, application time, 216

F

Fan gate, 242
 IKV version, 240-47
 method, 241
 narrow, 244f
 Fascia, RIM use, 15-17
 Fiber glass reinforcements, in urethanes, 225-36
 Filled polyurethane(s), 95
 Filling pattern method, 250-57
 Film gating, 241
 Fir-tree mixer, 249f
 Fixture(s), 20t
 Flaked glass, disadvantage, 228
 Flow, pressure drop, 243
 Foaming, use, 150
 Fox's equation, 47
 Free pour impingement mixing head, 271, 274
 cross section, 275f
 Fringed micelle crystallite(s), formation, 65-66

G

Gel permeation chromatography, polyurethane elastomers, 32
 Glass fiber(s), 97-110
 packing fraction, 98-100
 Glass fiber slurries, shear thinning, 102
 Glass flakes, 226
 reinforcement, surface quality, 229
 GPC--See Gel permeation chromatography
 Growth, 5, 15

H

Hagen-Poiseuille principle, 251
 Hammer-milled glass--See Milled glass fibers
 Hammett equation, 113
 Hard segment(s), 5
 and material type, 7t
 chain extender, 54
 content, definition, 29
 percentage vs. elastomer properties, 130t, 131t
 polyurethane elastomers, 27, 28f
 variations and use, 6
 Hard segment polymer(s), properties, 7t
 HDI--See 1,6-Hexamethylene diisocyanate
 High-polydispersity ratio(s), rationale, 42
 High-shear RRIM viscometer, 105-8
 HMG--See Milled glass fibers
 Hot process equipment, 272f

I

Impact strength, chopped integral strands, 232
 Impingement injection mixing, 238
 Impingement mixing, 12f
 equipment, 259-61
 maximum operational pressure, 261
 Reynolds number, 88
 IMR--See Internal mold release, 22
 Incompatible polyols, in polyurethanes, 86t
 Industrial consumer application(s), 4, 5t
 Injection molding, estimated capital, 21t
 Interior trim foam, market usage, 4
 Internal mold release, 22
 agent, requirements, 217
 economic advantages, 216
 multiple stream, 222

Internal mold release--Continued

- need, 216
- nylon system, 157
- RRIM, 23t
- technology, 23
- Intersegmented interactions,
 - absence, 47
- Isocyanate(s)
 - electron density, 112
 - polarized complexes, formation, 113
 - reaction with caprolactams, 138
 - reaction with organotin
 - catalysts, 112
 - reactivity with alkenes, 126
- Isocyanurate, urethane modified, 9
 - fiber length effects, 12t

J

- J-car fascia, molding with
 - IMR, 218,220

K

- Ketene acetals
 - formation of ketene aminals, 133
 - structure, 128
- Ketene aminal(s)
 - moisture effects, 127
 - preparation, 133
 - reactivity, 126
 - RIM polymerizations, 129-32
 - structure, 126
- Ketene aminal-isocyanate(s), 125-34
 - specific reaction, 126-28
- Krauss-Maffei head, 88

L

- Lactam(s), base catalyzed
 - polymerization, 136
- Lauryl lactam, 154
- Loss tangent, polyurethanes, 93,94f
- Low-pressure casting, 150
 - nylon systems, 160-61

M

- Market(s), automotive, 3-4
- MDI--See Modified diphenylmethane
 - 4,4'-diisocyanate
- Milled glass fibers, 226
 - bulk volume determination, 98
 - length requirement, 228
 - as reinforcement, flexural
 - modulus, 229,231t
 - tensile strength, effect, 232

Mineral reinforcement, 140

Mixing

- efficiency
 - predicting, 260
 - achieving, 88
- impingement, 238
- Mixing head, 263f
 - free pour impingement, 271,274
 - cross section, 275f
 - industrial application, 262
 - open molds, 274
 - small size, 261-62
- Modified diphenylmethane
 - 4,4'-diisocyanate
 - characteristics, 56
 - densitometer scans, 57,58f
 - differential scanning
 - calorimetry, 56
 - dynamic mechanical data, 56,63f
 - heat sag, 56
 - mechanical testing, 56
 - reaction, 129
 - X-ray diffraction, 56,57,58f,59f
 - Modified diphenylmethane
 - 4,4'-diisocyanate/ethylene glycol,
 - X-ray diffraction, 54,55f
- Mold(s)
 - cylindrical, flow front
 - profiles, 253f
 - design, problems, 250
 - nylon systems, 159-60
- Moldfilling
 - air entrapment, 240f
 - avoiding, 245,247,257
 - filling pattern method, 251
 - flow management, 239-47
 - island geometry, 245
 - polyurethane, 237-58
 - process, 11
- Molecular weight determination,
 - polyurethane
 - elastomers, 38,41f,42,43f

N

- Narrow fan gate, 244f
- NCO group--See Isocyanates
- Nonautomotive market(s), 4
- Nucleation, internal release
 - agents, 217
- Nylon(s), vs. urethanes, 154-58
- Nylon 6, 9,135-62
 - melting point, 135
 - particulate reinforcement, 140
 - RIM, 138-42
- Nylon block copolymer(s), 142-58
 - adsorption effects, 151f
 - dynamic modulus curves, 147f
 - effect of polyol content, 145t

- Nylon block copolymer(s)--Continued
 heat resistance, 146,149
 heat sag values, 149
 heat sag/flexural modulus, 149t
 immersion growth data, 153f
 moisture effect, 149
 molding processes, 150
 morphology, 146
 polyether effects on impact strength/stiffness, 147f
 prepolymer formation, 142
 properties, 144-45
 reactions, 142-44
 exotherm, 156f
 relative humidity effects, 152f
 structure, 146
 synthesis, 142
 temperature modulus response, 149t
 use of polyol rubber blocks, 150
 viscosity comparison, 155f
- Nylon processing, equipment, 269,271
- Nylon system(s)
 equipment requirements, 158-60
 gel times, 154
 injection rates, 157
 internal mold release, 157
 low-pressure casting, 160-61
 molds, 159-60
 monomers, 154
- O
- Open molds, mixing head, 274
- Organic-silicone hybrid technology--
 See Silicone-organic hybrid(s)
- Organotin catalyst(s)
 in urethane systems, 111-21
 reaction with isocyanates, 112-14
- Orthoester(s), formation of ketene
 aminals, 133
- Ovens, hot process equipment, 273f
- P
- Packing fraction
 calculation, 98
 chopped strand glass reinforcement, 99f
 as function of weight averages, 101f
- Paintability, internal release
 agents, 217
- Particle cone(s), difficulties, 100
- Particulate reinforcement, 140
- PC alloy
 capital, 22t
 hourly labor cost, 20,21t
- PEDA--See Polyether diamine
- Phase separation
 premature, 46
 segmented polyurethane(s), 95
- Phase-separation studies, 27-52
- Phenyl-isocyanate diadduct,
 structure, 127
- Physical cross-links
 decay, temperature effects, 76-80
 density and plasticizer effects, 78
- Plant(s), typical, 17
- Plaque thickness, 89
- Plasticizer(s), effect of
 cross-links, 76,79
- Polyamide(s)
 particulate reinforcement, 140
 preparation, 129
 solution derived, preparation, 133
- Polyether, structure, 142
- Polymerization
 rapid, 46
 shrinkage, compensation, 150
- Polyol(s)
 and polyurethanes, tensile properties, 93t
 characteristics, 30
 high-shear rate data, 108
 incompatible, in polyurethanes, 86t
 molecular weight increases, 46
 rheology, 97-110
- Polyol rubber block (s), use in nylon
 block copolymers, 150
- Polyurethane(s)
 amine additive effects, 53-64
 amorphous systems, 33
 glass transition temperatures, 48t
 block composition, 53
 crystalline systems, 45-47
 differential scanning calorimetry, 32,38,40f,41f
 dynamic mechanical spectra, 32,33
 dynamic mechanical temperature behavior, 93-95
 filled, 95
 flexural modulus-temperature behavior, 90,92f,93
 foam molding, mold-filling operation, 255
 gel permeation chromatography, 32
 hard-segment composition, 27, 28f
 incompatible polyols, 86t
 mechanical properties, 33
 moldfilling, 237-58
 molecular weight determination, 38,41f,42,43f
 noncrystalline systems, 47-49
 reinforced RIM
 capital, 22t
 hourly labor costs, 21t
 thickness for body panels, 18

Polyurethane(s)--Continued

- RIM, 15-26
 - production, 29,32
 - segmented, phase separation, 95
 - tensile properties, 42,93t
 - tensile stress-strain, 90,91f
 - transitional behavior, 93,94f
 - unfilled, 89-90
 - wide angle X-ray
 - scattering, 32,38,39f
- Premature phase separation, 46
- Pressure recording, reinforced RIM, 107f
- Process efficiency, 18
- Process energy cost comparison, 19t
- Processing, solid-filled system, 262, 266-67
- Productivity, 18t
- PU--See Polyurethane(s)
- PU-RIM--See Polyurethane(s), RIM

Q

Quartz, 140

R

- Reinforced RIM, 11
 - automotive, 4t
 - flow rate, 105
 - internal mold release, 23t
 - pipe diagram, 230f
 - pressure recording, 107f
 - volume recording, 107f
- Reinforced RIM viscometer
 - correction factors, 106,108
 - high shear, 105-8
- Resin transfer molding, 150
- Reynolds number, calculating, 260
- RIM
 - basic principle, 226
 - cycle, 214,215f
 - equipment, 259-78
 - flow diagram, 268f
 - low capacity, 267,269
 - medium capacity, 267,269
 - estimated capital, 21t
 - hourly labor cost, 20
 - process, 227f
 - processing, parameters used, 89t
- RIM-polyurethane(s), reaction systems, 84
- Rotational casting, 150,154
- RRIM--See Reinforced RIM
- Rubber
 - injection temperature and rubber sheet thickness, 284
 - state of cure, 279-91
 - in storage bulb, 282-84

Rubber--Continued

- temperature profiles, 279-91
- thermal properties, 282t
- Rubber vulcanization
 - injection temperature and state of cure, 286
 - mathematical treatment, 280
 - midplane temperature, 284t
 - as function of enthalpy, 288t
 - numerical calculation, 281
 - rubber sheet thickness effect, 285f
 - state of cure and cure time, 286t
 - by sulfur, 280

S

- Second-order reaction
 - adiabatic, 67
 - Arrhenius equation, 67
- Segmented polyurethane(s), in phase separation, 95
- Sheet-molding compound(s)
 - capital, 22t
 - hourly labor cost, 20,21t
 - tooling/fixtures, 20
- Silicone(s)
 - internal mold release technology, 213-24
 - tailormade, IMR agents, 219f
- Silicone-organic hybrid(s)
 - internal mold release, 218-21
 - agents, 221-22
 - paintability problems, 218
- SiO₂--See Quartz
- SMC--See Sheet-molding compound(s)
- Solid-filled systems
 - efficient mixing, 266
 - processing, 262,266-67
- Solvation effect, on dibutyltin dilaurate, 116
- Sprue gate, 242,249f
 - problems, 247
- Storage bulb, temperature in rubber vulcanization, 282-84
- Straight-line dependence, effect of RIM composition, 74,76
- Stress-strain, tensile,
 - polyurethanes, 90,91f
- Structure-property relationship(s),
 - polyurethane, 53-64,83-96

T

- Tensile elongation at break, with reinforcement, 234
- Tensile elongation values, with reinforcement, 235
- Tensile properties, polyurethane elastomers, 42

- Tensile strength data, with reinforcement, 233t
- Thin section moldings, flow management, 240f
- Tin catalyst(s)
activity, hydrolyzable chlorine effects, 116,120
role in isocyanate polarization, 114
- Tool(s), 20t
- Torsion pendulum data, polyurethanes, 93,94f
- Triethyl orthoacetate, 128
- Trim waste, 18-19
- Truncated vs. annular cones, 101f
- U
- Unfilled polyurethane(s), 89-90
- Urethane(s)
adiabatic reactor data, 71-73f
adiabatic temperature vs. rigid segments, 73f
components, 69t
cross-links, temperature effects, 70
DSC, 75,80
fiber glass reinforcements, 225-36
milled glass, 228
gel times, 154
morphology, 65-82
physical properties, 70
plasticizer modification, 69,74t
raw materials, 16
use for auto parts, 226
viscosity comparison, 155f
vs. nylon, 154-58
- Urethane-modified isocyanurate, fiber length effects, 12t
- Urethane reaction(s)
adiabatic reaction kinetics, 68
catalysis, mechanism, 111
dibutyltin dilaurate, catalysis mechanism, 118f
noncatalyzed, 113
organotin catalysis, 111-21
- Urethane segmented block copolymer(s), 5
- Urethane structural foam, market usage, 5t
- V
- Vinylamine(s), reactivity, 126
- Viscometry, cone and plate, 100-105
- Viscosity, equation, 102
- Volume recording, reinforced RIM, 107f
- Vykan, 140
- W
- Wide angle X-ray scattering, 32
polyurethane elastomers, 38,39f
- Wollastonite, 140
- X
- X-ray scattering
modified diphenylmethane 4,4'-diisocyanate, 57,58f,59f
wide angle, polyurethane elastomers, 32,38,39f

*Production by Meg Marshall
Indexing by Deborah Corson
Jacket design by Pamela Lewis*

*Elements typeset by Hot Type Ltd., Washington, D.C.
Printed and bound by Maple Press Co., York, Pa.*